# Qualitive and quantitive mass spectrometric analysis of neuroactive substances from single insect neurons

Inaugural-Dissertation
zur
Erlangung des Doktorgrades
der Mathematisch-Naturwissenschaftlichen Fakultät
der Universität zu Köln

vorgelegt von
Max Raoul Diesner
aus Frankfurt am Main

Köln
2018

Berichterstatter:
Dr. Susanne Neupert
Prof. Dr. Marcus Krüger

Tag der mündlichen Prüfung:
18.1.2019

## Abstract

Organisms need to constantly adapt their behavior to the changing environment as well as react towards changes in their internal state. The nervous system perceives and processes such stimuli and coordinates the corresponding reactions of the body. This system is based on regulated cell-cell communication, utilizing a wide range of different chemical signaling molecules and receptors. If one wants to fully grasp how neural circuits process, modulate and relay incoming information, then the involved neuroactive substances, their cellular distribution, temporal and quantitative dynamics have to be analyzed on single cell resolution. Single cell mass spectrometry (SCMS) allows the interrogation of chemical profiles from individual cells, including neuroactive substances such as neuropeptides and biogenic amines. Matrix assisted laser desorption/ionization – time-of-flight mass spectrometry (MALDI-TOF MS) has established itself as a fast and reliable tool for the analysis of neuropeptides from single neurons of invertebrates and vertebrates alike. However, the detection of small signaling molecules, such as biogenic monoamines, by MALDI-TOF SCMS has been challenging. Biogenic monoamines play key roles in orchestrating and modulating neural circuits, therefore a MALDI-TOF SCMS based method for their detection and quantification is highly desirable. Additionally, biogenic monoamines can be co-localized with neuropeptides. Therefore the development of a MALDI-TOF SCMS based method capable of detecting both neuroactive substances would help to reveal such overlapping expression profiles.

In the current thesis, I focused on the development of a MALDI-TOF SCMS based method that allows the detection and quantification of biogenic monoamines from single somata of insect neurons. The study focused on the insect octopaminergic/tyraminergic system, with an emphasis on octopamine (OA), which is considered to be homologous to the vertebrate noradrenalin/adrenalin system. By using chemical derivatization of amine moieties of OA and tyramine (TA) and an optimized sample preparation, I was able to lower the respective detection limits to single cell concentrations. Additionally, I could show that the chemical derivatization does not interfere with the detection of neuropeptides from the same sample, hence allowing the simultaneous detection of both substance classes. Further, I could show that absolute quantification of OA and TA is possible from single cell sample volumes using isotopically labeled synthetic standards. I used the developed protocol for the qualitative and quantitative analysis of OA/TA from genetically labeled and manually microdissected somata of interneurons from the fruit fly *Drosophila melanogaster*. Using the newly developed approach,

I analyzed intracellular OA/TA ratios, compared somatic OA titers between sexes and two different OAergic cell clusters and revealed that prolonged cooling of animals has an increasing effect on detectable OA titers in the analyzed neurons.

Furthermore, I used the developed protocol to analyze changes in somatic OA titers of aggression modulating OAergic neurons from the gnathal ganglion in socially naive and experienced adult male *D. melanogaster*. I could show that the somatic OA titer increases in these neurons when flies had social contact with the same sex compared to naive flies, which is possibly mediated by an input from pheromone detecting gustatory receptor neurons. To my knowledge, this is the first study to report a quantified increase of a somatic biogenic monoamine titer detected directly from individual isolated neurons of intact insect brains between two behavioral states by mass spectrometric analysis.

In a collaborative study, I employed the developed protocol to intracellular recorded descending dorsal unpaired median neurons from the Indian stick insect *Carausius morosus* and was able to confirm that these neurons contain OA and TA and thus could be OAergic.

Finally, as a starting point in an effort to create a map of neuropeptidergic neurons and their repertoire of neuroactive substances in adult *D. melanogaster*, I was involved in the analysis of single genetically labeled neuropeptidergic neuron somata using MALDI-TOF SCMS. In summary, we could describe a total of 10 different cell types characterized by their expressed neuropeptides and their location in the CNS. Future studies will focus on analyzing these cell types towards potential co-localized aminergic transmitters using the developed protocol.

# Zusammenfassung

Organismen müssen ihr Verhalten ständig an die sich verändernde Umwelt anpassen sowie auf Veränderungen in ihrem physiologischen Zustand reagieren. Das Nervensystem nimmt solche Reize wahr, verarbeitet sie und koordiniert die entsprechenden Reaktionen des Körpers. Dieses System basiert auf einer geregelten Zell-Zell-Kommunikation, bei der eine Vielzahl verschiedener chemischer Signalmoleküle und Rezeptoren zum Einsatz kommen. Um zu verstehen, wie neuronale Schaltkreise eingehende Informationen verarbeiten, modulieren und weiterleiten, müssen die beteiligten neuroaktiven Substanzen auf zellulärer Ebene charakterisiert und ihre zeitliche und quantitative Dynamik auf Einzelzellnivaeu analysiert werden. Die Einzelzell-Massenspektrometrie (SCMS) ermöglicht die Analyse von chemischen Profilen einzelner Zellen, einschließlich neuroaktiver Substanzen wie z.B. Neuropeptide und biogene Monoamine. Die matrixgestützte Laser Desorption/Ionisation – Flugzeit Massenspektrometrie (matrix assisted laser desorption/ionization mass spectrometry; MALDI-TOF MS) hat sich als schnelle und zuverlässige Methode zur Analyse von Neuropeptiden aus einzelnen Neuronen von Invertebraten und Vertebraten etabliert. Die Detektion von kleinen Signalmolekülen, wie z.B. biogenen Monoaminen, durch MALDI-TOF SCMS stellt jedoch bis heute eine analytische Herausforderung dar. Da biogene Monoamine eine Schlüsselrolle bei der Orchestrierung und Modulation neuronaler Schaltkreise haben, ist eine MALDI-TOF SCMS gestützte Methode für deren Nachweis und Quantifizierung äußerst erstrebenswert. Biogene Monoamine können zu dem mit Neuropeptiden kolokalisiert seien. Somit würde eine neu entwickelte durch MALDI-TOF SCMS gestützte Methode, mit der ein Nachweis beider neuroaktiven Substanzklassen aus einer Zellprobe möglich ist, es deutlich erleichtern entsprechend überlappende Expressionsmuster nachzuweisen.

In der vorliegenden Arbeit konzentrierte ich mich auf die Entwicklung einer MALDI-TOF SCMS basierten Methode, die den Nachweis und die Quantifizierung von biogenen Monoaminen aus einzelnen Insektenneuronen ermöglicht. Die Studie konzentrierte sich auf das octopaminerge/tyraminerge System von Insekten, mit dem Schwerpunkt auf Octopamin (OA), das als homolog zum Noradrenalin/Adrenalin-System der Wirbeltiere gilt. Durch die chemische Derivatisierung der Aminogruppe von OA und Tyramin (TA) und eine optimierte Probenvorbereitung konnte ich die jeweiligen Nachweisgrenzen auf Einzelzellkonzentrationen senken. Zudem konnte ich zeigen, dass die chemische Derivatisierung den Nachweis von Neuropeptiden aus derselben Probe nicht stört und somit den gleichzeitigen Nachweis beider

Substanzklassen ermöglicht. Außerdem konnte ich zeigen, dass die Quantifizierung von OA und TA aus Einzelzellprobenvolumina mit isotopenmarkierten synthetischen Standards möglich ist. Ich entwickelte das Protokoll zur qualitativen und quantitativen Analyse von OA/TA mittels genetisch markierten und manuell mikrodissektierten Somata von Interneuronen der Taufliege *Drosophila melanogaster*. Mit dem neu entwickelten Ansatz untersuchte ich intrazelluläre OA/TA Verhältnisse, verglich somatische OA-Titer zwischen den Geschlechtern sowie zwei verschiedenen OAergen Zellclustern und zeigte, dass eine Kühlung der Tiere vor der Präparation zu einem Anstieg der nachweisbaren OA-Titer in den analysierten Neuronen führt.

Darüber hinaus habe ich das entwickelte Protokoll verwendet, um Veränderungen in somatischen OA-Titern von aggressionsmodulierenden OAergen Neuronen aus dem gnathalen Ganglion in sozial naiven und erfahrenen erwachsenen männlichen *D. melanogaster* zu analysieren. Ich konnte zeigen, dass der somatische OA-Titer in diesen Neuronen zunimmt, wenn Fliegen sozialen Kontakt mit dem gleichen Geschlecht hatten, verglichen mit naiven Fliegen. Dies ist möglicherweise auf einen Input von gustatorische Rezeptorneuronen zurückführen welche Pheromone detektieren. Nach meiner Kenntnis ist dies die erste Studie, die einen quantifizierten Anstieg eines somatischen biogenen Monoamin-Titers zeigt, der direkt aus einzelnen isolierten Zellen eines intakten Insekten Gehirns zwischen zwei Verhaltenszuständen mittels massenspektrometrischer Analyse nachgewiesen wurde.

In einem Kooperationsprojekt untersuchte ich mit Hilfe des entwickelten Protokolls intrazellulär abgeleitete dorsal ungepaarte mediane Neurone der indischen Stabheuschrecke *Carausius morosus* in Bezug auf ihre aminerge Zusammensetzung. Ich konnte nachweisen, dass diese Neurone OA und TA enthalten und somit OAerg seien können.

Als Ausgangspunkt für die Erstellung einer Karte neuropeptiderger Neurone und ihrer Repertoires an neuroaktiven Substanzen in adulten *D. melanogaster*, war ich an der Analyse einzelner genetisch markierte neuropeptiderge Neuronenzellkörper mittels MALDI-TOF SCMS beteiligt. Insgesamt konnten wir 10 verschiedene Zelltypen beschreiben, die sich durch ihre Neuropeptidzusammensetzung und ihre Lage im Gehirn auszeichnen. Zukünftige Studien werden sich darauf konzentrieren, diese Zelltypen mit Hilfe des entwickelten Protokolls zur biogenen Monoamincharakterisierung auf mögliche Kolokalisierungen aminerger Transmitter zu analysieren.

# Table of Contents

Abstract ..... I

Zusammenfassung ..... III

Table of Contents ..... V

Abbreviations ..... VII

1. General Introduction ..... 1

2. Development of a MALDI-TOF MS based workflow for the identification and quantification of octopamine and tyramine from single identified *D. melanogaster* neurons ..... 28

- 2.1 Introduction ..... 29
- 2.2 Materials and Methods ..... 31
- 2.3 Results and Discussion ..... 35
  - 2.3.1 Analysis of non-derivatized and derivatized synthetic OA and TA ..... 35
  - 2.3.2 Detection of OA and TA from individual Drosophila neurons ..... 41
  - 2.3.3 Quantification of synthetic OA and TA ..... 43
  - 2.3.4 Stability of stored samples ..... 47
  - 2.3.5 Isomeric ion species and neuropeptide profiling ..... 49
  - 2.3.6 Discrimination of OA and DA ..... 50
  - 2.3.7 Quantification of OA and TA in VMlb somata ..... 52
  - 2.3.8 Temperature-dependent variability of detectable OA titers in VMlb neurons ..... 53
  - 2.3.9 Sexual dimorphism of VMlb OA concentrations ..... 54
  - 2.3.10 Quantification of OA from two OA/TA cell populations ..... 55
- 2.4 Conclusion ..... 57

3. Quantification of *Drosophila* VMlb octopamine titers in social driven male aggression by MALDI-TOF SCMS ..... 58

- 3.1 Introduction ..... 59
- 3.2 Materials and Methods ..... 63
- 3.3 Results and Discussion ..... 66
  - 3.3.1 Influence of age, sex and genetic construct on OA VMlb titers ..... 66
  - 3.3.2 Influence of social experience on VMlb OA titers ..... 67
- 3.4 Conclusion ..... 72

*4.* Mass spectrometric detection of octopamine and tyramine from intracellular recorded desDUM neurons of *Carausius morosus* ..... 73

- 4.1 Introduction ..... 74
- 4.2 Materials and Methods ..... 76
- 4.3 Results and Discussion ..... 79
- 4.4 Conclusion ..... 83

5. Mass spectrometric survey and mapping of neuropeptides in DIMMED neurons from the adult *Drosophila* brain ..... 84

- 5.1 Introduction ... 85
- 5.2 Materials and Methods ... 87
- 5.3 Results and Discussion ... 90
  - 5.3.1 Cell type #1: Allatostatin-C (Ast-C) neurons ... 92
  - 5.3.2 Cell type #2: Myosuppressin (DMS) neurons ... 94
  - 5.3.3 Cell type #3: Allatostatin-A (Ast-A) + myoinhibiting peptide (MIP) + Natalisin (Nat) neurons ... 94
  - 5.3.4 Cell type #4: CAPA neurons ... 97
  - 5.3.5 Cell type #5: Hugin/Pyrokinin (huginPK) neurons ... 99
  - 5.3.6 Cell type #6: Sulfakinin (SK) neurons ... 100
  - 5.3.7 Cell type #7: Corazonin (Cor)/short Neuropeptide F (sNPF) neurons ... 101
  - 5.3.8 Cell type #8: Pigment dispersing factor (PDF) neurons ... 103
  - 5.3.9 Cell type #9: Neuropeptide-like precursor 1 (NPLP1) neurons ... 103
  - 5.3.10 Cell type #10: Neuropeptide F (NPF) neurons ... 106
- 5.4 Conclusion ... 108

6. General Discussion ... 110
   - 6.1 Methodological aspects of the developed MALDI-TOF MS based approach ... 110
     - 6.1.1 Range of detectable analytes ... 111
     - 6.1.2 Limit of detection and quantification ... 113
     - 6.1.3 Sample isolation ... 114
   - 6.2 Applications and implications for further research ... 117
7. Conclusion ... 123
8. List of Figures ... 124
9. List of Tables ... 125
10. Bibliography ... 126
11. Part Publications ... 152
12. Acknowledgments ... 154
13. Erklärung ... 155
14. Curriculum vitae ... 156

## Abbreviations

| | |
|---|---|
| 1,5-DAN | 1,5-diaminonaphtalene |
| 5-HT | 5-Hydroxytryptamine/serotonin |
| 7-T | (z)-7-tricosense |
| ACh | acetylcholine |
| ACN | acetonitrile |
| CHCA | α–cyano-4-hydroxycinnamic acid |
| AD | adrenaline |
| Akh | adipokinetic hormone |
| AP | action potential |
| Ast-A | allatostatin-A |
| Ast-C | allatostatin-C |
| CA | 4-hydroxy-3-methoxycinnamaldehyde |
| cAMP | 3',5'-cyclic adenosine monophosphate |
| CE | capillary electrophoresis |
| CFME | carbon-fiber mircoelectrodes |
| Cha | choline acetyltransferase |
| CID | collision-induced dissociation |
| CNiFERs | cell-based neurotransmitter fluorescent engineered reporters |
| CNS | central nervous system |
| cVA | 11-*cis*-vaccenyl acetate |
| CPG | central pattern generator |
| DA | dopamine |
| DAG | diacylglycerol |
| DESI | desorption electrospray ionization |
| DPD | 2,5-dimethyl-1H-pyrrole-3,4-dicarbaldehyde |
| desDUM | descending dorsal unpaired median |
| DHB | 2,5-dihydroxybenzoic acid |
| DIM | DIMMED (transcription factor) |
| DMS | drosomyosuppressin |
| DTT | dithiothreitol |
| DUM | dorsal unpaired median |
| ECD | electrochemical detection |

| | |
|---|---|
| ER | endoplasmatic reticulum |
| ESI | electrospray ionization |
| FDA | US Food and Drug Administration |
| FRET | fluorescence resonance energy transfer |
| FSCV | fast-scan cyclic voltammetry |
| GABA | γ-aminobutyric acid |
| GFP | green fluorescent protein |
| GNG | gnathal ganglion |
| GPCR | G-protein-coupled receptors |
| GRASP | GFP reconstitution across synaptic partners |
| GRN | gustatory receptor neuron |
| HA | histamine |
| HPLC | high performance liquid chromatography |
| ICLI | inferior contralateral interneuron |
| $IP_3$ | 1,4,5-triphosphate |
| IS | internal standard |
| ISD | in-source decay |
| LDCV | large dense core vesicle |
| LEAP | large, episodically-releasing, amidating peptide producing cells, that contain the transcription factor DIMMED |
| LIF | laser-induced fluorescence detection |
| LINF | laser-induced native fluorescence detection |
| LOD | limit of detection |
| LOQ | limit of quantification |
| LLOQ | lower limit of quantification |
| MALDI | matrix-assisted laser desorption/ionization |
| MBON | mushroom body output neurons |
| MEKC | micellar elektrokinetic capillary chromatography |
| MIP | myoinhibitory peptide |
| MN | motor neuron |
| MP | bilaterial medial protocerebral neurons |
| MS | mass spectrometry |
| $MS^2$ | tandem mass spectrometry |
| MSI | mass spectrometry imaging |

| | |
|---|---|
| *m/z* | mass-to-charge ratio |
| NAD | noradrenaline |
| nanoLC | nano liquid chromatography |
| Nat | natalisin |
| NPF | neuropeptide F |
| NPLP1 | neuropeptide-like precursor 1 |
| OA | octopamine |
| OA(*d3*) | (±)-p-octopamine-α,β,β-d3 |
| OAR | octopamine receptors |
| ORN | olfactory receptors neurons |
| PAM | protocerebral anterior medial |
| PBS | phosphate buffer solution |
| PDF | pigment dispersing factor |
| PK | pyrokinin |
| PM | paired median |
| PP | precursor peptides |
| PPL1 | protocerebral posterior lateral 1 |
| PSD | post-source decay |
| PTM | posttranslational modification |
| PVK | periviscerokinin |
| rpm | revolutions per minute |
| RSD | relative standard deviation |
| SCMS | single cell mass spectrometry |
| SIMS | secondary ion mass spectrometry |
| SK | sulfakinin |
| sNPF | short neuropeptide F |
| TA | tyramine |
| TA(*d4*) | 2-(4-hydroxyphenyl)ethyl-1,1,2,2-d4-amine |
| Tβh | tyrosine-β-hydroxylase |
| TDC | tyrosine decarboxylase |
| TFA | trifluoroacetic acid |
| TK | tachykinin |
| TNT | tetanus neurotoxin light chain |
| TOF | time-of-flight |

| | |
|---|---|
| TrpA1 | transient receptor potential cation channel A1 |
| Tyr | tyrosine |
| UM | unpaired median neuron |
| UV | ultraviolet |
| VL | ventrolateral |
| VMlb | ventral midline labial |
| VMmd | ventral midline mandibular |
| VMmx | ventral midline maxillary |
| VNC | ventral nerve cord |
| VPM | ventral paired median |
| VUM | ventral unpaired median |

# 1. General Introduction

Organisms need to constantly adapt their behavior to the changing environment as well as react towards changes in their internal state. The nervous system perceives internal and external stimuli, integrates this information in the context to the current state of the organism and generates an appropriate reaction of the body. Regulated cell-cell communication is the basis for such targeted transduction, integration and modulation of information in the nervous system. For cell-cell communication in the nervous system, neurons can convert their electrical activity into the release of neuroactive substances targeting neurons and/or other cell types. Target cells express receptors which bind neuroactive substances with high specificity and selectivity. When a receptor binds to its specific ligand, intracellular signal cascades are activated altering the physiology and “behavior” of the corresponding cell, for example by changing gene expression or activation of membranous ion channels. A plethora of different neuroactive substances have been identified from nervous systems of invertebrates and vertebrates, and it has been shown that the cellular expression patterns, receptors and corresponding functions of a single neuroactive substance can be conserved throughout different evolutionary lineages (Bräunig & Pflüger 2001; Roeder 2005; Nässel & Wegener 2011).

In order to fully comprehend how the nervous system and underlying neural circuits shape and control the reactions of an organism, it is essential to analyze involved neuroactive substances, their cellular distribution, temporal and quantitative dynamics on a single cell resolution. However, neuroactive substances often show overlapping expression patterns in nervous system, e.g. biogenic monoamines and neuropeptides (Merighi 2011; Fricker 2012; Nässel 2018), which makes it challenging to reveal the full signaling capabilities of a given neuron. Thus, methodological approaches that enable the simultaneous detection of multiple classes of substances in a single experiment are highly desirable. Ideally, such methods would be quantitative to allow the analysis of changing neuroactive substance concentration in a given cell in relation to other signaling molecules, drugs or different behavioral states of the analyzed organism. Mass spectrometry (MS) offers the possibility to simultaneously detect and quantify different substance classes from biological samples such as single cells. For example, matrix assisted laser desorption/ ionization – time-of-flight single cell mass spectrometry (MALDI-TOF SCMS) is a widely used tool for the detection of neuropeptides from neuron somata of invertebrates and vertebrates alike (e.g. Li, Garden, et al. 2000; Neupert & Predel 2005; Rubakhin & Sweedler 2007; Neupert et al. 2007). However, the detection of potentially co-localized small neuroactive substances, like biogenic monoamines, has been challenging using this approach.

The main focus of the current thesis was the development of a MALDI-TOF SCMS based strategy for the detection and quantification of biogenic monoamines from single insect neuron somata. The focus laid on the insect octopamine (OA)/tyramine (TA) system, with an emphasis on OA, which is considered to be homologous to the vertebrate noradrenalin/adrenalin system. Moreover, since biogenic monoamines can be co-localized with neuropeptides in neurons, the simultaneous detection of these substance classes was investigated. To set the context of my work, I want to introduce insect nervous systems, OA and TA, neuropeptides and mass spectrometry as an analytical method in more detail in the following sections.

## Insect nervous systems and their role in neuroscience

Insect nervous systems are arranged in single units called ganglia organized in a metameric fashion, which is based on their segmental body plan. These ganglia can represent fusion products of so called neuromeres or represent a single neuromere. Neuromeres represent a segment specific part of the central nervous system (CNS) that contains the neural circuitry which processes sensory information and controls movement of segmental appendages and segmental muscles (Niven et al. 2008). Single neuromeres are linked by a pair of connectives, which are still present in fused ganglia as axonal tracts. The insect CNS is comprised of a brain (supraesophageal ganglion), the gnathal ganglion (GNG; old name subesophagial ganglion; Ito et al. 2014), and the ventral nerve cord (VNC). The brain is a fusion product of four pregnathal neuromeres, while the GNG represents a fusion product of the three gnathal neuromeres (Urbach & Technau 2003; Niven et al. 2008). The VNC consists of three thoracic ganglia, the pro-, meso- and metathoracic ganglion, connected to a varying number of abdominal ganglia. Ganglia in the VNC can be fused or remain free depending on the examined insect lineage, but in general represent a total of eleven neuromeres (Niven et al. 2008). Further, comparable to the vertebrate autonomic nervous system, a system of peripheral ganglia exists in insects, the stomatogastric nervous system. It is comprised of four main parts: the frontal ganglion, the hypocerebral ganglion and the paired/unpaired ingluvial and proventricular ganglia (Bilingsley & LeHane 1996; Hartenstein 1997).

Even though insect nervous systems are only comprised of a small number of neurons compared to mammal nervous systems, they produce a wide variety of complex behavior patterns such as mating, collision avoidance and spatial navigation as well as many properties of insect neurons show striking resemblance in their mammalian counterparts (Namiki et al. 2009). Moreover, extensive similarities of neuronal circuits underlying sensory systems, synaptic plasticity and neuromodulation between invertebrates and vertebrates suggest a deep homology between central parts of their distinct CNS (Strausfeld & Hirth 2013; Haberkern & Jayaraman 2016). The investigation of these “simple” nervous systems, therefore, facilitates our understanding of nervous systems in general on a broader scale (Namiki et al. 2009). Aside from these benefits, a multitude of practical advantages exist when working with insects and their nervous systems. Especially, their low cost mass rearing and short generation times facilitate fast repetition rates of experiments. Furthermore, the limited size and accessibility of insect nervous systems is highly beneficial for modern microscopy based methods, like immunohistochemistry or *in vivo* imaging, as well as electrophysiological applications. It is therefore not surprising that insects have established themselves as model organisms for the functional analysis of behavior and neuronal networks throughout the last century.

Another more recent driving force has been the development of non-invasive genetic tools for the targeted expression of reporter and effector genes like the GAL4/UAS system (Jarman et al. 1993) or the LaxA-LexAop system (Lai & Lee 2006) and their ongoing extension in the small fruit fly *D. melanogaster* (Yoshihara & Ito 2012). The combination of these tools with the fully sequenced *D. melanogaster* genome (Adams et al. 2000), enables the targeted analysis of gene expression by genetic labeling, as well as the targeted interference of gene expression rates via methods such as RNA interference (Roignant et al. 2003). Moreover, the system allows the activation or silencing of single neurons by light (Lima & Miesenböck 2005), temperature (Kitamoto 2001; McGuire et al. 2003) or the expression of ion channels (Luan et al. 2006) for the analysis of neuronal network functions. Furthermore, the GAL4/UAS system has been transferred to another insect model the red flour beetle *Tribolium castaneum* (Schinko et al. 2010), which will allow to use the depicted genetic tools in this insect species.

Finally, large scale projects which aim to decipher a high number of various insect transcriptomes and genomes, like the 1kite project (www.1kite.org) or the i5k project (i5k.github.io), in combination with the newly discovered CRISPR/Cas gene editing method (Jinek et al., 2012; Gasiunas et al., 2012) will allow the transfer of the already developed genetic tools to other insect species. In the current thesis, I used the GAL4/UAS system to label different subsets of neurons in adult *D. melanogaster* to allow their repeatable dissection and identification between different individual flies.

## Biogenic monoamines

Biogenic monoamines are small biogenic neuroactive substances which have a single functional amine moiety. The group of biogenic monoamine transmitter includes: the imidazole amines (histamine [HA]), catecholamines (adrenaline [AD], noradrenaline [NAD], dopamine [DA]), indolamines (serotonin [5-HT]), tryptamines (tryptamine), phenethylamines (e.g.: TA, OA, synephrine) and thyronamines (3-Iodothyronamine). Biogenic monoamines are versatile in their mode of action and can function as neurotransmitters, neuromodulators and/or neurohormones. They are involved in the regulation of nearly all vital functions in vertebrates and invertebrates alike, such as cardiovascular control, movement, endocrine regulation, circadian rhythms, learning and memory (e.g. Nässel & Winther, 2010).

All biogenic monoamines are synthesized from proteinogenic amino acids and their derivates, like tyrosine (Tyr), phenylalanine, tryptophan or histidine, via amino acid decarboxylases (Brady et al. 2012). They are synthesized in the cytosol of the neuron cell body as well as the nerve terminals, where they are stored and released from synaptic vesicles or large dense core vesicles (LDCV) by stimulus induced $Ca^{2+}$ dependent exocytosis. Cytosolic biogenic monoamines are actively transported into small synaptic vesicles or LDCVs by vesicular $H^+$ dependent monoamine transporters and can be co-localized with other neuroactive substances, like neuropeptides (Brady et al. 2012; Gallo et al. 2016). Nearly all biogenic monoamines are recognized by GPCR receptors, with the exception of 5-HT which binds to an ionotropic receptor (Wu et al. 2015). Secreted biogenic monoamines are inactivated either by degradation or reuptake. The primary mechanism for inactivation is cytosolic reuptake by specialized $Na^+/Cl^-$ dependent plasma membrane transporters (e.g.: DA transporter; Giros & Caron 1993; Ueno & Kume 2014). Cytosolic catabolism of monoamine transmitters after reuptake is mainly mediated by monoamine oxidases (Westlund et al. 1985; Eisenhofer 2004; Yamamoto & Vernier 2011) whereas extra-neuronal inactivation is mediated by catechol-o-methyltransferases (Eisenhofer 2004; Yamamoto & Vernier 2011). However, in invertebrates biogenic monoamine inactivation is enzymatically diverse and can also be mediated by Nacetylation, N-methylation, sulfation and other mechanisms (Sloley & Juorio 1995; Sloley 2004; Sotnikova & Gainetdinov 2010).

The analysis of the wide range involvement of biogenic monoamine signaling in complex behaviors and emotions led to the understanding that impairment of these systems can lead to severe disease and disorders such as depression, obsessive-compulsive disorder, neuropathic pain, and others (Pitman et al. 2011; Yousuf & Kerr 2016). Therefore, methods which allow us to foster our understanding of their cellular distribution, intracellular dynamics and effects on target cells are highly desirable. In this thesis I focused on two biogenic monoamines OA and TA in insect nervous systems, with an emphasis on OA.

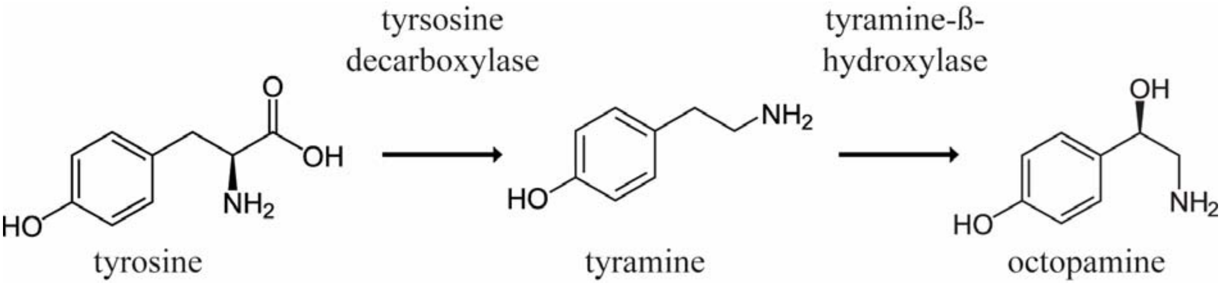

**Figure 1.1 Synthesis pathway of OA.** Tyrsoine is decarboxylated into TA, and TA is subsequently hydroxylated into OA.

## Octopamine

Octopamine, or p-hydroxyethanolamine, was first discovered in the salivary glands of *Octopus vulgaris* (Erspamer & Boretti 1951). It is synthesized by hydroxylation of its precursor TA, via the tyramine-β-hydroxlase (Tβh) in invertebrates (Fig. 1.1). OA is the most abundant biogenic monoamine transmitter in invertebrates (Verlinden et al. 2010; Fang et al. 2011), however, in vertebrates it is considered a trace amine and only found in very small amounts (Berry 2004). While OA function in the CNS of invertebrates is a subject of numerous studies and serves as a perfect model to investigate general features of neuromodulation, only recently interest in trace amine function in vertebrate nervous systems has resparked due to the discovery of mammalian trace amine receptors (Borowsky et al. 2001; Lindemann et al. 2005; khan & nawaz 2016). A growing body of evidence suggests an involvement of OAergic signaling in neurosynaptic transmission and seems to be connected to vertebrate neurological disorders like depression, migraine or Parkinson´s disease (khan & nawaz 2016). The chemical structure of OA is analogous to the vertebrate NAD and the invertebrate OA/TA signaling system is often seen as homologous to the vertebrate NAD/AD signaling system, due to similar functions in physiology and behavior as well as structural features (Roeder 2005; Verlinden et al. 2010). Furthermore, a recent phylogenetic analysis of biogenic monoamine receptors suggested that OAergic and adrenergic systems coexisted in the last common ancestor of bilaterians (Roeder 2005; Bauknecht & Jékely 2017). Adrenergic signaling seems to be unique to the deuterostome lineage and has no physiological relevance in invertebrates to date, while OA signaling in vertebrates was believed to be physiologically irrelevant as well (see above). Due to this lineage specificity and the fact that OA signaling has regulating effects in virtually all tested organs and tissues of insects it has been the subject of a plethora of studies as a potential target for insecticides (Roeder 2005; Verlinden et al. 2010; Farooqui 2012)

In insects, only a small number of neurons express OA as neuroactive substance, which has also been reported for other biogenic monoamines, projecting to most neuropil regions of the brain, the thoracic nervous system and peripheral organs. In the larval *D. melanogaster* CNS, for example, only around 80 OAergic neurons have been identified (Monastirioti et al. 1995; Selcho et al. 2012; Selcho et al. 2014), whereas the imago yields about 100 OAergic neurons (Monastirioti et al. 1995; Sinakevitch & Strausfeld 2006; Busch et al. 2009). Furthermore, the distribution and number of OAergic neurons has been studied in various insects including honey bees (Sinakevitch & Strausfeld 2006; Schröter et al. 2007), blowflies (Sinakevitch & Strausfeld 2006), cockroaches (Eckert et al. 1992; Sinakevitch et al. 2005), hawkmoths (Dacks et al. 2005), crickets (Sporhase-Eichmann et al. 1992), and locust (Konings et al. 1988). The projection patterns and terminal areas of these OAergic neurons seem to be conserved and analogous counterparts can be identified between different insect species (Braunig 1991; Bräunig & Pflüger 2001; Schröter et al. 2007; Busch et al. 2009; Busch & Tanimoto 2010). Mainly two populations of OAergic neurons have been described in insect nervsous systems; paired median (PM) and non-median neurons that can be located in the brain, the GNG and some segmental ganglia, as well as unpaired median neurons (UM) located solely in segmental ganglia and the GNG of insects (Bräunig & Pflüger 2001; Busch et al. 2009; Selcho et al. 2014). UM neurons can be subdivided into dorsal UM (DUM) and ventral UM (VUM) neurons depending on the cell body position at the midline of the respective ganglion (Bräunig & Pflüger 2001; Busch et al. 2009; Selcho et al. 2014). In *D. melanogaster* three clusters comprised of VUM and ventral PM (VPM) neurons located in the GNG have been described, with VUM neurons of the mandibular (VMmd) and maxillary (VMmx) cluster (8-9 VUM neurons in each cluster; Busch et al. 2009; Schneider et al. 2012) showing only innervation of the brain in various higher brain regions as well as the GNG. Individual VUMs of different clusters show very similar ramifications and projection patterns in the brain and it is suggested that they developed through a duplication of an evolutionary older set of OAergic VUMs (Busch et al. 2009; Busch & Tanimoto 2010). Because of their similarities in their projection patterns these neurons are characterized into morphological groups (Busch et al. 2009). Most VUMs of the labial cluster (VMlb; ~4-5 neurons) in adult *D. melanogaster*, however, send their projections towards the VNC with unknown targets (VUMd1-3; Busch et al. 2009; Schneider et al. 2012). Aside from these descending VUM neurons of the VMlb cluster, one pair of VPM neurons of the VMmd cluster, VPM1, project asymmetrical to the ipsilateral side of the thoracic neuromeres and the abdominal neuromeres (Busch et al. 2009). In the adult locust, homologous OAergic cells, so called descending DUM (desDUM) neurons, project to neuropil regions processing information of leg sensory organs (Bräunig & Burrows 2004). Finally, five sets of VPM neurons exist in *D. melanogaster*, with VPM1 and 2 neurons being located in the close vicinity of the VMmd cluster, VPM3 neurons at the VMmx cluster and VPM4 and 5 neurons at the VMlb cluster (Busch et al. 2009; Busch & Tanimoto 2010; see Fig. 1.2). Each VUM cluster develops from a single median precursor cell of the embryonic midline, while it has been suggested that VPM neurons develop from paired lateral neuroblasts (see Fig. 1.2; Klämbt et al. 1991; Busch & Tanimoto 2010).

OA solely mediates its regulatory and modulatory functions through G protein coupled receptors (GPCR) in insects. In the genetic model organism *D. melanogaster*, for example, five OA GPCRs have been identified with different binding affinities, second messenger cascades and distributions (Farooqui 2012; El-Kholy et al. 2015; Qi et al. 2017). These five OA receptors (OAR) are grouped into three classes based on their structural and signaling similarities to vertebrate adrenergic receptors: α-adrenergic-like receptors (OAMB [OctαR; two isoforms, OAMB-K3; OAMB-AS]; Octα2R [two isoforms, Octα2R-L; Octα2R-S]), β-adrenergic-like receptors (Octß1R; Octß2R; Octß3R) and octopamine/tyramine receptors (Farooqui 2012; El-Kholy et al. 2015; Qi et al. 2017). OAR elicit their function though G-proteins activating various second messenger cascades including cAMP, inositol 1,4,5-triphosphate ($IP_3$), and diacylglycerol (DAG). The latter second messenger cascades affect intracellular $Ca^{2+}$ concentrations, via $IP_3$ for example, or regulate phosphorylation via the protein kinase A, by cAMP, or protein kinase C by DAG (Farooqui 2012).

## Octopamine in insect behavior and physiology

DUM/VUMs are considered the main source of OA in the brain and the thoracic nervous system of insects. Subpopulations of gnathal DUM/VUMs innervate most neuropil regions of the insect brain and it has been shown that these are involved in controlling and regulating various complex behaviors, whereas thoracic and segmental DUM/VUM populations project to the periphery and are hypothesized to be the main source of peripheral OA signaling (Bräunig & Pflüger 2001; Roeder 2005; Farooqui 2007; Farooqui 2012).

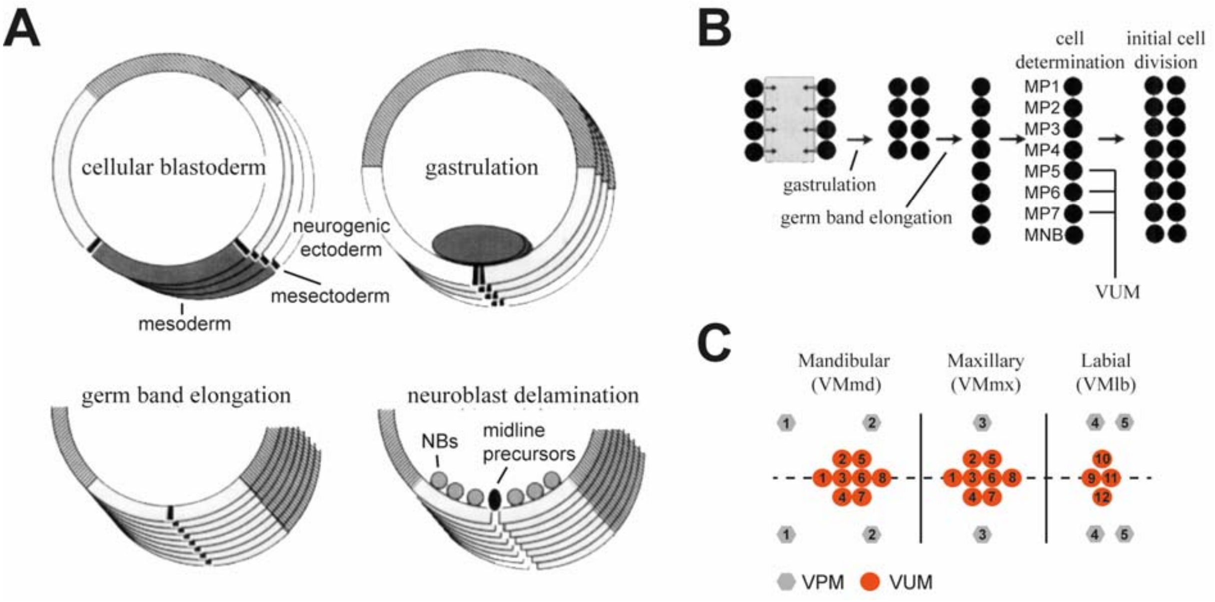
A
cellular blastoderm
gastrulation
neurogenic ectoderm
mesectoderm
mesoderm
germ band elongation
neuroblast delamination
NBs
midline precursors
B
cell determination
initial cell division
MP1
MP2
MP3
MP4
MP5
MP6
MP7
MNB
gastrulation
germ band elongation
VUM
C
Mandibular (VMmd)
Maxillary (VMmx)
Labial (VMlb)
VPM
VUM

**Figure 1.2 Development of VUM/VPM neurons in *D. melanogaster*.** (**A**) Development of the midline during four embryonic stages in *D. melanogaster*. Four midline precursor cells are located at both ends of the mesodermal anlage, forming the mesectoderm. During gastrulation, the mesoderm invaginates so that the midline precursor cells become juxtaposed at the ventral midline. During germ band elongation these precursor cells become a single line with eight cells per segment. Before these stem cells divide, they delaminate from the neuronal ectoderm into the neuroblast layer. (**B**) Schematic drawing of the development of the midline as described in (A). The midline consists of 7 medial precursor cells and the medial neuroblast. The medial precursor cells 5-7 develop into VUM neurons in *D. melanogaster*. (**C**) Outline of gnathal OAergic cell clusters and their VUM/VPM neurons in adult *D. melanogaster*. Numbers indicate a distinct morphological cell type with similar projections. Modified from (Klämbt et al. 1991; Busch & Tanimoto 2010).

OA signaling in the CNS involves modulating a plethora of different behaviors and underlying neuronal circuits such as reward and appetitive reinforcement (*D. melanogaster*: Schwaerzel et al. 2003; Schroll et al. 2006; Burke et al. 2012; *Apis mellifera*: Hammer 1993; Hammer & Menzel 1998; *Gryllus bimaculatus*: Unoki et al. 2005; Unoki et al. 2006), taste (*D. melanogaster*: LeDue et al. 2016), aggression (*D. melanogaster*: Hoyer et al. 2008; Zhou et al. 2008; Hoopfer 2016; Watanabe et al. 2017; *G. bimaculatus*: Stevenson et al. 2000; Stevenson

2005) and vision (*A. mellifera*: Erber & Kloppenburg 1995; *Locusta migratoria*: Stern et al. 1995; Stern 2009). Other processes modulated by OA in the CNS include the initiation, maintenance and modulation of motor patterns and motor circuits as described for walking and flying in locusts (*Schistocerca americana*: Sombati & Hoyle 1984; *Schistocerca gregaria*: Rillich et al. 2013), flight in the hawk moth (*Manduca sexta*: Claassen & Kammer 1986), larval locomotion and adult flight in the fruit fly (*D. melanogaster.* larvae: Saraswati et al. 2004; Fox et al. 2006; Selcho et al. 2012; Imago: Brembs et al. 2007; van Breugel et al. 2014), and walking in the stick insect (*Carausius morosus*, Büschges et al. 1993). Furthermore, the role of OA in sensitization and dishabituation has been studied in various insects such as in the visual system of the locust (*L. migratoria*: Stern 2009) or the honey bee proboscis extension reflex (PER; Mercer & Menzel 1982; Braun & Bicker 1992).

OA has also modulating effects in the periphery on skeletal and visceral muscles, organs and glands. In homology to the vertebrate adrenergic system, OA is involved in the physiological body adaptation during energy demanding tasks such as the fight or flight response (Stevenson et al. 2000). As response to "stressful" stimuli and subsequent hyperglycemia, OA can be released into the hemolymph, were it acts as a neurohormone, to increase hemolymphatic lipid and sugar concentrations by either affecting energy storages in the fat body directly (Fields & Woodring 1991) or by regulating the release of the neuropeptide adipokinetic hormone (Akh) from the *corpora cardiaca* (Pannabecker & Orchard 1986; Lorenz & Gäde 2009). Other peripheral effects of OA signaling involve the insect immune system, where OA mediates haemocyte activity, such as phagocytosis and nodule formation (Baines et al. 1992), and bounds to the surface of bacterial pathogens for better recognition (Dunphy & Downer 1994). Furthermore, OA can modulate sensory organs and neurons by increasing or decreasing receptor sensitivity, receptor density or affecting neurotransmitter release (Farooqui 2007). For example, it has been shown that OA sensitizes sensory neurons of the forewing stretch receptor in locust (Ramirez et al. 1993). Finally, OA acts on a wide range of different muscles e.g. on oviduct contraction (*D. melanogaster.*: Rodríguez-Valentín et al. 2006; *L. mirgatoria*: Orchard & Lange 1986), extensior-tibiae muscles in *S. gregaria* (Evans & O'Shea 1977) and body wall muscle in *D. melanogaster* larvae (Monastirioti et al. 1995; Selcho et al. 2012).

## Tyramine

Tyramine, or 4-Hydroxy-phenylethylamin, is not only the chemical precursor of OA but can rather act as neuroactive substance on its own. TA modulation is often described as antagonistic to OA mediated effects, homologous to adrenergic system in vertebrates. TA is synthesized by decarboxylation of Tyr via the tyramine-decarboxylase (Tdc, Fig. 1.1; Cole et al. 2005; Roeder 2005; Farooqui 2012). In *Drosophila*, two *Tdc* genes were described and subsequent gene products show Tdc activity *in vivo*, however *Tdc1* is expressed non-neurally, e.g. in malpighian tubules, rectal papillae and digestive tract musculature, whereas *Tdc2* is expressed solely in neurons (Cole et al. 2005).

Studies focusing on the effects of OA signaling often reduced TA to an intermediate product in the synthesis pathway of OA (Lange 2009; Farooqui 2012). Nowadays, a growing body of evidence is starting to overturn this picture and more studies focus on potential roles of TA signaling in physiology and behavior. However, unraveling the functions of TA signaling is difficult due to dependency of OA synthesis on TA and only limited access to selective and strong TA receptor antagonists (Lange 2009). Nevertheless, the identification of three *Drosophila* TA GPCRs (Oct/TyrR [TyrR], TyrRII, III; Saudou et al. 1990; Cazzamali et al. 2005; El-Kholy et al. 2015) and characterization of some of their signaling properties (Cazzamali et al. 2005; Bayliss et al. 2013; Farooqui 2012), as well as the analysis of their expression pattern in the CNS by creation of specific transgenetic driver lines in *D. melanogaster* (El-Kholy et al. 2015) has led to first insights in TA signaling in the fly and to the understanding that TA acts as independent neuroactive substances in the CNS.

## Tyramine in insect behavior and physiology

Tyramine is co-localized with OA in DUM/VUM neurons and it has been speculated that both substances can be co-released from OAergic neurons (Lange & da Silva 2007; Lange 2009; Pyakurel et al. 2016). Aside from co-releasing, neurons expressing exclusively TA have been described in the *D. melanogaster* larval brain and VNC by immunostainings against TA, OA and synthesizing enzymes (Monastirioti et al. 1995; Nagaya et al. 2002; Selcho et al. 2014). Furthermore, studies on the TA/OAergic innervation of the locust oviduct from abdominal DUM/VUMs and paired dorsal neurons revealed also potentially exclusive TAergic neurons (Stevenson et al. 1994; Donini & Lange 2004; Lange & da Silva 2007; da Silva & Lange 2008).

TA signaling has often been described as antagonistic to OA signaling, homologous to the adrenergic system in vertebrates. TA signaling is involved in regulating motor patterns and circuits, as it has been shown that increased neuronal TA titers decrease larval crawling distance in *D. melanogaster* (Nagaya et al. 2002; Saraswati et al. 2004; Fox et al. 2006) as well as reduce flight duration in adults (Brembs et al. 2007; Ryglewski et al. 2017). In the locust *S. gregaria* it has been shown that TA is modulating central pattern generators for walking and flight (Buhl et al. 2008; Rillich et al. 2013). Sensory systems can also be the target of TA modulation, which has been shown by a *D. melanogaster* tyramine receptor mutant *honoka*, which showed reduced behavioral responses to odorant repellents compared to wild type flies (Kutsukake et al. 2000). Furthermore, TA signaling modulates appetitive regulation as shown in the blowfly *Phormia regina*, where injections of TA led to a decreased PER with regard to experiences of appetitive and nonappetitive food flavors (Nisimura 2005). In *A. mellifera*, however, thoracic injection of TA led to an increased sugar responsiveness and a better performance in appetitive learning (Scheiner et al. 2002; Scheiner, Reim, et al. 2017), which is suggested to be mediated by caste specific differential expression of TA GPCRs in the honey bees fat body (Scheiner, Entler, et al. 2017).

## Neuropeptides

Neuropeptides are the most diverse neuroactive substances found in metazoan organisms and are involved in controlling and modulating a plethora of physiological processes and behavioral patterns such as food intake, reproduction or muscle control (Nässel 2002; Nässel & Winther 2010; Wegener & Veenstra 2015; Schoofs et al. 2017). The term neuropeptide was coined by David de Wied in the 70s who studied the activity of pituitary peptide hormones in rats on motivation, learning and memory (de Wied 1971; de Wied 2000). The proposed definition was that neuropeptides are produced and secreted by neurons and affect functions of the CNS (de Wied et al. 1974; de Wied 2000). A more recent and better fitting definition states that a neuropeptide is defined as a bioactive peptide, secreted by neurons or non-neuronal cells, with similarities in their expressed genetic information, synthesis, processing as well as their binding to similar receptor families affecting neuronal tissue (Kastin 2000; Fricker 2012).

Neuropeptides usually contain 2-100 amino acids and are produced by neurosecretory cells and interneurons in the nervous system but can also be expressed by various non-neuronal cells of the endocrine system (Zitnan 1996; Kingan & Adams 2000; Fricker 2012; Wegener & Veenstra

2015). A single cell is not limited to the expression of a distinct neuropeptide gene but can express multiple neuropeptide genes at the same time, sometimes even co-localized with classical neurotransmitter or biogenic monoamines (Fricker 2012; Nässel 2018). Neuropeptides are versatile in their mode of action and can act as neurotransmitter, neuromodulator and/or neurohormone depending on the secreting synapse or neuroheamal site (Nässel 2009; Nässel & Winther 2010).

Neuropeptides are produced in the cell body and are matured throughout the regulated secretory pathway, in contrast to classical neurotransmitters which are in general enzymatically synthesized at the synapse (Merighi 2011; Fricker 2012). Neuropeptide synthesis starts with the translation of a peptide-precursor, the prepropeptide or preprohormone, containing a signal peptide which guides the preproprotein to the rough endoplasmic reticulum (ER; Perone et al. 1997). As a first enzymatic step a signal peptidase removes the N-terminal signal sequence, which is rapidly degraded (Tuteja 2005). The resulting propeptide or prohormone can undergo further modification (e.g.: glycosylation) and is transported to the Golgi network, passing the network from the *cis*- to the *trans*-face, and subsequently packaged in LDCVs for further maturation, storage and ultimately secretion (Merighi 2011; Fricker 2012). During Golgi transit and maturation in LDCVs the propeptide is cleaved by endoproteases (furins, prohormone convertases) at designated internal dibasic and/or monobasic cleavage sites, such as Lys-Arg (KR), Lys-Lys (KK), Arg-Arg (RR), Arg (R) and Lys (K) (Veenstra 2000; Rholam & Fahy 2009; Fricker 2012). C-terminal basic amino acids, remaining from the endoprotease enzymatic cleavage, are subsequently removed by exoproteases (carboxyproteases) leading to mature and/or immature peptides (Merighi 2011; Fricker 2012). Often, a precursor is cleaved into multiple neuropeptides (isoforms) with structurally related C-terminal motifs. The C-terminal motif plays a crucial role during interaction of the neuropeptide and its designated receptor, in general a GPCR (Nässel & Winther 2010; Merighi 2011; Fricker 2012). Neuropeptides with a conserved structural motif are classified into neuropeptide families (Coast & Schooley 2011).

Subsequently, resulting peptides can be subjected to further modification during maturation. Such post-translational modifications (PTM) affect the activity and degradation of mature neuropeptides. Amidation of the C-terminus is a widespread PTM of neuropeptides and is necessary for proper receptor recognition (Kolhekar et al. 1997; Prigge et al. 2000). Cyclization of N-terminal Gln into pyroglutamate is another frequently observed PTM in neuropeptides (e.g.: corazonin; Veenstra 1989). Other PTMs involve the addition of functional groups to amino acid side chains such as sulfation of Tyr (Holman et al. 1986), phosphorylation (Browne et al. 1981; Gäde et al. 2006) and glycosylation (Lu et al. 2002).

This multifarious synthesis, processing and packaging of neuropeptides leads to a vast repertoire of different potential bioactive neuroactive substances. To unravel such neuropeptidergic systems it is vital to gain knowledge of their expressed and processed mature products as well as other co-expressed neuroactive substances on a single cell level in nervous systems.

## An introduction to mass spectrometry

The identification, structural characterization and quantification of organic and inorganic chemical compounds from complex sample mixtures, such as organs/tissues/cells and their extracts, is today mainly achieved by MS and adjacent technologies such as chromatography. All mass spectrometers are based on the same principle, which is the separation of ionized molecules by means of their mass-to-charge ratio (*m/z*) in the gas-phase. In order to achieve this separation, mass spectrometers are working under high vacuum to circumvent potential collisions or diversions of produced ions with air molecules such as nitrogen. All mass spectrometers have three main components; (1) an ion source, which produces negatively or positively charged analyte ions, (2) the mass-analyzer, which separates the produced ions by their *m/z* ratio, and (3) a detector, detecting the separated ions (Fig. 1.3). Finally, a mass spectrum is generated by plotting the relative abundance of detected ions in a defined scanned mass range against their *m/z* ratio (Figure 1.3 A). This basic outline, also termed MS-mode or $MS^1$, illuminates the chemical complexity of a given sample, with information regarding relative abundance and masses of ionized analyte molecules. Ultimately, masses of detected ions can be compared to databanks, such as METLIN (metlin.scripps.edu) or UNIPROT (www.uniprot.org), in which already identified substances are deposited and identified via “mass match”. However, this identification solely rests on the comparison of recorded masses without any information on the chemical structure of a recorded ion and is often seen as a non-conclusive verification.

To obtain information on the chemical structure of an analyte of interest, mass spectrometers utilize a second mode called $MS^2$ or tandem mass spectrometry, which involves fragmentation of the ion of interest, the so called precursor ion, into specific and reproducible product ions.

This process involves multiple sequential steps of MS analysis according to their *m/z* ratio (Fig. 1.3). After the generation of analyte ions in the source, they are separated by their *m/z* ratio in a first mass analyzer ($MS^1$). Distinct precursor ion species can now be filtered from the remaining ion background and subjected to fragmentation. A second mass analyzer ($MS^2$) than separates the produced ion fragments or product ions and ultimately guides them to the detector (Fig. 1.3). To date various fragmentation methods have been observed and developed, which can be exclusive to a given instrumentation, such as in-source decay (ISD; Brown & Lennon 1995; Sellami et al. 2012), post-source decay (PSD; Spengler et al. 1992; Kaufmann et al. 1994), collision-induced dissociation (CID; Levsen & Schwarz 1976; Mitchell Wells & McLuckey 2005), photodissociation methods (Brodbelt 2015), electron capture and transfer methods (Qi & Volmer 2016; Lermyte et al. 2018) and others.

The detection of specific analytes can be hampered from biological samples due to isometric and/or isobaric chemical compounds, substances with concentrations lower than the limit of detection (LOD) or ion suppression effects caused by salts, ion-pairing agents, endogenous compounds, and additives such as drugs or metabolites. In order to tackle such sample-derived problems and enable a successful detection by MS, mass spectrometers are often combined with chromatographic or electro kinetic separation techniques, enzymatic digestions, chemical derivatizations or a combination of these.

While MS or even $MS^2$ can give information about relative concentrations of sample analytes an absolute quantification of these compounds can be achieved by the addition of a known internal standard (IS) or reference with a defined concentration to the sample. While synthetic isotopically marked standards of a known substance are the gold standard, these can be very expensive or unavailable for purchase. To fill this gap, chemically related substances can be used instead, however, to guarantee a precise quantification their ionization properties and linear correlation compared to the ion of interest have to be assessed carefully. Another possibility for absolute quantification is to analyze synthetic standards of the analyte of interest before the main experiment, in a corresponding sample matrix with the identical instrumentation, and compare the obtained signal intensities from both experiments.

A variety of different ion sources, analyzers and detectors have been developed and combined in the last decade, leading to numerous analytical platforms with unique features and drawbacks. In this study, I used MALDI-TOF MS as the main analytical tool.

## Matrix-assisted laser desorption/ionization – time of flight mass spectrometry (MALDI-TOF MS)

MALDI is a soft ionization technique that allows the ionization of large organic molecules with little or no fragmentation during gas phase transition and ionization. The term was first coined by Michael Karas and colleagues 1985 (Karas et al. 1985), however, another group around Koichi Tanaka, who worked on the ionization of glycerin via cobalt-particles and a pulsed $N_2$ laser, received a quarter of the 2002 chemistry Nobel prize for their contribution to the development of MALDI.

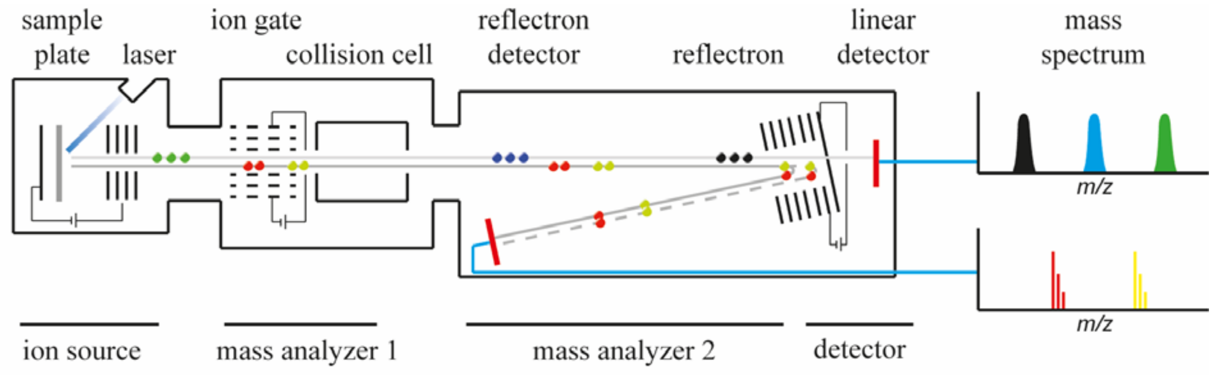

**Figure 1.3 Schematic of a MALDI-TOF mass spectrometer.** In MALDI-TOF MS, analyte ions are created by pulsed laser desorption of matrix and analyte molecules from the co-crystalized matrix sample spot in the MALDI ion source. Ions are electromagnetically accelerated from the source into the time-of-flight mass analyzer were they are separated by their *m/z* ratio. In linear mode ions directly hit the linear detector (light grey line) at the end of the flight tube. Detected ions generate Gaussian like signals in the mass spectrum (upper mass spectrum). In reflectron mode, ions of the same *m/z* ratio with differing kinetic energies are focused by the reflectron onto the reflectron detector (dark grey line), producing isotopically resolved signals (lower mass spectrum). For $MS^2$ experiments ions can be separated at the ion gate, after passing a first mass analyzer, and fragmented by e.g. a collision gas in the collision cell. Product ions are than separated in a second mass analyzer and detected by linear or reflectron mode.

In order to analyze biological samples, either intact tissues/cells (direct profiling), extracts of these or biofluids are placed on a sample carrier and are mixed with a dissolved matrix. During evaporation of the matrix solvent the matrix and sample co-crystallize and a dried-droplet sample spot results which is subsequently introduced into the mass spectrometer under a high vacuum. Matrix substances show strong optical absorption in ultraviolet (UV) or infrared wavelength ranges for excitement by corresponding pulsed lasers. Most matrices are acidic, however, they are often mixed with strong acids, such as trifluoroacetic acid (TFA) as an additional proton donator and to obtain a good crystallization (Hillenkamp & Peter-Katalinic 2007). The excited matrix molecules induce desorption of co-crystallized analyte and matrix molecules into the gas phase. Ionization of the analyte molecules is postulated to happen at least through two models: (1) the thermal model, high temperatures during laser irradiation facilitate proton transfer between the liquid matrix and the analyte (Lu et al. 2015), and the (2) lucky survivor model (Karas et al. 2000; Karas & Krüger 2003), which postulates ion formation by charge separation during fragmentation of analyte/matrix clusters. Due to the soft ionization, MALDI mainly produces singly charged ions $[M+H]^+$ (Karas et al. 2000), however, salt adduct ions can be observed which lead to increased ion masses ($[M+Na]^+$, + *m/z* 23; $[M+K]^+$, + *m/z* 39). Ionized analyte molecules are accelerated by an electric field, from the source into the TOF mass analyzer (Fig. 1.3). The TOF mass analyzer is a vacuum tube in which the accelerated ions can drift freely until they reach the detector or the reflectron. The TOF between the moment of acceleration and the detector of an ion is dependent on the *m/z* ratio and can therefore be used to separate ions. Due to the predominantly single charged ions produced by MALDI-TOF MS, it is possible to directly infer the molecular mass of an ion through their detected *m/z* ratio (Fig. 1.3).

Modern MALDI-TOF instruments have two measurement modes with separate detectors. The first mode is called linear mode. In linear mode ions drift through the TOF analyzer and hit the detector at the end of the flight tube. This mode generates ion signals with a relatively low resolution but is very sensitive especially in higher mass ranges larger than *m/z* 6000. Recorded ion signals in linear mass spectra usually show a Gaussian shaped “peak” without resolving isotopic patterns (Fig. 1.3). Deduced masses are given as average masses, since all possible isotopes are cumulated in a single signal. The second mode utilizes a second detector and an ion reflector, hence called reflectron mode. This mode enhances resolution via compensating small distribution-related differences of transmitted kinetic energy during acceleration in the ion source, for ions of the same *m/z* ratio, by reversing the ion flight direction through an electric field ion reflector (reflectron). Ions of the same *m/z* ratio but different kinetic energies penetrate the field of the ion reflector in an energy dependent manner, with higher energetic ions flying deeper into the field. Thus, ions are reflected at different depth leading to a nearly simultaneous impact at the second detector, which is located on the opposite site of the reflector. Ultimately, this leads to an improved ion signal resolution capable of resolving isotopic patterns. Deduced masses of ions detected with resolved isotopic patterns are given as monoisotopic mass ($[M+H]^+$), which is composed only of the most abundant isotopes (Fig. 1.3). All masses are given as monoisotopic masses in this thesis.

Common fragmentation methods applied in MALDI-TOF MS to elucidate the chemical structure of analyte ions are: laser induced dissociation (Macht et al. 2004) and connected methods such as ISD and PSD, in which the laser transmitted energy leads to fragmentation of the ion of interest in the source (ISD; Brown & Lennon 1995; Sellami et al. 2012) or after the source (PSD; Spengler et al. 1992; Kaufmann et al. 1994), and CID, where the precursor ions are fragmented by collision with an applied chemical inert gas such as argon or nitrogen (Levsen & Schwarz 1976; Mitchell Wells & McLuckey 2005).

MALDI-TOF MS offers some advantages over other MS techniques when analyzing minute volume samples such as single cells. Due to its high salt and buffer tolerance as well as its overall sensitivity, it is not only possible to directly interrogate the chemical profile of a given sample but also to obtain structural information of single analytes of interest from this sample, without the need for precedent sample fractionation and desalting (Li, Garden, et al. 2000; Hummon et al. 2006; Ong et al. 2015a). Furthermore, MALDI offers a straight forward sample preparation which is very time efficient and thus enables the rapid preparation of multiple samples in a single batch. Moreover, only small amounts of the chosen MALDI matrix are needed to allow a successful measurement, thus limiting dilution of the sample and enabling even detection of low concentrated analytes (Li, Garden, et al. 2000; Hummon et al. 2006; Ong et al. 2015a). Another advantage is the low sample consumption of MALDI in combination with the temporal disconnection of possible precedent chromatographic separation techniques, which allows not only the storage of prepared samples for longer periods of time, but also the repeated analysis of a given sample in different measuring modes and mass ranges as well as high sample throughputs (Li, Garden, et al. 2000; Hummon et al. 2006; Ong et al. 2015a).

## Neuropeptidomics

The identification and characterization of neuropeptides used to be a time and sample consuming complex undertaking. Neuropeptides had to be separated from the sample matrix, concentrated and often be subjected to further chemical processing in order to elucidate their primary structure by Edman degradation (Niall 1973). The identification and characterization of a single peptide could gulp up regularly thousands of individual animals to generate enough material for sequence analysis. In contrast to this, modern MS based neuropeptidomics are capable of detecting and characterizing many neuropeptides from small samples such as a single cell. The suffix "-omics" labels biological sub disciplines which focus on the global analysis of similar individual elements such as genes (genomics), metabolites (metabolomics), mRNA (transcriptomics), or the proteome (proteomics) of a single cell, cell cluster, organ, or organism at a defined point of time. Neuropeptidomics therefore, aims to unravel the complement of neuropeptides from a cell, tissue or extract of the nervous system (Yin et al. 2011; Lee 2016). Neuropeptidomics use MS based methods for the identification and sequence analysis of mature neuropeptides often in combination with genomic and/or transcriptomic data.

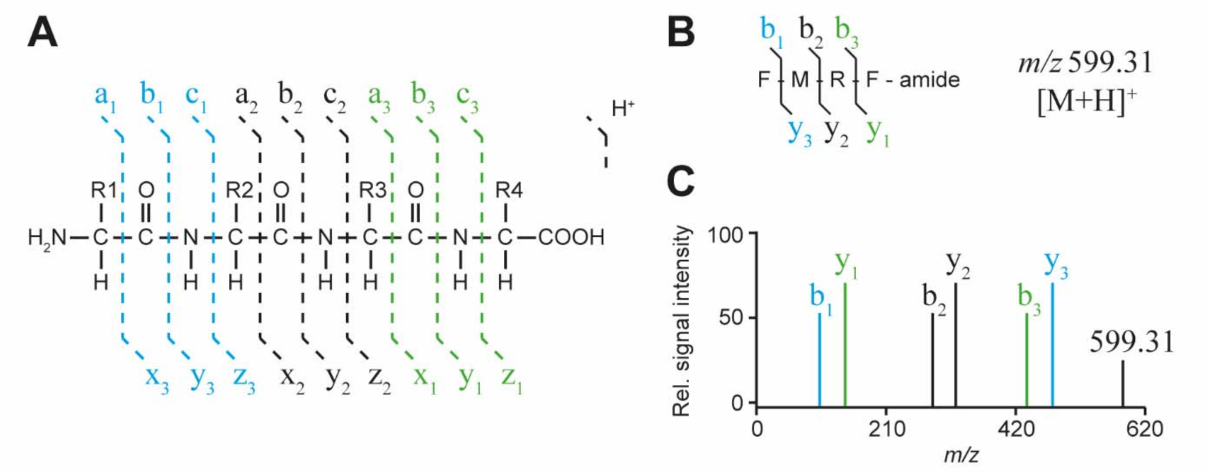

**Figure 1.4 Hypothetical fragmentation of the peptide FMRFamide by MS².** (**A**) Nomenclature of peptide fragments after Roepstorff & Fohlman, 1984. (**B**) Exemplary b- and y- fragments of the peptide FMRFamide and monoisotopic mass of the intact peptide. (**C**) Hypothetical MS$^2$ mass spectrum of the fragmented FMRFamdie peptide.

Neuropeptides consist of amino acids interconnected by peptide bonds, which can be fragmented during MS² experiments. Fragmentation can be observed at various positions of the peptide bond and even at amino acid side chains, depending on the energy and fragmentation method (Fig. 1.4). The resulting product ions can be used to deduce the amino acid sequence of an analyzed peptide. Sequencing by MS mainly rests on product ions generated by continuous fragmentation of peptide-bonds, giving rise to b- and y-fragments, whereas other fragmentation products such as short immonium ions and internal product ions, which derive from multiple backbone fragmentation, can serve as additional sequence confirmation (Fig. 1.4 A). The mass difference between two detected adjacent product ions of the same series (e.g.: b1-b2) allows to conclude the appropriate amino acid (Fig. 1.4 B, C). Often, resulting product ion/MS² mass spectra provide sufficient product ion information to allow *de novo* sequencing of the analyzed peptide by hand or appropriate computer algorithms. Furthermore, modern neuropeptidomics utilize different bioinformatic approaches for sequence elucidation and identification which involve *in silico* prediction of product ions from amino acid sequences, *in* *silico* prediction of cleavage sites and cleavage products from identified neuropeptide genes, databank driven comparative sequence identification, and cross validation and identification of sequences between mass spectrometric data and genomic and/or transcriptomic data sets.

## Single cell mass spectrometry (SCMS)

Cellular variability and heterogeneity is a necessity for individual biological and behavioral traits of organisms and targeted SCMS offers the possibility to elucidate how individual cells contribute to physiology and behavior, as well as pathologies and diseases, in multicellular organisms by determining their chemical profiles (e.g. Ong et al. 2015a). However, the analysis of single cells is still challenging due to the fragile nature of single cells, the low sample volume and the highly complex chemical composition. MS-based technologies are often the method of choice in small volume sample bioanalytical analysis because of a wide scope of detectable analyte classes, low sample consumption, low detection levels and combinability to numerous separation and concentration methods. Furthermore, MS allows not only identification but also structural characterization, quantitation, targeted and even untargeted analysis of given single cell chemical features. Chemical analysis can be focused on intracellular or secreted extracellular analytes, since the study at hand focuses on whole cell analyses, mostly methods dedicated to such are introduced in more detail.

The first step in single cell analysis is the identification of a cell of interest. Various approaches exist, depending on the sampled organism and the experimental setup. For identification the shape, color or position of a cell can be sufficient for a clear identification and subsequent isolation (Neupert & Predel 2005; Rubakhin et al. 2011). The uptake or intracellular injection of fluorescent neuronal markers (El Filali et al. 2003; Neupert & Predel 2005), the expression of fluorescent gene reporters in genetic model organisms (Neupert et al. 2007), CRISPR/Cas9 mediated gene tagging in non-model organisms or immunolabeling (Neupert et al. 2012) can be used *in vivo* or *ex vivo* to identify desired cell clusters or single cells and help to guide sample isolation.

Cell identification is followed by the isolation or extraction of the desired sample which can be achieved by various techniques. Manual microdissection with sharp needles and micro scissors of desired cell bodies is a fast and robust method and enables documentation and spatial localization, but relies heavily on an experienced experimentalist to prevent rapture-induced loss of analytes (Neupert & Predel 2005; Rubakhin & Sweedler 2007). Other recent developed solutions try to circumvent such bias by using computer assisted laser capture dissection and laser trapping for the isolation of cells from thin tissue sections (Espina et al. 2006; Park et al. 2016). A very elegant method is the direct sampling of cytoplasm from the cell body via patch-clamp capillaries, which enables pl volume samples with only limited danger of potential contaminations from the cellular matrix (Aerts et al. 2014). Often enzymatic treatments with collagenases or dispases for tissue dissociation are used to generate large amounts of single cells. When used in conjunction with fluorescent labeling techniques, this approach can be used to visually discriminate between cells of interest, and even automated cell sorting by flow cytometry is possible (Yew et al. 2009). Nevertheless, a change of environmental conditions, such as temperature or extracellular matrix, by enzymes, culture mediums or lasers can lead to significant changes in intracellular compositions of single cells and has to be evaluated with great caution (Nemes et al. 2012; Qi et al. 2017).

Since MALDI-TOF was the main analytical method of this study, therefore, SCMS approaches utilizing MALDI are discussed in more detail, with a few examples covering electrospray ionization (ESI), even though a wide array of different MS approaches has been subjected to SCMS (for review see Ong et al. 2015a; Armbrecht & Dittrich 2017). A frequently used method to analyze single neuron somata is direct SCMS by MALDI-TOF MS, which has been used to detect neuropeptides from single neurons with varying size and organismic origin such as rats (Rubakhin & Sweedler 2007; Ong et al. 2015), the great pond snail *Lymnaea* (Li et al. 1994; Jiménez et al. 1998; El Filali et al. 2003), the Californian sea hare *Aplysia californica* (Garden et al. 1996; Li et al. 1999; Li, Romanova, et al. 2000) and numerous insects (*Periplaneta americana*: Neupert & Predel 2005; Neupert & Gundel 2007; Neupert et al. 2009; Neupert et al. 2010; *D. melanogaster*: Neupert et al. 2007; *M. sexta*: Neupert, Huetteroth, et al. 2009*;* *Rhodnius prolixus*: Neupert et al. 2010; *L. migratoria*: Redeker et al. 2017). Furthermore, quantification with direct MALDI-TOF MS of neuropeptides from single *A. californica* neurons has been reported, using isotopic labeling and internal standards combined (Rubakhin & Sweedler 2008). However, to date no direct MALDI-TOF SCMS approach has been reported for the detection of small molecule neuroactive substances, like biogenic monoamines and others.

MALDI mass spectrometric imaging (MSI) represents another MALDI driven approach to investigate single cells. In MALDI MSI, a thin tissue section or a mixture of single cells is placed on a sample carrier, a stainless steel plate or a conductive glass slide, and registered by a scanner or a high resolution camera. The sample is then placed in the MS source and analyzed via MALDI in a continuous step-wise manner, whereby a mass spectrum is recorded at each laser position on the sample. Finally, by combining the registered photo and the localized mass spectra it is possible to obtain a spatial representation of a given mass on the sample, in a detection dependent and therefore semi quantitative manner. MALDI MSI with coarse spatial resolution (50-25 µm) has been used by studies focusing on lipids and neuropeptides from cultured single cells such as large *A. californica* neurons (Rubakhin et al. 2003), single mice peritonal macrophages (Yang et al. 2018) or single human breast cancer cells (Wang et al. 2016).

By using new developed ion source configurations (Koestler et al. 2008; Kompauer et al. 2016), laser optics (Römpp et al. 2010) and sophisticated sample preparation methods (Svatoš & Ibáñez 2014) the lateral resolution can be lowered to 10 µm or even below and thereby enable SCMS analysis directly from tissue sections. Moreover, these high resolution methods can be used to analyze lipids, peptides and metabolites at the subcellular level in unicellular organisms like *Paramecium caudatum* (Kompauer et al. 2016) or even three dimensional subcellular SCMS of early stage *Danio rerio* embryos (Dueñas et al. 2017).

Prior to SCMS, preceding separation and concentration methods, such as capillary electrophoresis (CE), nano liquid chromatography (nanoLC) or microfluidic devices, can be used expand the range of detectable analytes and quantification via extracted migration profiles can be achieved from low volume samples such as single cells. Even though the combination of CE-MALDI MS has been used to study a variety of different samples (Zuberovic et al. 2009; Pourhaghighi et al. 2011; Ye et al. 2015; Týčová et al. 2017), it is surprising that only few studies focus on CE-MALDI SCMS. Rubakhin and colleagues used CE-MALDI-TOF MS to analyze neuropeptide releasates from single *A. californica* neurons (Rubakhin et al. 2001; Fan et al. 2013), while another study focused on the detection of neuropeptides from single *Aplysia* neurons via a combination of CE-MALDI-TOF MS and radionuclide detection (Page et al. 2002).

A more frequently used combinatorial method is CE-ESI MS, which has been used successfully by different groups to detect not only proteins and neuropeptides but also small molecule metabolites, such as neuroactive substances, from single cells. Cao and Moini studied the α-

and β-chains of hemoglobin by subjecting a single human erythrocyte to CE-ESI MS (Cao & Moini 1999). Other studies focused on the metabolomic analysis of different single *A. californica* neurons and could detect >300 single chemical features including acetylcholine (ACh), DA and 5-HT (Lapainis et al. 2009; Nemes et al. 2011). Furthermore, CE-ESI SCMS guided comparative metabolomics with multivariate statistics has been used to elucidate small molecules that potentially affect blastomere cell fate in the 16-cell stage of *Xenopus leavis* (Onjiko et al. 2015). Proteomic approaches can be combined with CE-ESI SCMS and led recently to the identification of a total of 1709 protein groups from three different blastomeres of the 16-cell stadium of *X. leavis* (Lombard-Banek et al. 2016). Finally, CE- laser-induced fluorescence detection (LIF) and – native laser-induced fluorescence detection (LINF) have been used to analyze neuroactive substances, peptide and proteins of single cells with very low LODs (sub nM range; Kim et al. 2002; Lapainis et al. 2007; Cecala et al. 2012).

## Identification, localization and quantification of OA/TA and other biogenic monoamines in insect nervous tissues

In order to study biogenic monoamine function in behavior and physiology a wide variety of bioanalytical methods have been applied and developed to identify, locate and quantify these small neuroactive substances in the insect CNS. Localization of biogenic monoamines such as OA and TA in insects has been studied by means of immunohistochemistry directed against synthesizing enzymes or the molecule of interest directly (e.g. OA/TA, Monastirioti et al. 1995; Busch et al. 2009; Selcho et al. 2014). In genetic model organisms, such as *D. melanogaster* and *T. castaneum,* genetic labeling methods can be used to label potentially monoaminergic neurons, by targeting synthesizing enzyme genes (Busch et al. 2009; Selcho et al. 2014). Even though antibody guided immunohistochemistry is a reliable method, antibodies can cross react with alternate epitopes due to similar chemical structures, e.g. OA and TA, while stainings or labeling techniques focusing on synthesizing enzymes only give indirect evidence of the molecule of interest.

A common method for the identification and quantification of biogenic monoamines from biological samples, such as nervous tissue or body fluids, is the separation and purification by high performance liquid chromatography (HPLC) or CE coupled to electrochemical (ECD), LIF, or MS detection (Shin et al. 2018). While HPLC systems have been used to quantify biogenic monoamines in pooled samples of whole brains (Hardie & Hirsh 2006; Chen et al.

2013), CE has proven to be a more sensitive separation method with very low sample consumption (nl range). The combination of micellar elektrokinetic capillary chromatography (MEKC), which represents a modification of conventional CE by adding a surfactant as pseudo-stationary phase (micelles, e.g. SDS), amperometric ECD and synthetic standards led to the detection of 14 biogenic monoamines and their metabolites in single adult *D. melanogaster* head homogenates (Ream et al. 2003; Paxon et al. 2005). Furthermore, in a more recent study MEKC-ECD was used to quantify 24 metabolites and biogenic monoamines, such as TA, OA, DA and 5-HT from single *D. melanogaster* head homogenates (Kuklinski et al. 2010). A more recent study from the group of B. J. Venton combined CE with fast-scan cyclic voltammetry (CE-FSCV), which has the advantage of selective identification by recording analyte specific oxidation voltammograms, and quantified a total of four biogenic monoamines from single *Drosophila* brain homogenates from larvae, pupa and adults (Denno et al. 2016). Another promising method is the detection and quantification of amino acids and their corresponding neuroactive substances via LINF or flourescamine supported LIF coupled to CE (for review see Tseng et al. 2010). Piyankarage and colleagues, for example, described the detection and quantification of 13 amino acids from heamolymph samples of *D. melanogaster* larvae using CE-LIF (Piyankarage et al. 2008; Piyankarage et al. 2010). Furthermore, the detection of biogenic monoamines has been reported for pooled head homogenates of *D. melanogaster*, by CE coupled to MS (Phan et al. 2013).

Even tools for the real-time measurement of biogenic monoamine exocytosis and re-uptake *in vivo* have been developed and applied in vertebrates and invertebrates and often utilize carbon-fiber mircoelectrodes (CFME) in combination with ECD such as FSCV and amperometry (Shin et al. 2018). In general, these methods measure the change in current (nano amps) during oxidation and reduction of the molecule of interest at the CFME. Makos and colleagues used CFME-FSCV to analyze monoamine reuptake of exogenously applied DA in the *D. melanogaster* protocerebral anterior medial brain region and compared observed reuptake between wild type flies and a genetic driver line with a defective DA transporter gene (Makos et al. 2009). CFME-FSCV has also been used in conjunction with channelrhodopsin-2 mediated, neuron specific stimulation in order to analyze release and clearance of DA in the larval VNC of Drosophila (Borue et al. 2009; Vickrey et al. 2009). Finally, Majdi and colleagues could show, in a pioneering experiment, the successful measurement of optogenetically controlled OA release from single nerve varicosities of the body wall muscle in Drosophila larva (Majdi et al. 2015).

A quiet recently developed method is the endogenous imaging of biogenic monoamines and other neuroactive substances via selective fluorescent sensors, which can either be protein based and directly synthesized in model organisms or exogenously applied (for review see Liang et al. 2015). Some biosensors have been developed in the last years, targeting either glutamate or GABA, with varying sensitivity, from low nM to µM ranges and only two were tested *in vivo*; in *Caenorhabditis elegans* (Marvin et al. 2013) and mice (Okubo et al. 2010). However, Patriarchi and colleagues developed just recently an intensity-based genetically encoded DA sensor, dLight1, for endogenous imaging of DA in mice, with high spatiotemporal resolution and low LODs (nM range, switch on ~10 ms; Patriarchi et al. 2018). This was possible by cloning a circularly permuted GFP, which is also used in GcAMP6 (Chen et al. 2013), to a cytosolic loop of a human DA receptor. Furthermore, by using the same strategy they were able to produce similar constructs for the detection of other biogenic monoamines and neuropeptides alike. This potentially groundbreaking development will allow the direct imaging of releasing events of neuroactive substances in intact nervous systems.

A similar approach is the implantation of so called cell-based neurotransmitter fluorescent engineered reporters (CNiFERs) *in vivo*, which are altered HEK 293 cells. These cells express selective GPCRs in combination with fluorescence resonance energy transfer (FRET) based reporter system. Furthermore, they exhibit high selectivity and sensitivity, in the nM range, and their application has been shown to detect DA and NAD *in vivo* in mice (Muller et al. 2014). However, the use of CNiFERs is limited to larger organisms since the implanted cells have a size of about 50 µm, which is equivalent to a whole *Drosophila* antennal lobe.

Ultimately, MSI via MALDI or desorption electrospray ionization (DESI) has been used to investigate the localization and quantities of biogenic monoamines and other neuroactive small molecules from nervous tissue sections. DESI MS is a recently developed matrix free ionization technique which uses a capillary ejecting solvent via electrospray directly on the sample tissue, which is mounted on a moveable 3D sample stage (Ifa et al. 2007). By the repeated impact of fresh solvent droplets, secondary analyte containing droplets are ejected from the sample, ionized and ultimately sampled by the mass spectrometer through an elongated inlet capillary or sniffer positioned close to the sample surface. While modern MALDI MSI combines low µm-spatial resolution with a high degree of sensitivity and selectivity, analysis of small molecule neuroactive substacnes like biogenic monoamines by MALDI-TOF MS in general is a challenging task since most of these substances show poor ionization characteristics, fragmentation during ionization, overlaying or suppression by matrix clusters, and problematic mass isomers, e.g. OA and DA, which need further analysis like $MS^2$ for proper identification and detection. The development of new matrices and chemical derivatization compounds and procedures tackle these problems. Manier and colleagues used 4-hydroxy-3-methoxycinnamaldehyde (CA) as a targeted derivatization agent for metabolites and neuroactive substances containing amine moeties and reported the successful simultaneous detection of nine amino acids and neuroactive substances from pig brain and adrenal gland tissue sections (Manier et al. 2014). Another promising approach is the usage of pyrylium salts as derivatization agent and matrix alike, leading to the simultaneous detection and quantification of eleven neuroactive substacnes (seven amines) and their metabolites in rat brain sections (Shariatgorji et al. 2014; Shariatgorji et al. 2015). Pyrylium salts, however, are very expensive and difficult to obtain on the open market, in contrast to cheap derivatization agents like CA.

Two recent studies used DESI MS to detect and quantify GABA, glutamate and DA from rat brain tissue sections (Bergman et al. 2016; Fernandes et al. 2016). The detection of small molecule neuroactive substances by DESI can also be improved by targeted chemical derivatization, which has been shown for nine small molecule neuroactive substances, including DA, 5-HT and glutamate (Shariatgorji et al. 2016). The DESI ionization process is very soft and can be compared to normal ESI, bypassing the laser induced fragmentation of small molecule neuroactive substances and their metabolites observed during MALDI ionization. However, modern DESI systems show a very coarse spatial resolution, between 200-150 µm (Shariatgorji et al. 2016; Bergman et al. 2016), compared to low µm resolution (ca. 50-10µm) MALDI-TOF systems (Shariatgorji et al. 2014; Spengler 2015), which is a prerequisite to analyze insect nervous systems.

## Aim of this study

The main aim of this thesis is the development of a MALDI-TOF MS based method for the routine detection, identification and quantification of biogenic monoamines from single dissected neuron somata of intact insect nervous systems. The focus of the thesis lies on the insect OAergic/TAergic system, which is seen homologous to the vertebrate noradrenalin/adrenalin system. A prerequisite was that the newly developed method should be as simple, fast, cost effective and safe as comparable direct profiling MALDI-TOF SCMS approaches and work, if possible, without requiring prior sample fractionation. Moreover, due to the possible co-localization of biogenic monoamines and neuropeptides in neurons, the simultaneous detection of both substance classes from the same sample using such an approach should be investigated. The method should be established using single cells of the genetic model organism *D. melanogaster*, to enable a stable identification of single cells or cell clusters for dissection and have the possibility to alter neuroactive substance expression by using the large genetic *Drosophila* toolbox and also benefit from the extensive research on neuroactive substance expression patterns and neuronal circuits driving behavior in this model organism. Assuming a successful development and establishment, the protocol should be used to analyze expression patterns of OA/TA and/or neuropeptides in identified subsets of neurons, as well as analyze potential dynamic quantities of somatic OA/TA titers between cell clusters, sex, age, and behavioral states in *D. melanogaster* and other insects.

The thesis at hand is organized in five chapters (chapter 1 Introduction):

Chapter 2 is dedicated to the development of a MALDI-TOF SCMS protocol for the detection and quantification of OA and TA from single genetically labeled *D. melanogaster* neuron somata using on-plate chemical derivatizations, isotopically labeled internal standards and an advanced sample preparation.

Chapter 3 is dedicated to the analysis of changing somatic OA titers from gnathal *D. melanogaster* VMlb neurons in social driven male aggression using the developed MALDI-TOF SCMS approach.

Chapter 4 is dedicated to a collaborative study, in which the developed MALDI-TOF MS approach was used to identify somatic OA and TA from intracellular recorded desDUM neurons of the Indian stick insect *C. morosus*.

Chapter 5 is dedicated to the effort of creating a map of neuropeptidergic cells and their repertoire of neuroactive substances in adult *D. melanogaster* using conventional MALDI-TOF SCMS.

# 2. Development of a MALDI-TOF MS based workflow for the identification and quantification of octopamine and tyramine from single identified *D. melanogaster* neurons

The results of this chapter are already published in the following peer-reviewed article: Diesner, M; Neupert, S. *Quantification of Biogenic Amines from Individual GFP-Labeled Drosophila Cells by MALDI-TOF Mass Spectrometry.* Analytical chemistry, 2018, 90, 13, 8035-8043, DOI: 10.1021/acs.analchem.8b00961.

The authors contributions are as followed: MD and SN conceptualized experiments, MD and SN performed experiments (SN performed DPD VMlb experiments and dissected 9 samples from the VMlb 60 min data set, all other samples MD). MD analyzed the data, prepared figures and tables. MD and SN wrote the manuscript, SN funding. Text passages and figures of this chapter are taken or modified from the published article.

Parts of this chapter are adapted/modified/copied with permission from: Quantification of Biogenic Amines from Individual GFP-Labeled Drosophila Cells by MALDI-TOF Mass Spectrometry, Diesner M, Neupert S, Analytical chemistry, 2018, 90, 13, 8035-8043. Copyright 2018 American Chemical Society

A license for the adaptation/modification/copying was given to Max Diesner.

## 2.1 Introduction

Neuroactive substances such as biogenic monoamines and neuropeptides are central players in shaping physiology and behavioral patterns in metazoan organisms. These substances are produced in specific subpopulations of neurons throughout the CNS, however, they can be co-localized in specific neurons. In order to understand and investigate the distribution, quantities and functional effects of these substances in well-defined neuronal circuits and underlying single neurons, robust and highly sensitive measurement tools are needed. SCMS has become a key technology to interrogate the molecular profile of isolated cell samples, including neuroactive substances such as peptides, proteins, amino acids, and biogenic monoamines (Romanova et al. 2014; Qi et al. 2018; Zhang & Vertes 2018). The detection and quantification of biogenic amines from biological samples has been studied with various analytical techniques such as CE coupled to FSCV (Denno et al. 2016; Pyakurel et al. 2016), HPLC coupled to ECD (Hardie & Hirsh 2006; Chen et al. 2013), CE coupled to ESI-TOF MS (Aerts et al. 2014; Onjiko et al. 2015) and CE coupled to LIF or LINF (Kim et al. 2002; Lapainis et al. 2007; Cecala et al. 2012) even up to the level of single cells.

While the detection of neuropeptides using MALDI-TOF MS from single isolated neurons is a commonly used tool in neurobiology (e.g. Neupert et al. 2007; Rubakhin et al. 2011; Ong et al. 2015b), the analysis of small molecule neuroactive substances, such as biogenic monoamines, from single cells using MALDI-TOF MS is still challenging from an analytical point of view. The detection of these molecules by MALDI-TOF MS is limited due to the generation of intense matrix signals in the corresponding mass ranges of interest, in-source analyte instability, insufficient molecule ionization, or putative ion suppression events. Various studies focused on overcoming these persisting hurdles by developing chemical derivatization protocols (Chacon et al. 2011; Manier et al. 2014; Toue et al. 2014), alternative matrices (Shanta et al. 2012; Shariatgorji et al. 2012; Shariatgorji et al. 2014) and sample preparation protocols (Persike & Karas 2009) to increase ion stability and molecule ionization for an improved MALDI-TOF MS detection of small molecule substances. Furthermore, different groups reported the successful quantification of small molecules from dried droplet samples using MALDI-TOF MS in combination with internal standard application and an improved matrix preparation (Persike & Karas 2009; Persike et al. 2010; Chaptal et al. 2017).

Neuroactive substances, such as biogenic monoamines and neuropeptides, can be co-localized in specific neurons, but a method based on MALDI-TOF MS to identify and map single neurons regarding their aminergic compositions within an intact brain is still lacking. Therefore, the main goal of the thesis at hand was to develop a MALDI-TOF MS based method for the detection and quantification of biogenic monoamines from single cell samples. Furthermore, the developed protocol should also allow the detection of neuropeptides and related precursor peptides from the same sample.

Here, I focused on single neurons of the OA/TA system of the genetic model animal *D. melanogaster*, as it offers the possibility to use promoter-specific GAL4 driver lines to express fluorescent gene reporters in defined subsets of single cells or cell populations in the CNS. In *D. melanogaster* and other invertebrates, the biogenic monoamine OA, equivalent to norepinephrine in vertebrates, is synthesized in a two-step process; Tyr is decarboxylated by Tdc2 into TA (Cole *et al.*, 2005), which is followed by the hydroxylation of TA into OA by Tβh (see chapter 1, Fig. 1.1; Livingstone & Tempel 1983; Monastirioti et al. 1996). The functions and localizations of OA and TA in Drosophila have been studied extensively, mainly using genetic tools and immunohistochemistry (Python & Stocker 2002; Cole et al. 2005; Sinakevitch & Strausfeld 2006; Vömel & Wegener 2008; Busch et al. 2009; Selcho et al. 2012; Selcho et al. 2014); and is described in more detail in the general introduction (see chapter 1) of this thesis.

The detection and quantification of biogenic amines such as OA and TA from *D. melanogaster* tissue samples has been the focus of several studies using mainly HPLC or CE coupled to FSCV (Denno et al. 2016) or ECD (Ream et al. 2003; Paxon et al. 2005; Hardie & Hirsh 2006; Chen et al. 2013). However, all of these studies used whole brains in combination with sample homogenization which renders identification and quantification of biogenic amines from a single cell as well as unambiguous cell localization in an intact brain impossible. Moreover, when analyzing whole brains, or larger tissue parts, potential changes in biogenic monoamine concentration in single soma or cell populations could be concealed due to a potential upregulation or release in other neurons, reuptake by glia cells and inactivation mechanisms leading to a compensatory effect in the sample (Zhou et al. 2008).

The present study assessed the performance of two commercially available derivatization agents for enhancing MS sensitivity and stability of biogenic monoamines and investigated detection and quantification limits by combining on plate derivatization with isotopically labeled internal standards. Furthermore, fluorescence-guided microdissections in combination with a *Tdc2-GAL4* driver line crossed to a UAS-*mCD8::GFP* reporter line was used for a reliable identification and isolation of TA and OA synthesizing neurons. Moreover, the developed protocol was used to compare concentrations of OA and TA from individual isolated VMlb neurons of the GNG between females and males, investigated temperature-dependent changes in somatic OA/TA concentrations, and determined OA/TA titer differences in two cell populations at the single-cell level. Finally, to demonstrate that the application of the developed protocol is not interfering with the detection of neuropeptides, single neuropeptidergic *D. melanogaster* neurons were analyzed. The developed protocol for the characterization and quantification of biogenic monoamines of individual *D. melanogaster* neurons will help to foster our understanding of neuromodulation, plasticity and single neuron function in discrete neuronal circuits in the CNS.

## 2.2 Materials and Methods

### *Chemicals*

All used chemicals were purchased from SIGMA-Aldrich (Steinheim, Germany), if not stated otherwise.

### *Synthetic solutions*

Stock solutions of OA-hydrochloride, TA-hydrochloride, (±)-p-octopamine-α,β,β-d3 hydrochloride (OA[*d3*]), (CDN Isotopes, Pointe-Claire, Canada) and 2-(4-hydroxyphenyl)ethyl-1,1,2,2-d4-amine hydrochloride (TA[*d4*]; CDN Isotopes) were prepared in 50% MeOH/TraceSELECT® water at a concentration of 10 nmol/µl, stored at 4°C in darkness and were used to prepare dilution series. Stock solutions of synthetic biogenic amines were replaced after two months, dilution series after three weeks.

### *Derivatization reagents*

4-hydroxy-3-methoxycinnamaldehyde (CA) was prepared in 100% MeOH at a concentration of 23 mg/ml, as described by Manier and colleagues (Manier et al. 2014), and centrifuged at 13000 rpm at 4°C for 10 min. 5 µl of the supernatant was diluted in 150 µl 50% MeOH/TraceSELECT® water at a concentration of 0.76 mg/ml. According to Gatti and colleagues (Gatti et al. 2012), 2,5-dimethyl-1H-pyrrole-3,4-dicarbaldehyde (DPD) was dissolved in 50% MeOH/TraceSELECT® water at a concentration of 0.415 mg/ml. The mixture was vortexed for 30 s and sonicated for 2 min in ice water. Both solutions were centrifuged at 15000 rpm for 10 min at 4°C and stored at 4°C and darkness upon usage. Both derivatization solution were prepared fresh daily.

### *Fly strains*

Adult flies ≥ 5 days old of both sexes were used. Flies were raised on standard cornmeal, molasses, yeast, agar medium on a 12 h/12 h light-dark cycle at 25°C and 60% humidity. The following fly strains were used: *Tdc2-GAL4* (Cole et al. 2005); UAS-*mCD8::GFP* (Burke et al. 2012); *Tßh*$^{nM18}$*-GAL4* (Monastirioti et al. 1996; kindly provided by Manuela Ruppert, University Cologne); *c929-Gal4* (Hewes et al. 2003; kindly provided by Christian Wegener, University Würzburg); *Tßh*$^{nM18}$*,FM7; Tdc2-GAL4, Tdc2-GAL4* (*Tßh*$^{nM18}$*/Tdc2-GAL4*, this work). For visualization GAL4 lines were crossed to UAS-*mCD8::GFP*.

### *Quantification and standard curve calculation*

Preparation of dried droplet samples was modified from Persike and colleagues (Persike et al. 2010) and adapted for small volume samples. To calculate standard curves, either 300 nl or 18.4 nl of synthetic OA, TA, or a mixture of both, was applied onto a MALDI sample plate in a concentration range from 1000 to 0.1 fmol/µl. For standard curves measured in parent mode MS$^2$ (pMS$^2$), only samples in a range of 100 to 1 fmol/µl were analyzed. After applied synthetic solutions were allowed to air-dry, sample spots were covered with an equal volume (300/18.4 nl) of OA(*d3*), TA(*d4*), or a mixture of both with a constant concentration of 100 fmol/µl. After letting the spot air-drying a second time, each spot was covered with either 126 nl or 9.2 nl of CA or DPD. The resulting spot was allowed to air-dry again and ultimately covered with 300 nl or 18.4 nl α–cyano-4-hydroxycinnamic acid (CHCA) and dried under a constant airflow. CHCA was prepared fresh daily in 80% MeOH/TraceSELECT® water at a concentration of 1.43 mg/ml. The resulting mixture was centrifuged for 10 min at 15.000 rpm at 4 °C and stored at 4 °C and darkness until usage.

### *Single cell dissection*

Flies were either immobilized for 60 min or 15 min on ice, or directly removed from the vials using forceps. The brain was removed in dissection buffer (NaCl 126mM, KCl 5.4mM,

$NaH_2PO_4$ 0.17mM, $KH_2PO_4$ 0.22mM, pH 7.4) under an epifluorescence stereomicroscope. For single-cell dissections, brain samples were transferred to a fresh drop of ice cold dissection buffer containing 33% glycerol. To access single somata, the ganglionic sheath was carefully opened close to the position of the cell of interest using ultra-fine scissors, without changing the neuroarchitecture of the brain. Before the removal of the uncovered cell soma a pulled glass capillary with a tapered tip was connected to a rubber-tube and fitted to a mouthpiece. Then, the tip of the glass capillary was positioned over the cell soma of interest. By gently applying negative air pressure on the capillary by inhaling, the cell soma was removed from the tissue and loaded into the glass capillary. Subsequently, the isolated cell soma was transferred to a stainless steel MALDI-TOF target plate and released by applying gentle air pressure. Excessive dissection saline was removed using the same glass capillary and the remaining soma was left to dry at room temperature (rt). Residual glycerol surrounding the isolated soma was washed off with 50% MeOH/TraceSELECT® water. Washing was performed multiple times with a fresh glass capillary until the glycerol was completely removed. However, the placed cell soma was left uncovered by the washing solution to prevent a possible loss of analytes. Only one neuron soma was isolated from a single brain sample. Furthermore, a single dissection block, processing multiple brains, did not exceed one hour.

### *Single cell sample preparation for quantitative MALDI-TOF MS*

Dissected single cell samples were covered with 18.4 nl of an equimolar mixture of OA(*d3*) and TA(*d4*) with a concentration of 100 fmol/µl. After air-drying, 9.2 nl of CA or DPD were added to the sample spots and left to air-dry. Finally, the sample spots were covered with 18.4 nl of CHCA and dried under a constant stream of air. All solutions were applied using a pulled glass capillary fitted in a nanoliter micro injector (nanoliter 2000, World Precision Instruments, FL, USA). Between each application step, the remaining solution in the glass capillary was removed and the capillary rinsed two-times with 100% TraceSELECT® water, 50% MeOH/TraceSELECT® water followed by 100% MeOH before air-drying.

### *MALDI-TOF MS*

Mass spectra were acquired using an UltrafleXtreme MALDI-TOF/TOF mass spectrometer (Bruker Daltonik GmbH, Bremen, Germany). All MS acquisitions were performed under manual control in reflector positive ion mode. The instrument settings were optimized for the mass ranges of *m/z* 0-400 and *m/z* 600-4000, respectively. The instrument was calibrated for the mass range *m/z* 0-400 using prominent internal CHCA matrix ion signals as described earlier

(Persike & Karas 2009). For the mass range *m/z* 600-4000 the instrument was calibrated using an external synthetic peptide standard (Table 2.1). All mass spectra were acquired with 2000 laser shots with a laser frequency of 333 Hz.

### *MALDI-TOF/TOF tandem mass spectrometry*

Tandem mass experiments were performed using LIFT technology, with an acceleration set to 1 kV. The number of laser shots for a single MS$^2$ spectrum varied from 1000 to 2000 shots for biogenic monoamines and from 2000 to 5000 shots for neuropeptides, depending on ion signal quality. To verify OA and OA(*d3*), tandem mass spectra were acquired without collision gas. For the validation of TA and TA(*d4*), fragmentations were performed in CID mode, with argon as the collision gas. Resulting fragments of underivatized biogenic monoamines were compared to data provided in the Scripps Center for Metabolomics database (METLIN, https://metlin.scripps.edu/index.php). Peptide identities were verified by comparison of predicted (http://prospector.ucsf.edu) and experimentally obtained fragment ions. For quantification experiments of OA and TA, mass spectra were acquired in parent ion mode with fixed laser intensity. The parent ion window was set from *m/z* -0.4 to +6. Each mass spectrum was acquired with 2000 laser shots. In general, a signal was considered to be detected with an S/N ratio ≥ 3. The data obtained in these experiments were processed with the FlexAnalysis 3.4 software package (Bruker Daltonik GmbH, Bremen, Germany). For quantitative analysis, only unprocessed data were used.

**Table 2.1** Synthetic peptides used for instrument calibration in the range of *m/z* 600 - 4000.

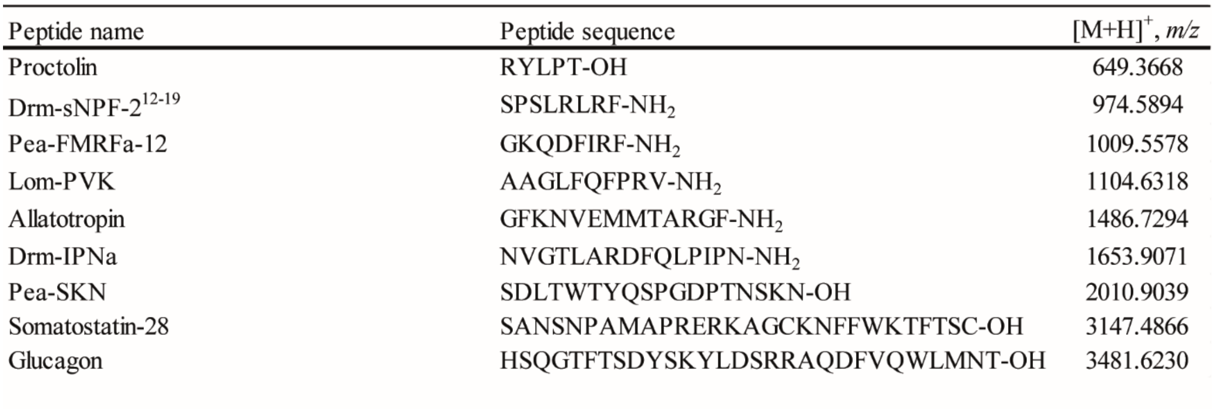

| Peptide name | Peptide sequence | $[M+H]^+$, *m/z* |
|---|---|---|
| Proctolin | RYLPT-OH | 649.3668 |
| Drm-sNPF-2$^{12-19}$ | SPSLRLRF-NH$_2$ | 974.5894 |
| Pea-FMRFa-12 | GKQDFIRF-NH$_2$ | 1009.5578 |
| Lom-PVK | AAGLFQFPRV-NH$_2$ | 1104.6318 |
| Allatotropin | GFKNVEMMTARGF-NH$_2$ | 1486.7294 |
| Drm-IPNa | NVGTLARDFQLPIPN-NH$_2$ | 1653.9071 |
| Pea-SKN | SDLTWTYQSPGDPTNSKN-OH | 2010.9039 |
| Somatostatin-28 | SANSNPAMAPRERKAGCKNFFWKTFTSC-OH | 3147.4866 |
| Glucagon | HSQGTFTSDYSKYLDSRRAQDFVQWLMNT-OH | 3481.6230 |

### *Method validation and Statistics*

Validation of standard curves followed the ±15/20 criteria published by the US Food and Drug Administration (FDA) for bioanalytical methods (FDA 2013). All data points for standard curve calculation are averages of at least three replicates. Linear ranges, accuracy, relative standard deviations (RSD) and linearity ($R^2$) were calculated with Microsoft Excel 2010 and/or R 3.1.3 (R Development Core Team). To compare OA titers between different octopaminergic cell populations, data points were tested for normal distribution using a one-sample Kolmogorov-Smirnov test and were either analyzed by student's t-test or one-way analysis of variance (ANOVA) for datasets with more than two groups. Comparative statistics were calculated in R 3.1.3.

### *Imaging of GFP expression*

For imaging of native GFP expression, brains were handled as described by Pitman and colleagues (Pitman et al. 2011). Brains were dissected in ice-cold phosphate-buffered saline (PBS, 1.86 mM $NaH_2PO_4$, 8.41 mM $Na_2HPO_4$, 175 mM NaCl) and fixed in 4% paraformaldehyde diluted in PBS for 90 min at rt (~21 °C) under vacuum (300 mbar). Then, samples were washed three times for 10 mins in PBS containing 0.1% Triton X-100 and one time in PBS before mounting in 90% glycerol/1% DABCO/9% PBS. Imaging was performed on a Zeiss LSM Meta 510 microscope (Zeiss AG, Jena, Germany), and resulting images were processed in Amira 5.4.2 (FEI, Hillsboro, OR). Reconstruction of brain surfaces was performed manually in Amira, while GFP-marked cells were visualized using voltex rendering.

## 2.3 Results and Discussion

### *2.3.1 Analysis of non-derivatized and derivatized synthetic OA and TA*

In order to evaluate the used analytical platform, a Bruker UltrafleXtreme MALDI-TOF/TOF mass spectrometer, and to assess ion stability and LODs for underivatized biogenic monoamines, different concentrations of synthetic TA and OA were analyzed with CHCA. Recorded mass spectra showed that TA as well as OA are unstable and undergo fragmentation during ionization (Fig. 2.1 A1, B1). OA (*m/z* 154.1) losses a mass equal to a water molecule ($H_2O$, *m/z* -18), producing a fragment ion at *m/z* 136.0, while TA (*m/z* 138.0) losses a mass equal to ammonia ($NH_3$, *m/z* -17), producing a fragment ion at *m/z* 121.0. From the ratios of the detected ion signals it can be deduced that OA shows a more unstable configuration compared to TA. Mass spectra of subsequent tandem experiments revealed product ions identical to fragments observed in the latter MS analysis (Fig. 2.1 A1, B1), which is also in consistency with fragmentation spectra deposited in the METLIN database. Furthermore, METLIN predicts fragmentation of the hydroxyl group at the phenol ring for OA and the fragmentation of the α-amine group of TA, matching the observed neutral losses. The mass spectrometric analysis of a dilution series of synthetic TA and OA with CHCA revealed a LOD of 100 fmol/µl for OA and 10 pmol/µl for TA, in MS and MS² mode. These relatively high detection limits are probably a direct result from the observed instability and poor ionization. To allow an unequivocal identification of TA and OA from biological samples as small as a single *D. melanogaster* neuron, the ion stability and ionization properties of resulting ions had to be notably increased.

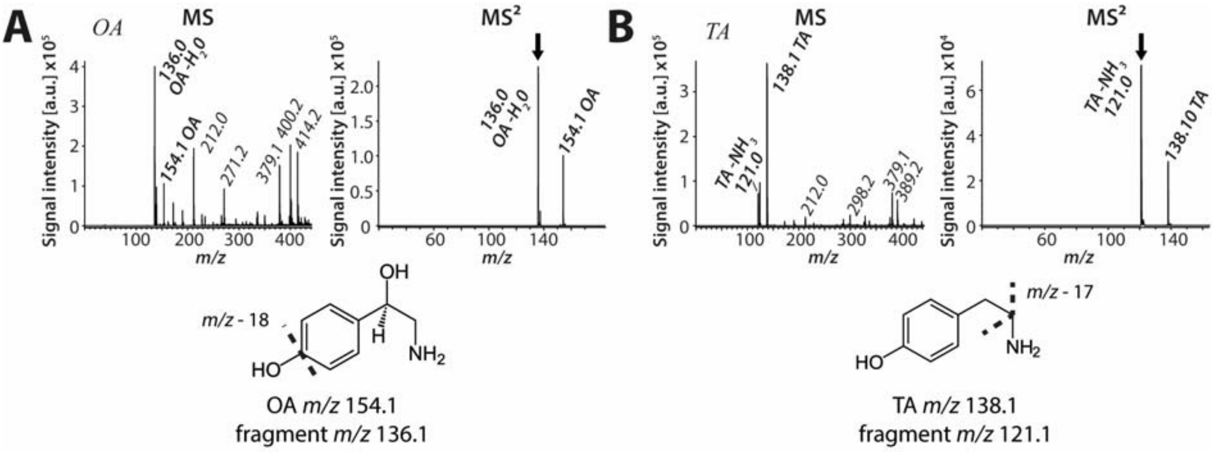

**Figure 2.1 Mass spectrometric analysis of underivatized synthetic OA and TA**. Both analyzed synthetic biogenic monoamines, OA (*m/z* 154.1; **A**) and TA (*m/z* 138.1; **B**), are unstable during ionization as represented by product ions at *m/z* 136.1 (OA) and *m/z* 121.0 (TA) in MS mode, which was confirmed by subsequent MS² experiments. Arrow = Product ion used for identification.

In recent years, derivatization reagents in corresponding protocols for the detection of monoamine neuroactive substances by MALDI-TOF MS have been developed, improving ion stability and ionization and leading ultimately to an improved specificity and sensitivity (Chacon et al. 2011; Shanta et al. 2012; Toue et al. 2014; Manier et al. 2014; Shariatgorji et al. 2015). Two derivatization agents, targeting primary amine groups, were tested in this study: CA which has been used for the detection of biogenic monoamines from rat frozen tissue section using MALDI-TOF MSI (Manier et al. 2014) and DPD which has been used for the improved detection of TA and OA using HPLC with diode array detection (Gatti et al. 2012). Both derivatization agents were picked because of their simple derivatization procedures which have been reported to occur at rt and need no additional chemical treatments of the sample

(Gatti et al. 2012; Manier et al. 2014). An exemplary reaction scheme of CA and DPD with OA is given in Figure 2.2.

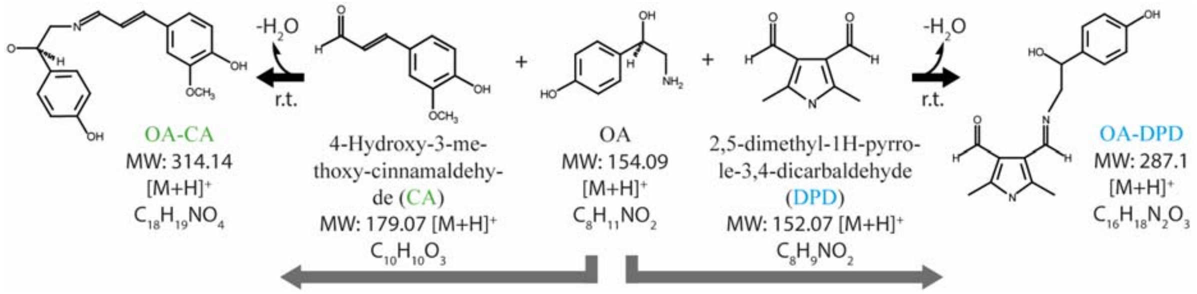

**Figure 2.2** Schematic reaction scheme of CA and DPD with OA (after Manier et al. 2014 and Gatti et al. 2012).

On-plate derivatization of synthetic biogenic monoamines with CA resulted in a mass shift of *m/z* +160 in resulting mass spectra (Fig. 2.3), as reported earlier (Manier et al. 2014). Recorded mass spectra of CA derivatized OA, OA-CA, revealed an intense ion signal at *m/z* 314.1, while MS analysis of TA-CA revealed an intense ion signal at *m/z* 298.1 (Fig. 2.3 A1, B1). Subsequent $MS^2$ analysis of OA-CA revealed a single product ion at *m/z* 296.1, mass identical to a water loss fragment. This fragment results probably from the same localized water loss which has been proposed earlier for underivatized OA. Comparison to recorded $MS^2$ mass spectra of an isotopically labeled synthetic OA standard, OA(*d3*), revealed a corresponding product ion at *m/z* 299.1 (Fig. 2.3 A2). Tandem mass spectra of TA-CA showed a fragmentation pattern consisting of four distinct product ions at *m/z* 120.8, 178.0, 243.0 and 296.0 using CID (Fig. 2.3 B1). To allow an unambiguously identification of TA-CA, recorded $MS^2$ mass spectra of TA-CA were compared to tandem mass spectra of a baseline ion signal at m/z 298.1 from samples containing only CA, leading to the discovery that only the ion signal at m/z 120.8 could be used to clearly identify TA-CA. To analyze the structural origin of this product ion from TA-CA, isotopically labeled synthetic TA(*d4*) was derivatized with CA and analyzed in MS and $MS^2$ mode (Fig. 2.3 B2). Recorded mass spectra of CA derivatized TA(*d4*) revealed a single major ion signal at *m/z* 302.1, matching putative TA(*d4*)-CA. Subsequent $MS^2$ experiments revealed that the product ion at *m/z* 120.8 used for identification of TA-CA originates of the TA side of TA-CA, since a corresponding fragment ion at *m/z* 124.8 was observed in TA(*d4*)-CA tandem mass spectra (Fig. 2.3 B1, B2). Furthermore, the resulting product ion used for TA-CA identification at *m/z* 120.8 probably results from a cleavage between the TA α-carbon and the amino group in TA-CA. While analyzing high concentrated, CA derivatized, synthetic OA and TA, small additional ion signals were recorded in the close vicinity of the major OA-CA and TA-CA ion signals (Fig. 2.3 A1, B1). Comparison to mass spectra recorded from derivatized deuterized standards, OA(*d3*) and TA(*d4*), revealed that these ion signals originate from the derivatized substances and were not related to the used derivate (Fig. 2.3 A2, B2). The ion signals were only detectable in high concentrated samples and were not detected in samples with concentration ≤ 1000nM (analyzed sample range).

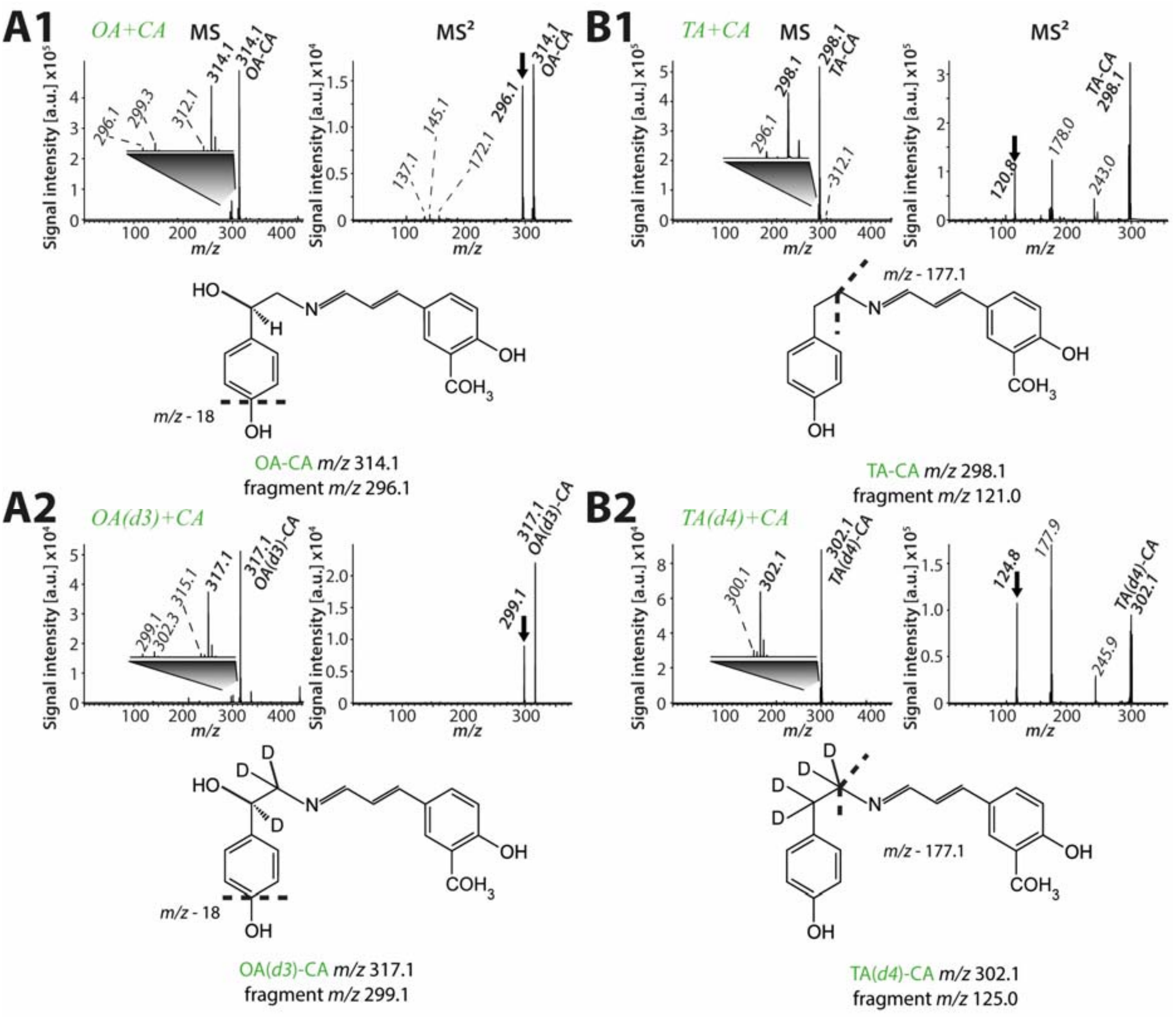

**Figure 2.3 MS and MS² mass spectra of OA-CA, OA(*d3*)-CA, TA-CA and TA(*d4*)-CA with suggested chemical structure of detected product ions used for identification**. (**A1**) MS and MS² mass spectra of CA derivatized synthetic OA and (**A2**) OA(*d3*) with suggested chemical structure of detected product ions used for OA/OA(*d3*) identification. (**B1**) MS and MS² mass spectra of CA derivatized synthetic TA and (**B2**) TA(*d4*) with suggested chemical structure of detected product ions used for TA/TA(*d4*) identification. Arrow = product ion used for identification.

Mass spectrometric analysis of different concentrations of TA and OA derivatized with CA revealed a striking increase in ion stability and ionization resulting in increased detection ratios with LODs as low as 5 fmol/µl for TA-CA and 25 fmol/µl for OA-CA. By using the MS² it was even possible to lower the LODs for the detection of TA-CA and OA-CA to 2.5 fmol/µl for TA-CA and 1 fmol/µl for OA-CA (Table 2.2).

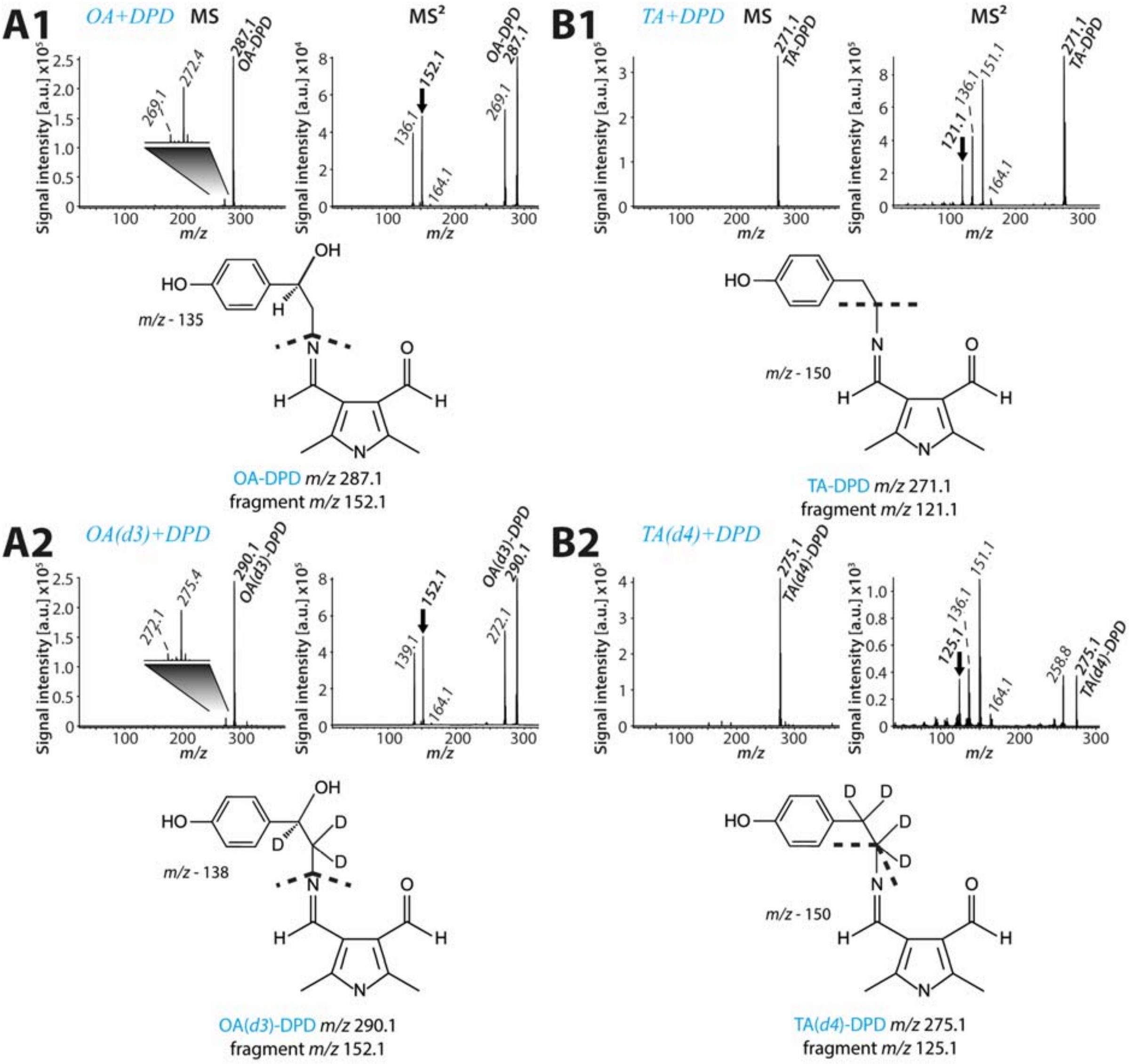

**Figure 2.4 MS and MS² mass spectra of DPD derivatized OA, OA(*d3*), TA and TA(*d4*) with suggested chemical structure of detected product ions used for identification**. (**A1**) Recorded MS and MS² mass spectra of DPD derivatized synthetic OA and (**A2**) OA(*d3*) with suggested chemical structure of detected product ions used for OA/OA(*d3*) identification. (**B1**) Recorded MS and MS² mass spectra of CA derivatized synthetic TA and (**B2**) TA(*d4*) with suggested chemical structure of detected product ions used for TA/TA(*d4*) identification. Arrow = product ion used for identification.

Mass spectrometric analysis of synthetic samples derivatized with DPD revealed a mass shift of *m/z* +133 for both TA (*m/z* 138.1 → *m/z* 271.1) and OA (*m/z* 154.1 → *m/z* 287.1; Fig. 2.4). Subsequent fragmentation spectra of OA-DPD showed three distinct ion signals at *m/z* 136.1, 152.1, and 269.1 and an ion pattern consisting of three ion signals at *m/z* 121.1, 136.1, and 151.1 for TA-DPD (Fig. 2.4). These results are in accordance with previous findings obtained by ESI

MS experiments (Gatti et al. 2012). To determine product ions for the clear identification of TA-DPD and OA-DPD, baseline ion signals matching TA-DPD and OA-DPD were analyzed by tandem mass spectrometry from samples containing only DPD. Comparison of the recorded $MS^2$ spectra of TA-DPD, OA-DPD and corresponding base line ion signals revealed that only the ion signals at *m/z* 152.1 for OA-DPD and *m/z* 121.1 for TA-DPD represent unique product ions for reliable identification. Tandem mass spectrometric analysis of isotopically labeled synthetic standards OA(*d3*) and TA(*d4*) revealed that the observed product ion at *m/z* 121.1 corresponds to the recorded product ion at *m/z* 120.8 observed in TA-CA samples and originates at the TA side of TA-DPD, whereas the product ion used for identification of OA-DPD (*m/z* 152.1) originates on the DPD side of OA-DPD (Fig. 2.4 A2, B2). Experimental determination of corresponding LODs revealed also a significant decrease in detection limits up to 10 fmol/µl in MS mode and 1 fmol/µl in $MS^2$ mode for both substances (Table 2.2).

**Table 2.2** Summary of experimentally determined LODs and LLOQs for OA-CA and TA-CA analysis in MS, $MS^2$, and $pMS^2$ mode. (*) = 300-nl samples; (**) = 18.4-nl samples.

| calculated values | MS [fmol/µl] | $MS^2$/$pMS^2$ [fmol/µl] |
|---|---|---|
| ***LOD*** | | |
| OA-CA | 25 | 1 |
| TA-CA | 5 | 2.5 |
| | | |
| OA-DPD | 10 | 1 |
| TA-DPD | 10 | 1 |
| ***LLOQ*** | | |
| OA-CA | 25*/25** | 2.5*/10** |
| TA-CA | 5*/10** | 5*/10** |

The observed LODs should be sufficient to detect TA and OA from biological samples, however, the analyzed sample volume of 300 nl was too large for SCMS, since addition of such a high volume to a single cell with a sample volume of about ~4-1.5 pl (cell diameter 7-10 µm) would lead to an extreme dilution of chemical features. Therefore, experiments were repeated with CA or DPD derivatized synthetic TA and OA with a sample volume of 18.4 nl. The recorded mass spectra confirmed previously determined LODs for both substances at 10 fmol/µl in MS mode and 1 fmol/µl (TA-CA 2.5 fmol/µl) in $MS^2$ mode (Table 2.2).

### 2.3.2 *Detection of OA and TA from individual Drosophila neurons*

To allow a reproducible cell identification among different brains, the *Tdc2-GAL4* line was crossed to a UAS-*mCD8::GFP* reporter line (Fig. 2.3 A1, A2). This line labels neurons that express Tdc2 and should therefore contain TA, and earlier studies, utilizing immunocytochemistry as well as genetic reporter lines, showed that most of these neurons also contain OA (Monastirioti et al. 1995; Busch et al. 2009). In order to evaluate the performance

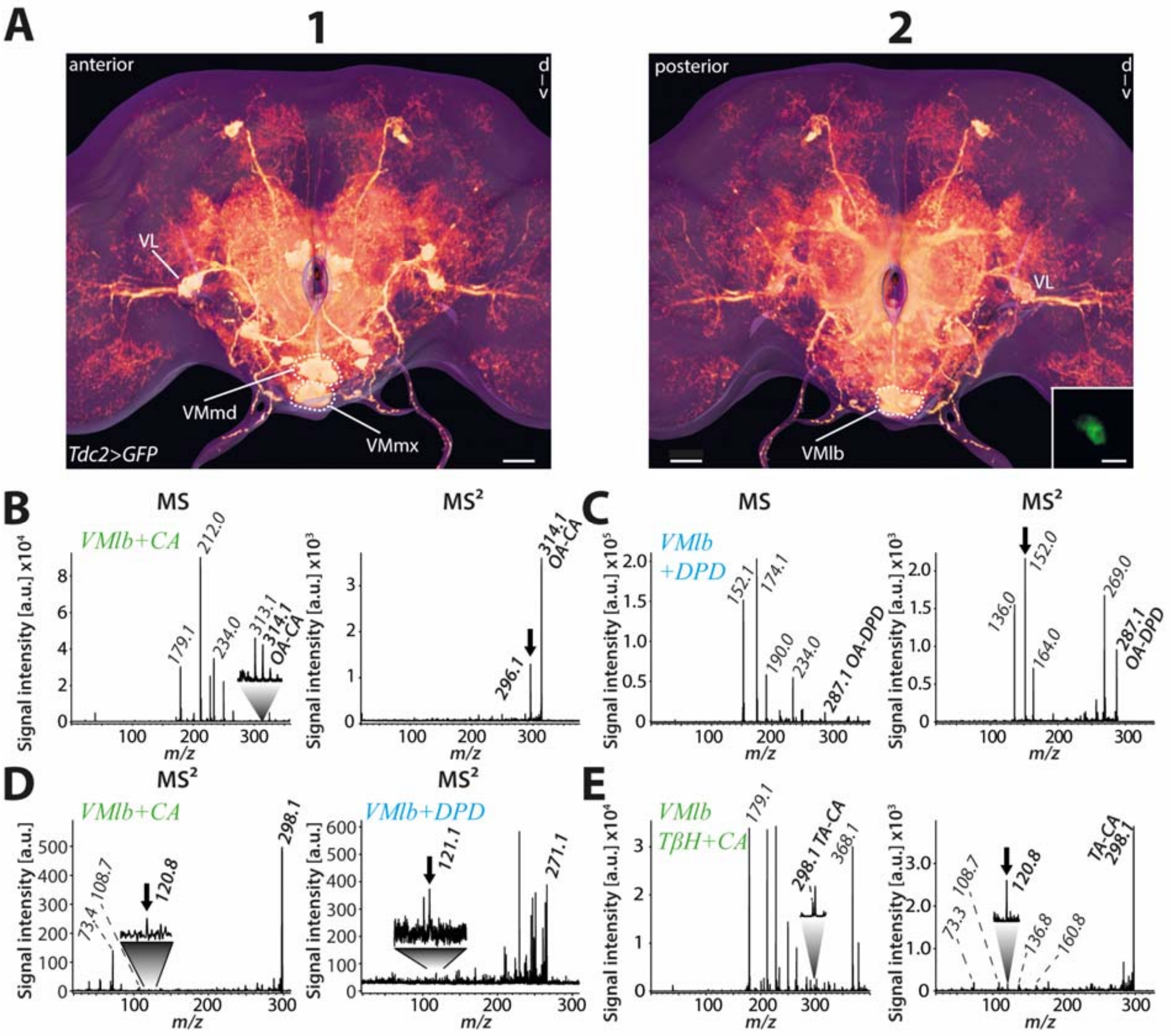

**Figure 2.5 Analysis of OA and TA from CA and DPD derivatized single *D. melanogaster* somata using direct MALDI-TOF MS.** Anterior (**A1**) and posterior (**A2**) views of a 3D reconstruction of a Tdc2>GFP labeled adult brain. VM, ventral midline; VL, ventrolateral cells; VMmx, VM maxillary cluster; VMmd, VM mandibular cluster; VMlb labial cluster. Scale bar = 25 µm. Inset A2: Isolated GFP-labeled soma on a sample plate. Scale bar = 10 µm. Detection (MS) and confirmation (MS²) of OA from individual dissected VMlb somata after (**B**) CA and (**C**) DPD derivatization. (**D**) Recorded tandem mass spectra for the confirmation of CA and DPD derivatized TA from single VMlb soma samples. (**E**) Mass spectra of a single CA derivatized Tβh$^{nM18}$/Tdc2>GFP VMlb soma yielding a prominent ion signal matching putative TA-CA at *m/z* 298.1 and subsequent confirmation by MS² of the corresponding precursor ion. Arrows = product ions used for identification.

of the developed protocol at the single cell level, VMlb neurons of the GNG were targeted (Fig. 2.3 A2). The VMlb clusters can be subdivided into two morphologically differentiable neuron subtypes according to their primary projection pathways: VPM and VUM neurons (see chapter 1; Busch et al. 2009). The primary projections of VPMs run toward the ventral foramen and develop asymmetric ramifications in the brain and the GNG, while VUM primary neurites run via one of three median tracts toward the posterior ventral area of the esophagus foramen from where they innervate the GNG and the thoracicoabdominal ganglia (Busch et al. 2009). These ascending and descending neurons seem to be involved in the neuronal pathway controlling aggression as well as reinforcing short-term memory among other behaviors (Zhou et al. 2008; Burke et al. 2012). Somata of these neurons are located close to the neuronal sheath and are therefore easily accessible for manual dissection. Moreover, these neurons showed an intense and consistent GFP labeling throughout nearly all dissected Tdc2>GFP brains, which is crucial for the reproducible dissection of neurons of interest under a fluorescence stereomicroscope. In the present study it was not possible to discriminate between the two neuron types, thus both neuron types were analyzed.

Single somata for SCMS were isolated in dissection buffer containing 33% glycerol, stabilizing neuron integrity and reducing the potential release of neuroactive substances from the soma into the axon without changing the biochemical profile of the neuron of interest (Rubakhin et al. 2003; Miao et al. 2005; Rubakhin et al. 2006; Rubakhin & Sweedler 2008). Only samples showing an intact fluorescence-labeled cell soma on the MALDI plate with no visible debris were chosen for further treatment and subsequent SCMS analysis (Fig. 2.5 A2, inset). Mass spectrometric analysis of CA treated single dissected VMlb somata revealed an ion signal at *m/z* 314.1 (Fig. 2.5 B). Subsequent tandem mass experiments confirmed this ion signal as OA-CA (Fig. 2.5 B). Recorded mass spectra of VMlb somata derivatized with DPD revealed an ion signal *m/z* 287.1, matching putative OA-DPD (Fig. 2.5 C). $MS^2$ mass spectra of this latter ion signal confirmed it as OA-DPD (Fig. 2.5 C). The detection of TA from CA or DPD derivatized samples, however, turned out to be inconsistent. In some derivatized VMlb samples a minor ion signal mass identical to TA-CA or TA-DPD was identified (not shown). Subsequent $MS^2$ experiments confirmed these ion signals as TA-CA and TA-DPD, respectively (Fig. 2.5 D). Furthermore, recorded $MS^2$ spectra of DPD derivatized single soma samples yielded additional ion signals of an unidentified origin compared to $MS^2$ mass spectra obtained from synthetic TA-DPD samples (Fig. 2.5 D; Fig. 2.4 B1).

To rule out whether this inconsistency of detection was caused by the applied derivatization protocol or resulted from a low titer of TA in the analyzed neurons, a second OA-devoid genetic driver line was analyzed. This *Tßh$^{nM18}$/Tdc2-GAL4* driver line is expressed in the same neuronal subpopulations as *Tdc2-GAL4*, moreover, the gene *Tßh* for the OA synthesizing enzyme is knocked out and labeled neurons therefore cannot synthesize OA. Furthermore, it has been shown that the initial *Tßh$^{nM18}$* line has elevated TA levels compared to wildtype flies and is completely devoid of OA (Monastirioti et al. 1996; Iliadi et al. 2017). Mass spectra of single VMlb somata of Tßh$^{nM18}$/Tdc2>GFP treated with CA revealed a clear ion signal at *m/z* 298.1, corresponding to putative TA-CA but no ion signal matching OA-CA (Fig. 2.5 E). Subsequent structure elucidation by MS² confirmed the ion signal as TA-CA (Fig. 2.5 E). This corroborates the hypothesis that the inconsistency of TA detection is due to a very low titer of TA in the analyzed VMlb neurons, which is at the lower boundary of the LOD (~2.5 fmol/µl) of the developed protocol.

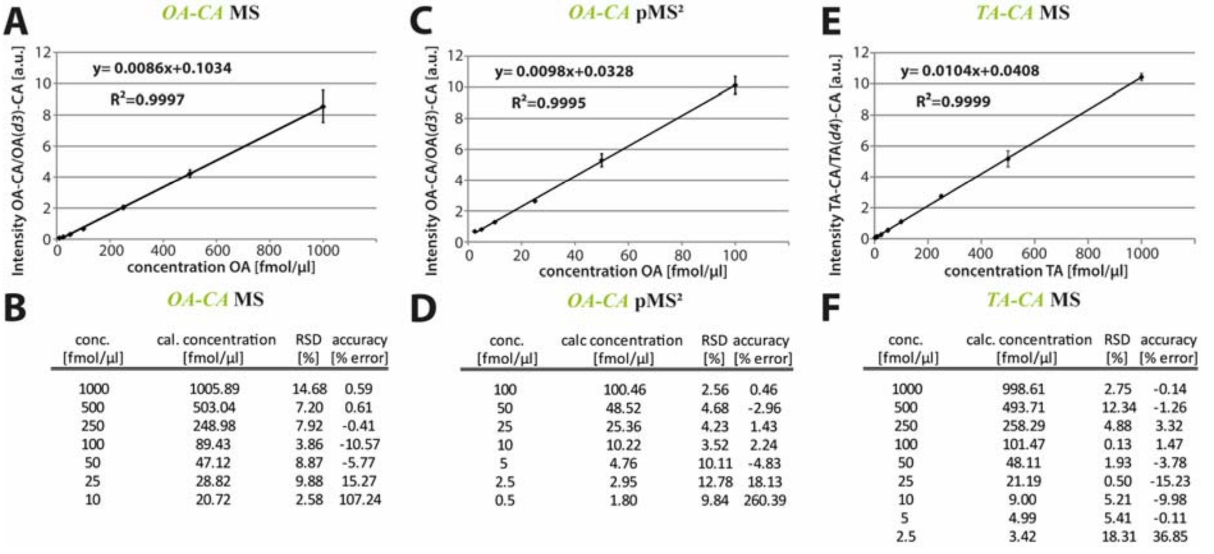

**B** *OA-CA* MS

| conc. [fmol/µl] | cal. concentration [fmol/µl] | RSD [%] | accuracy [% error] |
|---|---|---|---|
| 1000 | 1005.89 | 14.68 | 0.59 |
| 500 | 503.04 | 7.20 | 0.61 |
| 250 | 248.98 | 7.92 | -0.41 |
| 100 | 89.43 | 3.86 | -10.57 |
| 50 | 47.12 | 8.87 | -5.77 |
| 25 | 28.82 | 9.88 | 15.27 |
| 10 | 20.72 | 2.58 | 107.24 |

**D** *OA-CA* pMS²

| conc. [fmol/µl] | calc concentration [fmol/µl] | RSD [%] | accuracy [% error] |
|---|---|---|---|
| 100 | 100.46 | 2.56 | 0.46 |
| 50 | 48.52 | 4.68 | -2.96 |
| 25 | 25.36 | 4.23 | 1.43 |
| 10 | 10.22 | 3.52 | 2.24 |
| 5 | 4.76 | 10.11 | -4.83 |
| 2.5 | 2.95 | 12.78 | 18.13 |
| 0.5 | 1.80 | 9.84 | 260.39 |

**F** *TA-CA* MS

| conc. [fmol/µl] | calc. concentration [fmol/µl] | RSD [%] | accuracy [% error] |
|---|---|---|---|
| 1000 | 998.61 | 2.75 | -0.14 |
| 500 | 493.71 | 12.34 | -1.26 |
| 250 | 258.29 | 4.88 | 3.32 |
| 100 | 101.47 | 0.13 | 1.47 |
| 50 | 48.11 | 1.93 | -3.78 |
| 25 | 21.19 | 0.50 | -15.23 |
| 10 | 9.00 | 5.21 | -9.98 |
| 5 | 4.99 | 5.41 | -0.11 |
| 2.5 | 3.42 | 18.31 | 36.85 |

**Figure 2.6 Observed linearity, precision, and accuracy for 300-nl samples of OA-CA/OA(*d3*)-CA in MS and pMS² mode as well as TA-CA/TA(*d4*)-CA in MS mode.** (**A**, **B**) Observed Linearity, accuracy, and precision for OA-CA with OA(*d3*)-CA as IS in MS mode, (**C**, **D**) for OA-CA with OA(*d3*)-CA as internal standard in pMS² mode and (**E**, **F**) for TA-CA with TA(*d4*)-CA as IS in MS mode.

## *2.3.3 Quantification of synthetic OA and TA*

In order to enable robust quantification of TA and OA from biological samples, standard curves had to be constructed from experimentally analyzed synthetic samples. For initial testing, 300 nl sample spots consisting of either synthetic OA, TA or a mixture of both were applied in a concentration range of 1000 fmol/µl to 0.5 fmol/µl and covered by 300 nl of an internal standard comprising OA(*d3*), TA(*d4*) or a mixture of both at a fixed concentration of 100 fmol/µl. Finally, sample spots were treated with 126 nl CA or DPD and covered with 300 nl CHCA as matrix. For the construction of standard curves, each analyzed concentration was measured with at least three replicates and the average ion intensity ratios were calculated. Experimentally determined standard curves for samples derivatized with CA showed robust RSDs (<15/20%), excellent precision (<15/20%), and nearly perfect linearity values (OA-CA, $R^2 = 0.9997$; TA-CA, $R^2 = 0.9999$) in MS mode, which fulfilled the criteria set up by the FDA for bioanalytical method validation (FDA, 2013; Fig. 2.6 A, B, E, F). The experimentally determined lower limit of quantification (LLOQ) for OA-CA was 25 fmol/µl and 5 fmol/µl for TA-CA (Table 2.2, Fig. 2.6 B, F). The detection of small molecules can suffer from internal matrix ion signals, overlapping potential ion signals of interest as described earlier. A matrix ion signal at *m/z* 313.1 interfered with the OA-CA signal by overlapping the OA-CA ion signal with its second isotope. To resolve this problem, standard curve and LLOQs were determined by analyzing synthetic samples in a range from 100 fmol/µl to 1 fmol/µl in parent MS² mode (Fig. 2.6 C, D). By setting the precursor ion window from *m/z* -0.4 to +6 it was possible to quench the interference of the matrix ion signal from the analysis (Fig. 2.7 A). This resulted in an even lower LLOQ for OA-CA at 2.5 fmol/µl (Table 2.2, Fig. 2.6 C, D). Standard curves for TA-CA created from pMS² measurements showed no improvements and yielded the same LLOQ at 5

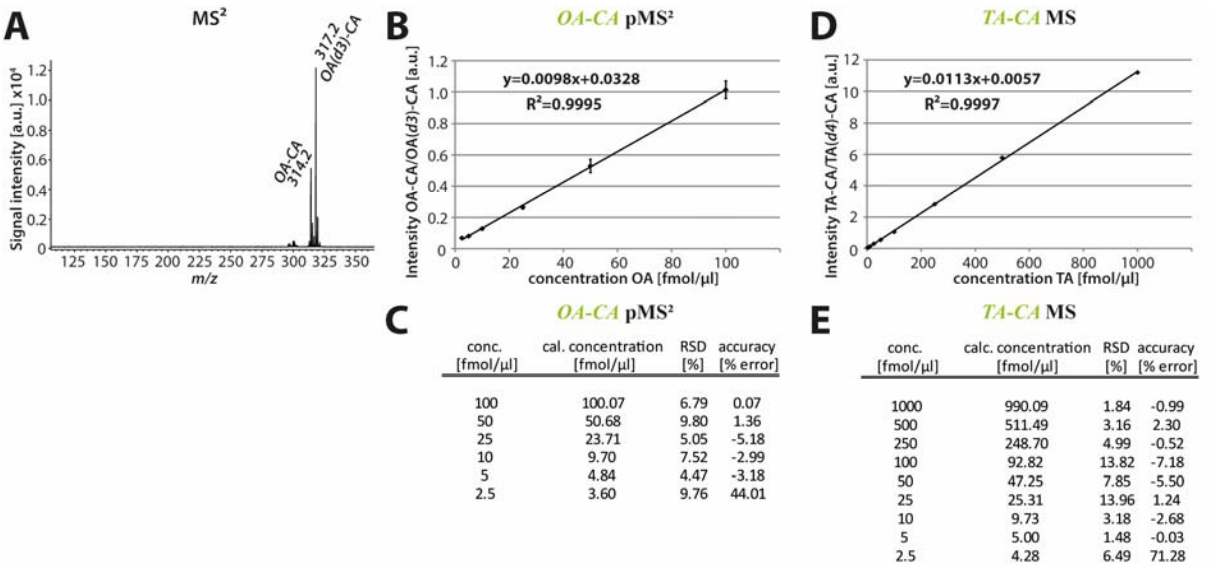

**C** OA-CA pMS²

| conc. [fmol/µl] | cal. concentration [fmol/µl] | RSD [%] | accuracy [% error] |
|---|---|---|---|
| 100 | 100.07 | 6.79 | 0.07 |
| 50 | 50.68 | 9.80 | 1.36 |
| 25 | 23.71 | 5.05 | -5.18 |
| 10 | 9.70 | 7.52 | -2.99 |
| 5 | 4.84 | 4.47 | -3.18 |
| 2.5 | 3.60 | 9.76 | 44.01 |

**E** TA-CA MS

| conc. [fmol/µl] | calc. concentration [fmol/µl] | RSD [%] | accuracy [% error] |
|---|---|---|---|
| 1000 | 990.09 | 1.84 | -0.99 |
| 500 | 511.49 | 3.16 | 2.30 |
| 250 | 248.70 | 4.99 | -0.52 |
| 100 | 92.82 | 13.82 | -7.18 |
| 50 | 47.25 | 7.85 | -5.50 |
| 25 | 25.31 | 13.96 | 1.24 |
| 10 | 9.73 | 3.18 | -2.68 |
| 5 | 5.00 | 1.48 | -0.03 |
| 2.5 | 4.28 | 6.49 | 71.28 |

**Figure 2.7 Quantification of synthetic OA and TA from CA derivatized 18.4 nl samples. (A)** Representative pMS² mass spectrum of an OA-CA/OA(*d3*)-CA sample and standard curves constructed from 18.4 nl volume samples for quantification of (**B**) OA-CA in pMS2 and (**D**) TA-CA in MS mode with observed linearity, accuracy, and precision (**C**, **E**).

fmol/µl as recorded from MS mode experiments, which was expected since no matrix ion signals interfere with the TA-CA ion signal at *m/z* 298.1 (Table 2.2).

The determined LLOQs and observed standard curve parameters were quiet encouraging, however, again the approach had to be scaled down to single cell volumes. Experiments for the construction of standard curves and determination of LLOQs were repeated with a sample volume of 18.4 nl for synthetic TA, OA, internal standards, matrix and 9.2 nl of derivatization agent.

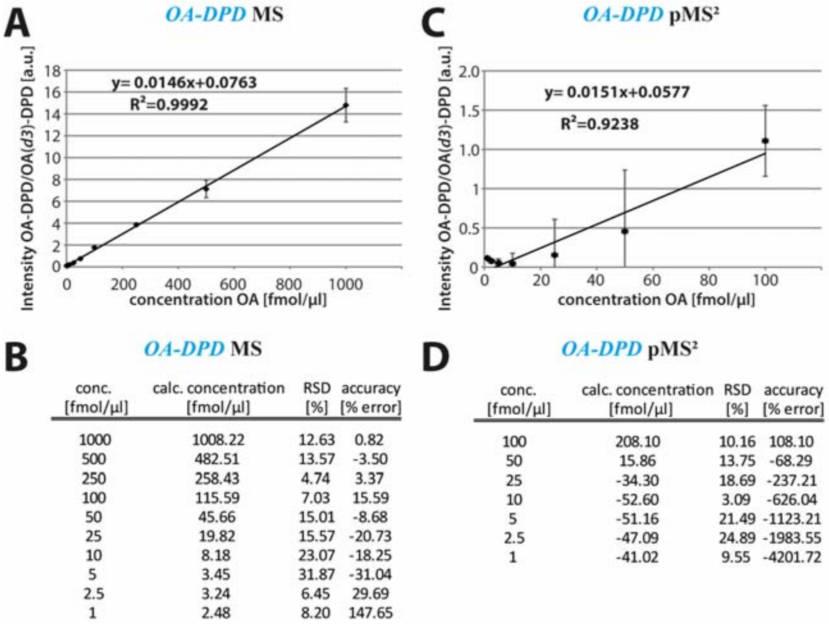

| conc. [fmol/µl] | calc. concentration [fmol/µl] | RSD [%] | accuracy [% error] |
|---|---|---|---|
| 1000 | 1008.22 | 12.63 | 0.82 |
| 500 | 482.51 | 13.57 | -3.50 |
| 250 | 258.43 | 4.74 | 3.37 |
| 100 | 115.59 | 7.03 | 15.59 |
| 50 | 45.66 | 15.01 | -8.68 |
| 25 | 19.82 | 15.57 | -20.73 |
| 10 | 8.18 | 23.07 | -18.25 |
| 5 | 3.45 | 31.87 | -31.04 |
| 2.5 | 3.24 | 6.45 | 29.69 |
| 1 | 2.48 | 8.20 | 147.65 |

| conc. [fmol/µl] | calc. concentration [fmol/µl] | RSD [%] | accuracy [% error] |
|---|---|---|---|
| 100 | 208.10 | 10.16 | 108.10 |
| 50 | 15.86 | 13.75 | -68.29 |
| 25 | -34.30 | 18.69 | -237.21 |
| 10 | -52.60 | 3.09 | -626.04 |
| 5 | -51.16 | 21.49 | -1123.21 |
| 2.5 | -47.09 | 24.89 | -1983.55 |
| 1 | -41.02 | 9.55 | -4201.72 |

**Figure 2.8 Observed linearity, precision, and accuracy for 300-nl samples of OA-DPD/OA(*d3*)-DPD in MS and pMS² mode.** (**A**, **B**) Observed Linearity, accuracy, and precision for OA-DPD with OA(*d3*)-DPD as IS in MS mode and (**C**, **D**) pMS² mode.

Experimentally determined standard curves for OA-CA showed nearly identical values in RSD (<15/20%), linearity (MS mode, $R^2 = 0.9997$; pMS² mode, $R^2 = 0.9995$) and precision (<15/20%) as reported for 300 nl samples (Fig. 2.7 B, C). However, in pMS² mode the LLOQ was increased to 10 fmol/µl due to day-to-day variation, possibly resulting from varying matrix interference (Table 2.2). Analysis of determined standard curves and LLOQs for TA-CA samples in MS and MS² mode were consistent with determined values from earlier analyzed 300 nl samples (Table 2.2, Fig. 2.7 D, E). A comparison to other quantitative techniques showedthat the developed protocol for OA and TA quantification is among the most sensitive methods published to date (Table 2.3). Furthermore, the presented protocol can operate with extremely low sample volumes (low nl range), which enables the direct interrogation of small biological samples like single cells. Often, extracts of such small samples have to be diluted to higher volumes in order to be introduced into separating or analyzing instruments, which can lead to analyte concentrations lower than the LOD of the used setup and ultimately missing them in the analysis.

**Table 2.3 Determined LOQs for OA (A) and TA (B) using different quantitative approaches.** Abbreviations: MALDI-TOF MS, matrix assisted laser desorption/ionization - time of flight mass spectrometry; MALDI-TOF pMS², matrix assisted laser desorption/ionization - time of flight precursor tandem mass spectrometry; HPLC-DAD-UV, high performance liquid chromatography with UV detection by diode array detector; UPLC-TUV, ultra-performance liquid chromatography with tunable ultra violet detector; CE-DAD-UV, capillary electrophoresis with UV detection by diode array detector; HPLC-FLD, high performance liquid chromatography with fluorescence detector; HPLC-MS/MS, high performance liquid chromatography with tandem mass spectrometric detection; CE-FSCV, capillary electrophoresis with fast-scan cyclic voltammetry detection; MEKC-EC, micellar electrokinetic capillary chromatography with electrochemical detection; CE-LINF, capillary electrophoresis with laser induced natural flouresence detection.

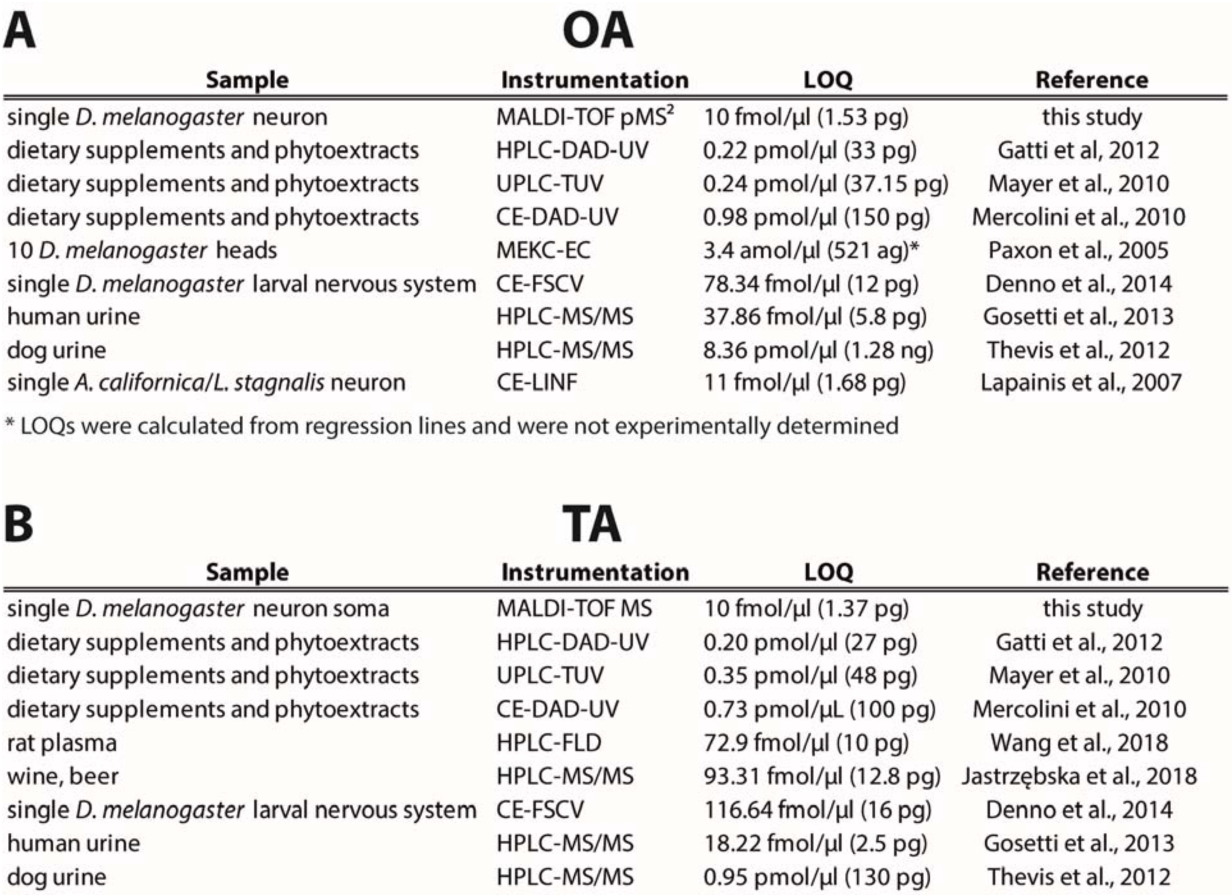

**A** **OA**

| Sample | Instrumentation | LOQ | Reference |
|---|---|---|---|
| single *D. melanogaster* neuron | MALDI-TOF pMS² | 10 fmol/µl (1.53 pg) | this study |
| dietary supplements and phytoextracts | HPLC-DAD-UV | 0.22 pmol/µl (33 pg) | Gatti et al, 2012 |
| dietary supplements and phytoextracts | UPLC-TUV | 0.24 pmol/µl (37.15 pg) | Mayer et al., 2010 |
| dietary supplements and phytoextracts | CE-DAD-UV | 0.98 pmol/µl (150 pg) | Mercolini et al., 2010 |
| 10 *D. melanogaster* heads | MEKC-EC | 3.4 amol/µl (521 ag)* | Paxon et al., 2005 |
| single *D. melanogaster* larval nervous system | CE-FSCV | 78.34 fmol/µl (12 pg) | Denno et al., 2014 |
| human urine | HPLC-MS/MS | 37.86 fmol/µl (5.8 pg) | Gosetti et al., 2013 |
| dog urine | HPLC-MS/MS | 8.36 pmol/µl (1.28 ng) | Thevis et al., 2012 |
| single *A. californica/L. stagnalis* neuron | CE-LINF | 11 fmol/µl (1.68 pg) | Lapainis et al., 2007 |

* LOQs were calculated from regression lines and were not experimentally determined

**B** **TA**

| Sample | Instrumentation | LOQ | Reference |
|---|---|---|---|
| single *D. melanogaster* neuron soma | MALDI-TOF MS | 10 fmol/µl (1.37 pg) | this study |
| dietary supplements and phytoextracts | HPLC-DAD-UV | 0.20 pmol/µl (27 pg) | Gatti et al., 2012 |
| dietary supplements and phytoextracts | UPLC-TUV | 0.35 pmol/µl (48 pg) | Mayer et al., 2010 |
| dietary supplements and phytoextracts | CE-DAD-UV | 0.73 pmol/µL (100 pg) | Mercolini et al., 2010 |
| rat plasma | HPLC-FLD | 72.9 fmol/µl (10 pg) | Wang et al., 2018 |
| wine, beer | HPLC-MS/MS | 93.31 fmol/µl (12.8 pg) | Jastrzębska et al., 2018 |
| single *D. melanogaster* larval nervous system | CE-FSCV | 116.64 fmol/µl (16 pg) | Denno et al., 2014 |
| human urine | HPLC-MS/MS | 18.22 fmol/µl (2.5 pg) | Gosetti et al., 2013 |
| dog urine | HPLC-MS/MS | 0.95 pmol/µl (130 pg) | Thevis et al., 2012 |

Analysis of constructed standard curves of 300 nl DPD derivatized OA samples revealed RSD values exceeding the 15/20% rule, showing poor precision and/or declined linearity (Fig. 2.8 A-D). This could result from an incomplete turnover, which is limited by the short reaction time during drying of the small volume of applied DPD, and therefore not qualifying for a robust quantification in conjunction with the developed protocol.

### 2.3.4 Stability of stored samples

Often it is desirable to store prepared samples for later analysis, however, storage under the wrong conditions can lead to a change in sample composition by sample degradation or unwanted chemical reactions driven by external effects like light or heat. To evaluate a potential degradation of OA-CA and TA-CA during sample storage, four triplicates of 18.4 nl sample spots were prepared and stored at either darkness or at the laboratory bench with access to light (no direct sunlight) for up to 69 h. The triplicate sample sets were analyzed at four different time points: immediately after sample preparation and after 6, 22.5, and 69 h. Samples stored in darkness showed no change in ion ratios between any of the measured time points from 0 h to 69 h (ANOVA, OA: $p = 0.56$, TA: $p = 0.67$; Fig. 2.9 A, B). Furthermore, no significant decrease in ion signal intensity (ANOVA, OA: $p = 0.48$; TA: $p = 0.90$) was detected, and RSDs showed robust values <15% for all samples (Fig. 2.9 E, F, I). The sample set which was stored at a lab bench with indirect access to daylight, however, showed a significant increase in signal ratios for OA-CA/OA(*d3*)-CA between 22.5 h and 69 h (ANOVA, $p = 0.03$; post-hoc-test, 22.30 h and 69.00 h, $p = 0.037$), while ratios recorded for TA-CA/TA(*d4*)-CA showed no significant changes over the analyzed time periods (ANOVA, $p = 0.59$; Fig. 2.9 C, D). Furthermore, observed RSDs exceeded the <15% rule for TA-CA/TA(*d4*)-CA samples after 69 h of storage under light conditions (Fig. 2.7 I), and ion signal intensities decreased significantly for both substances after 22.5 h (ANOVA, OA: $p = 3.10e\text{-}6$; TA: $p = 0.023$) and even more dramatically after 69 h (ANOVA, OA: $p = 2.41e\text{-}7$; TA: $p = 3.26e\text{-}6$; Fig. 2.7 G, H).

The observed degradation is possibly mediated by the absorption of photon energy from the indirect sunlight. Substances with aromatic rings have high optical (photon) absorption characteristics, which for example is a prerequisite for MALDI matrices (e.g. CHCA) to allow desorption and ionization of analyte molecules during laser excitation (Hillenkamp & Peter-Katalinic 2007). However, aromatic ring systems can be found in many organic substances, for example in OA, TA and CA (Fig. 2.1). Moreover, it is known that the level of absorption is dependent on the connected ligands of the core ring (Hillenkamp & Peter-Katalinic 2007). Thus, an explanation for the overall loss of signal intensity for samples stored with access to indirect sunlight points towards a preliminary excitation of the deposited matrix during storage and a direct degradation of CA derivatized OA and TA.

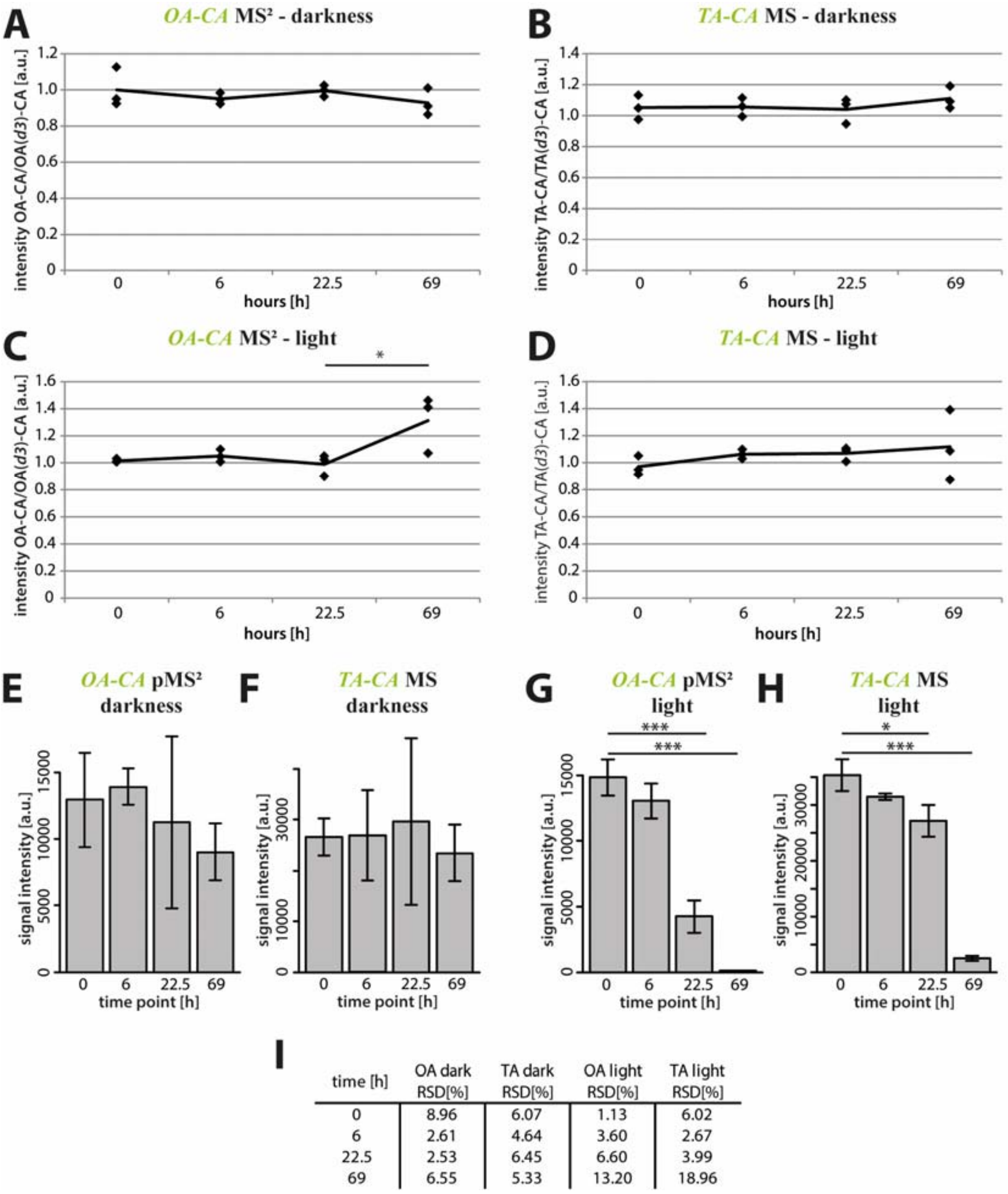

| time [h] | OA dark RSD[%] | TA dark RSD[%] | OA light RSD[%] | TA light RSD[%] |
|---|---|---|---|---|
| 0 | 8.96 | 6.07 | 1.13 | 6.02 |
| 6 | 2.61 | 4.64 | 3.60 | 2.67 |
| 22.5 | 2.53 | 6.45 | 6.60 | 3.99 |
| 69 | 6.55 | 5.33 | 13.20 | 18.96 |

**Figure 2.9 Effect of sample storage in light and dark conditions on detected OA-CA/OA(*d3*)-CA and TA-CA/TA(*d4*)-CA ratios, signal intensities and RSDs.** Samples stored in darkness showed no significant changes in sample/standard ratios (OA, **A**; TA, **B**; ANOVA, OA: $p = 0.56$, TA: $p = 0.67$), signal intensities (OA, **E**; TA, **F**; ANOVA, OA: $p = 0.48$; TA: $p = 0.90$) or RSDs (**I**). Samples stored with indirect access to day light showed an significant increase in detected OA-CA/OA(*d3*)-CA ratios (**C**) while TA-CA/TA(*d4*)-CA samples were unaffected (**D**). Signal intensities of samples stored in light conditions showed significantly decreased ion intensities after 22.5 h for both substances and increased RSDs with TA values exceeding 15% (**I**).

In summary, prepared samples can be stored for up to 69 h in darkness without any detectable sample degradation and storage in light conditions should be avoided.

### *2.3.5 Isomeric ion species and neuropeptide profiling*

Isomeric molecules of derivatized TA and OA, originating from the cell metabolism of *D. melanogaster* neurons, can potentially hamper robust quantitative analysis from these biological samples. They can contribute to detected ion signal ratios and thereby interfere with calculated substance concentrations. To resolve the problem of isomeric molecules originating from the sample background of *D. melanogaster* neurons, single somata of neuropeptidergic drosomyosuppressin (DMS)-expressing neurons, which do not belong to the OAergic/TAergic system labeled by c929>GFP (see chapter 5), were isolated and treated with CA and DPD before SCMS analysis.

Recorded mass spectra of CA or DPD treated DMS cell samples revealed only baseline ion signals matching derivatized TA and OA (CA, Fig. 2.8 B; DPD, Fig. 2.9 B). Subsequent $MS^2$ experiments of these baseline ion signals revealed no additional product ions, when compared to $MS^2$ spectra of corresponding baseline ions from samples containing only CA or DPD, which would correspond to isomeric molecules (CA, Fig. 2.10 E, F, I, J; DPD, Fig. 2.11 E, F, I, J). Therefore, interfering ion signals of isomeric molecules from the sample background, which are mass identical to the ion signals of interest, cannot be detected, however, their presence cannot be completely ruled out. Moreover, even though such molecules could be present their interference seems to be very limited and outside of the detection limit of the used instrument. To test a possible effect of the applied derivatization agents on the detection of neuropeptides, CA and DPD treated DMS cell samples were also analyzed in the mass range at *m/z* 600-4000. Recorded mass spectra of CA derivatized DMS samples revealed two ion signals at *m/z* 1247.6 and *m/z* 1407.5 (Fig. 2.10 C). Recorded mass spectra from tandem mass experiments of both precursor ions revealed product ions matching to predicted fragments of DMS and DMS-CA, and product ion spectra obtained from CA derivatized synthetic DMS (Fig. 2.10 D, G, H, K, L). Mass spectra obtained from DMS samples treated with DPD yielded similar results, with ion signals at *m/z* 1247.6 and *m/z* 1380.7, matching DMS and putative DMS-DPD (Fig. 2.11 C). Comparison of recorded $MS^2$ spectra to tandem mass spectra obtained from synthetic DMS derivatized with DPD confirmed the identity of the ion signals as DMS and DMS-DPD (Fig. 2.11 D, G, H, K, L). Furthermore, only minor ion signals of derivatized DMS were observed for both derivatization agents (CA, Fig. 2.10 C; DPD, Fig. 2.11 C). Hence, the developed protocol enables the detection of biogenic monoamines and neuropeptides from the same derivatized cell sample using either derivatization substance.

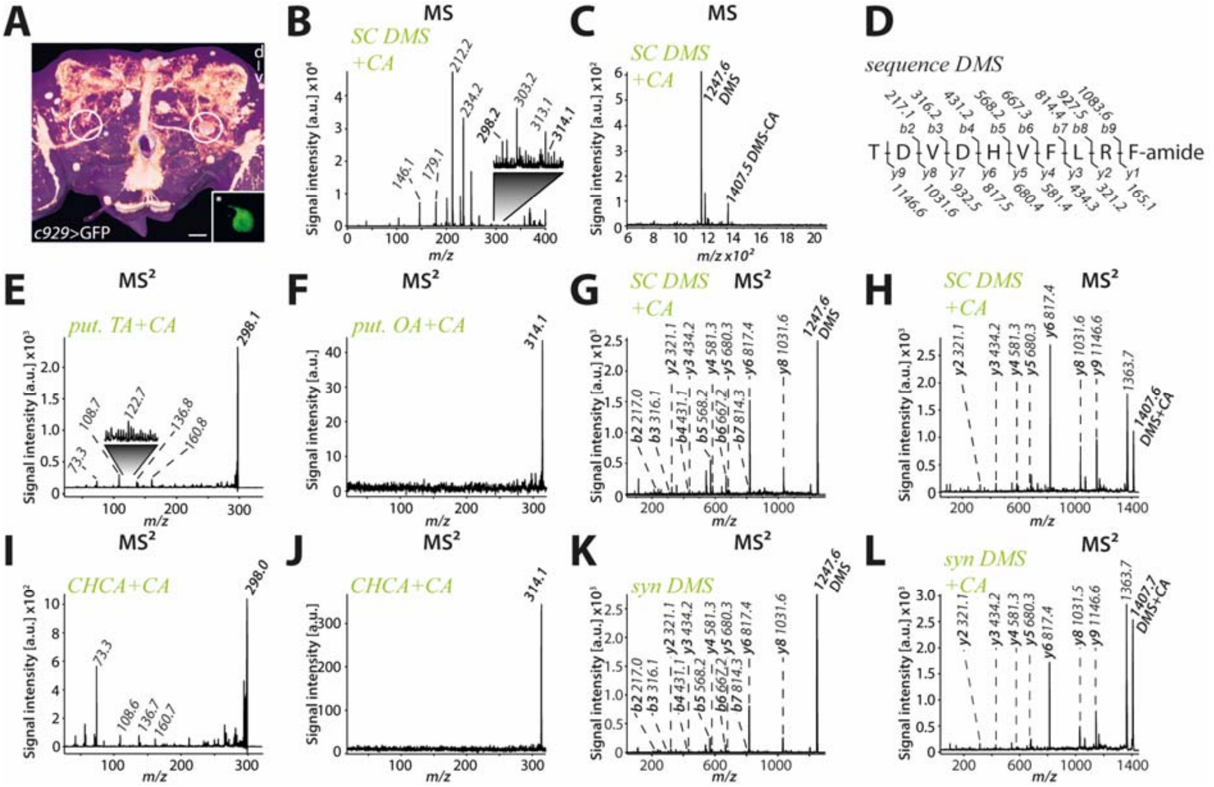

**Figure 2.10 Effect of sample derivatization by CA on the detection of neuropeptides and evaluation of possible isomeric species from the sample background of *D. melanogaster* neurons.** (**A**) Posterior view of a c929>GFP brain sample. Right circle: DMS cell body is marked. Left circle: Single DMS soma was isolated and placed onto a MALDI sample plate (insert). Scale bar = 25 µm. (**B**) Mass spectrum of a CA derivatized DMS cell in the mass range of *m/z* 0-400. (**C**) Mass spectrum of a CA derivatized DMS neuron in the mass range of *m/z* 600-2000 revealed two ion signals at *m/z* 1247.6 (put. DMS) and *m/z* 1407.5 (put. DMS-CA). (**D**) Amino acid sequence of DMS with predicted y-, and b-fragments. (**E**, **F**) Subsequent MS² analysis of background ion signals revealed no product ions matching (**E**) TA-CA or (**F**) OA-CA. Comparison to corresponding MS² spectra from samples containing only CA revealed no additional product ions (**I**, **J**). Tandem mass spectra of precursor ions *m/z* 1247.6 (**G**) and *m/z* 1407.5 (**H**) confirmed the ion signals as DMS and DMS-CA. (**K**, **L**) MS² mass spectra of syn. DMS and CA derivatized synthetic DMS matching the observed product ions from biological samples.

## 2.3.6 Discrimination of OA and DA

DA is another biogenic monoamine synthesized by *D. melanogaster* neurons and is mass identical to OA (METLIN; Wright 1987). Co-localization of the two biogenic monoamines has not been reported to date, however, to allow a clear distinction between the two substances and exclude a potential interference of DA in analyzed samples, synthetic DA was analyzed by the developed derivatization protocol in MS and MS² mode. Recorded mass spectra of CA derivatized synthetic DA revealed a major ion signal at *m/z* 314.1, matching putative DA-CA and OA-CA (Fig. 2.12 A). Tandem mass experiments of the latter precursor ion revealed numerous prominent product ion signals at *m/z* 137.0, 178.0, 190.0 and 259.0 (Fig. 2.12 B). is in consistency with results from an earlier study (Manier *et al.*, 2014). Synthetic DA samples

Comparison to recorded MS² mass spectra of OA-CA and of samples only containing CA revealed that the product ion at *m/z* 259.0 can be used to unambiguously identify DA-CA. This

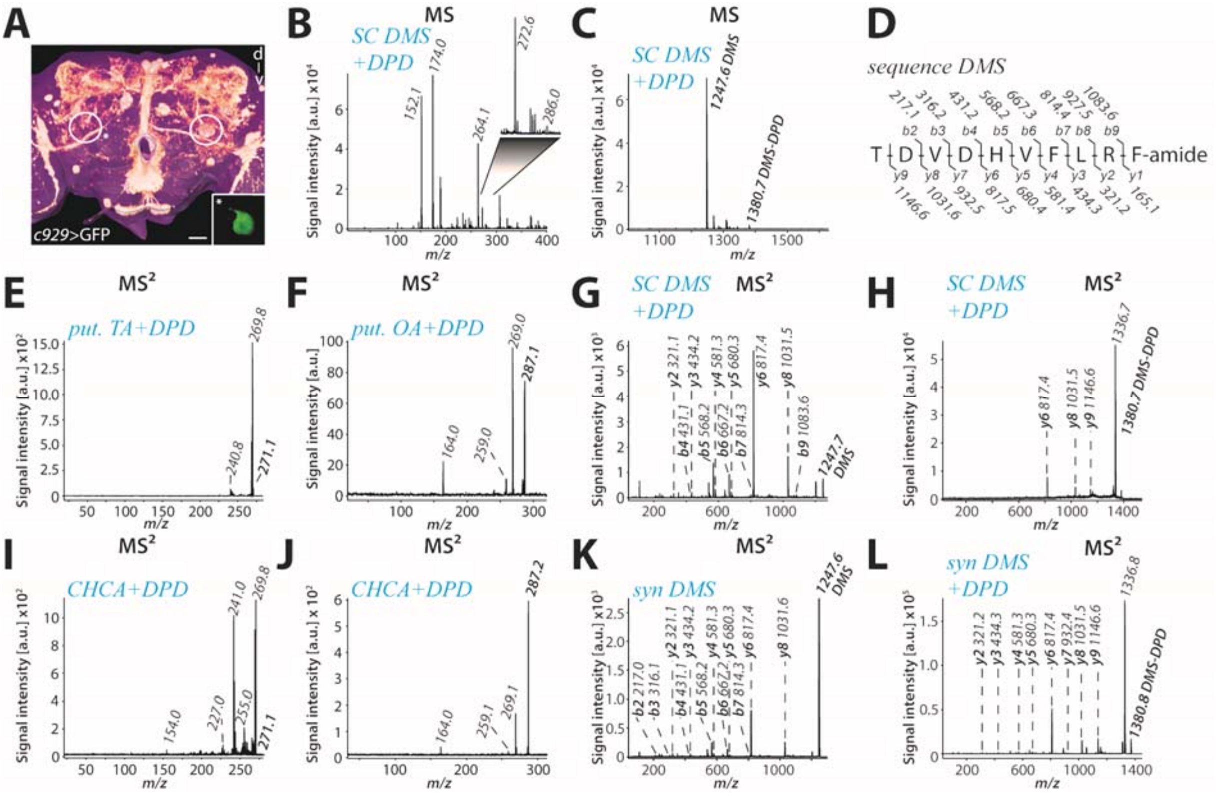

**Figure 2.11 Effect of sample derivatization by DPD on the detection of neuropeptides and evaluation of possible isomeric species from the sample background of *D. melanogaster* neurons.** (**A**) Posterior view of a c929>GFP brain sample with unmanipulated (right) and isolated DMS neuron soma (left circle). Inset = isolated soma on MALDI-TOF sample plate. Scale bar = 25 µm. (**B**) Mass spectrum of a DPD derivatized DMS cell in the mass range of *m/z* 0-400. (**C**) Mass spectrum of a DPD derivatized DMS neuron in the mass range of *m/z* 900-1800 revealed two ion signals at *m/z* 1247.6 (put. DMS) and *m/z* 1380.7 (put. DMS-DPD). (**D**) Amino acid sequence of DMS with predicted y-, and b-fragments. (**E**, **F**) Subsequent MS² analysis of background ion signals revealed no product ions matching (**E**) TA-CA or (**F**) OA-CA. Comparison to corresponding MS² spectra from samples containing only CA revealed no additional product ions (**I**, **J**). Tandem mass spectra of precursor ions *m/z* 1247.6 (**G**) and *m/z* 1380.7 (**H**) confirmed the ion signals as DMS and DMS-CA. (**K**, **L**) MS² mass spectra of synthetic DMS and CA derivatized synthetic DMS matching the observed product ions from biological samples.

derivatized with DPD showed an ion signal at *m/z* 287.1, matching putative DA-DPD and OA-DPD (Fig. 2.12 C). Subsequent MS² experiments of the ion signal revealed product ions at *m/z* 136.1, 151.1, 164.1, 242.1, 257.0 and 269.0 (Fig. 2.12 D). Comparison to MS² mass spectra recorded from samples containing OA-DPD or only DPD revealed that only the product ion at *m/z* 151.1 represents a unique fragment for a clear identification of DA-DPD. Thus, it is possible to discriminate between DA and OA in MS² mode using both derivatization agents, when analyzing OAergic neuron samples. Since no specific fragments of DA were detected in any analyzed neuron sample and VMlb neurons were never described as DAergic neurons, a possible interference of DA on OA measurements can be excluded with high certainty.

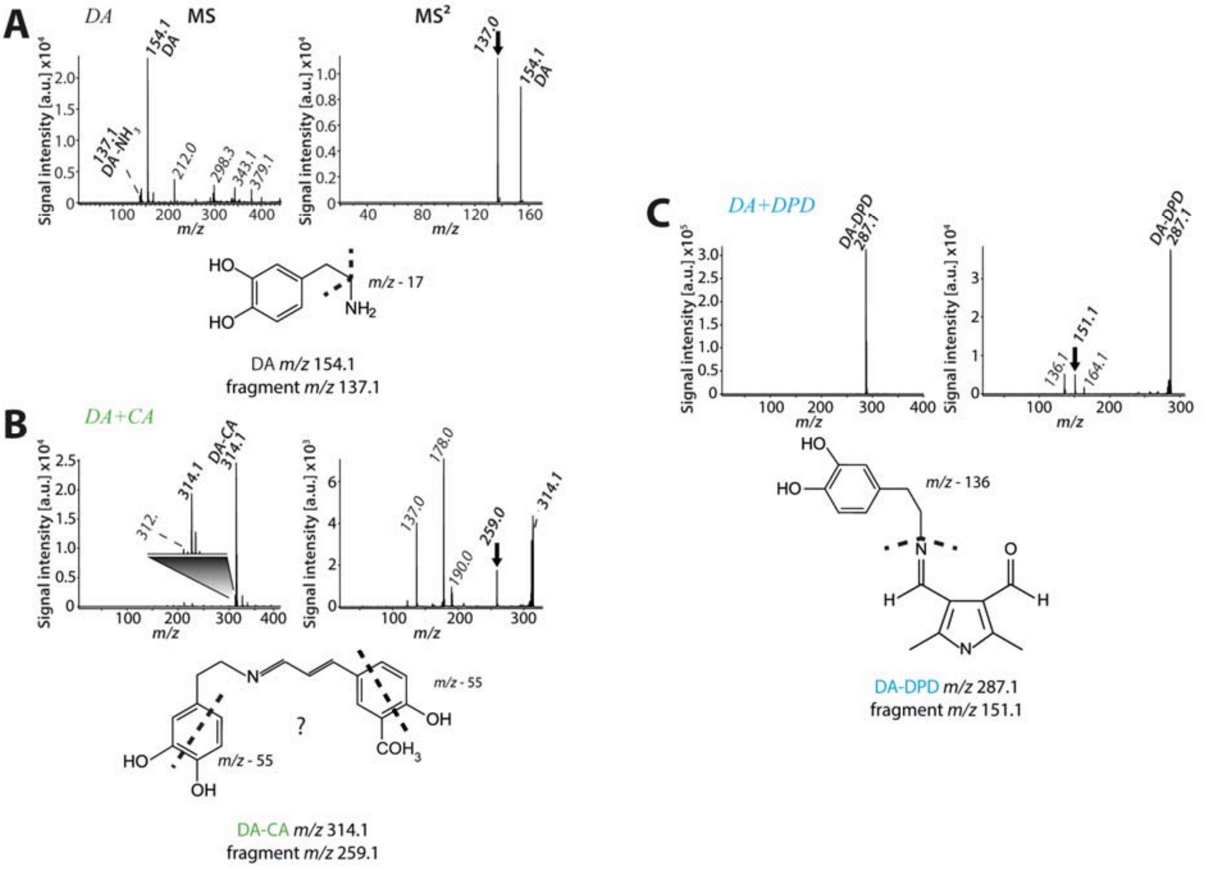

**Figure 2.12 MS and MS² mass spectra of underivatized, CA and DPD derivatized synthetic DA with suggested chemical structure of detected product ions used for DA identification**. (**A**) MS and MS² mass spectra of synthetic DA with suggested chemical structure of detected product ion used for DA identification. Comparison to product ion data obtained from METLIN database suggested an ammonia loss, originating from the amine group of the α-carbon. (**B**) MS and MS² mass spectra of CA derivatized synthetic DA with suggested product ion used for identification. MS² spectra of CA derivatized DA showed multiple major product ions identical to previously reported data by Manier et al., 2014. The product ion used for DA identification, *m/z* 259.0, suggests a breakage of one of the aromatic ring systems of DA-CA, however, which side is fragmented could not be confirmed. (**C**) MS and MS² mass spectra of DPD derivatized synthetic DA with suggested chemical structure of detected product ion used for DA identification. Comparison of MS² spectra of OA-DPD and DA-DPD revealed a unique product ion for identification (OA-DPD, *m/z* 152.1; DA-DPD, *m/z* 151.1). Arrow = product ion used for identification.

### *2.3.7 Quantification of OA and TA in VMlb somata*

To test the efficiency of the developed quantification protocol on biological samples, I prepared Tdc2>GFP-labeled VMlb neurons again. Single VMlb neurons of flies cooled for 1 h were isolated and treated with 18.4 nl IS, 9.2 nl CA and subsequently covered with 18.4 nl of CHCA. To minimize potential interference from repeated laser excitation of such a small sample and thereby guarantee reproducible measurements, data was acquired in the following order: (1)

$pMS^2$ mode for OA-CA quantification, (2) MS mode for TA-CA quantification and fingerprinting, (3) $MS^2$ mode for OA-CA and OA(*d3*)-CA confirmation, and (4) $MS^2$ mode TA-CA and TA(*d4*)-CA confirmation. Quantitative mass spectrometric analysis of 1 h cooled VMlb soma samples showed clear ion signals for OA-CA with an average concentration of 29.67 fmol/µl (n = 14, ± 7.49 fmol/µl; Fig. 2.13 A). Recorded TA-CA concentrations, however, were below the determined LLOQ, but $MS^2$ analysis revealed identification of TA-CA in 3 out of 14 samples. These findings corroborate the earlier stated hypothesis that VMlb neurons contain high levels of OA and only small quantities of TA, probably due to an ongoing conversion of TA into OA.

### 2.3.8 Temperature-dependent variability of detectable OA titers in VMlb neurons

Anaesthetization by cooling of animals prior to dissection or for transfer is a widely used technique, especially when working with insect models. Furthermore, some behavioral experiments use cold-shock anesthesia for blocking reconsolidation of trained memory (Krashes & Waddell 2008; Felsenberg et al. 2017; Cognigni et al. 2018). However, if and how exactly cooling influences single neuron biogenic monoamine titers of treated animals remains elusive. To test whether cooling has a pronounced effect on recordable TA/OA titers, two additional experimental groups were analyzed: (1) uncooled animals (t = 0) and (2) animals cooled for 15 min (t = 15). Quantitative mass spectrometric analysis of single VMlb soma samples from uncooled animals (1) revealed an average OA-CA concentration of 13.67 fmol/µl (n = 21, ± 3.25 fmol/µl; Fig. 2.13 A). Recorded TA-CA titers were lower than the determined LLOQ, but tandem MS revealed clear evidence for TA-CA in 13 of 21 cells (male, 7 of 11; female, 6 of 10). For the second experimental group, which was subjected to cooling for 15 min (2), recorded OA-CA titers had an average concentration of 17.38 fmol/µl (n = 17, ± 1.94 fmol/µl; Fig. 2.13 A). Again, recorded TA-CA titers lay below the determined LLOQ, however, in 10 of 17 cell samples (male, 7 of 9; female 3 of 8) the presence of TA-CA was verified by $MS^2$ spectra. Statistical comparison of recorded VMlb OA-CA titers from uncooled, 15 min cooled and 60 min cooled flies revealed significant higher OA titers in cooled animals compared to uncooled flies, and a significant higher OA titer in 60 min cooled flies compared to 15 min cooled and uncooled flies (ANOVA, uncooled x 15 min, $p = 0.02$; uncooled x 60 min, $p = 8.59e\text{-}14$; 15 min x 60 min, $p = 1.01e\text{-}9$; Fig. 2.13 A). These results demonstrate a direct correlation between the applied duration of cooling and detectable OA concentrations in the VMlb neurons. This could be mediated by a reduced neurotransmitter vesicle transport from the soma into the axon, whereas the synthesis process remains intact. In general, lower temperatures lead to a reduced activity in neurons which has been shown for the H1 neuron in the blowfly *Calliphora erythrocephala* (Warzecha et al. 1999) or the generation of action potentials in sensory neurons of the base of the tactile spine of *P. americana* (French 1985).

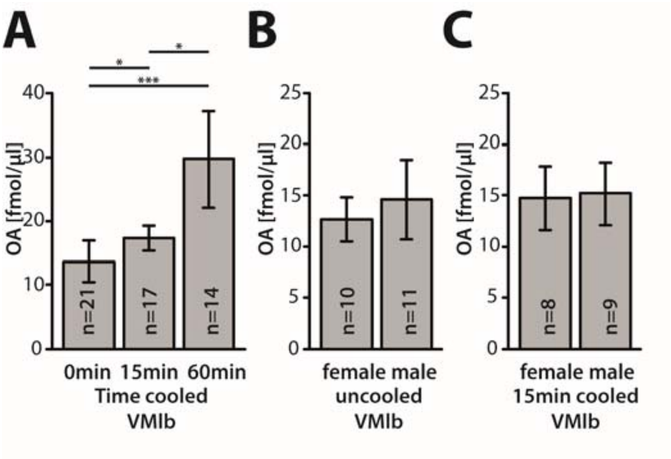

**Figure 2.13 Effect of cooling on recorded OA VMlb titers and statistical analysis of a potential sexual dimorphism in VMlb OA titers**. (**A**) Cooling of animals prior to dissection resulted in an increase of recordable VMlb OA titers over time. Significant differences were found between all three VMlb sample groups. (ANOVA, uncooled~15-min cooling, $p = 0.02$; uncooled~60-min cooling, $p = 8.59e\text{-}14$; 15 min~60 min, $p = 1.01e\text{-}9$). No sexual dimorphism was observed for (**B**) uncooled (t-test, $p = 0.17$) or (**C**) 15-min-cooled (t-test, $p = 0.97$) flies.

### *2.3.9 Sexual dimorphism of VMlb OA concentrations*

OA is a key player in modulating neuronal circuits and involved in reproduction, mating, and aggression in *D. melanogaster* in general (see chapter 1; Roeder 2005). However, it has been shown that sexual dimorphic OAergic neurons exist in females, controlling postmating behaviors (Rezával et al. 2014) and males, which are potentially involved in male specific aggression behavior (Certel et al. 2007; Certel et al. 2010; Hoopfer 2016). Furthermore, it has been shown that females contain less total neuronal OA in comparison to their male counterparts, while males contain less TA (Denno et al. 2016). To test whether such a sexual dimorphism is also pronounced in VMlb neurons, samples from uncooled male and female flies as well as 15 min cooled flies were analyzed towards their VMlb OA concentration and statistically compared. Recorded quantitative mass spectra of female VMlb neurons showed an average OA-CA concentration of 12.65 fmol/µl (n = 10, ± 2.04 fmol/µl) for uncooled animals and 17.37 fmol/µl (n = 8, ±1.79 fmol/µl) for 15 min cooled animals (Fig. 2.13 B, C). Quantitative SCMS of male VMlb soma samples revealed average OA-CA concentrations of 14.59 fmol/µl (n = 11 ± 3.70 fmol/µl) for uncooled animals and 17.40 fmol/µl (n = 9, ± 1.96

fmol/µl) for animals which had been subjected to 15 min cooling (Fig. 2.13 B, C). Statistical comparison of OA titers between sexes revealed no sexual dimorphism for both sample groups (uncooled, t-test, *p = 0.17*; 15 min cooled, t-test, *p = 0.97*; Fig. 2.13 B, C). Thus, no sexual dimorphism has been observed in the analyzed VMlb OA titers. The discrepancy of total OA content between males and females as shown by Denno et al., 2014 could arise from potentially male exclusive OAergic neurons, or from OAergic neurons which have sex specific releasing and synthesizing properties. One VUM neuron of the VMlb cluster, for example, has been shown to express the male variant of the sex determination factor *fruitless* ($fru^M$) and knock down of $fru^M$ via RNAi in three OAergic GNG neurons, including this $fru^M$ VUM VMlb neuron, led to higher male-male attraction in a behavioral test analyzing male-male aggression (Certel *et al.*, 2010). In the presented study, however, it was not possible to discriminate between specific VMlb neurons, and therefore a subcluster specific quantification was not possible. Future studies using more sophisticated UAS/GAL4 combinations will enable the targeted interrogation of somatic OA titers in this $fru^M$ OAergic VMlb neuron. Furthermore, it would be highly interesting to see whether knockdown of $fru^M$ leads to an altered somatic OA titer in these neurons.

### *2.3.10 Quantification of OA from two OA/TA cell populations*

Different cell populations are involved in different neuronal circuits, exhibiting variating activity frequencies and release modes, hence could have potentially the necessity for different somatic quantities of involved neuroactive substances. To test for variating OA/TA concentration between different OA/TA expressing cell populations, observed VMlb cell titers were compared to data obtained from somata of the ventrolateral cluster (VL), which is also labeled by Tdc2>GFP (Fig. 2.5 A). The VL population is comprised of two descending neurons per hemisphere with different projection patterns (OA-VL1 and OA-VL2) located between the antennal lobe and the ventrolateral protocerebrum in each brain hemisphere (Busch et al. 2009). OA-VL1 neurons project through the gnathal zone and the connective into all three thoracic neuromeres, whereas OA-VL2 runs posteriorly along the lateral margin of the gnathal zone (Busch et al. 2009). However, a discrimination between OA-VL1 and 2 was not possible during dissections. It has been shown that VL neurons directly modulate bitter gustatory receptor neurons (GRNs) output via a potential co-release of OA and TA, acting on the receptor Oct-TyrR (LeDue et al. 2016). However, whether VL neurons are indeed OAergic has been a matter of scientific discussion. Immunocytological stainings against Tβh showed no labeling of these cells (Zhou et al. 2008; Burke et al. 2012; Schneider et al. 2012), while other studies showed immunofluorescence against OA and TA in this cluster (Busch et al. 2009). To answer this question and compare OA titers between cell populations, VL neurons from male and female flies which were cooled for 15min on ice were analyzed by MALDI-TOF SCMS. Mass spectra from VL neurons revealed ion signals for OA-CA and TA-CA (n=9) lower than the LLOQ, however $MS^2$ experiments confirmed the presence of OA-CA in all samples and the presence of TA-CA in 5 out of 9 samples analyzed (Fig. 2.14 A, B). These results confirm the immunocytological findings that VL neurons contain OA - despite the lack of anti-Tβh immunofluorescence (Busch et al. 2009). Moreover, the confirmed presence of TA as the precursor of OA consolidates these findings even further. An explanation for the lack in Tβh immunofluorescence could be a timed expression of Tβh, rendering the soma Tβh free at given time points with an amount of OA stored in the VL somata. Another explanation would be a very low expression of Tβh, which would potentially also result in unlabeled VL neurons using immunohistochemistry. Furthermore, the target cells of VL neurons express Oct-TyrR, a receptor which reacts to both substances TA and OA in a similar fashion (Robb et al. 1994). This suggests that VL neurons probably do not need to produce large quantities of OA to modulate their downstream targets in comparison to OAergic VMlb neurons, since a co-release of TA and OA could be possible and sufficient to regulate downstream GRNs (LeDue et al. 2016).

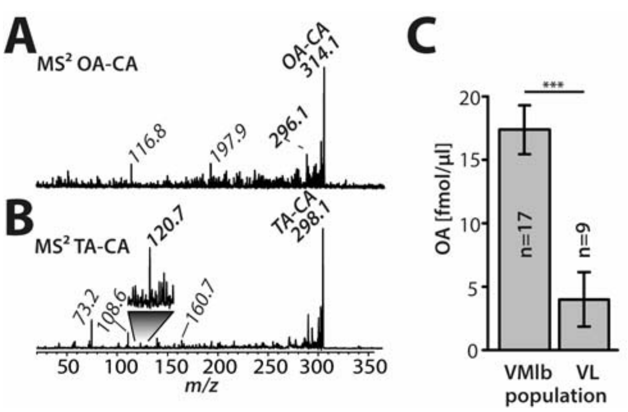

**Figure 2.14 Detection of OA-CA and TA-CA in VL neurons and comparison of OA-CA concentrations from VMlb and VL samples.** (**A**) $MS^2$ spectrum of putative OA-CA from a single isolated VL neuron. The ion identity was confirmed as OA-CA by the product ion *m/z* 296.1. (**B**) Confirmation of TA-CA from VL samples by tandem MS. The product ion *m/z* 120.7 confirmed the parent ion as TA-CA. (**C**) Statistical comparison of OA titers from VMlb and VL samples revealed a highly significant difference between the two cell populations (t-test, $p = 1.19e\text{-}10$).

Statistical comparison of recorded OA-CA titers was difficult since VL OA-CA titers were below the OA LLOQ based on FDA criteria. In order to circumvent this problem and render a statistical comparison of OA-CA titers between neuron populations possible, corresponding VL OA-CA concentrations were calculated from recorded $pMS^2$ spectra with an average concentration of 3.98 fmol/µl ($n = 9$, ± 2.03 fmol/µl). Statistical comparison of recorded VMlb and VL OA-CA titers showed a highly significant difference between the two cell clusters (t-test, $p = 1.19e\text{-}10$), highlighting that somata concentrations of neuroactive substances such as OA can vary tremendously between cell clusters with different functions, whereas intra-cluster variation seems to be limited (Fig. 2.14 C).

## 2.4 Conclusion

The developed protocol allows the identification and quantification of OA and TA from small-volume samples such as a single *D. melanogaster* soma (cell diameter 7-9 µm). Furthermore, the developed protocol is highly sensitive, reproducible, cost-effective, and fast and should be adaptable, with slight optimizations in terms of analytes of interest, soma size and type as well as organismic origin, to various single cell samples and other biogenic monoamines. Moreover, it allows the simultaneous detection of biogenic monoamines and neuropeptides in a single experiment without major interference on neuropeptide detection rates and fragmentation possibilities. Altogether, the developed protocol offers a wide range of application such as the characterization of cell-to-cell and cluster heterogeneity of neuroactive substance expression patterns and quantities, analyzing potential changes in neuroactive substance cell titers in behavioral analysis, physiological processes and natural or induced neuronal dysfunctions and pathologies. Following this idea, in Chapter 3 I focused on the analysis of potentially changing OA cell titers of VMlb neurons in socially driven aggression of male *D. melanogaster*.

# 3. Quantification of *Drosophila* VMlb octopamine titers in social driven male aggression by MALDI-TOF SCMS

The contributions are as followed: MD and SN conceptualized experiments, MD performed experiments, MD analyzed the data, SN funding.

## 3.1 Introduction

Aggression is an innate social behavior that can be observed in most sexually propagating metazoan animals (Lorenz 1963; Hoopfer 2016). This agnostic behavior commonly occurs between males trying to establish dominance, securing resources like food sources, territory or to enable access to reproductively active females. Aggression is not limited to the male sex; however, males often show a quantitatively higher aggression compared to females (Lorenz 1963). While aggression represents a part of the normal repertoire of behavior in animals and humans alike, violent aggression and maladaptive aggressive behavior in humans represents a major threat to public health and social cohesion (Craig & Halton 2009). Consistent with the observation in animals, human males show higher rates of aggressive behavior compared to females as they are ten times more likely to commit murder in comparison to females and are five times more likely to be under “correctional supervision” for criminal offences (data from the USA; Craig & Halton 2009).

In *D. melanogaster*, male aggressive behavior has been shown to be robust with different distinct behavioral actions such as wing threat, lunging, tussling and boxing (Dow & Schilcher 1975; Chen et al. 2002). This observed male aggression reflects, as in other species, competition over territory, resources or reproductive active females (Chen et al. 2002; Hoyer et al. 2008; Hoopfer et al. 2015), is genetically specified (Dierick & Greenspan 2006; Zwarts et al. 2011), connected to the fly’s social experience (Zhou et al. 2008; von Philipsborn et al. 2011; Inagaki et al. 2014; Andrews et al. 2014) and dependent on the internal state (Dickson 2008; Clowney et al. 2015; Hoopfer 2016). In *D. melanogaster* male and female show gender specific patterns in aggression, however, some agnostic actions are gender-independent (Nilsen et al. 2004). These sexually dimorphic behavioral aggression patterns require gender specific neuronal circuits or at least sex specific expression of neuronal effectors, such as receptors, in aggression promoting neuronal circuits. In *D. melanogaster* it has been shown that the male variant of the sex specific transcripts of *fruitless* (*fru*$^{M}$), a master regulator of sexual differentiation of the brain (Burtis 1993; Lee & Hall 2000), is needed for proper male aggressive behavior towards conspecific males, but also for courtship behavior towards females (Certel et al. 2007; Certel et al. 2010; Wang et al. 2012; Watanabe et al. 2017), suggesting a high interplay of the underlying neuronal circuits. Indeed, a recent study could show that a subset (8-10 neurons P1$^{a}$) of a male specific cluster of ~20 P1 neurons located at the lateral protocerebral complex, which have been shown to control and initiate male courtship behavior and song production (von Philipsborn et al. 2011; Kohatsu et al. 2011; Pan et al. 2012; Kallman et al. 2015; Clowney et al. 2015), promote also aggression when being activated by heat sensitive dTrpA1 (Hoopfer et al. 2015). *D. melanogaster* transient receptor potential cation channel A1 (TrpA1) is a temperature sensitive cation channel that can be expressed via the GAL4/UAS system and allows artificial activation of neurons by shifting corresponding flies to temperatures >28°C (Hamada et al. 2008). P1 neurons receive multiple sensory input from neurons involved in olfaction, gustation and audition and are seen as a central integrator for orchestrating courtship behavior and potentially aggression (Hoopfer et al. 2015; Auer & Benton 2016; Hoopfer 2016; Watanabe et al. 2017). Slow (<20 Hz) optogenetically activation of $P1^a$ neurons via red activatable channelrhodopsin (Inagaki et al. 2014) led to an increase in male-male aggression, while high optogenitcally activation (>30 Hz) of $P1^a$ neurons led to an increase in male-male courtship (Hoopfer et al. 2015). Furthermore, after optogenetically activation of P1 neurons male flies showed enhanced male-male aggression even after 10 mins, suggesting that activation of the $P1^a$ neurons leads to a persistent, fly-intrinsic internal state that enhances aggression (Hoopfer et al. 2015). However, how this state is maintained on a circuit level remains to be elucidated.

The decision to court or fight in male flies depends on the detection of cuticular hydrocarbons, which are produced in oenocytes (Kohl et al. 2015; Hoopfer 2016). These define a sex and species-specific pheromonal signature, which controls social behaviors such as aggression and courtship among others (Billeter et al. 2009; Fernandez et al. 2010; Kohl et al. 2015). Two specific male cuticular hydrocarbons, (z)-7-tricosense (7-T), which is detected by GRNs expressing Gr32a, and 11-*cis*-vaccenyl acetate (cVA), which is detected by olfactory receptors neurons (ORNs) expressing Or67d, have been shown to promote aggression and suppress male courtship behavior (Kurtovic et al. 2007; Wang et al. 2011). However, presentation of the two male pheromones alone is not sufficient to elicit normal levels of male aggression, a second cue such as a food source or a female has to be present in order to initiate male fighting (Yuan et al. 2014; Lim et al. 2014). By using GFP reconstitution across synaptic partners (GRASP), a technique in which two complementary fragments of GFP are expressed in different subsets of neurons and upon contact are fused to ubiquitous transmembrane proteins emitting light by excitation (Feinberg et al. 2008), recent studies could show that Gr32a GRNs project towards the GNG and form synaptic contacts with OAergic neurons in the GNG (Andrews et al. 2014). The same study showed that activation of Gr32a expressing GRNs via male cuticular hydrocarbon extracts evoked intracellular $Ca^{2+}$ response in subsets of OAergic GNG neurons, however, which of the *Tdc2-GAL4* labeled neurons were activated has not been specified yet

(Andrews et al. 2014). Furthermore, *fru*$^M$ second and third order neurons of these Gr32a GRNs project onto P1 neurons, regulating their activity (Clowney et al. 2015; Kallman et al. 2015). These *fru*$^M$ Gr32a pathways also converge onto tachykinin (TK) expressing *fru*$^M$ neurons, which have been shown to promote aggression (Asahina et al. 2014). Moreover, activation of these *fru*$^M$/TK neurons induces an arousal state, which induces aggressive behavior without the need for second cues such as food or male pheromones (Asahina et al. 2014).

Aside from the already mentioned peptidergic influence, a variety of different neuromodulators have been described to influence aggression. 5-HT and DA have been shown to regulate aggression in vertebrates and invertebrates alike (for review see Nelson & Trainor 2007; Zwarts et al. 2011). Two recent studies identified subsets of 5-HTergic (Alekseyenko et al. 2014) and DAergic neurons (Alekseyenko et al. 2013) that modulate aggression in *D. melanogaster*. Activation of 5-HT-PLP neurons via dTRPA1 led to an increased number of lunges, while silencing these neurons via expression of tetanus neurotoxin light chain (TNT), a proteolytic toxin cleaving synaptobrevin and thereby eliminating evoked synaptic vesicle release (Sweeney et al. 1995), reduced the total number of lunges in socially naive males (Alekseyenko et al. 2014). Furthermore, thermo-sensitive activation via TrpA1 or silencing via TNT of two DAergic subsets from the T1 cluster and from the PPM3 cluster lead to an increase in aggression. These two clusters project towards different areas of the central complex showing overlapping areas with expression of two different DA receptors, DD2R and DopR suggesting a modulatory role on aggression through these pathways (Alekseyenko et al. 2013).

Beside of 5-HT and DA, OA is also involved in shaping aggression in *D. melanogaster* and other invertebrates (see chapter 1; Roeder 2005). A recent study showed that *fru*$^M$ aSP2 neurons, which are located downstream of P1 neurons, are modulated by OA, probably via the OAMB receptor, and promote aggression when being genetically activated independently from general arousal (Watanabe et al. 2017). *Fru*$^M$ aSP2 neurons, however, seem not to influence aggression in a command like fashion, but rather exert a modulatory influence on agnostic behavior (Watanabe et al. 2017). *Fru*$^M$ aSP2 neurons receive input from P1 neurons, which also project downstream to cells specific for courtship (von Philipsborn et al. 2011), and from OAergic neurons (Watanabe et al. 2017). Flies fed with an OA receptor blocker mianserin and optogenetically activated P1 neurons showed reduced aggression, while genetic activation of aSP2 via NaChBac, a bacterial voltage-gated $Na^+$ channel that upon expression leads to the activation of the corresponding neuron (Ren et al. 2001; Luan et al. 2006), led to a partial rescue of the observed phenotype (Watanabe et al. 2017), suggesting a modulatory role of these neurons in aggression. By using GRASP in *fru$^M$* aSP2 neurons and OAergic neurons of the *Tdc2-GAL4* line, a potential OAergic input from Tdc2 neurons was shown (Watanabe et al. 2017). Furthermore, retrograde labeling experiments of synaptic regions of *fru$^M$* aSP2 neurons, utilizing photoactivatable GFP (Schneider et al. 2005), suggest that aside from other OAergic neurons, VUM/VPM neurons are possibly part of the OAergic input to these neurons (Watanabe et al. 2017).

Two subpopulations of VUM/VPM neurons of the Tdc2-GAL4 line have been shown to be required for normal levels of aggression. For three VUM/VPM neurons, the VPM1, VPM2 and VUMd3 (Busch et al. 2009), expression of the male specific *fru$^M$* transcription factor has been shown (Certel et al. 2007; Certel et al. 2010). Feminization by expression of *transformer* (Mundiyanapurath et al. 2009) in these neurons led to an increased male-male courtship, impairing male action selection (Certel et al. 2010). These neurons are interesting candidates for modulation of *fru$^M$* aSP2 neurons by OA, due to their expression of *fru$^M$* and their promotion of male-male courtship when being feminized. VPM1 and VPM2 neurons are located in the close vicinity of VMmd, whereas the VUMd3 neuron is located in the VMlb cluster (Busch et al. 2009). Another interesting VUM/VPM population, which has been shown to be essential for aggression, is a small subset of the VMlb cluster located in the GNG (Zhou et al. 2008). By using the yeast repressor GAL80, which blocks GAL4 activity by binding to its transcriptional activation domain (Suster et al. 2004), in OAergic neurons co-expressing choline acetyltransferase (Cha), the rate limiting enzyme for the production of acetylcholine (Salvaterra & McCaman 1985), they limited the GAL4 expression to a small subset of 2-5 VMlb OAergic neurons (Zhou et al. 2008). By a combination of this GAL4 expression in an OA devoid Tβh$^{nM18}$ line (Monastirioti et al. 1996) and subsequent activation of this labeled subset by NaChBac, they were able to rescue the Tβh$^{nM18}$ mediated phenotype, which showed highly reduced aggression behaviors (Zhou et al. 2008). However, a clear identification of the activated VMlb neurons in these experiments, their projections and targets remains unresolved.

As introduced, a subset of OAergic VMlb neurons are suggested to play an integral part of the neuronal circuit promoting male aggression in *D. melanogaster*, probably mediated by the activation of Gr32a expressing GRNs (Certel et al. 2007; Certel et al. 2010; Andrews et al. 2014). Since it has been shown that social experience/contact has a tremendous effect on aggression levels in males via male-specific pheromones, the question arouses whether such social experience/contact has a direct effect on detectable VMlb OA titers, which would corroborate a change of activity and hint towards a change in releasing frequency of OA from these neurons. In order to tackle this question, in this chapter single VMlb neurons, labeled by Tdc2>GFP (see chapter 2), were isolated from socially naïve and experienced male *D. melanogaster* and analyzed towards their OA content by using the protocol for quantitative MALDI-TOF SCMS (see chapter 2).

## 3.2 Materials and Methods

### *Chemicals*

All used chemicals were purchased from SIGMA-Aldrich (Steinheim, Germany), if not stated otherwise.

### *Synthetic solutions*

Stock solutions of OA-hydrochloride, TA-hydrochloride, OA(*d3*), (CDN Isotopes, Pointe-Claire, Canada) and TA(*d4*) (CDN Isotopes) were prepared in 50% MeOH/TraceSELECT® water at a concentration of 10 nmol/µl, stored at 4°C in darkness and were used to prepare dilution series. Stock solutions of synthetic biogenic amines were replaced after two months, dilution series after three weeks.

### *Derivatization reagent*

CA was prepared in 100% MeOH at a concentration of 23 mg/ml and centrifuged at 13000 rpm at 4°C for 10 min. 5 µl of the supernatant was diluted in 150 µl 50% MeOH/TraceSELECT® water at a concentration of 0.76 mg/ml and finally centrifuged for 10 mins at 13000 rpm and 4 °C, as described by Diesner & Neupert (Diesner & Neupert 2018; see chapter 2). The derivatization solution was prepared fresh daily.

### *Fly Strains*

5 days old adults of both sexes were used. Flies were raised on standard cornmeal, molasses, yeast, agar medium on a 12 h/12 h light-dark cycle at 25°C and 60% humidity. The following fly strains were used: *Tdc2-GAL4* (Cole et al. 2005; Bloomington #9313); 10xUAS-*IVS-mCD8::GFP* (Bloomington #32186).

### *Isolation experiments*

Initial experiments were conducted on 5 d old adult males and females which were reared in groups of about 20-30 flies. For isolation experiments, late male pupae were transferred into clean 1.5 ml Eppendorf tubes with a small hole in the cap for ventilation and filled with a small amount of standard *Drosophila* food. Isolation fly tubes were positioned in the climate chamber with at least 5 cm space between adjacent tubes to prevent potential “grouping effects”. For social experiments, 4-day old isolated males were grouped in pairs for 24 h in a fresh isolation vial.

### *Single cell dissection*

Single cell dissections were prepared as described earlier (Diesner & Neupert 2018; see chapter 2): Flies were immobilized 15 min on ice prior to dissection. The brain was removed in ice cold dissection buffer (NaCl 126 mM, KCl 5.4 mM, $NaH_2PO_4$ 0.17 mM, $KH_2PO_4$ 0.22 mM, pH 7.4) under an epifluorescence stereomicroscope. For single-cell dissections, brain samples were transferred to a fresh drop of ice cold dissection buffer containing 33% glycerol. The ganglionic sheath around the area of a GFP-labeled cell of interest was removed and the cell soma manually picked and transferred to a MALDI-TOF sample plate, by an uncoated glass capillary. Excessive dissection saline was removed using the same glass capillary. Residual glycerol surrounding the isolated soma was washed off with 50% MeOH/TraceSELECT® water. Washing was performed multiple times with a fresh glass capillary until the glycerol was completely removed. However, the placed cell soma was left uncovered by the washing solution to prevent a possible loss of analytes. Only one neuron soma was isolated from a single brain sample. Furthermore, a single dissection block, processing multiple brains, did not exceed one hour.

### *Single cell sample preparation for quantitative MALDI-TOF MS*

Samples were prepared as described by Diesner & Neupert (Diesner & Neupert 2018; see chapter 2). Dissected single cell samples were covered with 18.4 nl of an equimolar mixture of OA(*d3*) and TA(*d4*) with a concentration of 100 fmol/µl. After air-drying, 9.2 nl of CA were added to the sample spots and left to air-dry. Finally, the sample spots were covered with 18.4 nl of CHCA and dried under a constant stream of air. All solutions were applied using a pulled glass capillary fitted in a nanoliter micro injector (nanoliter 2000, World Precision Instruments, FL, USA). Between each application step, the remaining solution in the glass capillary was removed and the capillary rinsed two-times with 100% TraceSELECT® water, 50% MeOH/TraceSELECT® water followed by 100% MeOH before air-drying. CHCA was prepared fresh daily in 80% MeOH/TraceSELECT® water at a concentration of 1.43 mg/ml. The resulting mixture was centrifuged for 10 min at 15.000 rpm at 4 °C and stored at 4 °C and darkness until usage.

### *Quantification and standard curve calculation*

Preparation of dried droplet samples was modified from Persike and colleagues (Persike et al. 2010) and used as described in Diesner & Neupert, 2018 (see chapter 2). To calculate standard curves, 18.4 nl of an equimolar mixture of synthetic OA and TA was applied onto a MALDI sample plate in a concentration range from 100 to 2.5 fmol/µl. After applied synthetic solutions were allowed to air-dry, sample spots were covered with 18.4 nl of an equimolar mixture of OA(*d3*) and TA(*d4*) with a constant concentration of 100 fmol/µl. After letting the spot air-drying a second time, each spot was covered with 9.2 nl of CA. The resulting spot was allowed to air-dry again and ultimately covered with 18.4 nl CHCA and dried under a constant airflow.

### *MALDI-TOF MS*

Mass spectra were acquired using an UltrafleXtreme MALDI-TOF/TOF mass spectrometer (Bruker Daltonik GmbH, Bremen, Germany). All MS acquisitions were performed under manual control in reflector positive ion mode. The instrument was calibrated for the mass range *m/z* 0-400 using prominent internal CHCA matrix ion signals as described earlier (Persike & Karas 2009). All mass spectra were acquired with 2000 laser shots with a laser frequency of 333 Hz.

### *MS$^2$ experiments*

MS$^2$ experiments were performed using LIFT technology, with an acceleration set to 1 kV. The number of laser shots for a single MS$^2$ spectra varied from 1000 to 2000 shots, depending on ion signal quality. To verify OA and OA(*d3*), tandem mass spectra were acquired without collision gas. For the validation of TA and TA(*d4*), fragmentations were performed in CID mode, with argon as the collision gas. For quantification experiments of OA and TA, mass spectra were acquired in parent ion mode with fixed laser intensity. The parent ion window was set from *m/z* -0.4 to +6. Each mass spectrum was acquired with 2000 laser shots. In general, a signal was considered to be detected with an S/N ratio $\geq$ 3. The data obtained in these experiments were processed with the FlexAnalysis 3.4 software package (Bruker Daltonik GmbH, Bremen, Germany). For quantitative analysis, only unprocessed data were used.

### *Method validation and Statistics*

Validation of standard curves followed the ±15/20 criteria published by the FDA for bioanalytical methods (FDA 2013). All data points for standard curve calculation are averages of at least three replicates. Linear ranges, accuracy, RSDs and linearity ($R^2$) were calculated with Microsoft Excel 2010 and/or R 3.1.3 (R Development Core Team). Data points were tested for normal distribution using a one-sample Kolmogorov-Smirnov test and were analyzed by one-way analysis of variance (ANOVA). Comparative statistics were calculated in R 3.1.3.

## 3.3 Results and Discussion

### *3.3.1 Influence of age, sex and genetic construct on OA VMlb titers*

The age, sex and inserted genetic constructs can affect total neuroactive substance titers in nervous systems, which has been shown for biogenic monoamines in different developmental stages and various genetic lines in *D. melanogaster* (Fang et al. 2011; Denno et al. 2016). In the present chapter a different UAS-*mCD8::GFP* reporter line and age synchronized flies were used compared to previous experiments (see chapter 2; Diesner & Neupert 2018). To analyze a potential influence of the alternatively used genetic construct and the age on male and female VMlb OA titers, single VMlb somata of 5 d old male and female Tdc2>GFP *D. melanogaster* were dissected, their OA titers analyzed by MALDI-TOF SCMS and recorded results compared to an previously obtained dataset (see chapter 2; Diesner & Neupert 2018; Fig. 3.1 A, B). Recorded mass spectra of single VMlb somata of 15 min cooled 5 d old male flies revealed an average concentration of 16.13 fmol/µl OA (n =7; ± 3.55 fmol/µl; Fig. 3.1 B), while mass spectra of 5 d old females showed an average concentration of 17.25 fmol/µl OA (n = 7; ± 3.23 fmol/µl; Fig. 3.1 B). Statistical comparison to the data set from Diesner & Neupert 2018 (see chapter 2) from flies which were ≥ 5 d old and inhibited a different UAS-*mCD8::GFP* construct showed no significant differences in VMlb OA titers between all analyzed groups (ANOVA, $p = 0.995$; Fig. 3.1 B). The recorded results corroborate earlier findings of the dataset from Diesner & Neupert (2018), which did not show any sexual dimorphism in somatic VMlb OA titers (see chapter 2; Diesner & Neupert 2018). Additionally, the alternatively used genetic construct, the 10xUAS-*IVS-mCD8::GFP* reporter, as well as the synchronization of the age did also not affect somatic OA VMlb levels compared to previous results (Diesner & Neupert 2018; see chapter 2).

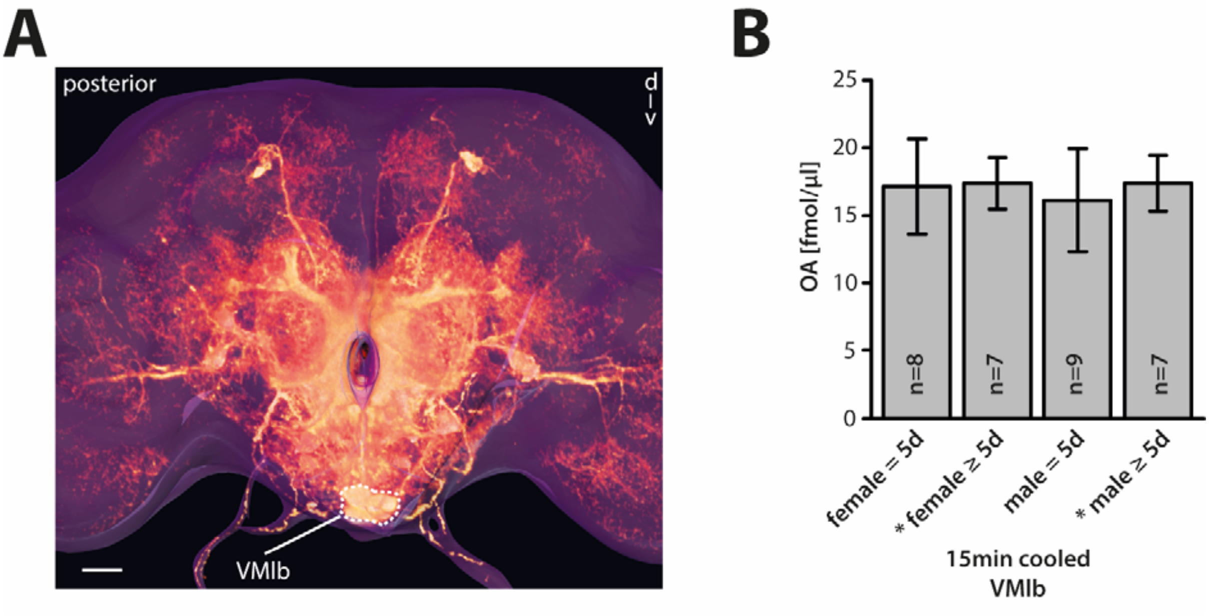

**Figure 3.1 OA VMlb titers do not differ between sexes, fly age and inserted genetic construct.** (**A**) Posterior view of a 3D reconstruction of a Tdc2>GFP labeled adult Drosophila brain. The VMlb cluster is highlighted. Scale bar = 25 µm (**B**) Statistical comparison of OA VMlb titers of groups of female and male flies with either fixed age and alternatively used reporter line (5d) or mixed age (≥5d) revealed no significant differences (ANOVA, *p = 0.995*). Asterisk = data adapted from chapter 2, Diesner & Nerupert, 2018.

### 3.3.2 *Influence of social experience on VMlb OA titers*

In order to analyze a potential effect of social contact on VMlb OA titers, late stage male Tdc2>GFP pupae were transferred to 1.5 ml Eppendorf tubes filled with a small drop of standard food and a small ventilation hole in the cap. After eclosion and a 5 d long social isolation, single VMlb neurons were dissected from these isolated males and OA titers analyzed by MALDI-TOF SCMS. Recorded mass spectra of VMlb neurons showed an average OA titer of 12.08 fmol/µl (n = 12; ± 1.63 fmol/µl), which was close to the LLOQ of the used quantitative MALDI-TOF SCMS technique (see chapter 2; Diesner & Neupert 2018). Statistical comparison to VMlb OA titers from 5 d old males reared in mixed groups showed a significant lower OA VMlb titer in isolated males (ANOVA, *p = 0.003*; Fig. 3.2). To verify that this decreased OA VMlb titer is a direct result of social experience, 4 d old isolated males were grouped in pairs for 24 h prior to OA VMlb analysis by MALDI-TOF SCMS. Mass spectra recorded by MALDI-TOF SCMS of single VMlb neurons of pairwise regrouped males revealed an average OA VMlb titer of 15.53 fmol/µl (n = 10; ± 2.43 fmol/µl; Fig. 3.2), which did not differ significantly compared to the observed titers from mixed group reared males (ANOVA, *p > 0.05*). However, comparison of OA VMlb titers between socially isolated males and pairwise regrouped flies showed a significant higher OA titer in regrouped flies (ANOVA, $p = 0.005$), suggesting a direct impact of social experience on OA VMlb titers.

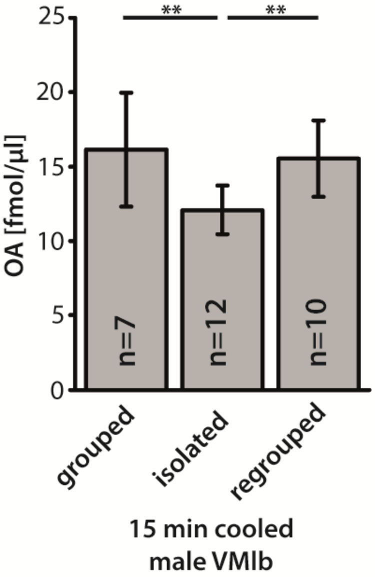

**Figure 3.2 Statistical comparison of OA VMlb titers recorded by MALDI-TOF SCMS in socially naïve and experienced 5 d old male *D. melanogaster*.** OA VMlb titers of male flies that were raised in mixed groups differed significantly from socially naïve males (ANOVA, $p = 0.003$). Pairwise regrouping of 4 d old males for 24 h led to a significant increase, compared to socially isolated males (ANOVA, $p = 0.005$), in OA VMlb titers, to about the same level as observed in grouped males (ANOVA, $p > 0.05$).

Finally, female OA VMlb titers from mixed grouped raised females (17.25 fmol/µl; ± 3.23 fmol/µl) showed nearly identical OA titers recorded from males which had been paired for 24 h (16.13 fmol/µl; ± 3.55 fmol/µl; Figure 3.1 B). This is not too surprising, since only three VUM/VPM neurons as well as second and third order downstream targets of Gr32a expressing GRNs express $fru^M$, and therefore show male specific characteristics (Certel et al. 2010; Weiss et al. 2011). It can be speculated that the neuronal circuit driving social interaction via Gr32a expressing GRNs, is somewhat similar in females and males and shows a similar upregulation of somatic OA titers in VMlbs. Furthermore, it is likely that the downstream targets of OAergic VUM/VPM neurons differ between males and females, leading to the activation or modulation of different microcircuits in the two sexes and ultimately to the sexual dimorphic behavioral output. However, whether female OAergic VMlb neurons indeed show a similar upregulation of somatic OA titers upon social interaction will be the focus of future studies.

The increased VMlb OA titer is likely a direct result by a higher activity of VMlb neurons which is mediated via the input from male pheromone sensing Gr32a expressing GRNs (Andrews et al. 2014). So far a direct correlation of a higher activity and increased somatic neuroactive substance content has not been shown, however, such a physiological reaction would be quiet conceivable. The higher activity of a neuron leads to a more frequent release of neuroactive substance and the faster diminished pool of the corresponding neurotransmitter, -modulator or -hormone has to be replenished accordingly, which ultimately leads to an increased synthesis rate and thus a higher somatic OA titer. Another explanation would be that the higher somatic concentration corresponds to a higher OA concentration per releasing event, with an unchanged activity frequency of VMlb neurons. Both possibilities would enable a longer activation of OA receptors on downstream targets and/or a more widespread volume transmission potentialy affecting other hitherto unreached targets.

The data presented in this chapter was recorded from single VMlb neurons, the same cell cluster which was analyzed in experiments described in chapter 2. The VMlb cluster can be separated into distinct subpopulations, VPM4 and 5, each comprised of 2 cells per brain as well as 4 VUM neuron classes (VUMd1-3, VUMa4; ~4-5 cells; see chapter 1; Busch et al. 2009; Busch & Tanimoto 2010; Schneider et al. 2012). However, in the presented experiments, as well as in experiments of chapter 2 (Diesner & Neupert 2018), it was not possible to differentiate between the different cell types during dissections. Moreover, although it is suggested that VPMs and VUMs do not share the same developmental origin (Klämbt et al. 1991; Busch & Tanimoto 2010) and due to the fact that different neuron clusters can have variating somatic neuroactive substance titers (see chapter 2; Diesner & Neupert 2018), it is interesting that all analyzed VMlb neurons share similar somatic OA concentrations. This hints towards similar capacities in OA synthesis, storage and release as well as similar inputs and activation of the analyzed neurons.

While the exact actions of single neurons comprised in this cluster have not been characterized, some functional data exists. VPM4 and 5 have been shown to be involved in short-term appetitive memory formation, partly via the α-adrenergic like OAMB receptor which is expressed in a subset of mushroom body targeting DA neurons, located in the protocerebral anterior medial (PAM) cluster (Burke et al. 2012). A more recent study showed that VUMa4 neurons, which are present in all three clusters, are involved in shifting the preference for ethanol containing food sources to a less attractive ethanol free food source upon activation, however, when activated with a broader subset of OAergic neurons this decision was reversed

(Claßen & Scholz 2018). The authors therefore argue that cell specific OA signaling orchestrates, in combination with olfactory cues, the decision of contrary behavioral outputs. Such a proposed principal could also hold true in the case of aggressive behavior, since socially naive flies show a more intense aggressive behavior, in combination with a lower OA titer in analyzed VMlb neurons compared to socially experience flies, which exhibited higher OA VMlb titers. Thus, a more intense OA signaling from VMlb neurons and potentially other co-activated OAergic VUM/VPM neurons in socially experienced flies could lead to a shift from a highly aggressive to a more moderate aggressive behavioral output.

While it has been shown that sexual experience can result in a long lasting state decreasing male-male aggression (Yuan et al. 2014) the question arises how such states are maintained in the CNS. Are these states maintained for example by a prolonged or increased release of neuromodulators from activated neurons, are target neurons affected in their signaling characteristics over such long time periods by activation of the corresponding receptors and their signaling cascades, and/or does the potentially altered aminergic signaling leads to a change in synaptic wiring in downstream neural circuits? A good example how experience can influence male specific synaptic wiring through aminergic signaling during development comes from the nematode *C. elegans*. In *C. elegans* it has been shown that OA and 5-HT control feeding related behaviors such as locomotion and aversive memory. 5-HT is responsible for controlling well-fed conditions while OA is involved in signaling starvation mediated behaviors (Harris et al. 2010; Churgin et al. 2017). Bayer & Hobert could show in a recent study that starvation of juvenile *C. elegans* leads to an altered male-specific pruning of neuronal connections, allowing the adult to retain juvenile sensory acuity and results in the loss of an adult behavioral sexual dimorphism (Bayer & Hobert 2018). Moreover, it was shown that during starvation the OA synthesizing gene *tßh-1* is upregulated in the sex-shared RIC interneuron and at the same time the OA receptor expressing downstream ADF neuron exhibits a downregulation of the 5-HT synthesizing enzyme *tryptophan hydroxylase-1* (Noble et al. 2013; Bayer & Hobert 2018). Finally, they could reveal that the pruning of male-specific connections depend on the expression of the *ser-4*/5-HT1A receptor in the downstream PHB neuron, thus suggesting that a higher OA release leads to a low 5-HT release and ultimately an low activation of *ser-4*/5-HT1A which directly controls synaptic connectivity (Bayer & Hobert 2018).

In male *D. melanogaster* it has been shown that repetitive fighting promotes a winning or losing state, which has also been shown in other species (Hsu et al. 2006; Kim et al. 2018). By coupling a winning or losing state to olfactory cues through classical conditioning, it has been shown that male flies can associate valence with these states and thus, such states could be maintained by the neuronal circuits responsible for appetitive and aversive memory (Kim et al. 2018). These circuits involve subsets of DAergic neurons of the PAM and protocerebral posterior lateral 1 (PPL1) clusters that target mushroom body Kenyon cells and it has been shown that PAM neurons receive modulating input by OA in adults, which is potentially released from VMlb neurons (Burke et al. 2012; Kim et al. 2018). Kenyon cells in the mushroom body receive sensory input from olfactory projection neurons while aversive valence is relayed via DAergic PPL1 neurons and appetitive valence is signaled by DAergic PAM neurons (Schwaerzel et al. 2003; Cognigni et al. 2018). It has been shown that olfactory cues are represented by the activity of small subpopulations of these Kenyon cells (Campbell et al. 2013; Lin et al. 2014; Cognigni et al. 2018). Furthermore, aversively reinforcing DAergic PPL1 neurons overlap with approach-promoting mushroom body output neurons (MBONs), while DAergic PAM neurons which have been described as largely appetitively reinforcing overlap with avoidance-promoting MBONs (Cognigni et al. 2018). It has been suggested that DA released by PPL1 or PAM neurons modulates synaptic plasticity between Kenyon cells and MBONs thus shaping MBON activity leading to aversive or approaching behaviors (Cognigni et al. 2018). In *D. melanogaster* larvae, which show a greatly reduced neuron number with a similar outline of connections between DAergic input neurons, Kenyon cells and MBONs, optogenetically activation of OA/TAergic neurons leads to induced appetitive memory formation and there is evidence that a physiological activation is mediated by sucrose detecting GRNs to OA/TAergic VUM neurons in the GNG (Schwaerzel et al. 2003; Schroll et al. 2006; Honjo & Furukubo-Tokunaga 2009). In summary, this suggests that the social interaction mediated enhanced VMlb OA concentration and an potentially corresponding enhanced OA release directly modulate appetitive PAM neurons and Kenyon cells and thus could lead to the formation of appetitive memory and long lasting internal states affecting the behavioral output (Burke et al. 2012; Cognigni et al. 2018). Aside from this, OAMB expressing *fru*$^{M}$ aSP2 neurons, which are located downstream of P1$^{a}$ neurons, have been shown to be activated by bath-applied OA in brain explants and optogenetical activation of P1$^{a}$ neurons with fed OA led to enhanced aggression in adult male *D. melanogaster* (Watanabe et al. 2017). Furthermore, first evidence has been provided that OAergic VUM/VPM neurons converge on *fru*$^{M}$ aSP2 neurons, aside from other OAergic neurons, and thus would hint towards a circuit that connects pheromone detecting

GRNs, OAergic VUM/VPM neurons and aggression promoting neurons (Zhou et al. 2008; Watanabe et al. 2017).

## 3.4 Conclusion

The protocol developed as part of this thesis (Diesner & Neupert 2018; see chapter 2) was used to elucidate an upregulation of somatic OA VMlb titers through social interaction in adult male *D. melanogaster*. To my knowledge this represents the first reported case of a mass spectrometric quantified change in somatic OA concentrations detected directly from individual cells of intact brains, between two behavioral states. While the upregulation of somatic neuroactive substance titers hints towards a more concentrated or prolonged release of these molecules, such a relationship has to be proven in future studies. Such studies could involve qualitative and quantitative measurement of released substances via cyclic voltammetry (Majdi et al. 2015; Pyakurel et al. 2016) or genetically encoded selective fluorescent sensors (Liang et al. 2015; Patriarchi et al. 2018) but also genetic encoded markers of neuronal activity such as GCaMP (Chen et al. 2013). Aside from analyzing somatic biogenic monoamine titers between behavioral states, the presented strategy yields also the possibility to analyze the temporal course of modulated somatic neuroactive substance titers in single neurons. Moreover, by combing the demonstrated SCMS protocol with the controlled application of neuroactive substances or drugs to brain explants or cell cultures their effect on somatic titers in neurons of interest could be studied.

# *4.* Mass spectrometric detection of octopamine and tyramine from intracellular recorded desDUM neurons of *Carausius morosus*

The results of this chapter are part of the manuscript: Stolz T, Diesner M, Neupert S, Hess M, Delgado E, Pflüger HJ, Schmidt J. *Descending octopaminergic interneurons modulate leg load evoked motor neuron activity in stick insects.* 2018, in preparation.

The results are also discussed in the connected
Ph.D. Thesis of Dr. Thomas Stolz (Stolz 2018).

The authors contributions to this collaborative project are as followed: TS, JS general conceptualization, TS and JS electrophysiological experiments, MD and SN single cell dissection and mass spectrometric experiments (MD contributed 12 samples and the blind sample, SN 2 samples), MH backfill experiments, ED and HJP anti-OA immunohistochemical experiments, the respective authors analyzed their collected data, TS and MD created figures, TS, JS, MD, SN, HJP wrote the manuscript.

## 4.1 Introduction

For animals locomotion is essential for their success and survival in their respective habitat. By using targeted locomotion it is possible to access food sources, find mating partners, evade predators or unfavorable environmental obstacles. However, neuronal systems coordinating locomotion have to be flexible due to their constant adaptation to a changing environment. This is especially true for animals using terrestrial based locomotion, due to the variable nature of the ground and encountered obstacles as well as due to the different locomotor modes such as walking, climbing and running.

Locomotion in general is coordinated by motor neurons (MNs) activating and inhibiting different subsets of skeletal muscles. MNs themselves are controlled by various interneurons that are part of larger neuronal circuits coordinating and generating rhythmic motor activity, so called central pattern generators (CPGs). In arthropods these CPGs are situated in the thoracic ganglions, while in vertebrates, CPGs are located in the spinal cord (Chrachri & Clarac 1987; Büschges et al. 1995; Marder & Rehm 2005; Kiehn 2006; Büschges et al. 2011). CPGs receive input from descending neurons of the brain and the GNG, which are crucial for the initiation, cessation, temporal coordination and selection of task-specific motor programs (Bidaye et al. 2014; Bidaye et al. 2017). Additionally, feedback from sensory leg organs, such as campaniform sensilla or femoral chordontonal organs, is used for the coordination of interneurons or MNs directly, thus offering the system a mechanism for adaptation and plasticity (Bässler & Büschges 1998; Windhorst 2007; Tuthill & Wilson 2016; Bidaye et al. 2017). Furthermore, the properties and connections of these single neuronal components of locomotor systems can be altered and tuned by neuromodulatory input (Katz & Harris-Warrick 1990; Marder 2012). This neuromodulatory input is essential for the needed flexibility and adaptation of these systems.

Neuromodulation of neuronal systems can be classified as intrinsic or extrinsic depending on whether the neuromodulatory neuron is an integral part of the target circuit or whether it is located outside of such (Katz 1995; Marder 2012). The release of corresponding neuroactive substances in intrinsic neuromodulation is depending on the activity of the neuronal circuit itself, whereas in extrinsic neuromodulation the release is decoupled of the activity of the target circuit (Katz 1995). A fitting example for intrinsic neuromodulation of locomotor systems are serotonergic neurons of a CPG controlling escape swimming in the mollusk *Tritonia diomedea*

(McClellan et al. 1994). A good example for extrinsic neuromodulation of locomotor systems represents the neuropeptidergic modulation of a multifunctional CPG controlling ingestion and egestion in *Aplysia.* (Jing et al. 2007). Here, the aplysian orthologue of the neuropeptide Y (aNPY) released from gut afferents within the CNS acts on a specific CPG interneuron to promote egestion (Jing et al. 2007; Taghert & Nitabach 2012).

While different neuroactive substances have been shown to affect the activity of locomotor systems (e.g. neuropeptides, amino acid derived transmitters; Katz 1995; Marder 2012) the focus in this study lied on the biogenic monoamine OA. In insects, the invertebrate noradrenalin homologue OA has been shown to affect various neuronal components of locomotor systems such as the activity of MNs, CPG neurons, coordinating neurons and sensory organs (Bräunig & Pflüger 2001; Roeder 2005; Marder 2012; see chapter 1). In the Indian stick insect *C. morosus* the activity of MNs is controlled by tonic depolarization as well as rhythmic excitatory and inhibitory inputs (Büschges 1998; Ludwar et al. 2005; Westmark et al. 2009; Rosenbaum et al. 2015), however, the underlying neural source of this tonic depolarization drive to MNs during walking is largely unknown. In order to elucidate potential neuroactive substance candidates Westmark and colleagues analyzed the pharmacological characteristics of the described tonic depolarization and suggested a modulatory role of OA in this system (Westmark et al. 2009). However, only limited data is available concerning the neuronal basis of this OAergic modulation in insect nervous systems.

The main sources of OA in insect nervous system are VPM/VUM/DUM neurons of the brain, GNG and segmental ganglia (see chapter 1). Gnathal OAergic desDUM neurons of the Locust have been shown to project to neuropil regions in the thoracic ganglia, which processes information of leg sensory organs and therefore represent interesting candidates for extrinsic OA modulation on thoracic locomotor systems controlling walking (Bräunig & Burrows 2004). Retrograde labelling experiments of GNG posterior connectives in *C. morosus* revealed a potentially homologous cluster of ~6 large neurons in the posterior part of the GNG with bilaterally descending axons (Heß 2008). Because of their morphological homology to the aforementioned desDUM neurons in the Locust, these neurons could be the source of thoracic OA modulation, however, whether these neurons indeed synthesize OA was not elucidated.

This chapter is dedicated to unravelling whether aforementioned desDUM neurons in *C. morosus* indeed contain somatic OA/TA. Simultaneously, the given aim allowed to test whether the developed MALDI-TOF SCMS protocol (see chapter 2; Diesner & Neupert 2018) is also applicable to single neurons which underwent intracellular recording. Therefore, electrophysiologically identified desDUM neurons were injected with dextran-tetramethylrhodamine for identification, dissected and subsequently analyzed by MALDI-TOF SCMS.

The described experiments were part of a larger effort to characterize the morphological and electrophysiological properties of *C. morosus* desDUM neurons and their impact on thoracic locomotor systems. My part of this project was to analyze the intracellular recorded desDUM neurons towards a potential OA/TA content by MALDI-TOF SCMS, therefore mainly these results are discussed. Readers who are interested in the electrophysiological in- and output of these neurons are referred to the doctoral thesis by T. Stolz (Stolz 2018; Stolz et al., 2018 *in preperation*).

## 4.2 Materials and Methods

### Chemicals

All used chemicals were purchased from SIGMA-Aldrich (Steinheim, Germany), if not stated otherwise.

### Synthetic solutions

Solutions of OA-hydrochloride, TA-hydrochloride, OA(*d3*), (CDN Isotopes, Pointe-Claire, Canada) and TA(*d4*) (CDN Isotopes) were prepared in 50% MeOH/TraceSELECT® water at a concentration of 100 fmol/µl, stored at 4°C in darkness. Prepared solutions of synthetic biogenic amines were replaced after three weeks.

### Derivatization reagents

CA was prepared in 100% MeOH at a concentration of 23 mg/ml and centrifuged at 13000 rpm at 4°C for 10 min. 5 µl of the supernatant was diluted in 150 µl 50% MeOH/TraceSELECT® water at a concentration of 0.76 mg/ml and finally centrifuged at 15000 rpm for 10 min at 4° C and stored at 4° C and darkness upon usage, as described by Diesner & Neupert (Diesner & Neupert 2018; see chapter 2).

### *Animals*

For all experiments female *C. morosus* from a colony maintained at the University of Cologne were used. Animals were reared at 28°C under a 12 h/12 h light-dark cycle, had access to water and were fed ad libitum with fresh cut parts of *Rubus sp.*.

### *Semi intact C. morosus preparations*

From adult female *C. morosus* all legs were removed at the mid-level of the coxa, except of one middle leg. The animal was attached to a platform using dental cement (Protemp II, 3M ESPE Dental AG, Seefeld, Germany) with the dorsal side pointing up. To gain access to the brain, the GNG, the mesothoracic ganglion and attached lateral nerves, the head capsule and thorax were opened dorsally by cutting corresponding rectangular windows into the cuticle. Subsequently, surrounding fat tissue, the gut and attached trachea were removed and the body cavity was rinsed and filled with saline (NaCl 180 mM; KCl 18 mM; $CaCl_2$ 8 mM; $MgCl_2$ 25 mM; HEPES buffer 10 mM; pH 7.2; Weidler & Diecke 1969).

### *Intracellular recordings*

For intracellular recordings of desDUM neurons, the still attached GNG was placed onto a wax coated steel platform. Small crystals of Pronase E (Merck, Darmstadt, Germany) were placed onto the ganglionic sheath for about 10-20 s to allow an optimal electrode penetration. Excessive enzyme was thoroughly washed off with fresh saline. Intracellular recordings were obtained from desDUM somata, located at the posterior part of the GNG. Borosilicate glass micropipettes (GB100-TF8P; Science Products, Hofheim, Germany) with resistances of 15-35 MΩ were manufactured on a filament puller (P-97; Sutter Instruments, Novato, CA, USA). The electrodes were filled with a mixture of 0.1 M KCl and 3 M $CH_3CO_2K$. Cells were identified by their large-amplitude (>70 mV), overshooting soma action potentials (APs), pronounced undershoot (>7 mV) and the generation of APs in response to gentle touch of the abdomen with a paintbrush. Membrane potentials were amplified with an intracellular amplifier (SEC-10L; NPI Electronics, Tamm, Germany) in bridge mode. Recordings were stored on a PC using Spike 2 software (Version 7.09, Cambridge Electronic Design, Ltd., Cambridge, UK).

### *Single cell dissection*

After intracellular recordings identified desDUM neurons, individual somata were marked by dextran-tetramethylrhodamine (5%, 3000 Dalton [MW], Invitrogen, Eugene, Oregon, USA) injection. After a successful staining the whole GNG was removed from the animal and transferred to a small silgard filled dissection dish with fresh saline. After a 30 min recovery time on ice, the isolated GNG was again transferred to an identical dissection dish filled with saline containing 33% glycerin (v/v). Marked cell bodies were visualized and dissected under a fluorescence stereomicroscope (Lumar V12; Carl Zeiss AG) using fine forceps (Dumont #5; Fine Science Tools, Heidelberg, Germany) and, immediately after isolation, transferred onto a MALDI sample plate using a glass capillary. Any excess dissection buffer was removed with the same glass capillary. Subsequently, remaining glycerol was washed off with 50% MeOH/$H_2O$ using a fresh glass capillary.

### *Sample preparation*

Sample preparation was adapted from Diesner & Neupert, 2018 (see chapter 2). Intact individual desDUM somata or small tissue parts of the anterior GNG were covered with 18.4 nl of isotopically marked internal standard, containing 100 fmol/µl OA(*d3*) and 100 fmol/µl TA(*d4*) dissolved in 50% MeOH/$H_2O$. Each sample was air-dried in darkness at room temperature. Subsequently, 9.2 nl of CA was applied and samples were air-dried again. In the last step, 18.4 nl of CHCA was applied as matrix solution and rapidly dried under a constant air-stream. For control experiments, biological samples were either replaced by 18.4 nl 100 fmol/µl synthetic OA and TA or, for blanks, only internal standard was used. CHCA was prepared fresh daily in 80% MeOH/TraceSELECT® water at a concentration of 1.43 mg/ml. The resulting mixture was centrifuged for 10 min at 15.000 rpm at 4 °C and stored at 4 °C and darkness until usage. All solutions were pipetted using a micro injector (Nanoliter 2000; World Precision Instruments, Sarasota, FL, USA) under a stereomicroscope (STEMI 2000; Carl Zeiss AG) equipped with a KL 1500 LED light source (Schott, Mainz, Germany).

### *MALDI-TOF MS*

Samples were analyzed with an UltrafleXtreme MALDI-TOF/TOF mass spectrometer (Bruker Daltonik Gmbh, Bremen, Germany) under manual control in reflectron positive ion mode in a mass range of *m/z* 0-400. All mass spectra were acquired with a fixed laser intensity. The instrument was calibrated using prominent matrix signals as reported earlier (Persike & Karas 2009; Diesner & Neupert 2018). 2000 laser shots per sample spot were accumulated for one MS spectrum. Fragmentation data to verify OA and OA(*d3*) were acquired in LIFT mode. $MS^2$ experiments to identify TA and TA(*d4*) were recorded in CID mode, with argon as the collision gas. All recorded data was analyzed using the FlexAnalysis 3.4 software package (Bruker Daltonik GmbH, Bremen, Germany).

## 4.3 Results and Discussion

To verify OA and TA in intracellular recorded desDUM neurons, electrophysiological identified and dextran-tetramethylrhodamine injected neurons were dissected, covered with 18.4 nl of IS, derivatized with 9.2 nl of CA, covered with 18.4 nl of CHCA and subsequently analyzed by MALDI-TOF SCMS. Intracellular labeling with dextran-tetramethylrhodamine was sufficient to identify labeled desDUM neurons under a fluorescence stereomicroscope, which is a prerequisite for manual dissection (Fig. 4.1 A, B). Recorded mass spectra of CA derivatized desDUM samples treated with internal standard revealed intense ion signals for putative OA-CA (*m/z* 314.1, n = 14) and low ion signals for TA-CA (*m/z* 298.1, n = 5) as well as the derivatized internal standards OA(*d3*)-CA (*m/z* 317.2) and TA(*d4*)-CA (*m/z* 302.2; Fig. 4.1 C). In order to verify a successful derivatization and identify the internal standards, ion signals of putative OA(*d3*)-CA (*m/z* 317.2) and TA(*d4*)-CA (*m/z* 302.2) were analyzed by tandem MS. Recorded product ion spectra of latter precursor ion signals confirmed these as the derivatized internal standards (Fig. 4.1 D). Subsequent fragmentation of putative OA-CA (*m/z* 314.1) and TA-CA (*m/z* 298.1) ion signals from desDUM samples revealed product ions matching signals obtained from CA derivatized samples containing synthetic OA and TA (Fig. 4.1 E-G). Control experiments from CA derivatized samples containing only IS revealed baseline ion signals matching putative OA-CA/TA-CA, however, subsequent tandem mass experiments revealed no product ions associated with OA-CA or TA-CA.

Finally, to rule out any potential interference from potentially isometric substances of OA-CA/TA-CA originating from the sample background, a small part of the anterior lateral GNG was dissected, treated with IS, derivatized with CA and subsequently analyzed by MALDI-TOF MS (Fig. 4.1 A). The recorded mass spectrum of the blind sample showed only baseline ion signals matching OA-CA/TA-CA and distinct ion signals for the derivatized IS (Fig. 4.2 B). The identity of the IS was confirmed by MS$^2$ (Fig. 4.2 C, D). Product ion spectra of baseline ion signals at *m/z* 298.1 (put. TA-CA) and *m/z* 314.1 (put. OA-CA) revealed no OA-CA/TA-CA specific product ions as well as no additional ion signals compared to blank samples (Fig. 4.2 C, D; Fig. 4.1 H). Thus, an influence from isomeric ion signals originating from the sample background can be excluded. In summary, these results confirm the presence of OA and TA in the intracellular recorded desDUM neurons.

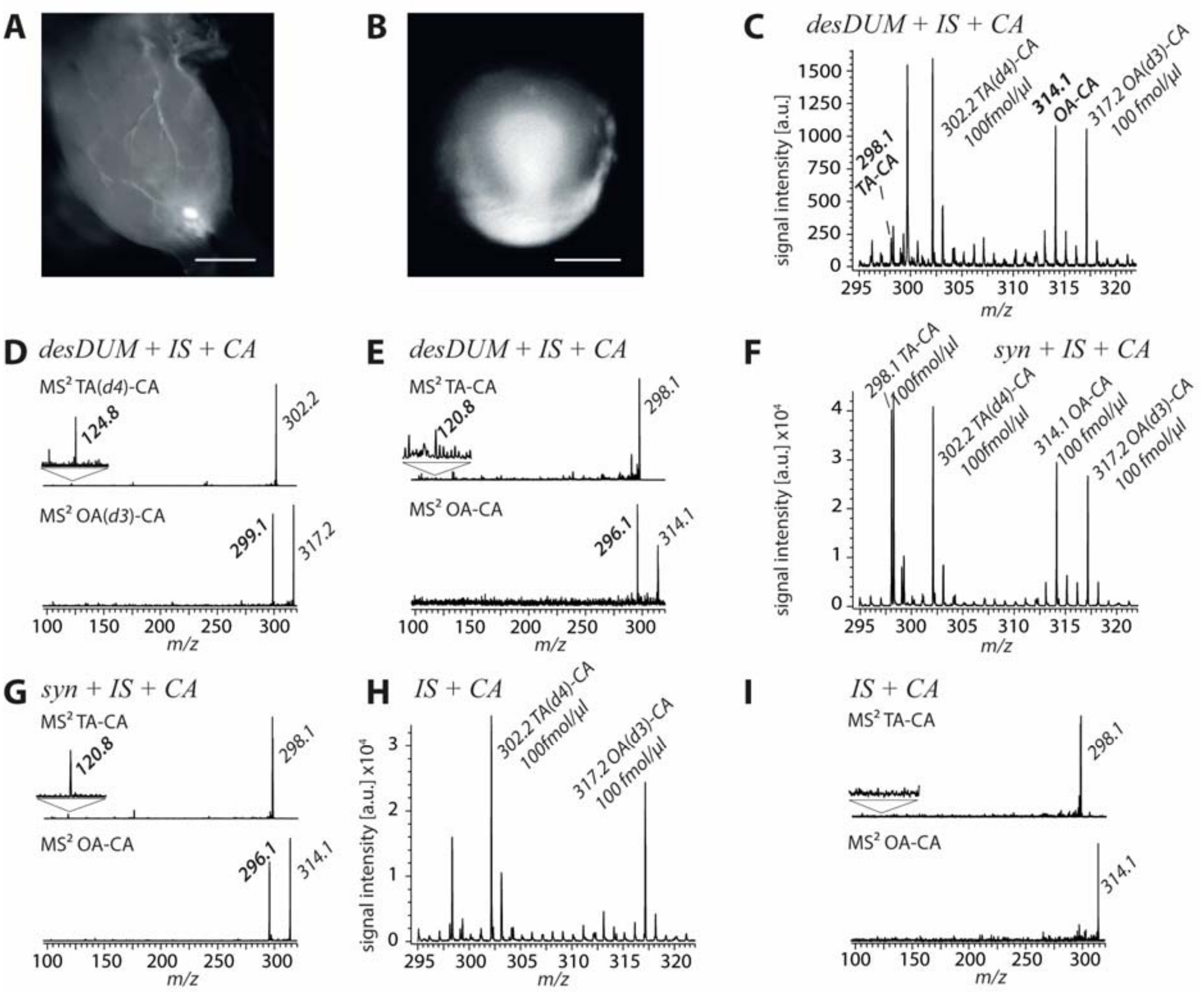

**Figure 4.1 Detection of OA and TA from an individual desDUM soma from the GNG of *C. morosus* by MALDI-TOF SCMS after intracellular recording and tetramethylrhodamine dextran injection.** (**A**) Isolated GNG with a dextran-tetramethylrhodamin injected desDUM soma after electrophysiological characterization; scale bar = 100 µm. (**B**) Intact dextran-tetramethylrhodamin labeled desDUM soma after dissection und transfer to a MALDI sample plate. Scale bar = 10 µm (**C**) Representative MALDI-TOF MS spectrum of a dissected single desDUM neuron soma after internal standard addition (*m/z* 302.2, TA[*d4*]-CA; *m/z* 317.2 OA[*d3*]-CA) and derivatization with CA. A clear ion signal for OA-CA (*m/z* 314.1) and a weak ion signal for TA-CA (*m/z* 298.1) were observed. (**D**) Tandem MS experiments of potentially derivatized ISs confirmed a successful derivatization. (**E**) Validation of putative OA-CA/TA-CA in desDUM soma samples by tandem MS. Product ion spectra showed unique product ions for each substance in accordance to standards (TA-CA, *m/z* 120.8; OA-CA, *m/z* 296.1). (**F**) Mass spectrum obtained of a CA derivatized control sample containing a mixture of synthetic 100 fmol/µl TA/OA and TA(*d4*)/OA(*d3*). (**G**) Tandem mass spectra of derivatized synthetic OA-CA and TA-CA with the major product ion signals for OA-CA (*m/z* 269.1) and TA-CA (*m/z* 120.8). (**H**) Mass spectra of a blank sample containing 100 fmol/µl deuterated TA(*d4*)-CA and OA(*d3*)-CA after chemical derivatization with CA. (**I**) Recorded tandem mass spectra of putative OA-CA/TA-CA ion signals from blank samples showed no product ions.

The SCMS results presented here confirm the presence of somatic OA and TA in the analyzed desDUM neurons. Moreover, immunohistochemical stainings against OA in the GNG of *C.*

*morosus*, which were carried out in the course of this study, revealing 4 to 10 (n = 4) OA-like immunoreactive cell bodies in the posterior GNG, further corroborate the here presented findings (Stolz et al., 2018 *in preparation*). However, the question remains whether these neurons indeed secrete OA and/or TA during activation. The release of OA from DUM neurons has first been studied in DUM neurons innervating the extensor-tibiae muscle (DUMETi) in the locust, using high $K^+$ saline activation and a radioenzyme assay for identification of OA (Morton & Evans 1984). A study by Martin Hammer could show that activation of the potentially OAergic ventral UM maxilar neuron 1 via intracellular current injection in honeybees mimicked OA effects on associative olfactory learning (Hammer 1993). Finally, in a recent study Majdi and colleagues could show the optogenetically controlled release of OA from Type II varicosities of OAergic VUM neurons in *D. melanogaster* larvae using cyclic voltammetry (Majdi et al. 2015). These studies indicate that activation of OAergic UM neurons indeed leads to a release of OA, however, it has been shown that DUM neurons can also co-release tyramine. Donini and Lange (2004) could show that DUM neurons of the 7th abdominal ganglion in female Locusts innervates the oviducts and release tyramine when activated by high $K^+$ concentrations (Donini & Lange 2004). Furthermore, in *D. melanogaster* larvae it was shown by CFME-FSCV that optogenitcally activation of *Tdc2* expressing neurons, which contain OA and TA, leads to a high release of OA in the VNC but also a potential co-release of TA (Pyakurel et al. 2016).

Biogenic monoamines can be co-localized and co-released with other neuroactive substances like neuropeptides or classical transmitters (Fricker 2012; Nässel 2018). However, co-localization of OA/TA with other neuroactive substances in DUM neurons seems to appear only rarely (Bräunig & Pflüger 2001). In the locust, for example, a co-localization of OA and the neuropeptide FMRFamide has been shown for the DUM-heart 1 neuron located in the abdominal ganglia 4-6 using immunohistochemistry (Stevenson et al. 1994; Bräunig & Pflüger 2001). Nevertheless, two recent independent studies analyzed neurons of the adult *D. melanogaster* brain using single cell transcriptomics and their results suggest a potential co-expression of eight different neuropeptides in OAergic neurons in general (Davie et al. 2018; Croset et al. 2018; Nässel 2018). Furthermore, experiments limiting the GAL4 expression in the OA/TA neuron labeling *Tdc2-GAL4* line using the Cha-GAL80 line, hint potentially towards a co-localization of acetylcholine in a subset of OAergic gnathal neurons (Zhou et al. 2008; Watanabe et al. 2017).

In the course of the project electrophysiological results showed that desDUM neurons not only show excitatory but also inhibitory effects on MN activity in *C. morosus* (Stolz 2018; Stolz et al., 2018 *in preparation*). Thus, it can be speculated that desDUM neurons contain a second neuroactive substance that would elicit such an inhibitory effect. Preliminary results from an immunhistchemical study in *C. morosus* using an antibody raised against *P. americana* MIP (GWQDLQGGW-$NH_2$) revealed 4 large cell bodies at the posterior end of the GNG, suggesting a potential co-localization of MIP and OA in some desDUM neurons (Sander Liessem, *personal communication*). A study using a genetic driver line labeling MIP expression in adult *D. melanogaster* show similar results, as this driver line labels multiple neurons at the midline of the GNG, which could overlap with OA/TAergic VUM neurons (Min et al. 2016). Moreover,

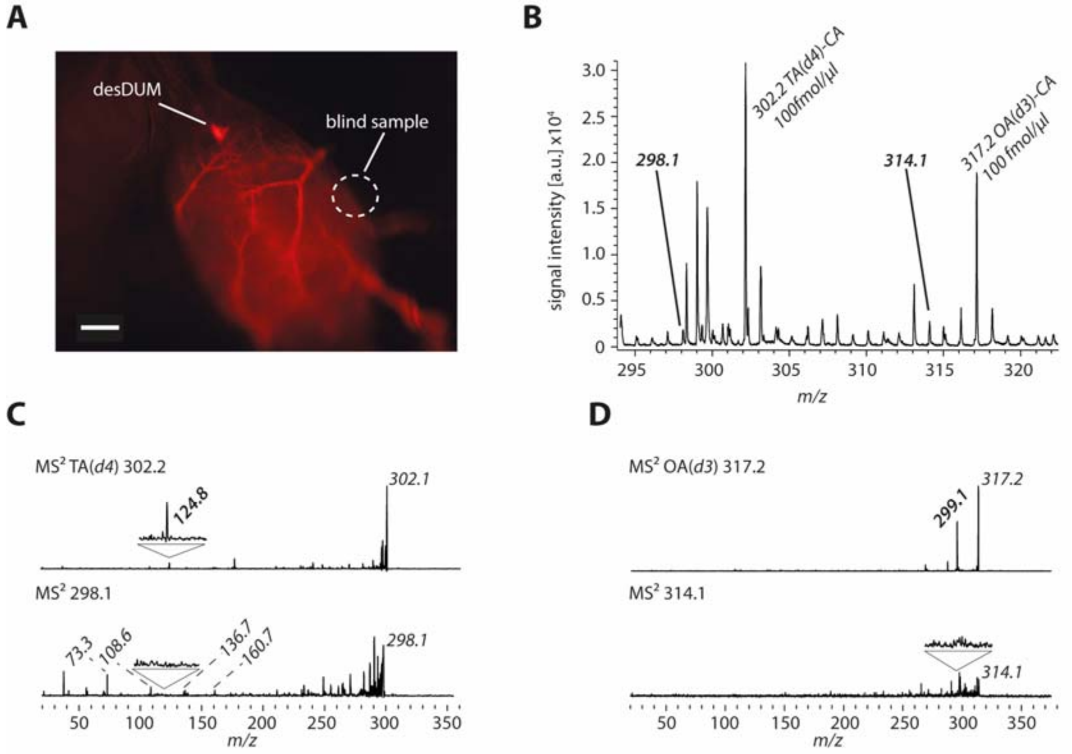

**Figure 4.2 Screening for potential OA-CA/TA-CA isomeric ion signals originating from nervous tissue of *C. morosus*.** (**A**) GNG of *C. morosus* after dissection and desDUM dextran-tetramethylrhodamine injection. The circle marks the area where the blind sample was cut out. Scale bar = 100 µm. (**B**) Detail view of the mass spectrum taken of the blind sample after IS application and derivatization by CA. Clear signals were recorded for TA(*d4*)-CA (*m/z* 302.2) and OA(*d3*)-CA (*m/z* 317.2). No distinct ion signals for either OA-CA or TA-CA were recorded. (**C**) MS$^2$ mass spectra after fragmentation of TA(*d4*)-CA (*m/z* 302.1) and the base ion signal at m/z 298.1. Fragmentation of *m/z* 302.1 revealed the unique product ion at *m/z* 124.8 identifying the signal as TA(*d4*)-CA. Fragmentation of *m/z* 298.1 showed no specific product ion for TA-CA. (**D**) Fragmentation spectra recorded from MS$^2$ experiments of OA(*d3*)-CA (*m/z* 317.2) and *m/z* 314.1. Mass spectrum recorded after fragmentation of *m/z* 317.2 revealed a product ion at m/z 299.1 confirming the ion signal as OA(*d3*)-CA. Fragmentation of *m/z* 314.1 showed no distinct signals for OA-TA.

the transcriptomic analysis of single OAergic neurons suggest that some of these neurons also express MIP (Croset et al. 2018; Nässel 2018). However, the analysis of potentially co-localized neuropeptides in desDUM neurons using the developed MALDI-TOF SCMS approach were unsuccessful. This could be due to the utilized matrix as previous experiments analyzing single *C. morosus* neuron somata with CHCA were also unsuccessful, while experiments using DHB were successful in the detection of multiple neuropeptides from similar samples (Sander Liessem, *personal communication*; Liessem et al. 2018). Thus, it would be interesting to repeat the here conducted experiments with DHB, in order to prove a potential co-localization of MIP and OA in desDUM neurons.

## 4.4 Conclusion

The developed MALDI-TOF SCMS approach (Diesner & Neupert 2018; see chapter 2) was used to detect and identify OA and TA from intracellular recorded gnathal desDUM neurons of adult *C. morosus*. The presented results not only confirmed the presence of OA and TA in the analyzed neurons but showed also that the within this thesis developed MALDI-TOF SCMS protocol can be combined with electrophysiological recordings. Therefore, the presented strategy enables the analysis of the chemical composition as well as the electrophysiological characteristics of a specific neuron in a single workflow. Such combinatorial workflows are highly desirable since they allow the in-depth analysis of the function of a given neuron in their corresponding neuronal circuits.

# 5. Mass spectrometric survey and mapping of neuropeptides in DIMMED neurons from the adult *Drosophila* brain

The results of this chapter are already published in the following peer-reviewed article: Diesner, M; Predel, R; Neupert, S. *Neuropeptide mapping of Dimmed cells of adult Drosophila brain*. Journal of the American Society of Mass Spectrometry, 2018, Epub ahead of print, DOI: 10.1007/s13361-017-1870-1.

The author contributions are as followed: SN conceptualized experiments, MD and SN performed experiments (Dissection of brains with removed single cells for mapping and subsequent 3D reconstruction SN, visual imaging of brains and 3D reconstructions MD; Repetition of single cell analysis SN and MD), MD and SN analyzed data, prepared figures and tables. MD, RP and SN wrote the manuscript. SN and RP funding.

Parts of this chapter have been adapted/modified/copied from the article with permission from Springer Customer Service Centre GmbH: Springer Nature, Journal of The American Society for Mass Spectrometry, Neuropeptide Mapping of Dimmed Cells of Adult Drosophila Brain, Diesner M, Predel, R, Neupert S, ©, 2018.

A license for the adaptation/modification/copying was given to Max Diesner with the licence number 4390870926882.

## 5.1 Introduction

Neuropeptides are key players in many physiological processes such as development, homeostasis, and reproduction and thereby shape the behavioral output of metazoan organisms in general (Nässel & Winther 2010). They represent the structurally most diverse group of neuroactive substances to date and mainly act on GPCRs. In *D. melanogaster* about 50 neuropeptide encoding genes have been identified to date, which give rise to an astonishing 96 potential bioactive products (Nässel & Winther 2010; Ida, Takahashi, Tominaga, Sato, Kume, Ozaki, et al. 2011; Ida, Takahashi, Tominaga, Sato, Kume, Yoshizawa-Kumagaye, et al. 2011; Jiang et al. 2013; Jung et al. 2014; Yeoh et al. 2017). The expression of a specific neuropeptide gene is not exclusive in a given neuron and extensive research on co-localization of neuropeptides exists (e.g. Nässel & Winther 2010; Nässel 2018). For example, in *D. melanogaster*, co-localized expression of five different neuropeptide genes has been shown in insulin producing cells of the *pars intercerebralis* (Brogiolo et al. 2001; Söderberg et al. 2012; Huang et al. 2016). Moreover, neuropeptides can further be co-localized with classical neurotransmitters but also with biogenic monoamines (Fricker 2012; Nässel 2018).

While neuropeptides can act as neurotransmitter, neuromodulator or neurohormone their function is often related to a modulatory or hormone like activity (Nässel & Winther 2010; Taghert & Nitabach 2012). In the *D. melanogaster* CNS most of these neurohormones are produced and secreted from large cells that display episodic release of amidated peptides (LEAP) cells (Park et al. 2008). Neurosecretory LEAP cells express the transcription factor DIMMED (DIMM), which promotes a neurosecretory/endocrine cell phenotype with an increased cell soma size. This increase in soma size in DIMM expressing neuroendocrine cells is accompanied by an upscaled capacity for neuropeptide production, storage and release which is necessary to raise or keep hemolymph titers of neurohormones at physiologically relevant concentrations. The DIMM mediated neurosecretory phenotype is independent of the expressed neuropeptide. Moreover, it has been shown that ectopic expression of DIMM in non-neuroendocrine cells, such as photoreceptors or motor neurons, activates the regulated secretory pathway and converts such cells from fast neurotransmission towards a neurosecretory phenotype (Hewes 2003; Hamanaka et al. 2010; Luo et al. 2017). Other described transcriptional roles of DIMM are regulating effects on cell growth and inhibiting apoptosis at different developmental stages in a cell type-specific manner (Liu et al. 2016). Finally, it has been reported that DIMM expression is not restricted to neuroendocrine cells, but has also been observed for neuropeptidergic interneurons with complex arborizations. However, even though most DIMM cells are peptidergic, not all peptidergic cells express DIMM (Park et al. 2008).

The reproducible identification of a neuron is one of the basic steps in characterizing its function in the CNS. While this can be achieved by e.g. retrograde dye labeling in larger insects, such classical approaches are of limited use in smaller insects like *D. melanogaster* due to the sheer limitation in size. It has to be noted that some studies tackled these size hurdles and were successful in labeling single neurons in developing and adult *D. melanogaster* (Rajashekhar & Singh 1994; Bossing & Technau 1994; Landgraf et al. 1997; Hsu & Bhandawat 2016). However, modern fly genetics with its thousands of genetic driver and reporter lines enables the routine fluorescent labeling and genetic modification of subpopulations or even single neurons with high accuracy and reproducibility. The creation of a *D. melanogaster DIMM-GAL4* driver line (*c929-GAL4*) in combination with fluorescent UAS reporter lines enables the systematic interrogation of co-localized neuroactive substances in neurosecretory neurons of the fly CNS (Hewes et al. 2000; Hewes et al. 2003; Park et al. 2008). For example, one study used affinity cell-capture or fluorescence activated cell sorting (FACS) to collect GFP-expressing DIMM neurons from adult *D. melanogaster* brain cell suspensions and subsequent MS analysis to elucidate neuropeptide expression among these neurons, identifying 42 peptides from 16 neuropeptide precursors (Yew et al. 2009). However, the analysis of pooled samples only allows conclusions to be drawn about the general expression of neuroactive substances in this cell population and render it impossible to correlate specific neuroactive substance profiles to specific DIMM neurons. In another study, Park and colleagues mapped the expression and co-localization of neuropeptides by immunohistochemistry and other neuropeptide labeling GAL-4 lines in 3rd instar *D. melanogaster* larva, by using the *c929-GAL4* line as reference (Park et al. 2008). Finally, even though a large body of data exists on neuroactive substance expression in the adult *D. melanogaster* CNS, a comprehensive map of DIMM neurons and their neuroactive substance profiles is missing to date.

Aside from immunohistochemistry, SCMS represents another powerful tool for the interrogation of neuroactive substances in a given neuron, as it allows the simultaneous detection and identification of a multitude of different chemical features from a single neuron sample in comparison to immunohistochemistry or genetic labeling (Li, Romanova, et al. 2000; Neupert et al. 2007; Nemes et al. 2013; Romanova et al. 2014; Ong et al. 2015b; Zhang & Vertes 2018; Qi et al. 2018; Diesner & Neupert 2018). The elegant combination of genetic labeling driven single neuron identification, somata microdissection and subsequent MALDI-TOF SCMS analysis has been successfully used to analyze neuropeptide expression in single neuron somata of adult *pdf*-expressing neurons and larval *hugin*-expressing neurons from intact *D. melanogaster* CNS preparations (Neupert et al. 2007). A similar approach which has been developed as part of this thesis, uses chemical derivatization and isotopically labeled ISs to detect, identify and even quantify the biogenic monoamines OA and TA from genetically labeled single dissected neuron somata of adult *D. melanogaster* (see chapter 2; Diesner & Neupert, 2018). Furthermore, the study could show that the used derivatization has only a limited effect on the detection of neuropeptides, hence allowing their simultaneous detection from a single sample (see chapter 2; Diesner & Neupert 2018).

This chapter is dedicated towards the creation of a map of DIMM neurons and their corresponding neuroactive substance repertoires in the adult brain of *D. melanogaster*. As a starting point, we used derivatization free MALDI-TOF SCMS to analyze the neuropeptidome of single GFP-expressing DIMM neurons from adult *D. melanogaster* brains of the *c929-GAL4* driver line with a soma size of ≥7 µm. Ten subpopulations of different DIMM neurons were analyzed on a single cell level and a total of 52 neuropeptide related products of 13 different neuropeptide precursors were identified. The resulting mass spectra provided information on (1) co-localization of neuropeptide products from differing neuropeptide genes as well as (2) major processing products of translated neuropeptide genes. Finally, the recorded SCMS data was compared with previously published results from studies using immunohistochemistry or genetic labeling to analyze neuropeptide expression. Altogether, this allowed us to map neuropeptide expression profiles to single DIMM cells and cell clusters.

## 5.2 Materials and Methods

### *Chemicals*

All used chemicals were purchased from SIGMA-Aldrich (Steinheim, Germany), if not stated otherwise.

### *Fly strains*

Adults of both sexes of *D. melanogaster* were used for experiments. Flies were reared on a standard agar, cornmeal, and yeast medium at 25 °C, 60% relative humidity and a 12 h: 12 h light-dark cycle. For cell identification, *c929-GAL4* was crossed to UAS-*mCD8::GFP* (*C929-*

*GAL4* was a present from Christian Wegener, University of Würzburg, Germany and UAS-*mCD8::GFP* was a present from Manuela Ruppert, University of Cologne, Germany).

### *Single cell dissection for mass spectrometry*

Cell dissection was adapted from Neupert *et al.*, 2007 and Diesner & Neupert 2018 (see chapter 2). Adult flies were immobilized on ice and brains were rapidly dissected in ice-cold saline buffer (125.94 mM NaCl, 5.37 mM KCl, 0.17 mM $NaH_2PO_4$, 0.22 mM $KH_2PO_4$, pH 7.2) with forceps and ultra-fine scissors under a stereofluorescence microscope (SteREO Lumar V12, Carl Zeiss AG, Goettingen, Germany). The dissected brains were transferred to a fresh drop of either saline buffer or saline buffer containing 33% glycerol. The ganglionic sheath around the area of a GFP-labeled cell of interest was removed and the cell soma manually picked and transferred to a MALDI-TOF sample plate, by an uncoated glass capillary (see chapter 2; Neupert et al. 2007; Diesner & Neupert 2018). Excessive dissection saline was removed using the same glass capillary. Residual dissection saline and/or glycerol surrounding the isolated soma was washed off with ice cold 50% MeOH/TraceSELECT® water. Washing was performed multiple times with a fresh glass capillary. However, the placed cell soma was left uncovered by the washing solution to prevent a possible loss of analytes. Finally, the dried sample was covered with matrix. Only samples with an intact cell body and no visual contaminations were prepared for further sample preparation.

### *Matirx application*

Solutions of 10 mg/ml 2,5-dihydroxybenzoic acid (DHB) dissolved in 20% acetonitrile (ACN), 1% formic acid, 79% HPLC grade water, 10 mg/ml CHCA dissolved in 60% ethanol, 36% ACN, 4% HPLC grade water or 10 mg/ml 1,5-diaminonaphtalene (1,5-DAN) dissolved in 50% ACN, 0.1% trifluoroacetic acid, 49.9% HPLC grade water were used as matrices. Prior to matrix application, the CHCA stock solution was diluted 1:3 with 50% methanol/water. Depending on the soma size, 9.2-18.4 nl of matrix was applied onto the dried samples using a nanoliter injector (World Precision Instruments, Berlin, Germany). For an even crystallization of DHB, freshly covered samples were rapidly dried using a conventional hairdryer.

### *MALDI-TOF MS*

Mass spectra were acquired in reflector positive ion mode under manual control on an UltrafleXtreme TOF/TOF mass spectrometer (Bruker Daltonics, Bremen, Germany) in a detection range of *m/z* 600–10,000. The instrument settings were optimized for the mass ranges of *m/z* 600–4000 and 3000–10,000, and calibrated using suitable synthetic peptide mixtures (Table 5.1; Table 2.1). Laser fluency was adjusted to provide the optimal signal-to-noise ratio. Data were collected using a laser beam diameter of 50 µm and random walk laser setting over the entire matrix spot. The data obtained in these experiments were processed with the FlexAnalysis 3.4 software package. MS/MS was performed with LIFT technology. LIFT acceleration was set at 1 kV. The number of laser shots used to obtain a spectrum varied from 5000 to 10,000, depending on signal quality. Peptide identities were verified using MS/MS fragmentation of corresponding ion signals, determination of the molecular mass of the fragments, and comparison of predicted (http://prospector.ucsf.edu) and experimentally obtained fragmentation patterns.

**Table 5.1** Synthetic peptides used for instrument calibration in the range of m/z 3000 – 10,000.

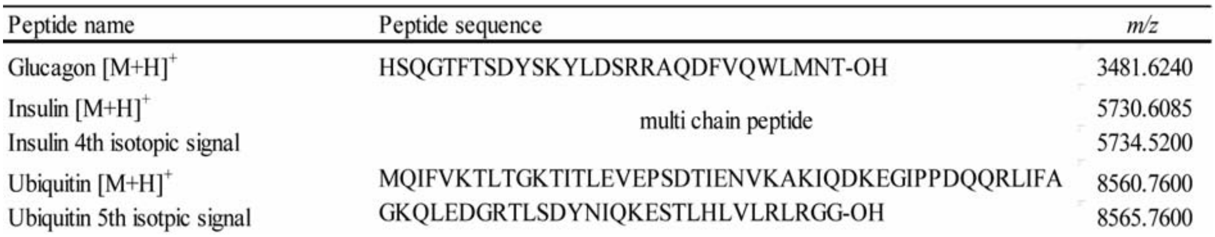

| Peptide name | Peptide sequence | *m/z* |
|---|---|---|
| Glucagon [M+H]$^+$ | HSQGTFTSDYSKYLDSRRAQDFVQWLMNT-OH | 3481.6240 |
| Insulin [M+H]$^+$ | multi chain peptide | 5730.6085 |
| Insulin 4th isotopic signal | | 5734.5200 |
| Ubiquitin [M+H]$^+$ | MQIFVKTLTGKTITLEVEPSDTIENVKAKIQDKEGIPPDQQRLIFA GKQLEDGRTLSDYNIQKESTLHLVLRLRGG-OH | 8560.7600 |
| Ubiquitin 5th isotpic signal | | 8565.7600 |

## *Drosophila peptide precursor sequences*

Neuropeptide precursor sequences were either obtained from blast searches at NCBI database (https://www.ncbi.nlm.nih.gov/) or from flybase (https://www.flybase.org). Signal peptides were predicted using the SignalP 4.1 server (www.cbs.dtu.dk/services/SignalP/). Potential cleavage sites were either manually assigned according to Veenstra 2000 (Veenstra 2000) or predicted *in silico* using the online suite Neuropred (http://stagbeetle.animal.uiuc.edu/cgi-bin/neuropred.py; Southey et al. 2006).

## *Documentation and single cell verification*

For documentation, microphotographs of corresponding brains were taken before and after single cell dissection with a stereo fluorescence microscope equipped with a digital camera (AxioCam MRc, Zeiss, Germany). For a more detailed mapping approach dissected brains were prepared after Pitman et al., 2011 (Pitman et al. 2011) for confocal microscopy. Therefore, brain samples were fixed in 4% paraformaldehyde dissolved in phosphate buffer solution (PBS) (1.86

mM $NaH_2PO_4$, 8.41 mM $Na_2HPO_4$, 175 mM NaCl) for 120 min at room temperature under vacuum. Samples were washed three times for 10 min in PBS containing 0.1% Triton-X 100 and two times for 10 min in PBS to remove excessive fixation solution and prevent over fixation. After mounting in glycerol containing 20% PBS and 50 mg/ml 1,4-diazabicyclo(2.2.2)octane, samples were analyzed using a Zeiss LSM 510 Meta confocal microscope equipped with a Plan-Apochromat 20x/0.75 objective. GFP was excited with an Argon laser at 488 nm and emission collected via a broad pass 505–550 filter. Serial optical sections were analyzed with a thickness of 0.3 to 0.8 µm. Contrast adjusted image stacks were used to reconstruct the brain surface whereas GFP expression was visualized by voltex function using the Amira 5.4.2 software package (FEI, Hillsboro, OR). The final figures were exported and processed to adjust brightness and contrast with Adobe Photoshop CS6 software (Adobe Systems, San Jose, CA).

## 5.3 Results and Discussion

The analysis of different adult c929>GFP brains by confocal microscopy showed a high degree of variation in GFP-labeled cell numbers (Fig. 5.1 A1-B2). This variation can probably be attributed to the fact that flies were not synchronized in age, sex or physiological state (hunger, mating etc.). While most of the larger DIMM positive neurons (≥10 µm) showed constant GFP-labeling, the number of GFP-labeled smaller neurons (<10 µm) varied tremendously, however, some smaller neurons showed also constant GFP-labeling between preparations (Fig. 5.1 B1, B2). Cells with a constant labeling could also be identified under the stereomicroscope with a high degree of certainty, which was a prerequisite for the repeated SCMS analysis of a specific neuron (Fig. 5.1 C1, C2). Due to the limitations in size for manual dissection, only neurons with cell soma of about 7 µm or larger were chosen for SCMS. Taken this altogether, a total set of 10 different single cells and cell populations were chosen for dissection and subsequent MALDI-TOF SCMS.

A total of 52 mature products of 13 different neuropeptide precursor genes from the 10 different cell types (Table 5.2) were detected. In the following sections each analyzed cell type is introduced and discussed.

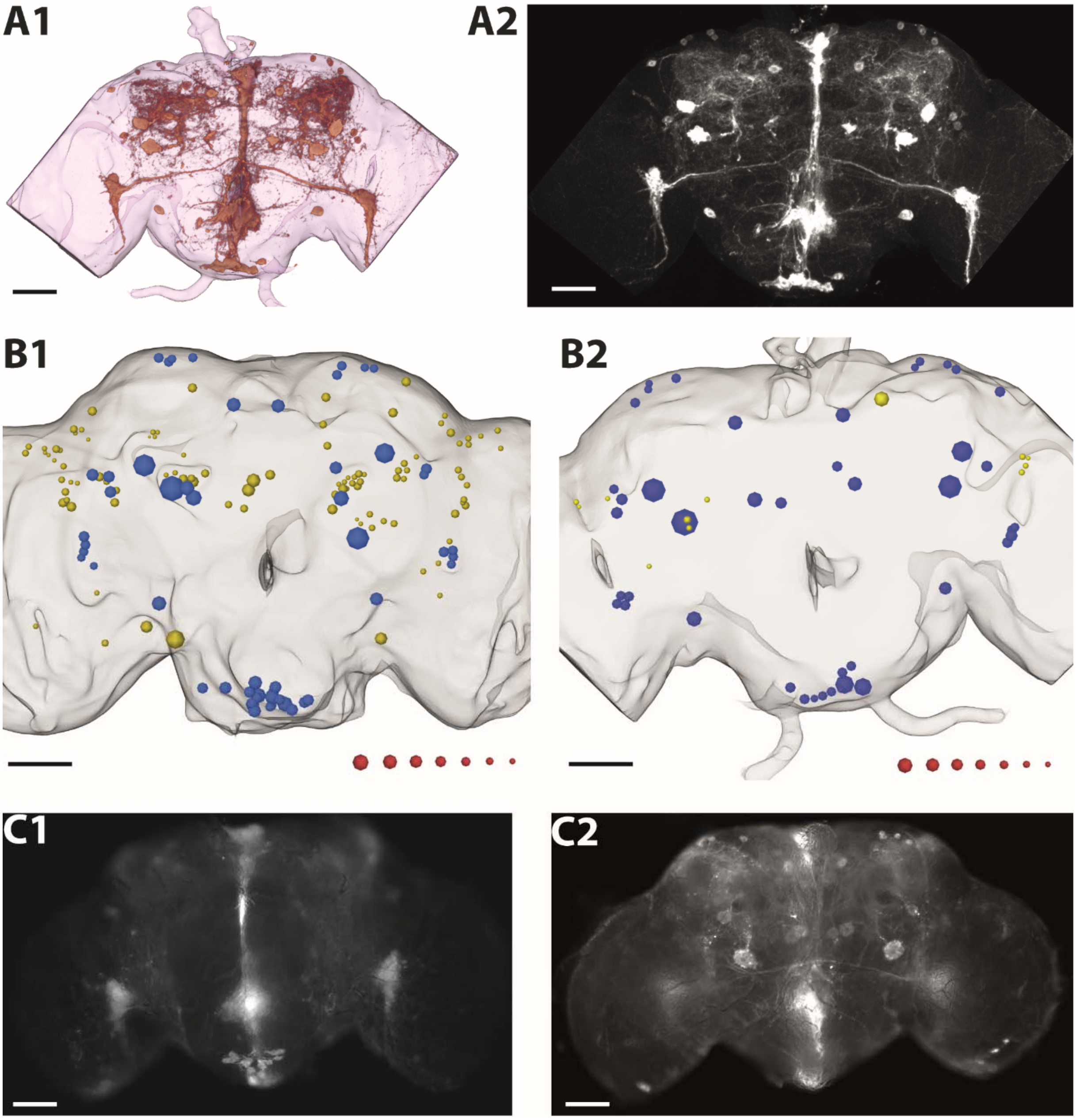

**Figure 5.1 Optical survey of the c929>GFP expression pattern in adult *D. melanogaster* brains**. (**A1**) Three dimensional reconstruction of detected c929>GFP labeling in an adult *D. melanogaster* brain and GNG. (**A2**) Maximum projection view of c929>GFP expression in an adult *D. melanogaster* brain and GNG recorded with confocal laser microscopy. (**B1**, **B2**) c929>GFP positive cell numbers vary considerably between different brain dissections. Schematic three dimensional reconstruction of c929>GFP-positive cell bodies in two different adult *D.melanogaster* brain and GNG preparations. Cell bodies which showed consistent labeling are marked in blue, while cell bodies showing fluctuating labeling are marked in yellow. Red size-markers from right to left: 3.5, 5.2, 6.8, 8.2, 9.6, 12.4, 14.0 µm. (**C1**) Anterior and posterior (**C2**) view of a dissected adult c929>GFP brain and GNG preparation under a fluorescence stereomicroscope as used for single cell dissection. Scale bar = 50µm.

### 5.3.1 *Cell type #1: Allatostatin-C (Ast-C) neurons*

SCMS analysis of a single large bilateral cell (soma size: 18-20 µm; n = 6) in the posterior medio-lateral protocerebrum revealed ion signals matching products of the Ast-C precursor and was therefore classified as Ast-C neuron (Fig. 5.2 A; FlyBase ID: FBgn0032336). The *D. melanogaster* precursor encodes a single putative Ast-C sequence. Two almost equimolar amounts of Ast-C with N-terminal Gln and N-terminal pyroglutamate were detected (Fig. 5.2 A). Both isoforms were identified earlier by mass spectrometry using an immunoaffinity cell enrichment of GFP-labeled DIMM neurons from the same *c929-GAL4* line (Yew et al. 2009). $MS^2$ experiments of the ion signal at *m/z* 1921.8 confirmed the ion signal as Ast-C with N-terminal Gln (Fig. 5.3 A). Comparison to results from a published immunocytochemical study showed a most likely match to the $PMP_2$ neuron described in the protocerebrum of adult *D. melanogaster* (Zitnan et al. 1993). However, an assignment of this neuron to the mapped Ast-C immunopositive DIMM neurons of the larval brain is not possible, since no cell was co-labeled by anti-Ast-C immunolabeling and c929>GFP driven fluorescence close to the position observed in the adult brain (Park et al. 2008). However, the described Ast-C cell could belong to a larval neuron lineage described as corpus allatum innervating neurosecretory neuron of the lateral protocerebrum 1 (CA-LP 1) innervating the larval ring gland (Siegmund & Korge 2001). Moreover, Price and colleagues described a single neuron as $PMP_2$ neuron in brains of third instar *D. melanogaster* larvae and adult *D. melanogaster* brains (Price et al. 2002). However, whether these larval $PMP_2$ neurons represent the same neuron or the same lineage as the adult DIMM positive Ast-C cell remains elusive. To date no direct function for the analyzed $PMP_2$ neuron has been described. Ast-C in general is associated with an allatostatic function (Wang et al. 2012) which is dependent on the stage and age of the insect analyzed (Bendena & Tobe 2012; Verlinden et al. 2015). Furthermore, it has been shown that Ast-C has myoinhibitory effects on the heart rate and crop contraction in *D. melanogaster* larvae and adults (Merte & Nichols 2002). Finally, a recently published study analyzing clock neurons showed a potential role of Ast-C in the circadian rhythm of the fly (Abruzzi et al. 2017). Non–amidated Ast-C products were the only neuropeptide products detected in this cell and therefore this DIMM cell do not likely process amidated peptides. This is interesting, since DIMM cells have been associated in general with the production and secretion of amidated peptides (Hewes et al. 2003; Park et al. 2008). However, in previous studies it was shown that some DIMM neurons express non-amidated peptides (Hamanaka et al. 2010; Park et al. 2008). Finally, this was the only analyzed DIMM cell type which processes non-amidated neuropeptides in this study.

**Table 5.2** Detected mature neuropeptides and precursor peptides (PP) by SCMS from identified DIMM neurons of the adult brain with GNG of *D. melanogaster*. * = peptides which were detected as sodium adduct in mass spectra

| Peptide name | Peptide sequence | $[M+H]^+$, *m/z* | Reference |
|---|---|---|---|
| ***Allatostatin-A (Ast-A)*** | | | |
| Ast-A-1 | VERYAFGL-NH$_2$ | 953.52 | Predel et al., 2004 |
| Ast-A-2 | LPVYNFGL-NH$_2$ | 921.43* | Yew et al., 2009 |
| Ast-A-3 | SRPYSFGL-NH$_2$ | 925.46 | Birgül et al., 1999 |
| Ast-A-4 | TTRPQPFNFGL-NH$_2$ | 1276.67 | Baggerman et al., 2002 |
| Ast-A-PP-1 | SPVIGQDQRSGDSDADVLLAADEMADNGGDNID-OH | 3360.47 | This study |
| ***Allatostatin-B, Myoinhibitory peptide (MIP)*** | | | |
| MIP-1 | AWQSLQSSW-NH$_2$ | 1091.52* | This study |
| MIP-2 | AWKSMNVAW-NH$_2$ | 1091.54* | Baggerman et al., 2002 |
| MIP-3 | RQAQGWNKFRGAW-NH$_2$ | 1603.83 | Yew et al., 2009 |
| MIP-4 | EPTWNNLKGMW-NH$_2$ | 1374.66* | Reiher et al. 2011 |
| MIP-5 | DQWQKLHGGW-NH$_2$ | 1253.62* | Baggerman et al., 2002 |
| ***Allatostatin-C (Ast-C)*** | | | |
| Ast-C [pQ] | pQVRYRQCYFNPISCF-NH$_2$ | 1904.89 | Yew et al., 2009 |
| Ast-C [Q] | QVRYRQCYFNPISCF-NH$_2$ | 1921.89 | Yew et al., 2009 |
| ***CAPA*** | | | |
| CAPA-tryptoPK$^{2\text{-}15}$ | GPSASSGLWFGPRL-NH$_2$ | 1430.75 | Predel et al., 2004 |
| CAPA-PP (CPPB) | GDAELRKWAHLLALQQVLD-OH | 2176.19 | Wegener et al., 2006 |
| CAPA-PP$^{2\text{-}19}$ | DAELRKWAHLLALQQVLD-OH | 2119.15 | This study |
| ***Corazonin*** | | | |
| Corazonin | pQTFQYSRGWTN-NH$_2$ | 1369.65 | Baggerman et al., 2002 |
| ***Diuretic hormone-31 (DH-31)*** | | | |
| DH-31 | TVDFGLARGYSGTQEAKHRMGLAAANFAGGP-NH$_2$ | 3149.57 | Reiher et al. 2011 |
| ***HuginPK (pyrokinin)*** | | | |
| PK | SVPFKPRL-NH$_2$ | 942.58 | Baggerman et al., 2002 |
| PK-PP | KSLQGTSKLDLGNHISAGSARGSLSPASPALSEA-OH | 3307.72 | This study |
| ***Myosuppressin (MS)*** | | | |
| MS | TDVDHVFLRF-NH$_2$ | 1247.65 | Nichols, 1992 |
| MS-PP | AVQGPPLCQSGIVEEMPPHIRKVCQALENSDQLTSALKSYINNEASALVANSDDLLKNYN-OH | 6484.22 | This study |
| ***Neuropeptide F (NPF)*** | | | |
| NPF | KNDVNTMADAYKFLQDLDTYYGDRARVRF-NH$_2$ | 3484.71 | Brown et al., 1999/ This study |
| NPF-PP-1 | SNSRPPR-OH | 813.43 | This study |
| NPF-PP-2 | GSLMDILRNHEMDNINLGKNANNGGEFARGFNEEEIF-OH | 4165.94 | This study |
| ***Neuropeptide-like precursor 1 (NPLP-1)*** | | | |
| APK | SVAALAAQGLLNAPK-OH | 1423.83* | Baggerman et al., 2002 |
| MTY | YIGSLARAGGLMTY-NH$_2$ | 1471.77 | Baggerman et al., 2002 |
| MTY$^{2\text{-}14}$ | IGSLARAGGLMTY-NH$_2$ | 1308.70 | This study |
| MTY$^{3\text{-}14}$ | GSLARAGGLMTY-NH$_2$ | 1195.62 | This study |
| IPN | NVGTLARDFQLPIPN-NH$_2$ | 1653.83 | Baggerman et al., 2002 |
| IPN$^{2\text{-}15}$ | VGTLARDFQLPIPN-NH$_2$ | 1539.86 | This study |
| DPK | NIATMARLQSAPSTHRDPK-OH | 2094.08 | Salisbury et al., 2013 |
| GAE$^{1\text{-}20}$ | NVAAVARYNSQHGHIQRAGA-OH | 2120.77 | Salisbury et al., 2013 |
| VQQ | NLGALKSSPVHGVQQ-OH | 1534.83* | Baggerman et al., 2005 |
| VQQ$^{1\text{-}14}$ | NLGALKSSPVHGVQ-OH | 1406.77* | Yew et al., 2009 |
| GAE$^{1\text{-}18}$-NH$_2$ | NVAAVARYNSQHGHIQRA-NH$_2$ | 1991.03 | Salisbury et al., 2013 |
| ***Natalisin (Nat)*** | | | |
| Nat-1$^{1\text{-}14}$ | EKLFDGYQFGEDMS-OH | 1665.71 | This study |
| Nat-2 | HSGSLDLDALMNRYEPFVPNR-NH$_2$ | 2430.19 | This study |
| Nat-3 | DKVKDLFKYDDLFYPHR-NH$_2$ | 2198.13 | This study |
| Nat-4 | HRNLFQVDDPFFATR-NH$_2$ | 1861.94 | This study |
| Nat-5 | LQLRDLYNADDPFVPNR-NH$_2$ | 2045.06 | This study |
| Nat-PP | LPPSLIATATKAALSHQRQQKQQQHQ-OH | 3036.64 | This study |
| ***Pigment-dispersing factor (PDF)*** | | | |
| PDF | NSELINSLLSLPKNMNDA-NH$_2$ | 1972.01 | Neupert et al., 2007 |
| ***Sulfakinin (SK)*** | | | |
| SK-1 | FDDYGHMRF-NH$_2$ | 1186.50 | Predel et al., 2004 |
| SK-2 | GGDDQFDDYGHMRF-NH$_2$ | 1658.66 | Baggerman et al., 2002 |
| ***Short neuropeptide F (sNPF)*** | | | |
| sNPF-1 | AQRSPSLRLRF-NH$_2$ | 1329.78 | Predel et al., 2004 |
| sNPF-1$^{4\text{-}11}$/ sNPF-2 | SPSLRLRF-NH$_2$ | 974.58 | Predel et al., 2004/ Wegener et al., 2006 |
| sNPF-3 | KPQRLRW-NH$_2$ | 982.61 | Yew et al., 2009 |
| sNPF-4 | KPMRLRW-NH$_2$ | 985.59 | Yew et al., 2009 |
| sNPF-PP-1 | EVSSAQGTPLSNLYDNLLQREYAGPVVFPNHQVE-OH | 3771.81 | This study |
| sNPF-PP-1$^{2\text{-}34}$ | VSSAQGTPLSNLYDNLLQREYAGPVVFPNHQVE-OH | 3642.82 | This study |
| sNPF-PP-2 | WFGDVNQKPI-OH | 1203.62 | Baggerman et al., 2002 |

### *5.3.2 Cell type #2: Myosuppressin (DMS) neurons*

Medial of cell type #1 a second very large bilaterial cell (soma size: 22-24 µm; n = 20) in the medio-lateral protocerebrum was analyzed by SCMS and revealed ion signals matching predicted products of the DMS precursor, and therefore was classified as DMS neuron (Fig. 5.2 B; FlyBase ID: FBgn0011581). The DMS precursor encodes a single putative DMS sequence and a putative long precursor peptide sequence (Vanden Broeck 2001). Both sequences were confirmed by SCMS of analyzed DMS neurons (Fig. 5.2 B). Comparison to a published immunocytochemical study, using an antibody directed against the peptide TDVDHVC in various developmental stages of *D. melanogaster*, revealed a most likely match of the analyzed MS neuron to the bilaterial medial protocerebral neurons 2 (MP2) in the imago and larva (McCormick & Nichols 1993). During development, the two MP2 neurons are the first neurons showing MS-immunopositive labeling, however, during metamorphosis one neuron is lost and in the imago only a single large MP2 neuron remains MS-immunopositive (McCormick & Nichols 1993). MP2 neurons project into to the ventral nerve cord with intense arborizations along the midline. MP2 DIMM neurons with MS-immunopositive labeling were also described in the larval *D. melanogaster* brain, resembling probably the same cell lineage (Park et al. 2008). A suggested co-localization with short neuropeptide F (sNPF) or other neuropeptides in MP2 neurons as described from larva, however, was not observed in our experiments. This finding is corroborated by the fact that immunostainings against sNPF in adults showed no labeling of a large cell in the same region as the described cell type #2 (Nässel et al. 2008). To date no functional description of the MP2 neuron has been published. However, it has been shown that DMS immunoreactive fibers innervate the heart, crop and anterior gut and that DMS has an inhibitory effect on these muscles (Dickerson et al. 2012).

### *5.3.3 Cell type #3: Allatostatin-A (Ast-A) + myoinhibiting peptide (MIP) + Natalisin (Nat) neurons*

Analysis with SCMS of a single bilateral cell located in the anterior ventro-lateral brain (soma size: 12-14 µm; n = 7) revealed ion signals matching predicted products of three different neuropeptide precursors, Ast-A, MIP and Nat, and the cell was therefore classified as Ast-A/MIP/Nat neuron (Fig. 5.2 C; FlyBase IDs: FBgn0015591, FBgn0036713, FBgn0085417). All four Ast-A paracopies encoded by the Ast-A precursor (Vanden Broeck 2001) as well as the first N-terminal precursor peptide were confirmed by mass spectra. The second present

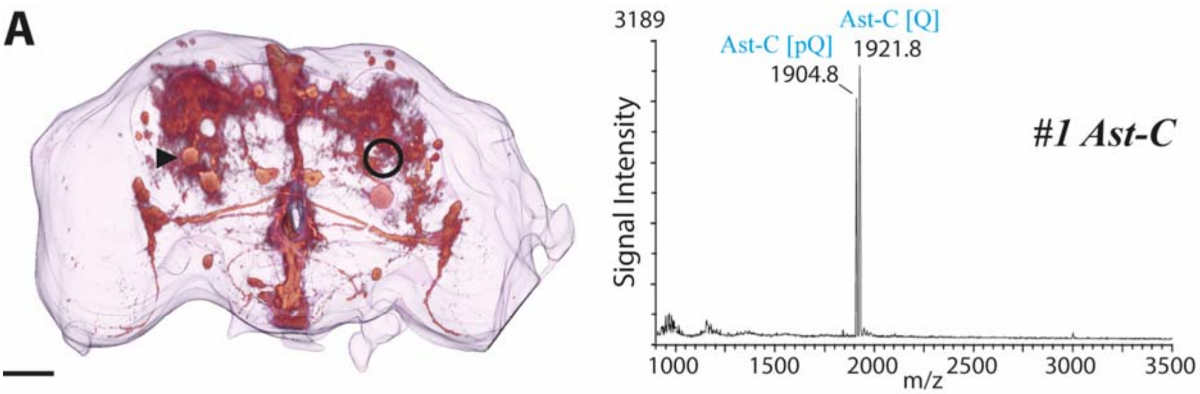

***MMKFVQILLCYGLLLTLFFALSEA***RPSGAETGPDSDGLDGQDAEDVRGAYGGGYDMPAQAIYPNIPMDRLQMLFAQYRPTYSAYLRSPTYGNVNELYRLPESKRQVRYRQCYFNPISCFRK

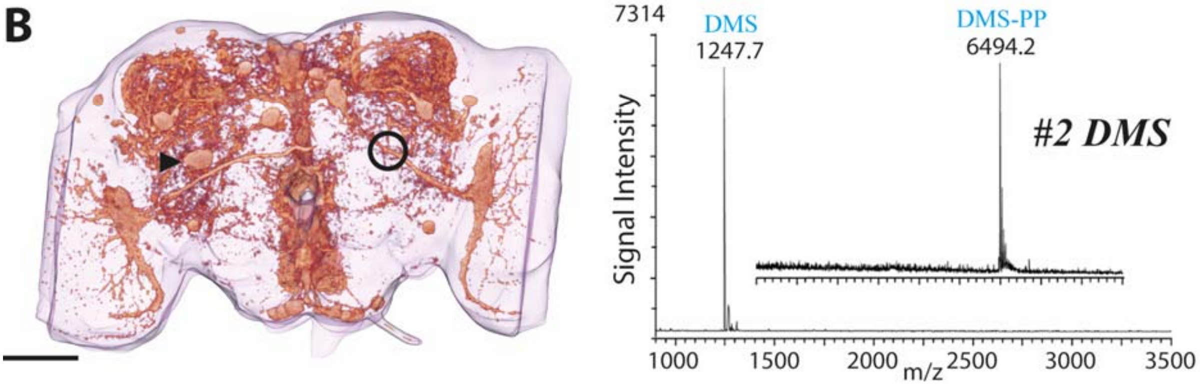

***MSFAQFFVACCLAIVLLAVSNTRA***AVQGPPLCQSGIVEEMPPHIRKVCQALENSDQLTSALKSYINNEASALVANSDDLLKNYNKRTDVDHVFLRFGKRR

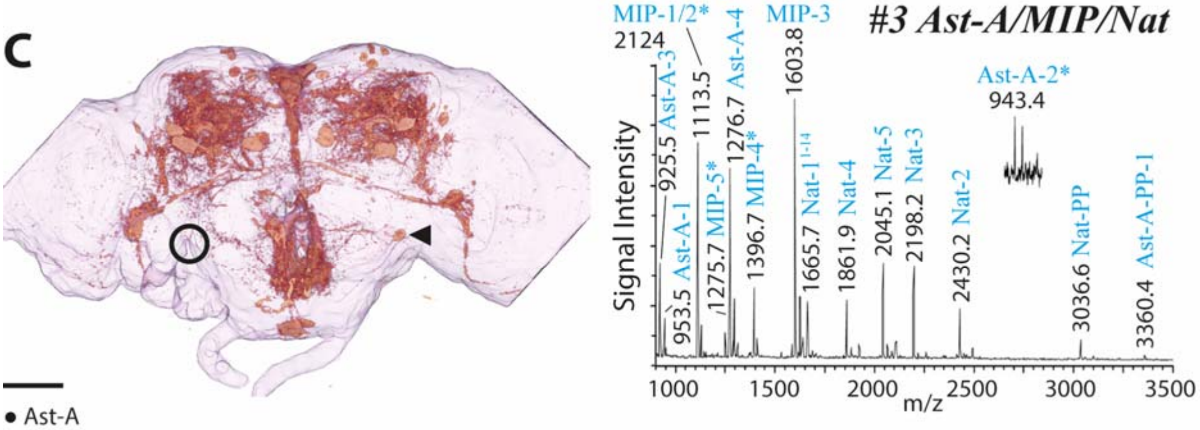

- Ast-A

***MNSLHAHLLLLAVCCVGYIAS***SPVIGQDQRSGDSDADVLLAADEMADNGGDNIDKRVERYAFGLGRRAYMYTNGGPGMKRLPVYNFGLGKRSRPYSFGLGKRSDYDYDQDNEIDYRVPPANYLAAERAVRPGRQNKRTTRPQFNFGLGRR

- MIP

***MAHTKTRRTYGFLMVLLILGSACG***NLVASGSAGSPPSNEPGGGGLSEQVVLDQLSESDLYGNNKRAWQSLQSSWGKRSSSGDVSDPDIYTGHFVPLVITDGTNTIDWDTFERLASGQSAQQQQQQPLQQQSQSGEDFDDLAGEPDVEKRAWKSMNVAWGKRRQAQGWNKFRGAWGKREPTWNNLKGMWGKRDQWQKLHGGWGKRSQLPSN

- Nat

***MRLTLAWLSLCLAIYCGGGHGH***GNVVLSLPPSLIATATKAALSHQRQQKQQQQHQKKDARVLFDSPADALRDMMHNGNGNGNGPMDSGKFSLSDVEQPAAQRSEDFNRNAYDLGARQSAPQEIAMGMELGMGLGLGPNNYRTTPPHRYWGQRCQGRSGGSGTSKCPQEYYRTMLAARNKEALSRLHMQLSSMQDSDSGASSSSDSEEEHVDDEEQSNNEVFMLLTGEQDLMKFLHWAMQVLYPIERPLGNLSDGAAENYYPGMFLWKKLNLSGHLEPPLIVDEPQYVLVRREKLFDGYQFGEDMSKENDPFIPPRGRKHSGSLDLDALMNRYEPFVPNRGKRDKVKDLFKYDDLFYPHRGKKHRNLFQVDDPFFATRGKKLQLRDLYNADDPFVPNRGKRHLTASAGKLGETMAGGGKWPDDSNNYWPLRMSTHKINGYDQSVRPSLSVEDAAASLASWRLPANRLHSTRSMSADLRQQLLLPHVRFIGNPNMRQQQQQQQQHQVKTSSWQAEERLRRSILAPGESNDAHETQLTLSHPA NPHLVTDTDNLNI

**Figure 5.2 Mapping of cell type #1-3**. (**A**) Localization of cell type #1, Ast-C neuron, corresponding mass spectrum and Ast-C precursor. The recorded mass spectrum shows ion signals for the N-terminal blocked [pQ] and unblocked [Q] form of Ast-C. (**B**) Localization of cell type #2, DMS neuron, corresponding mass spectrum and precursor. The recorded mass spectrum shows ion signals for the [pQ] form of DMS and the C-terminal PP. (**C**) Localization of cell type #3, Ast-A/MIP/Nat neuron, corresponding mass spectrum and related precursors. The recorded mass spectrum shows ion signals of mature peptide products and PP from all precursors and confirmed the co-localization of the three neuropeptide genes in these neurons for the first time. Asterisk: sodium adduct; arrowhead: localization unmanipulated soma; circle: localization dissected soma; scale bar = 50 µm. Signal peptide is given in bold italic, cleavage sites are given in red, identified sequences are given in blue, amidation sites are given in blue italic.

precursor, MIP, encodes five paracopies (Vanden Broeck 2001) which were all confirmed by SCMS in cell type #3. Furthermore, MIP-1, which is mass identical to MIP-2, was biochemically identified for the first time (Fig. 5.3 B, C). MIP-1 and 2, as well as 3 and 4, contain no Arg and were primarily detected as sodium adducts. Fragment spectra of mass identical MIP-1 and -2 as $[M+Na]^+$ revealed sufficient product ion signals for the confirmation of both peptides, however, a high number of unknown background ion signals were recorded. Unknown background ion signals can complicate manual and automated interpretation of product ion spectra by increasing possible false positive assignments of amino acids to ion signal pairs during *de novo* sequencing or by obscuring ion signals needed for sequence confirmation during matching of *in silico* predicted fragments to recorded product ion spectra. Thus, strategies to minimize occurring unknown background ion signals in product ion spectra can help to allow their fast and correct interpretation. A repeated analysis of the same cell type and corresponding fragmentation experiments of the putative MIP-1/2 $[M+Na]^+$ ion signal at *m/z* 1113.5 with 1,5-DAN, a matrix used for on-plate reducing of disulfide bonds (Fukuyama et al. 2006), resulted in much clearer $MS^2$ spectra. Even though the overall number of identifiable fragments was diminished, the extreme reduction of unknown background signals clarified the spectrum enormously (Fig. 5.3 B, C). Whether this effect is a general feature of 1,5-DAN on fragmentation of peptide sodium adducts, or if the amino acid sequence analyzed here resembles a unique case, remains elusive and will be the subject of future studies. Finally, products of a third multicopy peptide precursor, Nat, were detected in cell type #3 samples. Four of the five putative Nat paracopies were identified in corresponding mass spectra (Fig. 5.2 C; Jiang et al. 2013). Furthermore, only an N-terminal fragment of Nat-1 was recorded (Nat-$1^{1-14}$), suggesting cleavage of the putative internal Nat-1 Lys motive (Fig. 5.2 C). The analyzed cell type #3 likely corresponds to one of the few described Nat-immunopositive neurons from adult *D. melanogaster* brains, the inferior contralateral interneuron (ICLI; (Jiang et al. 2013). Moreover, a recent study investigating peptidergic control of satiety described the identical

ICLI neurons as part of an *MIP-GAL4* line, suggesting MIP expression in these cells (Min et al. 2016). Additionally, a third study described a tyraminergic input of these neurons by utilizing a genetic *tyramine-receptor-GAL4* (*TyrR-GAL4*) line, suggesting a key role of these ICLI neurons in male courtship (Huang et al. 2016; here IPS neuron). Additionally, the same study reported that these neurons also express MIP, confirming earlier results and corroborating the assumption that these neurons are identical to the analyzed cell type #3. Finally, comparison to a published immunocytochemistry study focusing on Ast-A, suggests that a single described neuron, the anterolateral tritocerebrum neuron 2 (ALT-2), is identical to the aforementioned ICLI neurons and to the described cell type #3 (Yoon & Stay 1995). The same study revealed that these neurons are visible for the first time during metamorphosis and explain their absence from the larval neuropeptidergic DIMM neuron map (Park et al. 2008). Cell type #3 represents the only observed cell type co-expressing three different neuropeptide genes in this study.

### *5.3.4 Cell type #4: CAPA neurons*

Mass spectrometric analysis of two large DIMM neurons (soma size: 16-17 µm; n = 6) in the GNG showed ion signals matching predicted products of the CAPA precursor and were therefore determined as CAPA neurons (Fig. 5.4 A; FlyBase ID: FBgn0039722). It has been shown that the *capa* and *pyrokinin* (*hugin*; see huginPK/ #5 cells) genes share a common evolutionary origin and it has been suggested that they result from a gene duplication during the emergence of hexapods (Derst et al. 2016). The proposed ancestor was a single gene encoding three distinct receptor ligands, which have separate designated names in insects: pyrokinins (PKs; Predel et al. 1999), periviscerokinins (PVKs; $CAP_{2B}$, (Predel et al. 1995; Huesmann et al. 1995), and the tryptoPKs (Veenstra 2014; Redeker et al. 2017). In *D. melanogaster* and other insects it has been shown that each of these neuropeptides activates a separate receptor (Park et al. 2002; Iversen et al. 2002; Kean et al. 2002; Meng et al. 2002; Rosenkilde et al. 2003; Cazzamali et al. 2005; Predel & Wegener 2006). However, the *D. melanogaster* CAPA precursor encodes two PVKs and one tryptoPK (Kean et al. 2002). Recorded mass spectra of CAPA neurons revealed only two ion signals, identifying an N-terminally truncated tryptoPK form and an N-terminally adjacent PP. This is not surprising since earlier studies suggested a cell type specific differential processing of the CAPA precursor in neuroendocrine cells from the abdominal ganglia of the VNC and corresponding cells from the GNG. Mass spectrometric analysis of adult abdominal hormone release sites (perisympathetic organs) revealed two mature PVKs and the mature tryptoPK, while mass

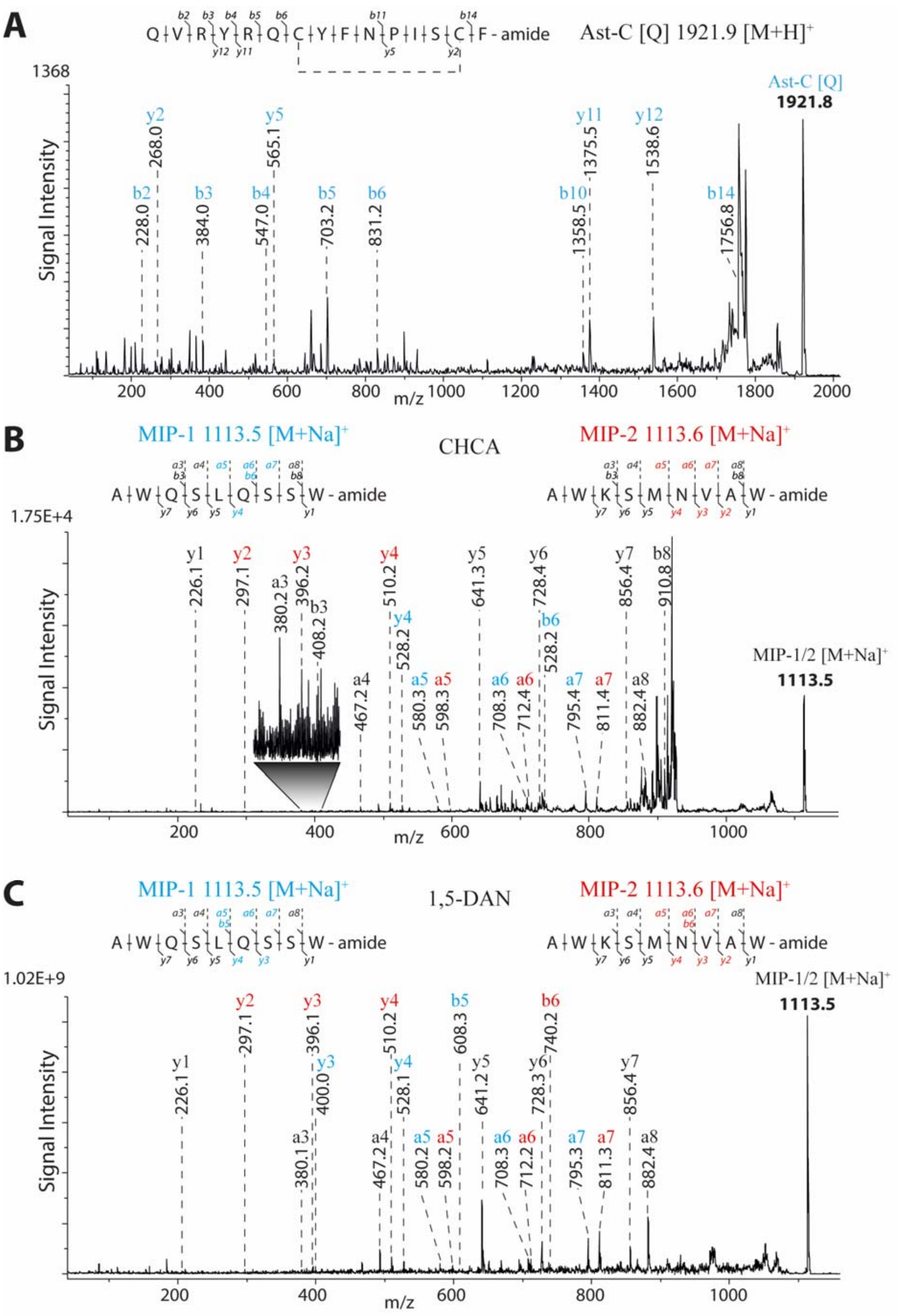
A
Q V R Y R Q C Y F N P I S C F - amide
b2 b3 b4 b5 b6 b11 b14
y12 y11 y5 y2
Ast-C [Q] 1921.9 [M+H]+
1368
Signal Intensity
y2 268.0
y5 565.1
y11 1375.5
y12 1538.6
b2 228.0
b3 384.0
b4 547.0
b5 703.2
b6 831.2
b10 1358.5
b14 1756.8
Ast-C [Q]
1921.8
200 400 600 800 1000 1200 1400 1600 1800 2000
m/z
B
MIP-1 1113.5 [M+Na]+
CHCA
MIP-2 1113.6 [M+Na]+
A W Q S L Q S S W - amide
a3 a4 a5 a6 a7 a8
b3 b6 b8
y7 y6 y5 y4 y1
A W K S M N V A W - amide
a3 a4 a5 a6 a7 a8
b3 b8
y7 y6 y5 y4 y3 y2 y1
1.75E+4
Signal Intensity
y1 226.1
y2 297.1
y3 396.2
a3 380.2
b3 408.2
y4 510.2
y4 528.2
y5 641.3
y6 728.4
b6 528.2
y7 856.4
b8 910.8
a4 467.2
a5 580.3
a5 598.3
a6 708.3
a6 712.4
a7 795.4
a7 811.4
a8 882.4
MIP-1/2 [M+Na]+
1113.5
200 400 600 800 1000
m/z
C
MIP-1 1113.5 [M+Na]+
1,5-DAN
MIP-2 1113.6 [M+Na]+
A W Q S L Q S S W - amide
a3 a4 a5 a6 a7 a8
b5
y7 y6 y5 y4 y3 y1
A W K S M N V A W - amide
a3 a4 a5 a6 a7 a8
b6
y7 y6 y5 y4 y3 y2 y1
1.02E+9
Signal Intensity
MIP-1/2 [M+Na]+
1113.5
y1 226.1
y2 297.1
y3 396.1
y3 400.0
y4 510.2
y4 528.1
b5 608.3
y5 641.2
b6 740.2
y6 728.3
y7 856.4
a3 380.1
a4 467.2
a5 580.2
a5 598.2
a6 708.3
a6 712.2
a7 795.3
a7 811.3
a8 882.4
200 400 600 800 1000
m/z

**Figure 5.3 MS² spectra of N-terminal unblocked AST-C, MIP-1 and MIP-2 from cell type #3 preparations.** Fragmentations of AST-C [Q] (**A**), mass identical MIP-1 and -2 with CHCA (**B**) and (**C**) 1,5-DAN as matrix. b-,y-,a- and c-fragments are labeled which confirm the predicted sequence of Ast-C [Q], MIP-2, and MIP-1. The usage of 1,5-DAN as matrix simplifies the sequence reconstruction of the analyzed sodium adducts of MIP-1 and -2 in resulting MS² mass spectra. Black fragment labels = mass identical for MIP-1 and 2.

spectrometric analysis of the adult retrocerebral complex yielded only truncated tryptoPK (Predel et al. 2004; Wegener et al. 2006). Therefore, the here obtained results corroborate these findings by confirming the absence of PVKs and the presence of the N-terminally truncated form of tryptoPK in the analyzed DIMM neurons. Transcriptomic analysis of abdominal ganglia and GNG showed no differences in detected CAPA transcripts (Neupert, Ragionieri, Predel, unpublished), hence this differential processing seems to be mediated by an expression of different processing enzymes in corresponding CAPA neurons. This represents the only reported case of differential neuropeptide precursor processing in *D. melanogaster* to this date.

### *5.3.5 Cell type #5: Hugin/Pyrokinin (huginPK) neurons*

Three DIMM cell populations in the GNG with a total of eight neurons (soma size 7-10 µm; n = 10; FlyBase ID: FBgn0028374) showed ion signals matching the huginPK precursor and thus were designated as huginPK neurons (Fig. 5.4 B). The huginPK precursor encodes two putative PKs, hug γ and PK (Meng *et al.*, 2002). Recorded mass spectra of analyzed DIMM neurons yielded ion signals for PK (SVPFKPRLamide, *m/z* 942.58) and a larger PP, the latter confirming the predicted length of the signal peptide (Fig. 5.4 B). Identical cells, identified by a *hugin-GAL4* line, were analyzed by SCMS in an earlier study, identifying also only PK in recorded mass spectra (Neupert et al. 2007). The here presented results corroborate these earlier findings. A previous study predicted also the cleavage of a second peptide from the precursor, hugin γ (QLQSNGEPAYRVRTPRLamide, *m/z* 1984.08; Meng et al. 2002). However, no corresponding ion signal were either detected in this study or an earlier study (Neupert et al. 2007). The expression patterns of huginPK neurons have been studied in great detail by immunocytochemistry and *huginPK-GAL4* driver lines in larvae and adults. Gnathal huginPK neurons send projections in the protocerebrum, the VNC, the retrocerebral complex as well as on to pharyngeal muscles (Siegmund & Korge 2001; Melcher & Pankratz 2005; Bader et al. 2007; Schlegel et al. 2016; Hückesfeld et al. 2016; King et al. 2017). The analyzed DIMM neurons are likely identical to these described GNG huginPK neurons. Furthermore, huginPK expression has been reported exclusively to DIMM neurons in larva (Park et al. 2008). Finally, huginPK neurons have been associated with linking the *D. melanogaster* circadian clock to locomotor activity in adults (King et al. 2017) as well as are necessary for the avoidance of bitter food sources and corresponding locomotor activity in larvae (Schlegel et al. 2016; Hückesfeld et al. 2016).

### *5.3.6 Cell type #6: Sulfakinin (SK) neurons*

Recorded mass spectra of two bilateral neurons located in the dorsal medium protocerebrum (soma size 11-14 µm, n = 3) showed ion signals matching products of the SK precursor and were thus designated as SK neurons (Fig. 5.4 C; FlyBase ID: FBgn0000500). The SK precursor encodes two putative SK paracopies and a smaller amidated peptide (Nichols et al. 1988). The two paracopies of SK, SK-1 and SK-2, were confirmed in recorded mass spectra of analyzed SK neurons, however, no ion signals were observed for the smaller peptide, SK-0, or PPs (Fig. 5.4 C). Moreover, SK-1 and 2 were only detected without sulfation, which was reported earlier and is needed for proper recognition by their corresponding receptor (Kubiak et al. 2002; Yew et al. 2009). This is due to the fact that detection of Tyr sulfation with MALDI-TOF MS operating in ion positive mode is not possible. The analyzed DIMM neurons are likely corresponding to the two medial protocerebrum cells (MP1), exhibiting extensive arborizations along the entire VNC, which were described in a study analyzing SK expression in different *D. melanogaster* developmental stages using a SK specific antiserum (Nichols & Lim 1996). MP1 neurons are also designated protocerebral descending neurons and seem to be highly conserved between insect taxa (Agricola & Braunig 1995). MP1 neurons are likely identical to the described SK-immunopositive DIMM neurons in larvae (Park et al. 2008). However, a suggested co-localization with AST-C in larvae could not be confirmed in the mass spectrometric analyzed adult neurons (Park et al. 2008). To date no function of the MP1 neurons has been published. However, a knockdown of DSK in DSK producing insulin cells in the *pars intercerebralis* has been shown to cause defective regulation of food intake, food choice and decreasing overall satiety (Söderberg et al. 2012; Nässel & Williams 2014). Furthermore, another study revealed that the Drosophila obesity-linked homologs *Transcription factor AP-2* and *Tiwaz* regulate octopamine signaling to initiate feeding (Williams et al. 2014; Nässel & Williams 2014). Octopamine then, in a negative feedback loop, induces expression of DSK to inhibit consummatory behavior (Williams et al. 2014; Nässel & Williams 2014). Finally, this *transcription factor AP-2* and *Tiwaz* controlled OA circuit regulating DSK secretion seems also to be involved in male aggression in *D. melanogaster* (Williams et al. 2014). Finally, the analyzed DIMM neurons are likely identical to the described larval CC-MS 2 neurons, which project into the larval ring gland (Siegmund & Korge 2001; Kean et al. 2002; Wegener et al.

2006). These neurons have also been described as DIMM positive in larvae (Park et al. 2008). CAPA in general has been shown to stimulate secretion in Malphighian tubules in *D. melanogaster* and other insects (Terhzaz et al. 2012; Halberg et al. 2015). Finally, this CAPA mediated secretion impacts desiccation and cold tolerance in *D. melanogaster* (Terhzaz et al. 2015).

### *5.3.7 Cell type #7: Corazonin (Cor)/short Neuropeptide F (sNPF) neurons*

Recorded mass spectra of single cells of a dorso-lateral DIMM cell population (soma size 7-9 µm, n = 7), comprised of four neurons, revealed ion signals matching to products of the Cor and sNPF precursor and were therefore defined as Cor/sNPF neurons (Fig. 5.5 A; FlyBase ID: FBgn0013767). The Cor precursor encodes a single putative corazonin peptide with an N-terminal Gln for potential pyroglutamyl formation (Veenstra 1994). Recorded mass spectra could only confirm the presence of the pyroglutamyl form of corazonin, while the unprocessed form with a free Gln was not detected (Fig. 5.5 A). The sNPF precursor encodes four putative sNPF paracopies, which were all confirmed in corazonin/sNPF neuron mass spectra (Vanden Broeck 2001; Fig. 5.5 A). sNPF-1 has an internal single Arg cleavage site and the potential usage would result in an truncated sNPF-1 form which would be sequence and therefore mass identical to sNPF-2. Comparison of the recorded relative ion signal intensities of sNPF precursor products indicate the usage of this internal cleavage site, since only small ion signals of the intact sNPF-1 form have been detected from the analyzed cells. Furthermore, a long precursor related peptide was identified, which follows directly the signal peptide in the sNPF precursor, in a complete and truncated form, missing the first N-terminal amino acid. This indicates a potential usage of the signal peptide with different lengths. The ion signal of mature Cor was always the most intense ion signal recorded in mass spectra of analyzed Cor/sNPF neurons. Comparison to a study analyzing expression patterns of corazonin viaimmunocytochemistry and *in situ* hybridization showed that the analyzed Cor/sNPF neurons are likely identical to the described DLP neurons (Choi et al. 2005). Moreover, another study analyzing sNPF expression patterns using immunohistochemistry, a *sNPF-GAL4* driver line and *in situ* hybridization, described a cell population in the same location as DLN1 (Nässel et al. 2008). A third study suggested a co-expression of Cor and sNPF in the DLP/DLN1 neurons by immunocytochemistry and a *Cor-GAL4* driver line (Kapan et al. 2012). The co-localization of Cor and sNPF has also been reported for the same neurons expressing DIMM in the larva (Park et al. 2008). The recorded mass spectra of analyzed Cor/sNPF neurons thus corroborate these earlier findings. It has been shown that these neurons are part of the circadian clock in *D. melanogaster* (Helfrich-Förster 2003; Schubert et al. 2018).

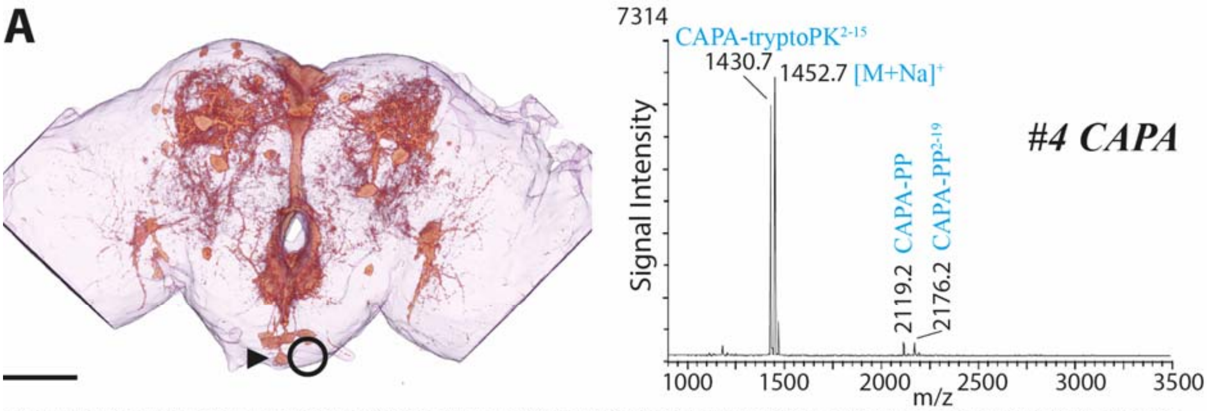

***MKSMLVHIVLVIFIIAEFSTA***ETDHDKNRRGANMGLYAFPRVGRSDPSLANSLRDGLEAGVLDGIYGDASQEDYNEADFQKKASGLVAFPRVGRGDAELRKWAHLLALQQVLDKRTGPSASSGLWFGPRLGKRSVDAKSFADISKGQKELN

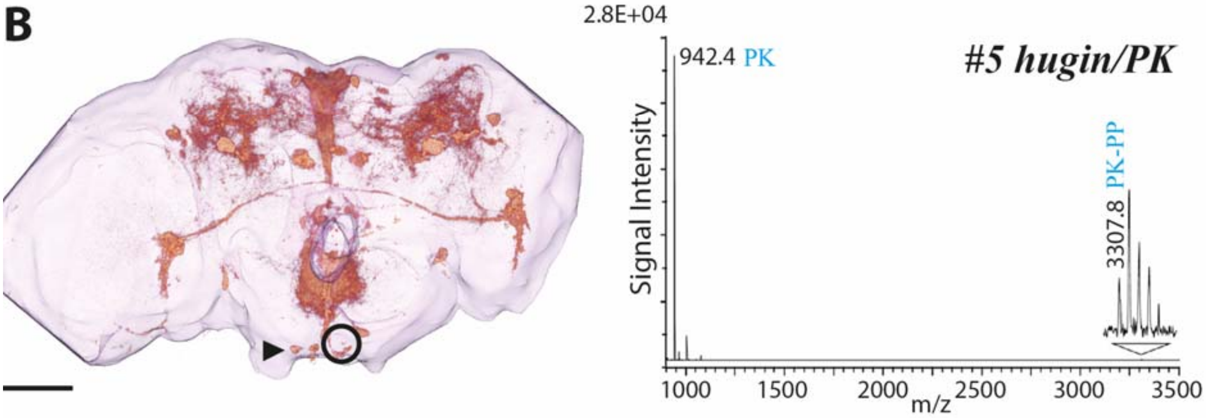

***MCGPSYCTLLLIAASCYILVCSHA***KSLQGTSKLDLGNHISAGSARGSLSPASPALSEARQKRAMGDYKELTDIIDELEENSLAQKASATMQVAAMPPQGQEFDLDTMPPLTYYLLLQKLRQLQSNGEPAYRVRTPRLGRSIDSWRLLDAEGATGMAGGEEAIGGQFMQRMVKKSVPFKPRLGKRAQVCGGD

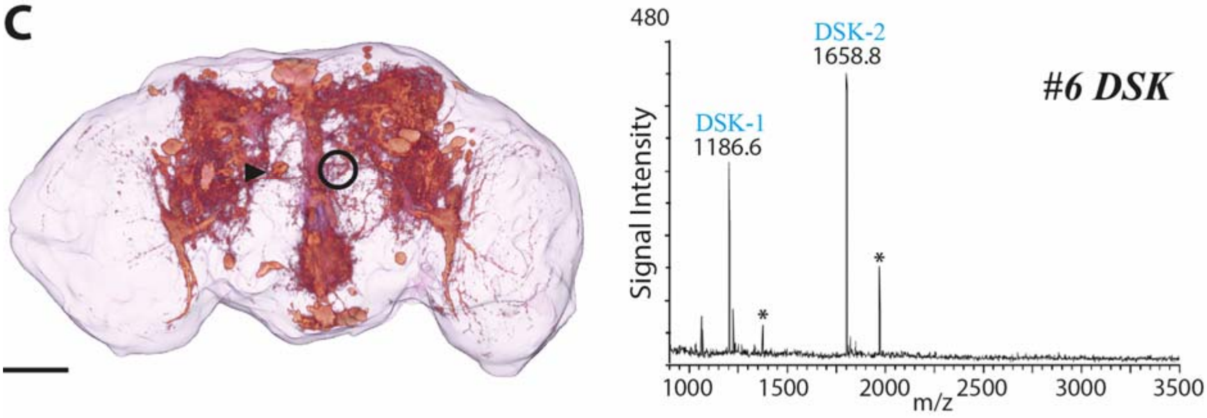

***MGPRSCTHFATLFMPLWALAFCFLVVLPIPAQT***TSLQNAKDDRRLQELESKIGGEIDQPIANLVGPSFSLFGDRRNQKTMSFGRRVPLISRPIIPIELDLLMDNDDERTKAKRFDDYGHMRFGKRGGDDQFDDYGHMRFGR

**Figure 5.4 Mapping of cell type #4-6**. (**A**) Localization of cell type #4, CAPA neuron, corresponding mass spectrum and CAPA precursor. The recorded mass spectrum shows ion signals of truncated CAPA-typroPK and a CAPA-PP, confirming the differential processing of the CAPA precursor in neuroendocrine cells of the GNG (shown here) and abdominal ganglia. (**B**) Localization of cell type #5, hugin/PK neuron, corresponding mass spectrum and hugin/PK precursor. The recorded mass spectrum shows ion signals for mature PK and a PK-PP. (**C**) Localization of cell type #6, DSK neuron, corresponding mass spectrum and DSK precursor. The recorded mass spectrum shows ion signals for DSK-1 and -2 without sulfation. Sulfation of Tyr cannot be detected in positive ion mode MALDI-TOF MS. Asterisk: sodium adduct; arrowhead: localization unmanipulated soma; circle: localization dissected contralateral soma; scale bar = 50 µm. Signal peptide is given in bold italic, cleavage sites are given in red, identified sequences are given in blue, amidation sites are given in blue italic.

### *5.3.8 Cell type #8: Pigment dispersing factor (PDF) neurons*

Mass spectrometric analysis of four medium sized (soma size: 9-11 µm, n = 5) neurons in the lateral protocerebrum revealed a single ion signal matching the PDF precursor and these neurons were therefore classified as PDF neurons (Fig. 5.5 B; FlyBase ID: FBgn0023178). The PDF precursor contains a single putative neuropeptide which was identified in recorded mass spectra. The analyzed DIMM neurons correspond to the described PDF-immunopositive large ventral lateral clock neurons (l-LNv; Helfrich-Förster 2003), which are part of the neuronal circadian clock in *D. melanogaster*. These cells were already analyzed by SCMS in an earlier study, using a *pdf-GAL4* line to mark these neurons (Neupert et al. 2007). Our results corroborate the prior findings, since recorded mass spectra were nearly identical. Even though a potential co-localization with NPF has been suggested for some l-LNvs, by a study using an *npf-GAL4* line and immunocytochemistry (Choi et al. 2005), mass spectra from this study as well as the previous study could not confirm this (Neupert et al. 2007). However, since NPF expression is controlled in a time depending manner it is possible that the analyzed neurons were not in the right time window or only cells which does not express NPF have been analyzed. Finally, L-LN$_v$ activity has been associated with arousal and promoting a waking state during the morning phase of *D. melanogaster* (Shang et al. 2008; Shang et al. 2013; Liang et al. 2017).

### *5.3.9 Cell type #9: Neuropeptide-like precursor 1 (NPLP1) neurons*

SCMS of two bilateral DIMM neurons in the dorso-lateral protocerebrum (soma size 11 µm, n = 2) revealed ion signals matching the NPLP1 precursor and were therefore determined as NPLP1 neurons (Fig. 5.5 C; FlyBase ID: FBgn0035092). The NPLP1 precursor encodes two putative sequences with a C-terminal amidation motif and several more without an amidation motif as PTM (Baggerman et al. 2002). However, the predicted sequences show a high degree of variation in their amino acid composition when compared to each other. Recorded mass spectra showed ion signals of 11 NPLP1 related peptides, with all of them being already reported in earlier peptidomic studies of the *D. melanogaster* CNS (Baggerman et al. 2002; Schoofs & Baggerman 2003; Predel et al. 2004; Yew et al. 2009; Salisbury et al. 2013). In contrast to other analyzed cell types, NPLP1 neurons showed multiple additional ion signals matching truncated forms of identified NPLP1 peptides (Fig. 5.5 C). Two peptides were identified with a C-terminally remaining Lys, (NIATMARLQSAPSTHRDPK-OH, *m/z* 2094.09; SVAALAAQGLLNAPK-OH, *m/z* 1423.83) from the dibasic cleavage site Arg-Lys, as reported earlier (Baggerman et al. 2002). A likely homologous NPLP1 peptide with the same remaining Lys has been reported from the yellow fever mosquito, *Aedes aegypti* (NIQSLLRTGMLPSIAPK-OH, NPLP1-6; Predel et al. 2010). Furthermore, one peptide (NVAAVARYNSQHGHIQRAGA-OH, $GAE^{1-20}$, *m/z* 2120.77) showed a C-terminally truncated form with an amidated C-treminus (NVAAVARYNSQHGHIQRA-$NH_2$). This suggests an additional C-terminal processing by exopeptidases until the amidation motif is unblocked and can be subsequently processed. Moreover, this is supported by the detection of other C-terminal truncated NPLP1 peptides from the same cell type (VQQ, Fig. 5.5 C, Table 5.2). Comparison to results from an immunocytochemical study using an antisera raised against the *D. melanogaster* NPLP1 peptide IPNamide revealed a highly possible match between the two analyzed DIMM neurons and two described adult IPNamide-immunopositive interneurons in the dorso-lateral protocerebrum (Verleyen et al. 2003). In the larva three IPNamide-immunopositive cell populations were described from the brain, the SP3, MP2 and DC cell clusters, however, none of these neurons exhibited any processes (Verleyen et al. 2003).Furthermore, no DIMM cells expressing NPLP1 were described for larva (Park et al. 2008). To date only VQQ of the NPLP1 derived peptides has been attributed with a function in Drosophila. VQQ activates a receptor guanylate cyclase and thereby stimulates fluid transport, increases cGMP in Malphigian tubules and ultimately signals environmental salt stress to the whole organism (Overend et al. 2012). Furthermore, a potential role in the *D. melanogaster* circadian clock has been suggested since IPNamide is expressed in DN1 clock neurons (Shafer et al. 2006).

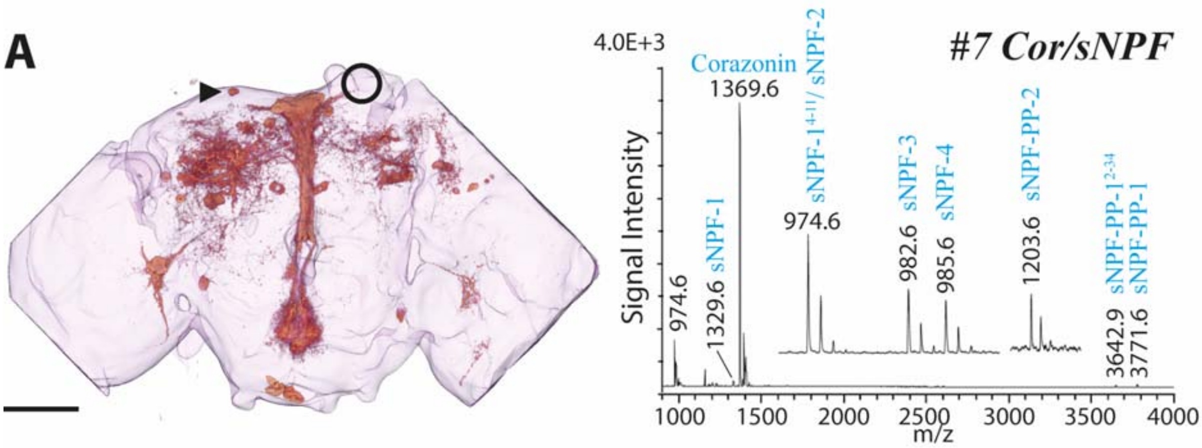

- Cor

***MLRLLLLPLFLFTLSMCMG***QTFQYSRGWTNGKRSFNAASPLLANGHLHRASELGLTDLYDLQDWSSDRRLERCLSQLQRS
LIARNCVPGSDFNANRVDPDPENSAHPRLSNSNGEVLYSSANIPNRHRSNELLEELSAAG GASAEPNVFGKH

- sNPF

***MFHLKRELSQGCALALICLVSLQMQQPAQA***EVSSAQGEHLVQPPPEKQSSKDSFLGTPLSNLYDNLLQREYAGPVVFPNH
QVERKAQRSPSLRLRFGRSDPDMLNSIVEKRWFGDVNQKPIRSPSLRLRFGRRDPSLPQMRRTAYDDLLERELTLNSQQQ
QQQLGTEPDSDLGADYDGLYERVVRKPQRLRWGRSVPQFEANNADNEQIERSQWYNSLLNSDKMRRMLVALQQQYEIPENV
ASYANDEDTDTDLNNDTSEFQREVRKPMRLRWGRSTGKAPSEQKHTPEETSSIPPKTQN

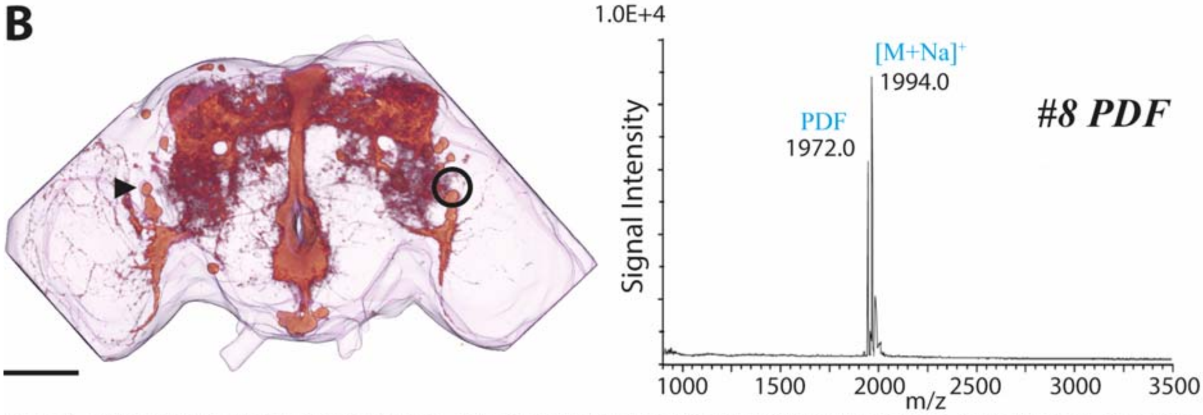

***MARYTYLVALVLLAICCQWGYCGA***MAMPDEERYVRKEYNRDLLDWFNNVGVGQFSPGQVATLCRYPLILENSLGPSVPIR
KRNSELINSLLSLPKNMNDAGK

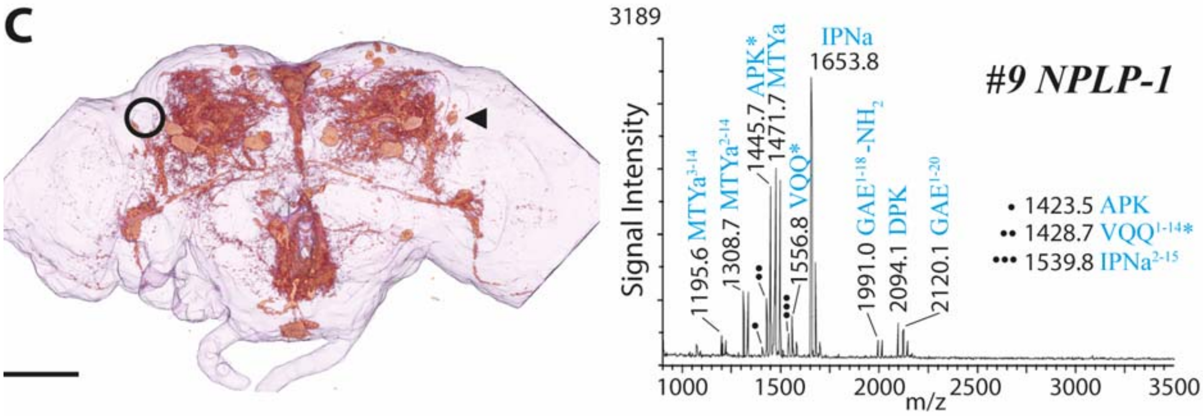

***MQAVLQSAHSSRRLMLLLSMLLNAAI***QPRSIIVSATDDVANVSPCEMESLINQLMSPSPEYQLHASALRNQLKNLLRERQ
LAVGEEQPLGEYPDYLEEDKRSVAALAAQGLLNAPKRSLATAKNGQLPTAEPGEDYGDADSGEPSEQKRYIGSLARAGGL
MTYGKRNVGTLARDFQLPIPNGKRNIATMARLQSAPSTHRDPKRNVAAVARYNSQHGHIQRAGAEKRNLGALKSSPVHGV
QQKREDEELLPAAAPDYADPMQSYWWYPSYAGYADLDWNDYRRAEKRFLDTSKDPELFGIHGNDATTAEPADEAYMESDA
EAGSEQLPSPQKRHIGAVYRSGFLPSYRYLRSPGGSSGFGGAGGRFSRSGRDARQFV

**Figure 5.5 Mapping of cell type #7-9.** (**A**) Localization of a Cor/sNPF neuron described as cell type #7, recorded mass spectrum and peptide precursors. The mass spectrum shows ion signals of Cor, the four predicted sNPF sequences and two additional sNPF PPs. (**B**) Localization of cell type #8, PDF neuron, corresponding mass spectrum and precursor. The recorded mass spectrum shows ion signals for mature PDF and its sodium adduct. (**C**) Localization of cell type #9, NPLP-1 neuron, corresponding mass spectrum and precursor. The recorded mass spectrum shows ion signals for various different NPLP-1 peptides and some truncated forms of these. Asterisk: sodium adduct; arrowhead: localization unmanipulated soma; circle: localization dissected contralateral soma; scale bar = 50 µm. Signal peptide is given in bold italic, cleavage sites are given in red, identified sequences are given in blue, amidation sites are given in blue italic.

### *5.3.10 Cell type #10: Neuropeptide F (NPF) neurons*

Recorded mass spectra of a single bilateral DIMM neuron in the dorsal medium protocerebrum (soma size 13-14 µm, n = 3), postereo-lateral of the DIMM positive *pars intercerebralis* cell group, revealed ion signals of the NPF precursor and was thus identified as NPF neuron (Fig. 5.6; FlyBase ID: FBgn0027109). The NPF precursor encodes a single putative NPF sequence and one putative precursor related sequence which have never been properly identified and confirmed by peptidomics to date (Brown et al. 1999). MS$^2$ experiments of putative mature NPF from designated DIMM NPF neurons revealed that the processed mature NPF is shorter than suggested, indicating a complete proteolytic processing of a monobasic Arg cleavage site at position 30 of the precursor (Fig. 5.6 B). Furthermore, two precursor related sequences were identified in recorded mass spectra unraveling the complete processing of the NPF precursor in the analyzed DIMM neurons for the first time (Fig. 5.6). Comparison to other studies using antisera directed against *D. melanogaster* NPF or an *npf-GAL4* driver line showed a correlation between the analyzed NPF DIMM neurons and described interneurons, either anti-NPF-immunopositive or GFP positive, innervating the dorsal and lateral protocerebrum as well as the ventral nerve cord (Brown et al. 1999; Wen et al. 2005; Krashes et al. 2009). Furthermore, the analyzed NPF neurons likely correlate to the described larval NPF-immunopositive DIMM neurons (Park et al. 2008). However, a co-localization of NPF and DH-31 as described for one larval DIMM neuron could not be convincingly confirmed (Park et al. 2008), even though a small ion signal matching mature DH-31 was found in a single recorded mass spectrum. While to date no study focused on the function of the described cell type #10 a large body of knowledge has been published on NPF function in invertebrates (Nässel & Wegener 2011). In *D. melanogaster* larvae, NPF signaling regulates motivation to feed (Wu et al. 2003; Wu et al. 2005), gustatory mediated food ingestion (Shen & Cai 2001) and feeding in general (Wu et al. 2003) . Furthermore, it has been associated with modulating alcohol sensitivity (Wen et al. 2005), behavioral and sensory responses to stress (Xu et al. 2010), aggression (Dierick & Greenspan 2007) and learning (Krashes et al. 2009).

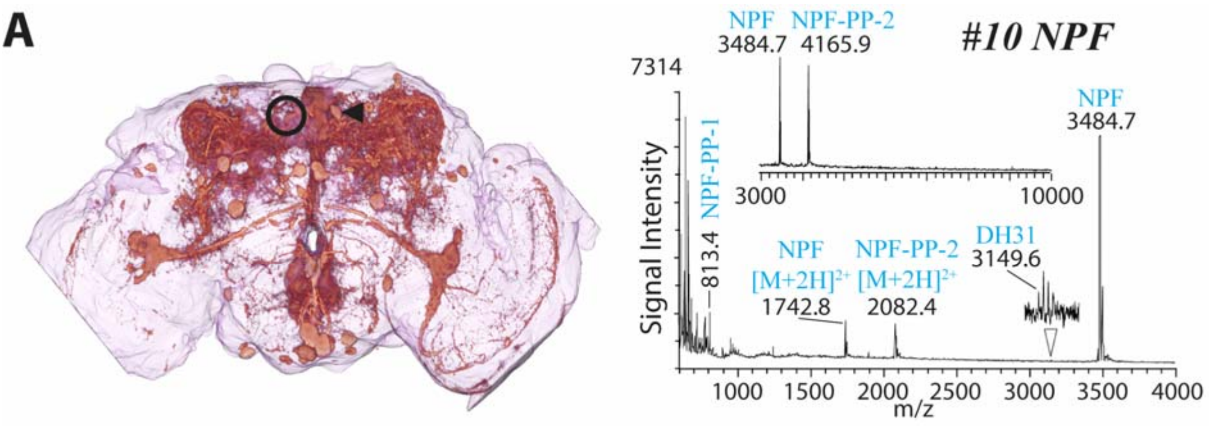

- NPF

***MCQTMRCILVACVALALLAAGCRVEA***SNSRPPRKNDVNTMADAYKFLQDLDTYYGDRARVRFGKRGSLMDILRNHEMDNI
NLGKNANNGGEFARGFNEEEIF

- DH31

***MTNRCACFALAFLLFCLLAISSIEA***APMPSQSNGGYGGAGYNELEEVPDDLLMELMTRFGRTIIRARNDLENSKRTVDFGLAR
GYSGTQEAKHRMGLAAANFAGGPGRRRRSETDV

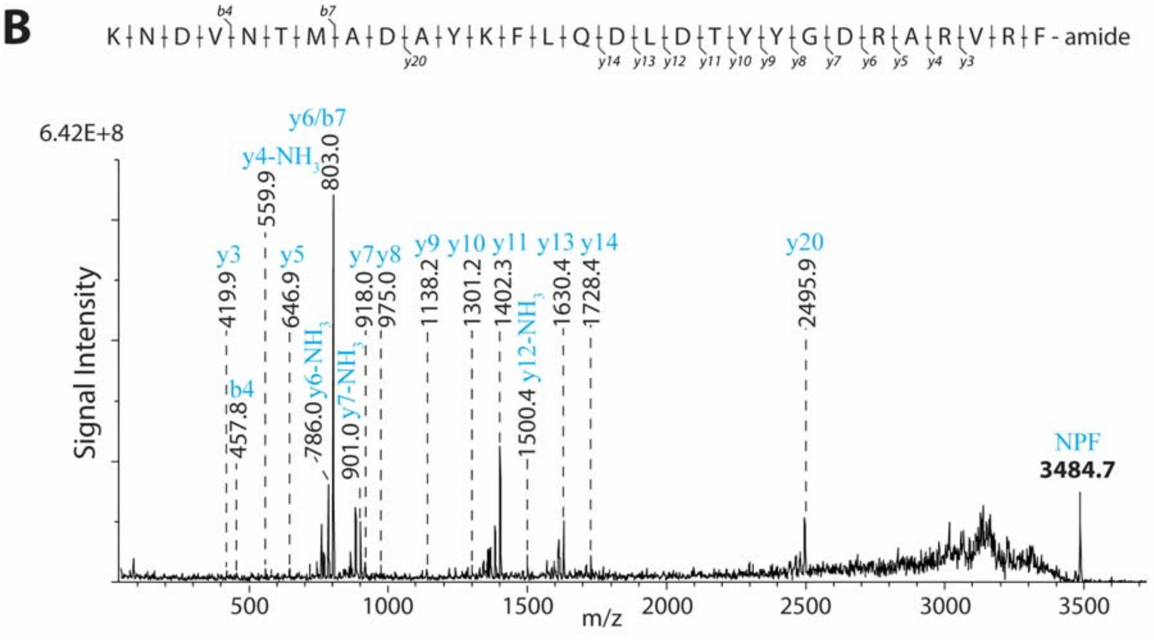

**Figure 5.6 Mapping of cell type #10.** (**A**) Localization of cell type #7, NPF neuron, corresponding mass spectrum and precursors. The recorded mass spectra show ion signals of NPF and two PP, confirming the complete processing of the NPF precursor. A small ion signal of DH31 was recorded in one sample preparation, however, it is not clear whether this signal originates from a contamination or represents a co-localization of the two precursors in cell type #10. (**B**) Recorded MS² mass spectrum of fragmented NPF from a cell type #10 sample preparation. The identified mature NPF is shorter in comparison to the originally predicated sequence. Arrowhead: localization undissected soma; circle: localization dissected contralateral soma; scale bar = 50 µm. Signal peptide is given in bold italic, cleavage sites are given in red, identified sequences are given in blue, amidation sites are given in blue italic.

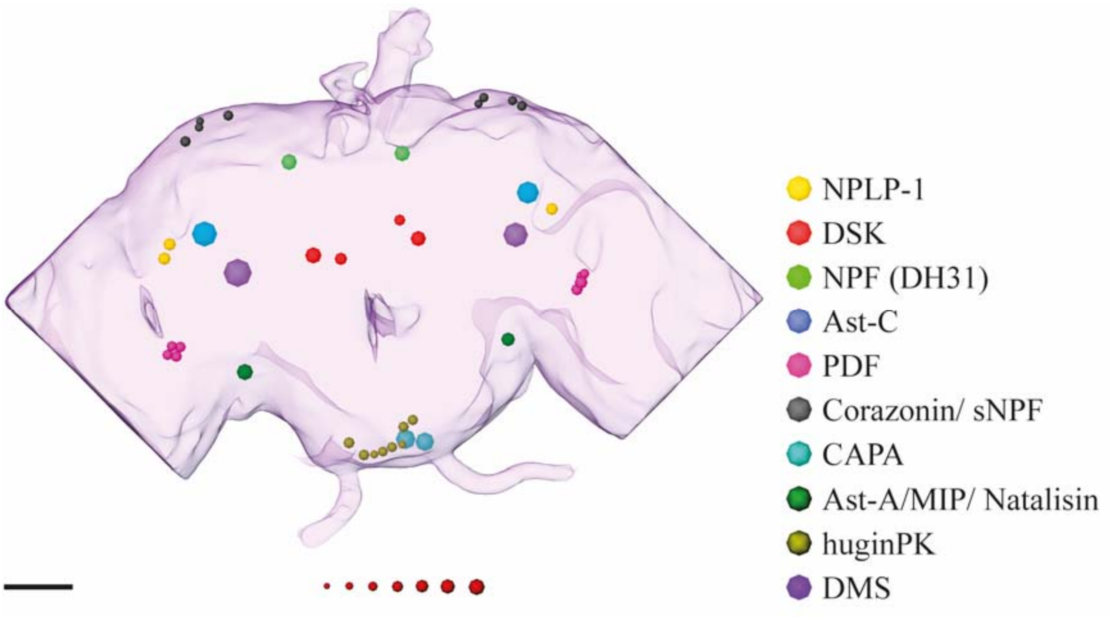

**Figure 5.7 Overview of SCMS analyzed DIMM neurons in the brain and GNG of adult *D. melanogaster*.** Scale bar = 50 µm; red size-markers from left to right: 3.5, 5.2, 6.8, 8.2, 9.6, 12.4, 14.0 µm.

## 5.4 Conclusion

By using GFP guided single cell microdissections and SCMS, the neuropeptidome of a total set of 10 clearly identified DIMM cell populations and single neurons were analyzed in the adult *D. melanogaster* brain and GNG (Fig. 5.7). Analyzed DIMM populations included not only neuroendocrine cells that project into the retrocerebral complex but also a number of interneurons with varying projections in the brain and/or the VNC. Mass spectrometric analysis of DIMM neurons revealed a total of 52 neuropeptide related products from 13 neuropeptide precursors, covering all mature neuropeptides from the observed precursors which have been described in earlier studies. In some cases, mature neuropeptides could be biochemically identified and confirmed for the first time, such as the natalisins, NPF and MIP-1. Overall 18 neuropeptides and PPs were detected for the first time. Furthermore, the here detected and identified neuropeptides and PPs allow to unravel cell specific processing of individual neuropeptide precursors. The here presented data can be implemented into existing virtual standard brain atlases such as Virtual Fly Brain (https://www.virtualflybrain.org/) or Fly Circuit (http://www.flycircuit.tw/).

With the presented results the basis for a map of DIMM neurons and their neuroactive substance repertoires has been laid. The now available data can be used as reference when analyzing potentially co-localized neuroactive substances, such as biogenic monoamines or classical neurotransmitter in neuropeptidergic DIMM neurons. For example, the within this thesis developed MALDI-TOF SCMS protocol could be used to analyze possible co-localized biogenic monoamines in DIMM neurons, using the presented data as a control (see chapter 2; Diesner, Predel, et al. 2018). Furthermore, the presented SCMS approaches could be applied to the *c929-GAL4* driver line in combination with other GAL4 driver lines, labeling neurons expressing aminergic or classical transmitter synthesizing enzymes to corroborate presented and future SCMS results and ease data interpretation. Ultimately, the presented data created by such complementary methods can help to increase our understanding of the distribution and interaction of neuroactive substances and thus of their functions in the CNS.

# 6. General Discussion

In the current thesis I developed a new MALDI-TOF MS approach for the detection and quantification of two biogenic monoamines, OA and TA, from single isolated neuron somata. Moreover, it was shown that the developed approach also holds the possibility to detect neuropeptides from the same single cell sample. In the following sections I want to point out the methodological aspects, limitations and drawbacks of this method, as well as discuss the obtained results in the light of possible applications and future research.

## 6.1 Methodological aspects of the developed MALDI-TOF MS based approach

In order to overcome persisting challenges in MALDI driven qualitative and quantitative biogenic monoamine analysis several different approaches, such as chemical derivatization of biogenic monoamines for their improved detection (Manier et al. 2014; Gatti et al. 2012), isotopically labeled ISs and an optimized sample preparation for a robust quantification (Persike & Karas 2009; Persike et al. 2010) were combined in a single workflow for the first time. In order to allow the qualitative and quantitative analysis of OA and TA of single neuron somata samples this workflow was successfully miniaturized to low nl volumes (see chapter 2; Diesner & Neupert 2018). Moreover, the developed workflow holds the possibility to interrogate potentially co-localized neuropeptides from the same single cell sample, which is based on the utilized MALDI matrix CHCA, which is capable of sufficiently ionizing derivatized biogenic monoamines and neuropeptides alike (see chapter 2; Diesner & Neupert 2018). The enhanced detection of the targeted biogenic monoamines OA and TA, the miniaturization of the workflow and the limited chemical complexity of the single cell samples further enabled to omit a sample fractionation by CE, as utilized in other analytical setups (e.g. Paxon et al. 2005; Lapainis et al. 2007; Nemes et al. 2013; Aerts et al. 2014; Denno et al. 2016; Lombard-Banek et al. 2016). Finally, the straight forward sample preparation and scalability of the developed workflow should allow to analyze biogenic monoamines and/or neuropeptides from single isolated neuron somata of variating size and organismic origin, as shown for single neuron somata of *D. melanogaster* and *C. morosus* in this thesis, as well as shown for the similar derivatization free MALDI-TOF approach used in this thesis and previous studies (see chapter 2-5; Li, Garden, et al. 2000; Neupert & Predel 2005; Neupert et al. 2007; Rubakhin & Sweedler 2007; Diesner, Predel, et al. 2018).

### *6.1.1 Range of detectable analytes*

The developed approach utilizes derivatization of the amine moieties of the targeted biogenic monoamines, OA and TA, in combination with the widely used CHCA matrix to improve their detection and quantification by MALDI-TOF SCMS. Furthermore, the developed protocol also allows the detection of neuropeptides from the same sample. While this approach has been successfully applied to detect amol amounts of OA and TA from biological samples as shown throughout this thesis (see chapter 2-4; Diesner & Neupert 2018), the question arises whether this approach is also beneficial for the detection of other amine containing metabolites as well as neuroactive substances from single cell samples. The first utilized derivatization agent CA has been used to derivatize other amine containing metabolites and neuroactive substances, such as amino acids, DA, GABA, and 5-HT, as well as the second utilized derivatization agent DPD has been used to derivatize amino acids, aside from OA and TA (Gatti et al. 2010; Manier et al. 2011; Gatti et al. 2012; Manier et al. 2014). These earlier findings in combination with the presented results for OA, TA as well as DA from this thesis (see chapter 2; Diesner & Neupert 2018) let one hypothesize that both derivatization agents should also be beneficial for an enhanced MALDI-TOF MS driven detection of other amine containing metabolites and neuroactive substances from single cell samples. Nevertheless, the derivatization as well as the overall developed workflow house some drawbacks that can hamper the detection of other amine containing metabolites and neuroactive substances. The high number of intense CHCA matrix related ion signals observed in the low mass range limits the overall number of potentially detectable low mass analyte ion signals (Persike & Karas 2009; Persike et al. 2010; Shariatgorji et al. 2012; Shariatgorji et al. 2014). Moreover, the ionization properties of the MALDI matrix as well as the chemical composition of the sample can lead to ion suppression effects, hampering a successful detection of certain analytes (Krause et al. 1999; Duncan et al. 2008). While the developed workflow as well as the derivatization free MALDI-TOF SCMS approach profit from the overall reduced chemical complexity of a single cell sample and are thus probably not as affected as multi-cell samples, such effects cannot be completely ruled out as they can be apparent in every multi-analyte sample analysis using MALDI-TOF MS (Duncan et al. 2008). Furthermore, the derivatization of a targeted biogenic monoamine by the utilized derivatization agents not only affects the absolute mass of a targeted analyte, but can also potentially lead to the detection of high intensity product ions upon fragmentation that not directly relate to the targeted analyte (Manier et al. 2014). These high intensity product ions can render it difficult or impossible to validate an unambiguous identification of the targeted analyte in relation to other isobaric/isometric analytes (Manier et al. 2014). However, this seems to be limited to small molecule analysis, as it was shown that the CA and DPD derivatized neuropeptide DMS, analyzed from synthetic samples as well as single DMS expressing neuropeptidergic neuron somata of adult *D. melanogaster*, showed the successful generation of b- and y- product ions upon fragmentation (see chapter 2; Diesner & Neupert 2018). Additionally, the utilized derivatization agents only showed a limited turn-over of the analyzed neuropeptide in biological samples (CA-DMS signal intensity 15% compared to underivatized DMS signal; DPD-DMS signal intensity 2.75% compared to underivatized DMS signal, chapter 2; Diesner & Neupert 2018), thus allowing the detection and fragmentation of the underivatized neuropeptide from a corresponding sample (see chapter 2; Diesner & Neupert 2018). However, if this applies to neuropeptide analysis in general using the developed approach will have to be investigated by future studies. Moreover, the CHCA matrix utilized in the developed workflow enables the detection of neuropeptides in a mass range up to *m/z* 4000 (e.g. Neupert & Predel 2005; Neupert et al. 2005; Neupert, Huetteroth, et al. 2009; Diesner, Gallot, et al. 2018). However, CHCA shows a preference towards Arg containing peptides and thus Arg free sequences can be potentially missed when using the developed approach (Leszyk 2010).

As a consequence of these drawbacks each new targeted biogenic monoamine or amine containing substance has to be evaluated carefully for an unambiguous identification and detection in biological samples using the developed approach. This evaluation should rest on analyzing synthetic samples in a range of multiple magnitudes in conjunction with an isotopically standard, in order to allow an experimental determination of the LOD and LLOQ as well as to investigate possible product ions for a unambiguous identification, as shown in this thesis and a previous study (see chapter 2; Manier et al. 2014; Diesner & Neupert 2018). Further, possible isobaric/isometric analytes should be ideally investigated in a similar fashion. After a successful experimental determination of the LOD/LLOQs as well as suitable product ions for an unambiguous identification, biological samples should always be cross validated by analyzing a cell or tissue sample that should be devoid of the respective analyte as well as screen resulting product ion spectra towards unidentified ion signals, as shown in this thesis (see chapter 2, 4; Diesner & Neupert 2018; Stolz 2018; Stolz et al. 2018 *in preparation*). Thus, unaccounted isobaric/isometric analytes can further be excluded from the sample analysis that can potentially originate from the sample background.

Nevertheless, future studies could overcome parts of the presented limitations in terms of qualitative analysis of a given targeted analyte by switching between the two tested derivatization agents. Moreover, future studies could also use alternative MALDI matrices such as DHB, which produces another set of matrix background ions compared to CHCA, potentially allowing the successful detection of a masked derivatized analyte, as well as expanding the range of detectable neuropeptides to mass ranges > *m/z* 4000 and Arg free sequences, as used within this study for the derivatization free detection of neuropeptides from single neuropeptidergic *D. melanogaster* neuron somata and previous studies (see chapter 5; e.g. Li, Garden, et al. 2000; Rubakhin et al. 2003; Rubakhin & Sweedler 2007; Redeker et al. 2017; Liessem et al. 2018; Diesner, Predel, et al. 2018). However, whether DHB shows the same performance in qualitative and quantitative analysis of derivatized biogenic monoamines has to be investigated by future studies.

### 6.1.2 *Limit of detection and quantification*

The developed workflow shows LODs as low as 18.4 amol (1 fmol/µl, in 18.4 nl samples) for the two analyzed biogenic monoamines, OA and TA, when using DPD, and 18.4 amol for OA and 46 amol for TA when using CA as chemical derivatization agent (OA, 1 fmol/µl; TA, 2.5 fmol/µl; in 18.4 nl samples; see chapter 2; Diesner & Neupert 2018). These experimentally determined LODs are in the range of the most sophisticated analytical setups that have been used to investigate biogenic monoamines and small metabolites in general from single cells or neuronal tissues: CE-µESI-MS (LOD 60 amol, experimentally determined for ACh and His, Met; Nemes et al. 2013; Onjiko et al. 2015), MEKC-ECD (LOD 3.4 amol for OA, calculated from regression plots; Paxon et al. 2005), CE-FSCV (LOD 78 fmol for OA, calculated from regression plots; Denno et al. 2015), CE-LIF (LOD 11 fmol/µl for OA, experimentally determined but no absolute detection limit given, Lapainis et al. 2007). In the latter techniques the LOD corresponds to the LLOQ, however, this holds not true for the developed MALDI-TOF MS approach (see chapter 2; Diesner & Neupert 2018). Nevertheless, the determined LLOQ of 184 amol for OA and TA (10 fmol/µl, in 18.4 nl samples) using CA as derivatization agent, is still within the grasp of the latter chromatographic supported methodological approaches (see chapter 2; Paxon et al. 2005; Lapainis et al. 2007; Nemes et al. 2013; Romanova et al. 2014; Onjiko et al. 2015; Denno et al. 2015; Diesner & Neupert 2018). Aside from the LLOQ the developed MALDI-TOF SCMS approach shows a good working range over three orders of magnitudes in MS and two orders of magnitudes in $MS^2$ mode (see chapter 2; Diesner & Neupert 2018).

The developed workflow also enables the detection of co-localized neuropeptides from the same sample, however, only qualitative analysis was performed in this thesis and no exact LODs were determined (see chapter 2; Diesner & Neupert 2018). A previous study has reported low amol LODs for the analysis of neuropeptides from single neurons, using CHCA driven MALDI-TOF MS analysis (~20 amol; Neupert & Predel 2005), as utilized in the derivatization free MALDI-TOF SCMS analysis as well as in the developed workflow (see chapter 2, 5; Diesner et al. 2018; Diesner & Neupert 2018). The MALDI-TOF MS analysis of CA and DPD derivatized single somata from neuropeptidergic neurons of adult *D. melanogaster* showed only a limited turn-over of the expressed DMS neuropeptide by the respective derivatization agents (CA-DMS signal intensity 15% compared to underivatized DMS signal; DPD-DMS signal intensity 2.75% compared to underivatized DMS signal, chapter 2; Diesner & Neupert 2018). Under the assumption that the observed limited turn-over applies to other neuropeptides as well, the developed workflow should also allow detection of neuropeptides in the amol range with slightly increased values compared to previously reported LODs (Neupert & Predel 2005).

### 6.1.3 Sample isolation

Single neuron somata were isolated manually from insect nervous systems using tapered glass capillaries for subsequent qualitative and quantitative MALDI-TOF MS analysis in this thesis (see chapter 2-5; Diesner & Neupert 2018; Diesner, Predel, et al. 2018). This approach has been used extensively in the analysis of single cells and offers a straight forward sample isolation (e.g. Li, Garden, et al. 2000; Neupert & Predel 2005; Rubakhin & Sweedler 2007; Neupert et al. 2007; Nemes et al. 2013), however, some drawbacks remain. The manual dissection and transfer of a single cell can lead to mechanical stress, which can induce exocytosis of neuroactive substances from the targeted neuron or even lead to membrane raptures with subsequent loss of cytoplasm or complete cell disintegration (Rubakhin et al. 2003; Ye et al. 2006; Rubakhin & Sweedler 2007; Rubakhin & Sweedler 2008; Nemes et al. 2012). In order to minimize the potential exocytosis of biogenic monoamines from targeted neuron somata during manual isolation and transfer, dissections were performed in a buffer containing 33% glycerol (see chapter 2-4; Diesner & Neupert 2018; Stolz 2018; Stolz et al. 2018 *in preparation*). Glycerol has been shown to increase neuron integrity as well as to reduce the exocytosis of neuroactive substances during isolation of single neurons, without significantly changing the cells metabolic profile (Rubakhin et al. 2003; Miao et al. 2005; Rubakhin et al. 2006; Rubakhin & Sweedler 2008). Moreover, cell integrity was visually controlled throughout the dissection and transfer process and only intact cell somata were analyzed. To further limit the potential loss of analytes by exocytosis, insects were anaesthetized by cooling and dissected in ice cold dissection buffer, which leads to a reduced action potential generation and a general halt of neuronal activity and thus a reduced exocytosis (French 1985; Warzecha et al. 1999; Cognigni et al. 2018). These applied precautions should reduce the overall loss of neuroactive substances during sample isolation, however, they can also potentially lead to an artificial rise of somatic neuroactive substances. Enzymatic activity has been shown to be preserved in glycerol stabilized cells, however, such an stabilization can also lead to enhanced enzyme activity (Raibekas & Massey 1997; Rubakhin et al. 2003). Such a preserved or even enhanced enzymatic activity in combination with the reduced exocytosis due to the applied cooling and ice cold dissection buffers can lead to an enhancement of somatic biogenic monoamine titers in analyzed neuron somata, as suggested by the results from single VMlb neurons of adult *D. melanogaster* that had been subjected to different time of cooling prior to somata isolation (see chapter 2; Diesner & Neupert 2018). In order to minimize this effect, but still benefit from the anaesthetization of the flies as well as the reduced exocytosis during dissections, the cooling time was kept to a maximum of 15 mins in all further quantitative experiments (see chapter 2; Diesner & Neupert 2018). Furthermore, excessive glycerol can hamper sample preparation as well as the subsequent detection of analytes and has to be removed prior to the addition of other chemicals or MALDI-TOF MS analysis (Rubakhin et al. 2003). Excessive glycerol is washed off with 50% MeOH/50% water applied by a glass capillary to minimize such effects (chapter 2-4; Diesner & Neupert 2018; Diesner, Predel, et al. 2018). However, to exclude a preliminary extraction of neuroactive substances from a respective sample due to this washing procedure, extra care was taken that the dissected somata are not covered by the washing solution in quantitative experiments (see chapter 2, 3; Diesner & Neupert 2018). Another potential problem during somata isolation is small debris from adjacent neuronal and glial projections as well as presynaptic terminals which can remain on the extracellular surface of the targeted cell soma after dissection. These structures may be small in size but can contain vesicles in which neuroactive substances are highly concentrated, thus leading to their detection and false positive qualitative and quantitative results (Aerts et al. 2014). Even though somata were visually examined after the transfer to the sample plate for such debris, it cannot be completely ruled out that the analyzed samples were completely debris free. Aside from this, the length of the remaining axon attached to the dissected soma could also potentially affect the recordable biogenic amine titers, as axons yield large numbers of vesicles, which are packed with high concentrations of neuroactive substances and are trafficked towards the release sites of a neuron

(Brady et al. 2012). In order to minimize such a potential effect, the length of the axon was always kept as short as possible during dissections throughout all experiments.

All of the discussed methodological drawbacks from the sample isolation and preparation procedures can affect the detectable somatic titers of the targeted biogenic monoamines, even though the applied workflow tries to minimize such effects by addressing each drawback individually. However, due to the mixed nature of the different effects (increase/decrease of somatic titers), it cannot be clearly determined if and to what extend the recorded titers differ from somatic *in vivo* concentrations. Nevertheless, the robust quantitative results obtained from the analysis of single VL and VMlb OA/TAergic neuron somata of adult *D. melanogaster* within this thesis suggest that these effects are stable between different sample preparations and thus does not limit the capability to detect and quantify stable and changing somatic OA/TA titers from manually isolated single insect neuron somata (see chapter 2, 3; Diesner & Neupert 2018).

A very elegant way to overcome most of these drawbacks is the direct sampling of cytoplasm from the neuron soma of interest by a patch clamp or a sharp capillary (Aerts et al. 2014; Onjiko et al. 2017a; Onjiko et al. 2017b). This approach minimizes the risk of contaminations from the remaining cell matrix debris as well as leakage of cytoplasm. Such an sampling approach has been successfully used to analyze metabolites by CE-ESI-MS from mouse thalamic neuron and astrocyte somata (extracted sample volume ~3 pl; Aerts et al. 2014) as well as single blastomeres of 8-32 cell stages of *X. laevis* embryos (extracted sample volume ~10 nl; Onjiko et al. 2017a; Onjiko et al. 2017b). Future studies will have to investigate whether this technique is also applicable to the here analyzed OA/TAergic interneurons of *D. melanogaster*, which have an even smaller sample volume compared to the aforementioned analyzed mouse thalamic neuron and astrocyte somata (VMlb cell diameter 10-7 µm, total somatic volume ~4-1.5 pl). Moreover, such future studies have also to assess whether this sample isolation process can be successfully combined with the developed workflow.

## 6.2 Applications and implications for further research

The developed MALDI-TOF MS workflow enables the detection and quantification of OA and TA from single neuron somata that were isolated from intact brain dissections. The workflow was established and validated using single genetically labeled OA/TAergic neurons of the model organism *D. melanogaster*. Moreover, by using this approach it was possible to reveal for the first time differences in somatic OA titers among single *D. melanogaster* neurons from two distinct cell populations, the VMlb and VL cluster, as well as an upregulation of somatic VMlb OA titers upon social contact in socially isolated male *D. melanogaster* (see chapter 2, 3; Diesner & Neupert 2018). VL neurons showed in average a significantly lower somatic OA titer in comparison to VMlb neurons, while both neuron populations showed TA detection only in some of the analyzed samples (see chapter 2; Diesner & Neupert 2018). These results match to previous findings of immunohistochemical studies that showed that VL neurons were immunopositive for OA and TA but showed no immunoreactivity against the OA synthesizing enzyme Tßh, whereas VMlb neurons showed positive immunoreactivity against OA, TA as well as Tßh (Busch et al. 2009; Schneider et al. 2012). This significant difference in somatic OA titers between the two analyzed cell populations suggests a differential release of OA/TA ratios from these neurons, as downstream targets express different sets of OA receptors. VL neurons target bitter sensing GRNs in the GNG, enhancing the excitability of these neurons through the Oct-TyrR (LeDue et al. 2016). The Oct-TyrR has been shown to be activated by OA as well as TA and leads in both cases to similar $CA^{2+}$ responses in targeted bitter sensing GRNs (Robb et al. 1994; LeDue et al. 2016). Thus, it can be concluded that VL neurons do not need high OA concentrations in order to modulate bitter GRNs, but rather can co-release OA and TA in similar concentrations, reflecting the recorded OA/TA titers (see chapter 2; Diesner & Neupert 2018). Subpopulations of VMlb neurons on the contrary, have been shown to modulate OAMB receptor expressing DAergic PAM neurons that control appetitive reward and Octβ2R expressing DAergic neurons that control appetitive motivation (Burke et al. 2012). OAMB and Octβ2R show an 2-3 magnitude lower $EC_{50}$ value for OA compared to TA (Han et al. 1998; Maqueira et al. 2005), leading to the conclusion that VMlb neurons use preferentially OA to modulate downstream targets, also reflecting the detected OA/TA titers. Moreover, the detection of an enhanced VMlb OA titer in regrouped males point towards a similar direction. Socially isolated *D. melanogaster* males have been reported to show a more intense aggressive behavior towards conspecifics, which is accompanied by a lower OA VMlb titer in comparison to grouped raised males (see chapter 3; Zhou et al. 2008). When isolated males are regrouped for 24 h this discrepancy in OA VMlb titers is abolished (see chapter 3). However, it has to be noted that it was not possible to discriminate between different specific VMlb neurons during the dissections, as the utilized *Tdc2-GAL4* line labels all subsets of VMlb neurons in this cluster (see chapter 2, 3; Busch et al. 2009; Schneider et al. 2012; Diesner & Neupert 2018). Furthermore, it has been shown in *D. melanogaster* that the activation of single OA VUM neurons can lead to a shift of preference towards a less attractive food source while the activation of a broader set of OAergic VUM neurons can reverse this decision (Claßen & Scholz 2018). Thus, one could speculate that this change of the behavioral output also holds true for the analyzed aggression paradigm and thus could hint towards a higher frequency in OA release from VMlb neurons upon social interaction in male *D. melanogaster* (see chapter 3). Moreover, to this day no OA or TA specific pre-synaptic transporter for a rapid re-uptake of OA and TA has been identified in *D. melanogaster*, thus hinting further towards a direct correlation between the detected somatic OA and TA titers and their release in corresponding neurons (Donly & Caveney 2005). However, future studies have to prove such a correlation and investigate to what extent this correlation applies. This would be possible by monitoring the release of the targeted biogenic monoamines by using cyclic voltammetry (Majdi et al. 2015; Pyakurel et al. 2016) or newly developed genetically encoded selective fluorescent sensors *in vivo* (Liang et al. 2015; Patriarchi et al. 2018), in combination with the subsequent analysis of the corresponding somatic titers by MALDI-TOF MS in single neurons.

Moreover, the question arises how this enhanced OA titer is achieved upon social contact in male *D. melanogaster*. Andrews et al. (2014) could show that male cuticular hydrocarbons evoke intracellular $Ca^{2+}$ responses in OA VUM neurons via Gr32a expressing sensory neurons. Furthermore, Pyakurel et al. (2016) could show that the release of OA in a VNC preparation of the third larva of *D. melanogaster* is correlated with the activation frequency of OA/TAergic neurons, using FSCV and optogentic activation of OA/TAergic neurons. By interpreting these results in the light of the postulated hypothesis that there is a direct correlation between the detected somatic OA/TA titers and the released content, it can be further speculated that the enhanced OA titer is a direct result of the activation of the analyzed neurons. In order to prove such a correlation, in future studies single VMlb neurons could be artificially activated with different frequencies, using the targeted expression of light activatable ion channels such as ReaChR or CsChrimson (Inagaki et al. 2014; Titlow et al. 2015), and subsequently analyzed towards their somatic OA titers using the developed workflow. Furthermore, it would be interesting to see whether the enhanced OA titer is accompanied by an upregulation of the OA synthesis enzyme Tßh, which could be investigated by using fluorescent protein tags *in vivo* or single cell qPCR in combination with artificial VMlb neuron activation and analysis of somatic OA/TA titers from these or identical manipulated neuron somata (Inagaki et al. 2014; Bayer & Hobert 2018).

Assuming that the somatic biogenic monoamine titers correlate with the released content of a respective neuron, the developed MALDI-TOF MS approach could be a valuable tool in further dissecting the function of single OAergic *D. melanogaster* neurons in physiological and behavioral studies, such as the analyzed VMlb neurons in the male social driven aggression paradigm (see chapter 3; Zhou et al. 2008). As previous studies have shown that a subpopulation of the VMlb cluster is necessary for driving socially mediated male aggression, it would be interesting to further dissect this cluster using the developed approach. As it was not possible to reproducibly determine which single VMlb neurons were analyzed in this study, due to the utilized *Tdc2-GAL4* line, future studies could use the *ChaT-GAL80* repressor line to specifically limit the labeling to aggression mediating neurons in the VMlb cluster (Zhou et al. 2008; Schneider et al. 2012; Claßen & Scholz 2018). Thus, it would be possible to determine whether these aggression modulating VMlb neurons show the same enhanced OA titer upon social contact or whether these neurons are unaffected and the shift in the behavioral response towards a reduced aggression to conspecifics indeed results from the upregulation of OA signaling in other VMlb neurons. Moreover, it would also be possible to investigate the temporal dynamics of the observed upregulation of somatic OA titers in VMlb neurons, by analyzing different sets of VMlb neurons after a timed social contact and subsequent analysis of corresponding VMlb OA titers after different time intervals.

As shown throughout this thesis, the developed workflow allows a solid framework for the detection and quantification of biogenic monoamines from single dissected neurons (chapter 2-4; Diesner & Neupert 2018). However, so far only the detection and quantification of OA and TA have been analyzed in greater detail, thus future studies should investigate in what extent this developed approach is beneficial for the detection and quantification of other biogenic monoamines. Preliminary results from this thesis, analyzing DA derivatization, as well as a previous study show that other biogenic monoamines are also derivatized by the utilized derivatization agents, thus theoretically allowing also their low detection by the developed approach, with previously discussed drawbacks taken into account (see chapter 2; Manier et al. 2014; Diesner & Neupert 2018). Nevertheless, by potentially expanding the range of detectable biogenic monoamines using the developed workflow, it will be possible to analyze other corresponding signaling pathways in *D. melanogaster*.

Other future applications of the developed MALDI-TOF MS workflow could aim at more basal questions, such as how a given genetic construct affects the somatic and potentially correlating released quantities of biogenic amines in a targeted neuron. Besides this, it would further be interesting to see how the synthesis of OA is influenced by artificially altering the balance between Tyr, TA and OA in OAergic neurons. This analysis would allow to directly elucidate whether and how a change of the precursors of TA and OA directly affect the turnover of the subsequent product. This could be achieved by genetically altering the expression of the TA synthesizing enzyme Tdc2 or neuronal Tyr transporters combined with subsequent MALDI-TOF MS driven analysis of the corresponding neuron soma. Assuming a successful detection and quantification of DA and 5-HT from single *D. melanogaster* somata samples by the developed workflow, it would also be possible to analyze the effect of biogenic monoamine recycling on somatic titers. This could be addressed by pharmacologically blocking or genetically altering the expression of corresponding biogenic monoamine presynaptic transporters in combination with artificial activation of the targeted neuron by light or temperature (Asahina et al. 2014; Inagaki et al. 2014) and subsequent MALDI-TOF driven analysis of the resulting somatic titers.

All of the aforementioned applications of the developed MALDI-TOF approach, however, are based on the genetic labeling tool box in *D. melanogaster*. However, the detection and quantification of biogenic monoamines using this workflow is not limited to genetic model organisms like *D. melanogaster* or *T. castaneum*, but can also be applied to other organisms in which comparable genetic tools have not been established. By identifying single neurons by electrophysiology and subsequent intracellular dye labeling, as shown for the analysis of desDUM neurons of the Indian stick insect *C. morosus* (see chapter 4; Stolz 2018; Stolz et al. 2018 *in preparation*), it is possible to apply this workflow also to other organisms. In the current thesis, the derivatization supported MALDI-TOF MS driven analysis of electrophysiological identified and intracellular labeled desDUM neurons from *C. morosus* could unambiguously show that these neurons contain OA and TA (see chapter 4; Stolz 2018; Stolz et al. 2018 *in preparation*). Thus, there is a high probability that at least the majority of the observed effects of these neurons on targeted CPGs is mediated by OA signaling, which is in accordance with previous reports from *C. morosus* (see chapter 4; Westmark et al. 2009; Stolz 2018; Stolz et al.

2018 *in preparation*). Moreover, the developed workflow also potentially allows the quantification of OA and TA from these neurons, however, in respect to the utilized intracellular recording technique it remains open how the penetration and removal of the recording capillary, as well as the utilized capillary buffer alters the intracellular quantities of neuroactive substance titers. Future studies could address this issue by analyzing somatic biogenic monoamine titers of genetically labeled and intracellular recorded neurons as well as corresponding unpenetrated neurons from brain dissections of physiological and age synchronized adult *D. melanogaster* using the developed approach (Juusola et al. 2016; Diesner & Neupert 2018). However, a more practicable way to allow quantification of such neurons would be to use the workflow in combination with perforated patch-clamp recordings that do not have the need for cell penetration and have been shown to have minimal impact on intracellular pathways (Lippiat 2008; Linley 2013). Furthermore, a previous study could show that neurons that have been analyzed with perforated patch-clamp recordings are suitable for MALDI-TOF MS analysis, in combination with intracellular dye labeling (Neupert et al. 2018).

Aside from biogenic monoamines, neuropeptides represent another class of important neuroactive substances. Moreover, it has been shown that biogenic monoamines and neuropeptides can be co-localized in neurons throughout the CNS in vertebrates and invertebrates alike (Hökfelt et al. 1987; Nässel 2018). Thus, a potential simultaneous detection of biogenic monoamines and neuropeptides by the developed workflow was investigated in this thesis (chapter 2; Diesner & Neupert 2018). By analyzing single somata of DMS expressing neuropeptidergic neurons of adult *D. melanogaster* as well as synthetic DMS samples with the developed workflow, it was shown that the utilized derivatization agents only leads to a minimal turn-over of the tested neuropeptide and that even derivatized neuropeptides can be successfully identified by tandem mass spectrometric analysis (chapter 2; Diesner & Neupert 2018). Moreover, by using the *DIMM-GAL4* driver line (*c929-GAL4*) crossed to a suitable UAS-*mCD8::GFP* reporter line in combination with subsequent derivatization free MALDI-TOF SCMS allowed to systematically analyze the neuropeptidome of single neurosecretory neurons of the adult *D. melanogaster* brain. By using this approach a total of 10 different cell types were described based on their location in the brain and their expressed neuropeptidome (chapter 5; Diesner, Predel, et al. 2018). Moreover, this approach further allowed to investigate the cell specific processing of corresponding neuropeptide precursors in the targeted neurons. While this analysis showed that such a mapping approach is suitable to reveal co-localization of neuropeptides, future studies can use the now available data in combination with the newly developed approach to investigate potential co-localizations of biogenic monoamines and neuropeptides in these neurosecretory neurons. Furthermore, future studies could also expand this mapping approach to other driver lines labeling neurons that express biogenic monoamines synthesizing enzymes, such as the utilized *Tdc2-Gal4* line. Additionally, future studies could also utilize the more sophisticated genetic tools available in *D. melanogaster*, such as the intersectional split-GAL4 technique (Dionne et al. 2018), in order to label neurons from overlapping expression profiles of different driver lines such as aminergic and peptide labeling GAL4 lines. This would allow to limit the number of labeled neurons and ease data interpretation.

# 7. Conclusion

In this thesis a new derivatization supported MALDI-TOF MS workflow was developed that enables the routine detection and quantification of two biogenic monoamines, OA and TA, from single isolated neuron somata. The workflow is highly sensitive, reproducible, fast, and cost-effective as well as exhibits only minimal interference on the detection and identification of potentially co-localized neuropeptides from the same sample. It further holds the potential to be beneficial in the detection and quantification of other biogenic monoamines such as DA from corresponding single neuron somata samples. The ability to qualify and quantify neuroactive substances such as OA and TA from genetically labeled neurons of model organisms such as *D. melanogaster* offers a wide range of applications like characterizing cell-to-cell and cluster heterogeneity, analyzing potential changes in neuroactive substance cell titers among different physiological and behavioral states, natural or induced neuronal dysfunctions and pathologies, as well as in relation to artificially applied neuroactive substances or drugs.

However, this workflow is not limited to the analysis of neurons from model organsims with a genetic labeling toolbox. It can be combined with electrophysiological recordings and subsequent intracellular dye application for the identification of single neurons from organisms where no comparable genetic tool box has been established. Moreover, such combinatorial approaches are highly desireable as they hold the possibility to characterize neurons in their physiological, morphological and neurochemical properties.

Future studies should combine this approach with techniques that allow to monitor the releasing of neuroactive substances *in vivo*, such as FSCV (Majdi et al. 2015; Pyakurel et al. 2016) or genetically encoded selective fluorescent sensors (Liang et al. 2015; Patriarchi et al. 2018), to investigate how the somatic neuroactive ratios of OA and TA and other neuroactive substances relate to the actual released quantities.

# 8. List of Figures

**Figure 1.1** Synthesis pathway of OA.. 5

**Figure 1.2** Development of VUM/VPM neurons in *D. melanogaster*. 8

**Figure 1.3** Schematic of a MALDI-TOF mass spectrometer. 15

**Figure 1.4** Hypothetical fragmentation of the peptide FMRFamide by $MS^2$. 18

**Figure 2.1** Mass spectrometric analysis of underivatized synthetic OA and TA. 36

**Figure 2.2** Schematic reaction scheme of CA and DPD with OA (after Manier *et al.*, 2014 and Gatti *et al.*, 2012). 37

**Figure 2.3** MS and $MS^2$ mass spectra of OA-CA, OA(*d3*)-CA, TA-CA and TA(*d4*)-CA with suggested chemical structure of detected product ions used for identification. 38

**Figure 2.4** MS and $MS^2$ mass spectra of DPD derivatized OA, OA(*d3*), TA and TA(*d4*) with suggested chemical structure of detected product ions used for identification. 39

**Figure 2.5** Analysis of OA and TA from CA and DPD derivatized single D. melanogaster somata using direct MALDI-TOF MS. 41

**Figure 2.6** Observed linearity, precision, and accuracy for 300-nl samples of OA-CA/OA(*d3*)-CA in MS and $pMS^2$ mode as well as TA-CA/TA(*d4*)-CA in MS mode 43

**Figure 2.7** Quantification of synthetic OA and TA from CA derivatized 18.4 nl samples. 44

**Figure 2.8** Observed linearity, precision, and accuracy for 300-nl samples of OA-DPD/OA(*d3*)-DPD in MS and $pMS^2$ mode 45

**Figure 2.9** Effect of sample storage in light and dark conditions on detected OA-CA/OA(*d3*)-CA and TA-CA/TA(*d4*)-CA ratios, signal intensities and RSDs 48

**Figure 2.10** Effect of sample derivatization by CA on the detection of neuropeptides and evaluation of possible isomeric species from the sample background of *D. melanogaster* neurons. 50

**Figure 2.11** Effect of sample derivatization by DPD on the detection of neuropeptides and evaluation of possible isomeric species from the sample background of *D. melanogaster* neurons. 51

**Figure 2.12** MS and $MS^2$ mass spectra of underivatized, CA and DPD derivatized synthetic DA with suggested chemical structure of detected product ions used for DA identification. 52

**Figure 2.13** Effect of cooling on recorded OA VMlb titers and statistical analysis of a potential sexual dimorphism in VMlb OA titers. 54

**Figure 2.14** Detection of OA-CA and TA-CA in VL neurons and comparison of OA-CA concentrations from VMlb and VL samples. 56

**Figure 3.1** OA VMlb titers do not differ between sexes, fly age and inserted genetic construct 67

**Figure 3.2** Statistical comparison of OA VMlb titers recorded by MALDI-TOF SCMS in socially naïve and experienced 5d old male *D. melanogaster*. 68

**Figure 4.1** Detection of OA and TA from an individual desDUM soma from the GNG of *C. morosus* by MALDI-TOF SCMS after intracellular recording and tetramethylrhodamine dextran injection. 80

**Figure 4.2** Screening for potential OA-CA/TA-CA isomeric ion signals originating from nervous tissue of C. morosus. 82

**Figure 5.1** Optical survey of the c929>GFP expression pattern in adult D. melanogaster brains. 91

**Figure 5.2** Mapping of cell type #1-3. ........ 96
**Figure 5.3** MS² spectra of N-terminal unblocked AST-C, MIP-1 and MIP-2 from cell type #3 preparations...... 99
**Figure 5.4** Mapping of cell type #4-6. ........ 103
**Figure 5.5** Mapping of cell type #7-9. ........ 106
**Figure 5.6** Mapping of cell type #10 ........ 107
**Figure 5.7** Overview of SCMS analyzed DIMM neurons in the brain and GNG of adult *D. melanogaster*. ..... 108

# 9. List of Tables

**Table 2.1** Synthetic peptides used for instrument calibration in the range of m/z 600 - 4000. ........ 34
**Table 2.2** Summary of experimentally determined LODs and LLOQs for OA-CA and TA-CA analysis in MS, MS², and pMS² mode ........ 40
**Table 2.3** Determined LOQs for OA and TA using different quantitative approaches........ 47
**Table 5.1** Synthetic peptides used for instrument calibration in the range of m/z 3000 – 10,000 ........ 89
**Table 5.2** Detected mature neuropeptides and peptides precursor (PP) by SCMS from identified DIMM neurons of the adult brain with GNG of *D. melanogaster*........ 93

# 10. Bibliography

**Abruzzi, K.C. et al.,** 2017. RNA-seq analysis of Drosophila clock and non-clock neurons reveals neuron-specific cycling and novel candidate neuropeptides. *PLoS Genetics*, **13**, e1006613.

**Adams, M.D. et al.,** 2000. The genome sequence of Drosophila melanogaster. *Science*, **5461**, pp.2185–2195.

**Aerts, J.T. et al.,** 2014. Patch clamp electrophysiology and capillary electrophoresis–mass spectrometry metabolomics for single cell characterization. *Analytical Chemistry*, **86**, pp.3203–3208.

**Agricola, H.J. & Braunig, P.,** 1995. Comparative aspects of peptidergic signaling pathways in the nervous systems of arthropods. *EXS*, **72**, pp.303–327.

**Alekseyenko, O. V. et al.,** 2014. Single serotonergic neurons that modulate aggression in Drosophila. *Current Biology*, **24**, pp.2700–2707.

**Alekseyenko, O. V et al.,** 2013. Single dopaminergic neurons that modulate aggression in Drosophila. *Proceedings of the National Academy of Sciences*, **110**, pp.6151–6156.

**Andrews, J.C. et al.,** 2014. Octopamine neuromodulation regulates Gr32a-linked aggression and courtship pathways in Drosophila males. *PLoS Genetics*, **10**, e1004356.

**Armbrecht, L. & Dittrich, P.S.,** 2017. Recent advances in the analysis of single cells. *Analytical Chemistry*, **89**, pp.2–21.

**Asahina, K. et al.,** 2014. Tachykinin-expressing neurons control male-specific aggressive arousal in drosophila. *Cell*, **156**, pp.221–235.

**Auer, T.O. & Benton, R.,** 2016. Sexual circuitry in Drosophila. *Current Opinion in Neurobiology*, **38**, pp.18–26.

**Bader, R., Wegener, C. & Pankratz, M.J.,** 2007. Comparative neuroanatomy and genomics of hugin and pheromone biosynthesis activating neuropeptide (PBAN). *Fly*, **1**, pp.228–231.

**Baggerman, G. et al.,** 2002. Peptidomics of the larval Drosophila melanogaster central nervous system. *The Journal of Biological Chemistry*, **277**, pp.40368–74.

**Baines, D., DeSantis, T. & Downer, R.G.H.,** 1992. Octopamine and 5-hydroxytryptamine enhance the phagocytic and nodule formation activities of cockroach (Periplaneta americana) haemocytes. *Journal of Insect Physiology*, **38**, pp.905–914.

**Bässler, U. & Büschges, A.,** 1998. Pattern generation for stick insect walking movements - Multisensory control of a locomotor program. *Brain Research Reviews*, **27**, pp.65–88.

**Bauknecht, P. & Jékely, G.,** 2017. Ancient coexistence of norepinephrine, tyramine, and octopamine signaling in bilaterians. *BMC Biology*, **15**, 6.

**Bayer, E.A. & Hobert, O.,** 2018. Past experience shapes sexually dimorphic neuronal wiring through monoaminergic signalling. *Nature*, **7721**, pp.117–121.

**Bayliss, A., Roselli, G. & Evans, P.D.,** 2013. A comparison of the signalling properties of two tyramine receptors from Drosophila. *Journal of Neurochemistry*, **125**, pp.37–48.

**Bendena, W.G. & Tobe, S.S.,** 2012. Families of allatoregulator sequences: a 2011 perspective *Canadian Journal of Zoology*, **90**, pp.521–544.

**Bergman, H.-M. et al.,** 2016. Quantitative mass spectrometry imaging of small-molecule neurotransmitters in rat brain tissue sections using nanospray desorption electrospray ionization. *The Analyst*, **141**, pp.3686–3695.

**Berry, M.D.,** 2004. Mammalian central nervous system trace amines. Pharmacologic amphetamines, physiologic neuromodulators. *Journal of Neurochemistry*, **90**, pp.257–271.

**Bidaye, S.S. et al.,** 2014. Neuronal control of Drosophila walking direction. *Science*, **344**, pp.97–101.

**Bidaye, S.S., Bockemühl, T. & Büschges, A.,** 2017. Six-legged walking in insects: how CPGs, peripheral feedback, and descending signals generate coordinated and adaptive motor rhythms. *Journal of Neurophysiology*, **119**, pp.459-475.

**Bilingsley, P.F. & LeHane, M.J.,** 1996. Structure and ultrastructure of the insect midgut. In *Biology of the Insect Midgut*. Springer Netherlands, pp. 3–30.

**Billeter, J.C. et al.,** 2009. Specialized cells tag sexual and species identity in Drosophila melanogaster. *Nature*, **7266**, pp.987–991.

**Borowsky, B. et al.,** 2001. Trace amines: Identification of a family of mammalian G protein-coupled receptors. *Proceedings of the National Academy of Sciences*, **98**, pp.8966–8971.

**Borue, X. et al.,** 2009. Quantitative evaluation of serotonin release and clearance in Drosophila. *Journal of Neuroscience Methods*, **179**, pp.300–308.

**Bossing, T. & Technau, G.M.,** 1994. The fate of the CNS midline progenitors in Drosophila as revealed by a new method for single cell labelling. *Development*, **120**, pp.1895–906.

**Brady, S. et al.,** 2012. *Basic Neurochemistry*, Academic Press.

**Braun, G. & Bicker, G.,** 1992. Habituation of an appetitive reflex in the honeybee. *Journal of Neurophysiology*, **67**, pp.588–598.

**Braunig, P.,** 1991. Suboesophageal DUM Neurons Innervate the Principal Neuropiles of the Locust Brain. *Philosophical Transactions of the Royal Society B: Biological Sciences*, **1264**, pp.221–240.

**Bräunig, P. & Burrows, M.,** 2004. Projection patterns of posterior dorsal unpaired median neurons of the locust subesophageal ganglion. *Journal of Comparative Neurology*, **478**, pp.164–175.

**Bräunig, P. & Pflüger, H.-J.,** 2001. The unpaired median neurons of insects. *Advacnes in Insect Physiology*, **28**, pp.185-266.

**Brembs, B. et al.,** 2007. Flight initiation and maintenance deficits in flies with genetically altered biogenic amine levels. *Journal of Neuroscience*, **41**, pp.11122–11131.

**van Breugel, F., Suver, M.P. & Dickinson, M.H.,** 2014. Octopaminergic modulation of the visual flight speed regulator of Drosophila. *Journal of Experimental Biology*, **217**, pp.1737–1744.

**Brodbelt, J.S.,** 2015. Photodissociation mass spectrometry: New tools for characterization of biological molecules. *Chemical Society Reviews*, **43**, pp.2757–2783.

**Vanden Broeck, J.,** 2001. Neuropeptides and their precursors in the fruitfly, Drosophila melanogaster. *Peptides*, **22**, pp.241–54.

**Brogiolo, W. et al.,** 2001. An evolutionarily conserved function of the drosophila insulin receptor and insulin-like peptides in growth control. *Current Biology*, **11**, pp.213–221.

**Brown, M.R. et al.,** 1999. Identification of a Drosophila brain-gut peptide related to the neuropeptide Y family. *Peptides*, **20**, pp.1035–42.

**Brown, R.S. & Lennon, J.J.,** 1995. Sequence-specific fragmentation of matrix-assisted laser-desorbed protein/peptide Ions. *Analytical Chemistry*, **67**, pp.3990–3999.

**Browne, C.A., Bennett, H.P.J. & Solomon, S.,** 1981. Isolation and characterization of corticotropin- and melanotropin-related peptides from the neurointermediary lobe of the rat pituitary by reversed-phase liquid chromatography. *Biochemistry*, **20**, pp.4538–4546.

**Buhl, E., Schildberger, K. & Stevenson, P.A.,** 2008. A muscarinic cholinergic mechanism underlies activation of the central pattern generator for locust flight. *Journal of Experimental Biology*, **211**, pp.2346–2357.

**Burke, C.J. et al.,** 2012. Layered reward signalling through octopamine and dopamine in Drosophila. *Nature*, **492**, pp.433-437.

**Burtis, K.C.,** 1993. The regulation of sex determination and sexually dimorphic differentiation in Drosophila. *Current Opinion in Cell Biology*, **6**, pp.1006–1014.

**Busch, S. et al.,** 2009. A map of octopaminergic neurons in the Drosophila brain. *The Journal of Comparative Neurology*, **513**, pp.643–67.

**Busch, S. & Tanimoto, H.,** 2010. Cellular configuration of single octopamine neurons in Drosophila. *Journal of Comparative Neurology*, **518**, pp.2355–2364.

**Büschges, A.,** 1998. Inhibitory synaptic drive patterns motoneuronal activity in rhythmic preparations of isolated thoracic ganglia in the stick insect. *Brain Research*, **783**, pp.262–271.

**Büschges, A., Kittmann, R. & Ramirez, J. -M,** 1993. Octopamine effects mimick state-dependent changes in a proprioceptive feedback system. *Journal of Neurobiology*, **24**, pp.598–610.

**Büschges, A., Schmitz, J. & Bässler, U.,** 1995. Rhythmic patterns in the thoracic nerve cord of the stick insect induced by pilocarpine. *The Journal of Experimental Biology*, **198(Pt 2)**, pp.435–56.

**Büschges, A., Scholz, H. & El Manira, A.,** 2011. New moves in motor control. *Current Biology*, **21**, pp.513–524.

**Campbell, R.A.A. et al.,** 2013. Imaging a population code for odor identity in the Drosophila mushroom body. *Journal of Neuroscience*, **33**, pp.10568–10581.

**Cao, P. & Moini, M.,** 1999. Separation and detection of a- and B- chains of hemoglobin of a single intact red blood cell using capillary electrophoresis. *Journal of the American Society for Mass Spectrometry*, **10**, pp.184–186.

**Cazzamali, G., Klaerke, D.A. & Grimmelikhuijzen, C.J.P.,** 2005. A new family of insect tyramine receptors. *Biochemical and Biophysical Research Communications*, **338**, pp.1189–1196.

**Cecala, C. et al.,** 2012. A hyphenated optical trap capillary electrophoresis laser induced native fluorescence system for single-cell chemical analysis. *The Analyst*, **137**, pp.2965–2972.

**Certel, S.J. et al.,** 2007. Modulation of Drosophila male behavioral choice. *Proceedings of the National Academy of Sciences*, **104**, pp.4706–4711.

**Certel, S.J. et al.,** 2010. Octopamine neuromodulatory effects on a social behavior decision-making network in Drosophila males. *PLoS ONE*, **10**, e13248.

**Chacon, A. et al.,** 2011. On-tissue chemical derivatization of 3-methoxysalicylamine for

MALDI-imaging mass spectrometry. *Journal of mass spectrometry*, **46**, pp.840–846.

**Chaptal, V. et al.,** 2017. Quantification of detergents complexed with membrane proteins. *Scientific Reports*, **7**, 41751.

**Chen, A. et al.,** 2013. Dispensable, redundant, complementary, and cooperative roles of dopamine, octopamine, and serotonin in Drosophila melanogaster. *Genetics*, **193**, pp.159–176.

**Chen, S. et al.,** 2002. Fighting fruit flies: A model system for the study of aggression. *Proceedings of the National Academy of Sciences*, **99**, pp.5664–5668.

**Chen, T.-W. et al.,** 2013. Ultrasensitive fluorescent proteins for imaging neuronal activity. *Nature*, **7458**, pp.295–300.

**Choi, Y.J. et al.,** 2005. Comparative analysis of Corazonin-encoding genes (Crz's) in Drosophila species and functional insights into Crz-expressing neurons. *Journal of Comparative Neurology*, **482**, pp.372–385.

**Chrachri, A. & Clarac, F.,** 1987. Induction of rhythmic activity in motoneurons of crayfish thoracic ganglia by cholinergic agonists. *Neuroscience Letters*, **77**, pp.49–54.

**Churgin, M.A. et al.,** 2017. Antagonistic serotonergic and octopaminergic neural circuits mediate food-dependent locomotory behavior in Caenorhabditis elegans. *The Journal of Neuroscience*, **37**, pp.2636–16.

**Claassen, D.E. & Kammer, A.E.,** 1986. Effects of octopamine, dopamine, and serotonin on production of flight motor output by thoracic ganglia of Manduca sexta. *Journal of Neurobiology*, **17**, pp.1–14.

**Claßen, G. & Scholz, H.,** 2018. Octopamine shifts the behavioral response from indecision to approach or aversion in Drosophila melanogaster. *Frontiers in Behavioral Neuroscience*, **12**, 131.

**Clowney, E.J. et al.,** 2015. Multimodal chemosensory circuits controlling male courtship in Drosophila. *Neuron*, **87**, pp.1036–1049.

**Coast, G.M. & Schooley, D.A.,** 2011. Toward a consensus nomenclature for insect neuropeptides and peptide hormones. *Peptides*, **32**, pp.620–631.

**Cognigni, P., Felsenberg, J. & Waddell, S.,** 2018. Do the right thing: neural network mechanisms of memory formation, expression and update in Drosophila. *Current Opinion in Neurobiology*, **49**, pp.51–58.

**Cole, S.H. et al.,** 2005. Two functional but noncomplementing Drosophila tyrosine decarboxylase genes: Distinct roles for neural tyramine and octopamine in female fertility. *Journal of Biological Chemistry*, **280**, pp.14948–14955.

**Craig, I.W. & Halton, K.E.,** 2009. Genetics of human aggressive behaviour. *Human Genetics*, **126**, pp.101–113.

**Croset, V., Treiber, C.D. & Waddell, S.,** 2018. Cellular diversity in the Drosophila midbrain revealed by single-cell transcriptomics. *eLife*, **7**, e34550.

**Dacks, A.M. et al.,** 2005. Octopamine-immunoreactive neurons in the brain and subesophageal ganglion of the hawkmoth Manduca sexta. *The Journal of Comparative Neurology*, **488**, pp.255–268.

**Davie, K. et al.,** 2018. A single-cell transcriptome atlas of the aging Drosophila brain. *Cell*, **174**, pp.982-998.

**Denno, M.E., Privman, E. & Venton, B.J.,** 2016. Analysis of neurotransmitter tissue content of Drosophila melanogaster in different life stages. *ACS Chemical Neuroscience*, **6**, pp.117–123.

**Derst, C. et al.,** 2016. Evolution of neuropeptides in non-pterygote hexapods. *BMC Evolutionary Biology*, **16**, 51.

**Dickerson, M. et al.,** 2012. Structure-activity and immunochemical data provide evidence of developmental- and tissue-specific myosuppressin signaling. *Peptides*, **36**, pp.272–279.

**Dickson, B.J.,** 2008. Wired for sex: The neurobiology of Drosophila mating decisions. *Science*, **5903**, pp.904–909.

**Dierick, H.A. & Greenspan, R.J.,** 2006. Molecular analysis of flies selected for aggressive behavior. *Nature Genetics*, **38**, pp.1023–1031.

**Dierick, H.A. & Greenspan, R.J.,** 2007. Serotonin and neuropeptide F have opposite modulatory effects on fly aggression. *Nature Genetics*, **39**, pp.678–682.

**Diesner, M., Gallot, A., et al.,** 2018. Mating-induced differential peptidomics of neuropeptides and protein hormones in Agrotis ipsilon moths. *Journal of Proteome Research*, **17**, pp.1397-1414.

**Diesner, M. & Neupert, S.,** 2018. Quantification of biogenic amines from individual GFP-labeled Drosophila cells by MALDI-TOF mass spectrometry. *Analytical Chemistry*, **90**, pp.8035-8043.

**Diesner, M., Predel, R. & Neupert, S.,** 2018. Neuropeptide mapping of Dimmed cells of adult Drosophila brain. *Journal of the American Society for Mass Spectrometry*, **29**, pp. 890-902.

**Dionne, H. et al.,** 2018. Genetic reagents for making split-GAL4 lines in Drosophila. *Genetics*, **209**, pp.31–35.

**Donini, A. & Lange, A.B.,** 2004. Evidence for a possible neurotransmitter/neuromodulator role of tyramine on the locust oviducts. *Journal of Insect Physiology*, **50**, pp.351–361.

**Donly, B.C. & Caveney, S.,** 2005. A transporter for phenolamine uptake in the arthropod CNS. *Archives of Insect Biochemistry and Physiology*, **59**, pp.172–183.

**Dow, M.A. & Schilcher, F. von,** 1975. Aggression and mating success in Drosophila melanogaster. *Nature*, **254**, p.511.

**Dueñas, M.E., Essner, J.J. & Lee, Y.J.,** 2017. 3D MALDI mass spectrometry imaging of a single cell: spatial mapping of lipids in the embryonic development of zebrafish. *Scientific Reports*, **7**, 14946.

**Duncan, M.W., Roder, H. & Hunsucker, S.W.,** 2008. Quantitative matrix-assisted laser desorption/ionization mass spectrometry. *Briefings in Functional Genomics & Proteomics*, **7**, pp.355–70.

**Dunphy, G.B. & Downer, R.G.H.,** 1994. Octopamine, a modulator of the hemocytic nodulation response of nonimmune Galleria-Mellonella larvae. *Journal of Insect Physiology*, **40**, pp.267–272.

**Eckert, M. et al.,** 1992. The octopaminergic system within the ventral nerve cord of the American cockroach. *Acta Biologica Hungarica*, **43**, pp.201–211.

**Eisenhofer, G.,** 2004. Catecholamine Metabolism: A Contemporary View with Implications for Physiology and Medicine. *Pharmacological Reviews*, **56**, pp.331–349.

**El-Kholy, S. et al.,** 2015. Expression analysis of octopamine and tyramine receptors in Drosophila. *Cell and Tissue Research*, **361**, pp.669–684.

**Erber, J. & Kloppenburg, P.,** 1995. The modulatory effects of serotonin and octopamine in the visual system of the honey bee (Apis mellifera L.). *Journal of Comparative Physiology A*, **176**, pp.111–118.

**Erspamer, V. & Boretti, G.,** 1951. Identification and characterization, by paper chromatography, of enteramine, octopamine, tyramine, histamine and allied substances in extracts of posterior salivary glands of octopoda and in other tissue extracts of vertebrates and invertebrates. *Archives internationales de pharmacodynamie et de thérapie*, **88**, pp.269–332.

**Espina, V. et al.,** 2006. Laser-capture microdissection. *Nature Protocols*, **2**, pp.586–603.

**Evans, P.D. & O'Shea, M.,** 1977. An octopaminergic neurone modulates neuromuscular transmission in the locust. *Nature*, **5634**, pp.257–259.

**Fan, Y. et al.,** 2013. Stimulation and release from neurons via a dual capillary collection device interfaced to mass spectrometry. *The Analyst*, **138**, pp.6337–6346.

**Fang, H., Vickrey, T.L. & Venton, B.J.,** 2011. Analysis of biogenic amines in a single Drosophila larva brain by capillary electrophoresis with fast-scan cyclic voltammetry detection. *Analytical Chemistry*, **83**, pp.2258–2264.

**Farooqui, T.,** 2007. Octopamine-mediated neuromodulation of insect senses. *Neurochemical Research*, **32**, pp.1511–1529.

**Farooqui, T.,** 2012. Review of octopamine in insect nervous system. *Open Access Insect Physiology*, **4**, pp.1-17.

**FDA,** 2013. Guidance for Industry: Bioanalytical Method Validation.

**Feinberg, E.H. et al.,** 2008. GFP reconstitution across synaptic partners (GRASP) defines cell contacts and synapses in living nervous systems. *Neuron*, **57**, pp.353–363.

**Felsenberg, J. et al.,** 2017. Re-evaluation of learned information in Drosophila. *Nature*, **7649**, pp.240–244.

**Fernandes, A.M.A.P. et al.,** 2016. Direct visualization of neurotransmitters in rat brain slices by desorption electrospray ionization mass spectrometry Imaging (DESI - MS). *Journal of The American Society for Mass Spectrometry*, **27**, pp.1944–1951.

**Fernandez, M. de la P. et al.,** 2010. Pheromonal and behavioral cues trigger male-to-female aggression in Drosophila. *PLoS Biology*, **11**, e1000541.

**Fields, P.E. & Woodring, J.P.,** 1991. Octopamine mobilization of lipids and carbohydrates in the house cricket, Acheta domesticus. *Journal of Insect Physiology*, **37**, pp.193–199.

**El Filali, Z. et al.,** 2003. Retrograde labeling of single neurons in conjunction with MALDI high-energy collision-induced dissociation MS/MS analysis for peptide profiling and structural characterization. *Analytical Chemistry*, **75**, pp.2996–3000.

**Fox, L.E., Soll, D.R. & Wu, C.-F.,** 2006. Coordination and modulation of locomotion pattern generators in Drosophila larvae: effects of altered biogenic amine levels by the tyramine β hydroxlyase mutation. *The Journal of Neuroscience*, **26**, pp.1486–1498.

**French, A.S.,** 1985. The effects of temperature on action potential encoding in the cockroach tactile spine. *Journal of Comparative Physiology A*, **156**, pp.817–821.

**Fricker, L.D.,** 2012. *Neuropeptides and Other Bioactive Peptides: From Discovery to*

*Function*, Morgan & Claypool Life Sciences.

**Fukuyama, Y., Iwamoto, S. & Tanaka, K.,** 2006. Rapid sequencing and disulfide mapping of peptides containing disulfide bonds by using 1,5-diaminonaphthalene as a reductive matrix. *Journal of Mass Spectrometry*, **41**, pp.191–201.

**Gäde, G. et al.,** 2006. Unique translational modification of an invertebrate neuropeptide: a phosphorylated member of the adipokinetic hormone peptide family. *The Biochemical Journal*, **393(Pt 3)**, pp.705–13.

**Gallo, V.P. et al.,** 2016. *Catecholaminergic System of Invertebrates: Comparative and Evolutionary Aspects in Comparison With the Octopaminergic System*, Elsevier Inc.

**Garden, R.W. et al.,** 1996. Excess salt removal with matrix rinsing: Direct peptide profiling of neurons from marine invertebrates using matrix-assisted laser desorption/ionization time-of-flight mass spectrometry. *Journal of Mass Spectrometry*, **31**, pp.1126–1130.

**Gatti, R. et al.,** 2010. 2,5-Dimethyl-1H-pyrrole-3,4-dicarbaldehyde as a precolumn derivatization reagent for HPLC/UV detection of amino acids. *Journal of Pharmaceutical and Biomedical Analysis*, **53**, pp.207–211.

**Gatti, R. et al.,** 2012. Determination of octopamine and tyramine traces in dietary supplements and phytoextracts by high performance liquid chromatography after derivatization with 2,5-dimethyl-1H-pyrrole-3,4-dicarbaldehyde. *Journal of Chromatography A*, **1220**, pp.92–100.

**Giros, B. & Caron, M.G.,** 1993. Molecular characterization of the dopamine transporter. *Trends in Pharmacological Sciences*, **14**, pp.43–9.

**Haberkern, H. & Jayaraman, V.,** 2016. Studying small brains to understand the building blocks of cognition. *Current Opinion in Neurobiology*, **37**, pp.59–65.

**Halberg, K.A. et al.,** 2015. Tracing the evolutionary origins of insect renal function. *Nature Communications*, **6**, pp.1–10.

**Hamada, F.N. et al.,** 2008. An internal thermal sensor controlling temperature preference in Drosophila. *Nature*, **7201**, pp.217–220.

**Hamanaka, Y. et al.,** 2010. Transcriptional Orchestration of the Regulated Secretory Pathway in Neurons by the bHLH protein DIMM. *Current Biology*, **20**, pp.9–18.

**Hammer, M.,** 1993. An identified neuron mediates the unconditioned stimulus in associative olfactory learning in honeybees. *Nature*, **366**, p.59-63.

**Hammer, M. & Menzel, R.,** 1998. Multiple sites of associative odor learning as revealed by local brain microinjections of octopamine in honeybees. *Learning & Memory*, **5**, pp.146–56.

**Han, K.A., Millar, N.S. & Davis, R.L.,** 1998. A novel octopamine receptor with preferential expression in Drosophila mushroom bodies. *The Journal of Neuroscience*, **18**, pp.3650–3658.

**Hardie, S.L. & Hirsh, J.,** 2006. An improved method for the separation and detection of biogenic amines in adult Drosophila brain extracts by high performance liquid chromatography. *Journal of Neuroscience Methods*, **153**, pp.243–249.

**Harris, G. et al.,** 2010. The monoaminergic modulation of sensory-mediated aversive responses in Caenorhabditis elegans requires glutamatergic/peptidergic cotransmission. *The Journal of Neuroscience*, **30**, pp.7889–7899.

**Hartenstein, V.,** 1997. Development of the insect stomatogastric nervous system. *Trends in Neurosciences*, **20**, pp.421–427.

**Helfrich-Förster, C.,** 2003. The neuroarchitecture of the circadian clock in the brain of Drosophila melanogaster. *Microscopy Research and Technique*, **62**, pp.94–102.

**Heß, M.,** 2008. *The role of octopamine and DUM-neurons in the modulation of motor activity in the stick insect Carausis morosus.* Bachelor Thesis, University Cologne.

**Hewes, R.S. et al.,** 2003. The bHLH protein Dimmed controls neuroendocrine cell differentiation in Drosophila. *Development*, **130**, pp.1771-1781.

**Hewes, R.S.,** 2003. The bHLH protein Dimmed controls neuroendocrine cell differentiation in Drosophila. *Development*, **130**, pp.1771–1781.

**Hewes, R.S., Schaefer, A.M. & Taghert, P.H.,** 2000. The cryptocephal gene (ATF4) encodes multiple basic-leucine zipper proteins controlling molting and metamorphosis in Drosophila. *Genetics*, **155**, pp.1711–1723.

**Hillenkamp, F. & Peter-Katalinic, J.**, 2007. *MALDI MS: A Practical Guide to Instrumentation, Methods and Applications*, Weinheim, Wiley-VCH.

**Hökfelt, T. et al.,** 1987. Coexistence of peptides with classical neurotransmitters. *Experientia*, **43**, pp.768–780.

**Holman, G.M., Cook, B.J. & Nachman, R.J.,** 1986. Isolation, primary structure and synthesis of leukomyosuppressin, an insect neuropeptide that inhibits spontaneous contractions of the cockroach hindgut. *Comparative Biochemistry and Physiology C-Pharmacology Toxicology & Endocrinology*, **85**, pp.329–333.

**Honjo, K. & Furukubo-Tokunaga, K.,** 2009. Distinctive neuronal networks and biochemical pathways for appetitive and aversive memory in Drosophila larvae. *Journal of Neuroscience*, **29**, pp.852–862.

**Hoopfer, E.D.,** 2016. Neural control of aggression in Drosophila. *Current Opinion in Neurobiology*, **38**, pp.109–118.

**Hoopfer, E.D. et al.,** 2015. P1 interneurons promote a persistent internal state that enhances inter-male aggression in Drosophila. *eLife*, **4**, pp.1–27.

**Hoyer, S.C. et al.,** 2008. Octopamine in male aggression of Drosophila. *Current Biology*, **18**, pp.159–167.

**Hsu, C.T. & Bhandawat, V.,** 2016. Organization of descending neurons in Drosophila melanogaster. *Scientific Reports*, **6**, pp.1–14.

**Hsu, Y., Earley, R.L. & Wolf, L.L.,** 2006. Modulation of aggressive behaviour by fighting experience: mechanisms and contest outcomes. *Biological reviews of the Cambridge Philosophical Society*, **81**, pp.33–74.

**Huang, J. et al.,** 2016. Neuromodulation of courtship drive through tyramine-responsive neurons in the Drosophila brain. *Current Biology*, **26**, pp.2246–2256.

**Hückesfeld, S., Peters, M. & Pankratz, M.J.,** 2016. Central relay of bitter taste to the protocerebrum by peptidergic interneurons in the Drosophila brain. *Nature Communications*, **7**, 12796.

**Huesmann, G.R. et al.,** 1995. Amino acid sequence of CAP2b, an insect cardioacceleratory peptide from the tobacco hawkmoth Manduca sexta. *FEBS Letters*, **371**, pp.311–314.

**Hummon, A.B., Amare, A. & Sweedler, J. V,** 2006. Discovering new invertebrate neuropeptides using mass spectrometry. *Mass spectrometry reviews*, **25**, pp.77–98.

**Ida, T., Takahashi, T., Tominaga, H., Sato, T., Kume, K., Yoshizawa-Kumagaye, K., et al.,** 2011. Identification of the endogenous cysteine-rich peptide trissin, a ligand for an orphan G protein-coupled receptor in Drosophila. *Biochemical and Biophysical Research Communications*, **414**, pp.44–8.

**Ifa, D.R. et al.,** 2007. Development of capabilities for imaging mass spectrometry under ambient conditions with desorption electrospray ionization (DESI). *International Journal of Mass Spectrometry*, **259**, pp.8–15.

**Iliadi, K.G., Iliadi, N. & Boulianne, G.L.,** 2017. Drosophila mutants lacking octopamine exhibit impairment in aversive olfactory associative learning. *European Journal of Neuroscience*, **46**, pp.2080–2087.

**Inagaki, H.K. et al.,** 2014. Optogenetic control of Drosophila using a red-shifted channelrhodopsin reveals experience-dependent influences on courtship. *Nature Methods*, **11**, pp.325–332.

**Ito, K. et al.,** 2014. A systematic nomenclature for the insect brain. *Neuron*, **81**, pp.755–765.

**Iversen, A. et al.,** 2002. Molecular cloning and functional expression of a Drosophila receptor for the neuropeptides capa-1 and -2. *Biochemical and Biophysical Research Communications*, **299**, pp.628–633.

**Jarman, A.P. et al.,** 1993. The Regulation and Function of the Helix-Loop-Helix Gene, Asense, in Drosophila Neural Precursors. *Development*, **119**, pp.19–29.

**Jiang, H. et al.,** 2013. Natalisin, a tachykinin-like signaling system, regulates sexual activity and fecundity in insects. *Proceedings of the National Academy of Sciences*, **110**, pp.3526-3534.

**Jiménez, C.R. et al.,** 1998. Direct mass spectrometric peptide profiling and sequencing of single neurons reveals differential peptide patterns in a small neuronal network. *Biochemistry*, **37**, pp.2070–2076.

**Jing, J. et al.,** 2007. From hunger to satiety: reconfiguration of a feeding network by Aplysia neuropeptide Y. *Journal of Neuroscience*, **27**, pp.3490–3502.

**Jung, S.H. et al.,** 2014. Identification of a novel insect neuropeptide, CNMa and its receptor. *FEBS Letters*, **588**, pp.2037–2041.

**Juusola, M. et al.,** 2016. Electrophysiological method for recording intracellular voltage responses of Drosophila photoreceptors and interneurons to light stimuli in vivo. *Journal of visualized experiments*, **112**, 54142.

**Kallman, B.R., Kim, H. & Scott, K.,** 2015. Excitation and inhibition onto central courtship neurons biases drosophila mate choice. *eLife*, **4**, e11188.

**Kapan, N. et al.,** 2012. Identified peptidergic neurons in the Drosophila brain regulate insulin-producing cells, stress responses and metabolism by coexpressed short neuropeptide F and corazonin. *Cellular and Molecular Life Sciences*, **69**, pp.4051–4066.

**Karas, M., Bachmann, D. & Hillenkamp, F.,** 1985. Influence of the wavelength in high-irradiance ultraviolet laser desorption mass spectrometry of organic molecules. *Analytical Chemistry*, **57**, pp.2935–2939.

**Karas, M., Glückmann, M. & Schäfer, J.,** 2000. Ionization in matrix-assisted laser desorption/ionization: Singly charged molecular ions are the lucky survivors. *Journal of Mass Spectrometry*, **35**, pp.1–12.

**Karas, M. & Krüger, R.,** 2003. Ion formation in MALDI: The cluster ionization mechanism. *Chemical Reviews*, **103**, pp.427–439.

**Kastin, A.J.,** 2000. What is a neuropeptide? *Trends in Neurosciences*, **23**, pp.113-114.

**Katz, P.S.,** 1995. Intrinsic and extrinsic neuromodulation of motor circuits. *Current opinion in Neurobiology*, **6**, pp.799–808.

**Katz, P.S. & Harris-Warrick, R.M.,** 1990. Neuromodulation of the crab pyloric central pattern generator by serotonergic/cholinergic proprioceptive afferents. *The Journal of Neuroscience*, **10**, pp.1495–1512.

**Kaufmann, R., Kirsch, D. & Spengler, B.,** 1994. Sequencing of peptides in a time-of-flight mass-spectrometer - evaluation of postsource decay following matrix-assisted laser-desorption ionization (MALDI). *International Journal of Mass Spectrometry and Ion Processes*, **131**, pp.355–385.

**Kean, L. et al.,** 2002. Two nitridergic peptides are encoded by the gene capability in Drosophila melanogaster. *American journal of physiology. Regulatory, integrative and comparative physiology*, **282**, pp.1297–1307.

**khan, M. zahid & nawaz, W.,** 2016. The emerging roles of human trace amines and human trace amine-associated receptors (hTAARs) in central nervous system. *Biomedicine and Pharmacotherapy*, **83**, pp.439–449.

**Kiehn, O.,** 2006. Locomotor circuits in the mammalian spinal cord. *Annual Review of Neuroscience*, **29**, pp.279–306.

**Kim, W.-S. et al.,** 2002. Ascorbic acid assays of individual neurons and neuronal tissues using capillary electrophoresis with laser-induced fluorescence detection. *Analytical Chemistry*, **74**, pp.5614–5620.

**Kim, Y.-K. et al.,** 2018. Repetitive aggressive encounters generate a long-lasting internal state in *Drosophila melanogaster* males. *Proceedings of the National Academy of Sciences*, **115**, pp.1099-1104

**King, A.N. et al.,** 2017. A peptidergic circuit links the circadian clock to locomotor activity. *Current Biology*, **27**, pp.1915–1927.e5.

**Kingan, T.G. & Adams, M.E.,** 2000. Ecdysteroids regulate secretory competence in Inka cells. *The Journal of Experimental Biology*, **203**, pp.3011–3018.

**Kitamoto, T.,** 2001. Conditional modification of behavior in Drosophila by targeted expression of a temperature-sensitive shibire allele in defined neurons. *Journal of Neurobiology*, **47**, pp.81–92.

**Klämbt, C., Jacobs, J.R. & Goodman, C.S.,** 1991. The midline of the drosophila central nervous system: A model for the genetic analysis of cell fate, cell migration, and growth cone guidance. *Cell*, **64**, pp.801–815.

**Koestler, M. et al.,** 2008. A high-resolution scanning microprobe matrix-assisted laser desorption/ionization ion source for imaging analysis on an ion trap/Fourier transform ion cyclotron resonance mass spectrometer. *Rapid Communications in Mass Spectrometry*, **22**, pp.3275–3285.

**Kohatsu, S., Koganezawa, M. & Yamamoto, D.,** 2011. Female contact activates male-specific interneurons that trigger stereotypic courtship behavior in Drosophila. *Neuron*, **69**, pp.498–508.

**Kohl, J., Huoviala, P. & Jefferis, G.S.X.E.,** 2015. Pheromone processing in Drosophila.

*Current Opinion in Neurobiology*, **34**, pp.149–157.

**Kolhekar, A.S. et al.,** 1997. Neuropeptide amidation in Drosophila: separate genes encode the two enzymes catalyzing amidation. *The Journal of Neuroscience*, **17**, pp.1363–1376.

**Kompauer, M., Heiles, S. & Spengler, B.,** 2016. Atmospheric pressure MALDI mass spectrometry imaging of tissues and cells at 1.4-µm lateral resolution. *Nature Methods*, **14**, pp.90–96.

**Konings, P.N.M. et al.,** 1988. Immunocytochemical demonstration of octopamine-immunoreactive cells in the nervous system of Locusta migratoria and Schistocerca gregaria. *Cell and Tissue Research*, **251**, pp.371–379.

**Krashes, M.J. et al.,** 2009. A neural circuit mechanism integrating motivational state with memory expression in Drosophila. *Cell*, **139**, pp.416–427.

**Krashes, M.J. & Waddell, S.,** 2008. Rapid consolidation to a radish and protein synthesis-dependent long-term memory after single-session appetitive olfactory conditioning in Drosophila. *The Journal of Neuroscience*, **28**, pp.3103–3113.

**Krause, E., Wenschuh, H. & Jungblut, P.R.,** 1999. The dominance of arginine-containing peptides in MALDI-derived tryptic mass fingerprints of proteins. *Analytical Chemistry*, **71**, pp.4160–4165.

**Kubiak, T.M. et al.,** 2002. Cloning and functional expression of the first Drosophila melanogaster sulfakinin receptor DSK-R1. *Biochemical and Biophysical Research Communications*, **291**, pp.313–320.

**Kuklinski, N.J. et al.,** 2010. Determination of salsolinol, norsalsolinol, and twenty-one biogenic amines using micellar electrokinetic capillary chromatography-electrochemical detection. *Electrophoresis*, **31**, pp.1886–1893.

**Kurtovic, A., Widmer, A. & Dickson, B.J.,** 2007. A single class of olfactory neurons mediates behavioural responses to a Drosophila sex pheromone. *Nature*, **7135**, pp.542–546.

**Kutsukake, M. et al.,** 2000. A tyramine receptor gene mutation causes a defective olfactory behavior in Drosophila melanogaster. *Gene*, **245**, pp.31–42.

**Lai, S.L. & Lee, T.,** 2006. Genetic mosaic with dual binary transcriptional systems in Drosophila. *Nature Neuroscience*, **9**, pp.703–709.

**Landgraf, M. et al.,** 1997. The origin, location, and projections of the embryonic abdominal motorneurons of Drosophila. *The Journal of Neuroscience*, **24**, pp.9642–9655.

**Lange, A.B.,** 2009. Tyramine: From octopamine precursor to neuroactive chemical in insects. *General and Comparative Endocrinology*, **162**, pp.18–26.

**Lange, A.B. & da Silva, R.,** 2007. Neural and hormonal control of muscular activity of the spermatheca in the locust, Locusta migratoria. *Peptides*, **28**, pp.174–184.

**Lapainis, T. et al.,** 2007. A multichannel native fluorescence detection system for capillary electrophoretic analysis of neurotransmitters in single neurons. *Analytical and Bioanalytical Chemistry*, **387**, pp.97–105.

**Lapainis, T., Rubakhin, S.S. & Sweedler, J. V.,** 2009. Capillary electrophoresis with electrospray ionization mass spectrometric detection for single-cell metabolomics. *Analytical Chemistry*, **81**, pp.5858–5864.

**LeDue, E.E. et al.,** 2016. Starvation-induced depotentiation of bitter taste in Drosophila. *Current Biology*, **26**, pp.2854–2861.

**Lee, G. & Hall, J.C.,** 2000. A newly uncovered phenotype associated with the fruitless gene of Drosophila melanogaster : Aggression-like head interactions between mutant males. *Behavior Genetics* , **30**, pp.263–275.

**Lee, J.E.,** 2016. Neuropeptidomics: Mass spectrometry-based identification and quantitation of neuropeptides. *Genomics & Informatics*, **14**, pp.12–19.

**Lermyte, F. et al.,** 2018. Radical solutions: Principles and application of electron-based dissociation in mass spectrometry-based analysis of protein structure. *Mass Spectrometry Reviews*, **37**, pp.750–771.

**Leszyk, J.D.,** 2010. Evaluation of the new MALDI matrix 4-chloro-alpha-cyanocinnamic acid. *Journal of Biomolecular Techniques*, **21**, pp.81–91.

**Levsen, K. & Schwarz, H.,** 1976. Stoßaktivierungsmassenspektrometrie - eine neue Sonde zur Strukturbestimmung von Ionen in der Gasphase. *Angewandte Chemie*, **88**, pp.589–599.

**Li, K.W. et al.,** 1994. Direct peptide profiling by mass spectrometry of single identified neurons reveals complex neuropeptide-processing pattern. *Journal of Biological Chemistry*, **269**, pp.30288–30292.

**Li, L. et al.,** 1999. In situ sequencing of peptides from biological tissues and single cells using MALDI-PSD/CID analysis. *Analytical Chemistry*, **71**, pp.5451–5458.

**Li, L., Romanova, E. V., et al.,** 2000. Peptide profiling of cells with multiple gene products: Combining immunochemistry and MALDI mass spectrometry with on-plate microextraction. *Analytical Chemistry*, **72**, pp.3867–3874.

**Li, L., Garden, R.W. & Sweedler, J. V,** 2000. Single-cell MALDI: a new tool for direct peptide profiling. *Trends in Biotechnology*, **18**, pp.151–160.

**Liang, R., Broussard, G.J. & Tian, L.,** 2015. Imaging chemical neurotransmission with genetically encoded fluorescent sensors. *ACS Chemical Neuroscience*, **6**, pp.84–93.

**Liang, X., Holy, T.E. & Taghert, P.H.,** 2017. A series of suppressive signals within the Drosophila circadian neural circuit generates sequential daily outputs. *Neuron*, **94**, pp.1173–1189.e4.

**Liessem, S. et al.,** 2018. Transcriptomic and Neuropeptidomic Analysis of the Stick Insect, Carausius morosus. *Journal of Proteome Research*, **17**, pp.2192–2204.

**Lim, R.S. et al.,** 2014. How food controls aggression in Drosophila. *PLoS ONE*, **9**, e105626.

**Lima, S.Q. & Miesenböck, G.,** 2005. Remote control of behavior through genetically targeted photostimulation of neurons. *Cell*, **121**, pp.141–152.

**Lin, A.C. et al.,** 2014. Sparse, decorrelated odor coding in the mushroom body enhances learned odor discrimination. *Nature Neuroscience*, **17**, pp.559-568.

**Lindemann, L. et al.,** 2005. Trace amine-associated receptors form structurally and functionally distinct subfamilies of novel G protein-coupled receptors. *Genomics*, **85**, pp.372–385.

**Linley, J.E.,** 2013. Perforated whole-cell patch-clamp recording. *Methods in molecular biology (Clifton, N.J.)*, **998**, pp.149–157.

**Lippiat, J.D.,** 2008. Whole-cell recording using the perforated patch clamp technique. *Methods in Molecular Biology*, **491**, pp.141–149.

**Liu, Y. et al.,** 2016. Drosophila insulin-like peptide 1 (DILP1) is transiently expressed during non-feeding stages and reproductive dormancy. *Scientific Reports*, **6**, 26620.

**Livingstone, M.S. & Tempel, B.L.,** 1983. Genetic dissection of monoamine neurotransmitter synthesis in Drosophila. *Nature*, **5912**, pp.67–70.

**Lombard-Banek, C., Moody, S.A. & Nemes, P.,** 2016. Single-cell mass spectrometry for discovery proteomics: Quantifying translational cell heterogeneity in the 16-Cell frog (Xenopus) embryo. *Angewandte Chemie*, **55**, pp.2454–2458.

**Lorenz, K.,** 1963. *Das sogenannte Böse*, Wien: Dr. G. Borotha-Schoeler Verlag.

**Lorenz, M.W. & Gäde, G.,** 2009. Hormonal regulation of energy metabolism in insects as a driving force for performance. *Integrative and Comparative Biology*, **49**, pp.380–392.

**Lu, I.-C. et al.,** 2015. Ionization mechanism of matrix-assisted laser desorption/ionization. *Annual Review of Analytical Chemistry*, **8**, pp.21–39.

**Lu, J. et al.,** 2002. Isolation and structure-bioactivity characterization of glycosylated N-pro-opiomelanoconin isoforms. *Journal of Neuroendocrinology*, **14**, pp.869–879.

**Luan, H. et al.,** 2006. Functional dissection of a neuronal network required for cuticle tanning and wing expansion in Drosophila. *The Journal of neuroscience*, **26**, pp.573–584.

**Ludwar, B.C. et al.,** 2005. Modulation of membrane potential in mesothoracic moto- and interneurons during stick insect front-leg walking. *Journal of Neurophysiology*, **94**, pp.2772–2784.

**Luo, J., Liu, Y. & Nässel, D.R.,** 2017. Transcriptional reorganization of Drosophila motor neurons and their muscular junctions toward a neuroendocrine phenotype by the bHLH protein Dimmed. *Frontiers in Molecular Neuroscience*, **10**, pp.1–20.

**Macht, M., Asperger, A. & Deininger, S.O.,** 2004. Comparison of laser-induced dissociation and high-energy collision-induced dissociation using matrix-assisted laser desorption/ionization tandem time-of-flight (MALDI-TOF/TOF) for peptide and protein identification. *Rapid Communications in Mass Spectrometry*, **18**, pp.2093–2105.

**Majdi, S. et al.,** 2015. Electrochemical measurements of optogenetically stimulated quantal amine release from single nerve cell varicosities in Drosophila larvae. *Angewandte Chemie*, **54**, pp.13609–13612.

**Makos, M.A. et al.,** 2009. In vivo electrochemical measurements of exogenously applied dopamine in Drosophila melanogaster. *Analytical Chemistry*, **81**, pp.1848–1854.

**Manier, M.L. et al.,** 2014. A derivatization and validation strategy for determining the spatial localization of endogenous amine metabolites in tissues using MALDI imaging mass spectrometry. *Journal of Mass Spectrometry*, **49**, pp.665–673.

**Manier, M.L. et al.,** 2011. Reagent precoated targets for rapid in-tissue derivatization of the anti-tuberculosis drug isoniazid followed by MALDI imaging mass spectrometry. *Journal of the American Society for Mass Spectrometry*, **22**, pp.1409–1419.

**Maqueira, B., Chatwin, H. & Evans, P.D.,** 2005. Identification and characterization of a novel family of Drosophilaβ-adrenergic-like octopamine G-protein coupled receptors. *Journal of Neurochemistry*, **94**, pp.547–560.

**Marder, E.,** 2012. Neuromodulation of neuronal circuits: Back to the future. *Neuron*, **76**, pp.1–11.

**Marder, E. & Rehm, K.J.,** 2005. Development of central pattern generating circuits. *Current Opinion in Neurobiology*, **15**, pp.86–93.

**Marvin, J.S. et al.,** 2013. An optimized fluorescent probe for visualizing glutamate neurotransmission. *Nature Methods*, **10**, pp.162–170.

**McClellan, A.D., Brown, G.D. & Getting, P.A.,** 1994. Modulation of swimming in Tritonia: excitatory and inhibitory effects of serotonin. *Journal of Comparative Physiology*, **174**, pp.257–266.

**McCormick, J. & Nichols, R.,** 1993. Spatial and temporal expression identify dromyosuppressin as a brain-gut peptide in Drosophila melanogaster. *Journal of Comparative Neurology*, **338**, pp.279–288.

**McGuire, S.E. et al.,** 2003. Spatiotemporal Rescue of Memory Dysfunction in Drosophila. *Science*, **5651**, pp.1765–1768.

**Melcher, C. & Pankratz, M.J.,** 2005. Candidate gustatory interneurons modulating feeding behavior in the Drosophila brain. *PLoS Biology*, **9**, pp.1618–1629.

**Meng, X. et al.,** 2002. The Drosophila hugin gene codes for myostimulatory and ecdysis-modifying neuropeptides. *Mechanisms of Development*, **117**, pp.5–13.

**Mercer, A.R. & Menzel, R.,** 1982. The effects of biogenic amines on conditioned and unconditioned responses to olfactory stimuli in the honeybee Apis mellifera. *Journal of Comparative Physiology A*, **145**, pp.363–368.

**Merighi, A.,** 2011. *Neuropeptides: Methods and Protocols*, Humana Press.

**Merte, J. & Nichols, R.,** 2002. Drosophila melanogaster myotropins have unique functions and signaling pathways. *Peptides*, **23**, pp.757–763.

**Miao, H., Rubakhin, S.S. & Sweedler, J. V,** 2005. Subcellular analysis of D-aspartate. *Analytical Chemistry*, **77**, pp.7190–7194.

**Min, S. et al.,** 2016. Identification of a peptidergic pathway critical to satiety responses in drosophila. *Current Biology*, **26**, pp.814–820.

**Mitchell Wells, J. & McLuckey, S.A.,** 2005. Collision-induced dissociation (CID) of peptides and proteins. *Methods in Enzymology*, **1993**, pp.148–185.

**Monastirioti, M. et al.,** 1995. Octopamine immunoreactivity in the fruit fly Drosophila melanogaster. *Journal of Comparative Neurology*, **356**, pp.37–54.

**Monastirioti, M., Linn, C.E. & White, K.,** 1996. Characterization of Drosophila tyramine beta-hydroxylase gene and isolation of mutant flies lacking octopamine. *The Journal of Neuroscience*, **16**, pp.3900–3911.

**Morton, D.B. & Evans, P.D.,** 1984. Octopamine release from an identified neurone in the locust. *Journal of Experimental Biology*, **113**, pp.269–287.

**Muller, A. et al.,** 2014. Cell-based reporters reveal in vivo dynamics of dopamine and norepinephrine release in murine cortex. *Nature Methods*, **12**, pp.1245–1252.

**Mundiyanapurath, S. et al.,** 2009. Feminizing cholinergic neurons in a male Drosophila nervous system enhances aggression. *Fly*, **3**, pp.179–184.

**Nagaya, Y. et al.,** 2002. A trace amine, tyramine, functions as a neuromodulator in Drosophila melanogaster. *Neuroscience Letters*, **329**, pp.324–328.

**Namiki, S. et al.,** 2009. Reconstruction of virtual neural circuits in an insect brain. *Frontiers in Neuroscience*, **3**, pp.206–213.

**Nässel, D.R. et al.,** 2008. A large population of diverse neurons in the Drosophila central nervous system expresses short neuropeptide F, suggesting multiple distributed peptide functions. *BMC Neuroscience*, **9**, 90.

**Nässel, D.R.,** 2009. Neuropeptide signaling near and far: How localized and timed is the action of neuropeptides in brain circuits? *Invertebrate Neuroscience*, **9**, pp.57–75.

**Nässel, D.R.,** 2002. Neuropeptides in the nervous system of Drosophila and other insects: multiple roles as neuromodulators and neurohormones. *Progress in Neurobiology*, **68**, pp.1–84.

**Nässel, D.R.,** 2018. Substrates for neuronal cotransmission with neuropeptides and small molecule neurotransmitters in Drosophila. *Frontiers in Cellular Neuroscience*, **12**, 83.

**Nässel, D.R. & Wegener, C.,** 2011. A comparative review of short and long neuropeptide F signaling in invertebrates: Any similarities to vertebrate neuropeptide Y signaling? *Peptides*, **32**, pp.1335–1355.

**Nässel, D.R. & Williams, M.J.,** 2014. Cholecystokinin-like peptide (DSK) in Drosophila, not only for satiety signaling. *Frontiers in Endocrinology*, **5**, 219.

**Nässel, D.R. & Winther, A.M.E.,** 2010. Drosophila neuropeptides in regulation of physiology and behavior. *Progress in Neurobiology*, **92**, pp.42–104.

**Nelson, R.J. & Trainor, B.C.,** 2007. Neural mechanisms of aggression. *Nature Reviews Neuroscience*, **8**, pp.536–546.

**Nemes, P. et al.,** 2011. Metabolic differentiation of neuronal phenotypes by single cell CE-ESI-MS. *Analytical Chemistry*, **83**, pp.6810–6817.

**Nemes, P. et al.,** 2013. Qualitative and quantitative metabolomic investigation of single neurons by capillary electrophoresis electrospray ionization mass spectrometry. *Nature Protocols*, **8**, pp.783–799.

**Nemes, P. et al.,** 2012. Single-cell metabolomics: Changes in the metabolome of freshly isolated and cultured neurons. *ACS Chemical Neuroscience*, **10**, pp.782–792.

**Neupert, S. et al.,** 2018. Analysis of single neurons by perforated patch clamp recordings and MALDI-TOF mass spectrometry. *ACS Chemical Neuroscience*, **9**, pp.2089–2096.

**Neupert, S., Huetteroth, W., et al.,** 2009. Conservation of the function counts: Homologous neurons express sequence-related neuropeptides that originate from different genes. *Journal of Neurochemistry*, **111**, pp.757–765.

**Neupert, S. et al.,** 2005. Identification of tick periviscerokinin, the first neurohormone of Ixodidae: Single cell analysis by means of MALDI-TOF/TOF mass spectrometry. *Biochemical and Biophysical Research Communications*, **338**, pp.1860–1864.

**Neupert, S. et al.,** 2007. Single-cell peptidomics of drosophila melanogaster neurons identified by Gal4-driven fluorescence. *Analytical Chemistry*, **79**, pp.3690–3694.

**Neupert, S. et al.,** 2010. Two capa-genes are expressed in the neuroendocrine system of Rhodnius prolixus. *Peptides*, **31**, pp.408–411.

**Neupert, S. & Gundel, M.,** 2007. Mass spectrometric analysis of FMRFamide-like immunoreactive neurons in the prothoracic and subesophageal ganglion of Periplaneta americana. *Peptides*, **28**, pp.11–17.

**Neupert, S. & Predel, R.,** 2005. Mass spectrometric analysis of single identified neurons of an insect. *Biochemical and Biophysical Research Communications*, **327**, pp.640–645.

**Neupert, S., Rubakhin, S.S. & Sweedler, J. V,** 2012. Targeted single-cell microchemical analysis: MS-based peptidomics of individual paraformaldehyde-fixed and immunolabeled neurons. *Chemistry & Biology*, **19**, pp.1010–1019.

**Neupert, S., Schattschneider, S. & Predel, R.,** 2009. Allatotropin-related peptide in cockroaches: Identification via mass spectrometric analysis of single identified neurons. *Peptides*, **30**, pp.489–494.

**Niall, H.D.,** 1973. Automated Edman Degradation: The protein sequenator. *Methods in Enzymology*, **1950**, pp.942–1010.

**Nichols, R. & Lim, I.A.,** 1996. Spatial and temporal immunocytochemical analysis of drosulfakinin (Dsk) gene products in the Drosophila melanogaster central nervous system. *Cell and Tissue Research*, **283**, pp.107–116.

**Nichols, R., Schneuwly, S.A. & Dixon, J.E.,** 1988. Identification and characterization of a Drosophila homologue to the vertebrate neuropeptide cholecystokinin. *Journal of Biological Chemistry*, **263**, pp.12167–12170.

**Nilsen, S.P. et al.,** 2004. Gender-selective patterns of aggressive behavior in Drosophila melanogaster. *Proceedings of the National Academy of Sciences*, **101**, pp.12342–12347.

**Nisimura, T.,** 2005. Experiential effects of appetitive and nonappetitive odors on feeding behavior in the blowfly, Phormia regina: A putative role for tyramine in appetite regulation. *Journal of Neuroscience*, **33**, pp.7507–7516.

**Niven, J.E., Graham, C.M. & Burrows, M.,** 2008. Diversity and Evolution of the Insect Ventral Nerve Cord. *Annual Review of Entomology*, **53**, pp.253–271.

**Noble, T., Stieglitz, J. & Srinivasan, S.,** 2013. An integrated serotonin and octopamine neuronal circuit directs the release of an endocrine signal to control C. elegans body fat. *Cell Metabolism*, **18**, pp.672–684.

**Okubo, Y. et al.,** 2010. Imaging extrasynaptic glutamate dynamics in the brain. *Proceedings of the National Academy of Sciences*, **107**, pp.6526–6531.

**Ong, T.-H. et al.,** 2015a. Mass spectrometry-based characterization of endogenous peptides and metabolites in small volume samples. *Biochimica et Biophysica Acta (BBA) - Proteins and Proteomics*, **1854**, pp.732–740.

**Ong, T.H. et al.,** 2015b. Classification of large cellular populations and discovery of rare cells using single cell matrix-assisted laser desorption/ionization time-of-flight mass spectrometry. *Analytical Chemistry*, **87**, pp.7036–7042.

**Onjiko, R.M. et al.,** 2017a. Metabolic comparison of dorsal versus ventral cells directly in the live 8-cell frog embryo by microprobe single-cell CE-ESI-MS. *Analytical methods: Advancing Methods and Applications*, **34**, pp.4964–4970.

**Onjiko, R.M. et al.,** 2017b. Microprobe capillary electrophoresis mass spectrometry for single-cell metabolomics in live frog Xenopus laevis embryos. *Journal of Visualized Experiments*, **130**.

**Onjiko, R.M., Moody, S.A. & Nemes, P.,** 2015. Single-cell mass spectrometry reveals small molecules that affect cell fates in the 16-cell embryo. *Proceedings of the National Academy of Sciences*, **112**, pp.6545–6550.

**Orchard, I. & Lange, A.B.,** 1986. Pharmacological profile of octopamine receptors on the lateral oviducts of the locust, Locusta migratoria. *Journal of Insect Physiology*, **32**, pp.741–745.

**Overend, G. et al.,** 2012. The receptor guanylate cyclase Gyc76C and a peptide ligand, NPLP1-VQQ, modulate the innate immune IMD pathway in response to salt stress. *Peptides*, **34**, pp.209–218.

**Page, J.S., Rubakhin, S.S. & Sweedler, J. V.,** 2002. Single-neuron analysis using CE combined with MALDI MS and radionuclide detection. *Analytical Chemistry*, **74**, pp.497–503.

**Pan, Y., Meissner, G.W. & Baker, B.S.,** 2012. Joint control of Drosophila male courtship behavior by motion cues and activation of male-specific P1 neurons. *Proceedings of the National Academy of Sciences*, **109**, pp.10065–10070.

**Pannabecker, T., & Orchard, I.,** 1986. Pharmacological properties of octopamine-2 receptors in locust neuroendocrine tissue. *Jounral of Insect Physiology*, **32**, pp.909–915.

**Park, D. et al.,** 2008. Mapping peptidergic cells in Drosophila: where DIMM fits in. *PloS ONE*, **3**, e1896.

**Park, J. et al.,** 2016. Single-cell transcriptional analysis reveals novel neuronal phenotypes and interaction networks involved in the central circadian clock. *Frontiers in Neuroscience*, **10**, 481.

**Park, Y., Kim, Y.-J. & Adams, M.E.,** 2002. Identification of G protein-coupled receptors for Drosophila PRXamide peptides, CCAP, corazonin, and AKH supports a theory of ligand-receptor coevolution. *Proceedings of the National Academy of Sciences*, **99**, pp.11423–11428.

**Patriarchi, T. et al.,** 2018. Ultrafast neuronal imaging of dopamine dynamics with designed genetically encoded sensors. *Science*, **6396**, eaat4422.

**Paxon, T.L. et al.,** 2005. Microcolumn separation of amine metabolites in the fruit fly. *Analytical Chemistry*, **77**, pp.5349–5355.

**Perone, M.J., Windeatt, S. & Castro, M.G.,** 1997. Intracellular trafficking of prohormones and proneuropeptides: Cell type-specific sorting and targeting. *Experimental Physiology*, **82**, pp.609–628.

**Persike, M. et al.,** 2010. Quantitative determination of acetylcholine and choline in microdialysis samples by MALDI-TOF MS. *Analytical Chemistry*, **82**, pp.922–929.

**Persike, M. & Karas, M.,** 2009. Rapid simultaneous quantitative determination of different small pharmaceutical drugs using a conventional matrix-assisted laser desorption/ionization time-of-flight mass spectrometry system. *Rapid Communications in Mass Spectrometry*, **23**, pp.3555–3562.

**Phan, N.T.N. et al.,** 2013. Capillary Electrophoresis Mass Spectrometry based Detection of Drugs and Neurotransmitters in Drosophila Brain. *Analytical Chemistry*, **85**, pp.8448-8454.

**von Philipsborn, A.C. et al.,** 2011. Neuronal Control of Drosophila Courtship Song. *Neuron*, **69**, pp.509–522.

**Pitman, J.L. et al.,** 2011. A pair of inhibitory neurons are required to sustain labile memory in the Drosophila mushroom body. *Current Biology*, **21**, pp.855–861.

**Piyankarage, S.C. et al.,** 2008. Hemolymph amino acid analysis of individual Drosophila larvae. *Analytical Chemistry*, **80**, pp.1201–1207.

**Piyankarage, S.C. et al.,** 2010. Hemolymph amino acid variations following behavioral and genetic changes in individual Drosophila larvae. *Amino Acids*, **38**, pp.779–788.

**Pourhaghighi, M.R., Busnel, J.M. & Girault, H.H.,** 2011. High-sensitive protein analysis by FESI-CE-MALDI-MS. *Electrophoresis*, **32**, pp.1795–1803.

**Predel, R. et al.,** 1999. Differential distribution of pyrokinin-isoforms in cerebral and abdominal neurohemal organs of the American cockroach. *Insect Biochemistry and Molecular Biology*, **29**, pp.139–144.

**Predel, R. et al.,** 2010. Neuropeptidomics of the mosquito Aedes aegypti. *Journal of Proteome Research*, **9**, pp.2006–2015.

**Predel, R. et al.,** 2004. Peptidomics of CNS-associated neurohemal systems of adult Drosophila melanogaster: a mass spectrometric survey of peptides from individual flies. *The Journal of Comparative Neurology*, **474**, pp.379–392.

**Predel, R. et al.,** 1995. Periviscerokinin (Pea-PVK): A novel myotropic neuropeptide from the perisympathetic organs of the American cockroach. *Peptides*, **16**, pp.61–66.

**Predel, R. & Wegener, C.,** 2006. Biology of the CAPA peptides in insects. *Cellular and Molecular Life Sciences*, **63**, pp.2477–2490.

**Price, M.D. et al.,** 2002. Drosophila melanogaster flatline encodes a myotropin orthologue to Manduca sexta allatostatin. *Peptides*, **23**, pp.787–794.

**Prigge, S.T. et al.,** 2000. New insights into copper monooxygenases and peptide amidation: Structure, mechanism and function. *Cellular and Molecular Life Sciences*, **57**, pp.1236–1259.

**Pyakurel, P., Privman Champaloux, E. & Venton, B.J.,** 2016. Fast-scan cyclic voltammetry (FSCV) detection of endogenous octopamine in Drosophila melanogaster ventral nerve cord. *ACS Chemical Neuroscience*, **8**, pp.1112–1119.

**Python, F. & Stocker, R.F.,** 2002. Immunoreactivity against choline acetyltransferase, γ-aminobutyric acid, histamine, octopamine, and serotonin in the larval chemosensory system of Drosophila melanogaster. *Journal of Comparative Neurology*, **453**, pp.157–167.

**Qi, M. et al.,** 2018. Single cell neurometabolomics. *ACS Chemical Neuroscience*, **9**, pp.40–50.

**Qi, Y. & Volmer, D.A.,** 2016. Structural analysis of small to medium-sized molecules by mass spectrometry after electron-ion fragmentation (ExD) reactions. *Analyst*, **141**, pp.794–806.

**Qi, Y. xiang et al.,** 2017. A new Drosophila octopamine receptor responds to serotonin. *Insect Biochemistry and Molecular Biology*, **90**, pp.61–70.

**Raibekas, A.A. & Massey, V.,** 1997. Glycerol-assisted restorative adjustment of flavoenzyme conformation perturbed by site-directed mutagenesis. *The Journal of Biological Chemistry*, **272**, pp.22248–22252.

**Rajashekhar, K.P. & Singh, R.N.,** 1994. Neuroarchitecture of the Tritocerebrum of Drosophila-melangaster. *Journal of Comparitive Neurology.*, **349**, pp.633–645.

**Ramirez, J.M., Büschges, A. & Kittmann, R.,** 1993. Octopaminergic modulation of the femoral chordotonal organ in the stick insect. *Journal of Comparative Physiology A*, **173**, pp.209–219.

**Ream, P.J. et al.,** 2003. Micellar electrokinetic capillary chromatography-electrochemical detection for analysis of biogenic amines in Drosophila melanogaster. *Analytical Chemistry*, **75**, pp.3972–3978.

**Redeker, J. et al.,** 2017. Identification and distribution of products from novel tryptopyrokinin genes in the locust, Locusta migratoria. *Biochemical and Biophysical Research Communications*, **486**, pp.70–75.

**Ren, D. et al.,** 2001. A prokaryotic voltage-gated sodium channel. *Science*, **5550**, pp.2372–

2375.

**Rezával, C. et al.,** 2014. Sexually dimorphic octopaminergic neurons modulate female postmating behaviors in drosophila. *Current Biology*, **24**, pp.725–730.

**Rholam, M. & Fahy, C.,** 2009. Processing of peptide and hormone precursors at the dibasic cleavage sites. *Cellular and Molecular Life Sciences*, **66**, pp.2075–2091.

**Rillich, J., Stevenson, P.A. & Pflueger, H.J.,** 2013. Flight and walking in Locusts-cholinergic co-activation, temporal coupling and its modulation by biogenic amines. *PLoS ONE*, **8**, e62899.

**Robb, S. et al.,** 1994. Agonist-specific coupling of a cloned Drosophila octopamine/tyramine receptor to multiple second messenger systems. *The EMBO journal*, **13**, pp.1325–1330.

**Rodríguez-Valentín, R. et al.**, 2006. Oviduct contraction in Drosophila is modulated by a neural network that is both, octopaminergic and glutamatergic. *Journal of Cellular Physiology*, **209**, pp.183–198.

**Roeder, T.,** 2005. TYRAMINE AND OCTOPAMINE: Ruling Behavior and Metabolism. *Annual Review of Entomology*, **50**, pp.447–477.

**Roignant, J.Y. et al.,** 2003. Absence of transitive and systemic pathways allows cell-specific and isoform-specific RNAi in Drosophila. *Rna*, **9**, pp.299–308.

**Romanova, E. V. et al.,** 2014. Small-volume analysis of cell-cell signaling molecules in the brain. *Neuropsychopharmacology*, **39,** pp.50–64.

**Römpp, A. et al.,** 2010. Histology by mass spectrometry: Label-free tissue characterization obtained from high-accuracy bioanalytical imaging. *Angewandte Chemie*, **49**, pp.3834–3838.

**Rosenbaum, P. et al.,** 2015. Task-dependent modification of leg motor neuron synaptic input underlying changes in walking direction and walking speed. *Journal of Neurophysiology*, **114**, pp.1090–1101.

**Rosenkilde, C. et al.,** 2003. Molecular cloning, functional expression, and gene silencing of two Drosophila receptors for the Drosophila neuropeptide pyrokinin-2. *Biochemical and Biophysical Research Communications*, **309**, pp.485–494.

**Rubakhin, S.S. et al.,** 2001. Analysis of cellular release using capillary electrophoresis and matrix assisted laser desorption/ionization-time of flight-mass spectrometry. *Electrophoresis*, **22**, pp.3752–3758.

**Rubakhin, S.S. et al.,** 2011. Profiling metabolilites and peptides in single cells. *Nature Methods*, **8**, S20-29.

**Rubakhin, S.S. et al.,** 2006. Profiling signaling peptides in single mammalian cells using mass spectrometry. *Analytical Chemistry*, **78**, pp.7267–7272.

**Rubakhin, S.S., Greenough, W.T. & Sweedler, J. V.,** 2003. Spatial profiling with MALDI MS: Distribution of neuropeptides within single neurons. *Analytical Chemistry*, **75**, pp.5374–5380.

**Rubakhin, S.S. & Sweedler, J. V.,** 2007. Characterizing peptides in individual mammalian cells using mass spectrometry. *Nature Protocols*, **8**, pp.1987–1997.

**Rubakhin, S.S. & Sweedler, J. V,** 2008. Quantitative measurements of cell-cell signaling peptides with single-cell MALDI MS. *Analytical Chemistry*, **80**, pp.7128–7136.

**Ryglewski, S., Duch, C. & Altenhein, B.,** 2017. Tyramine actions on Drosophila flight behavior are affected by a glial dehydrogenase/reductase. *Frontiers in Systems Neuroscience*, **11**, 68.

**Salisbury, J.P. et al.,** 2013. A rapid MALDI-TOF mass spectrometry workflow for Drosophila melanogaster differential neuropeptidomics. *Molecular Brain*, **6**, 60.

**Salvaterra, P.M. & McCaman, R.E.,** 1985. Choline acetyltransferase and acetylcholine levels in Drosophila melanogaster: a study using two temperature-sensitive mutants. *The Journal of Neuroscience*, **5**, pp.903–910.

**Saraswati, S. et al.,** 2004. Tyramine and Octopamine have opposite effects on the locomotion of Drosophila larvae. *Journal of Neurobiology*, **58**, pp.425–441.

**Saudou, F. et al.,** 1990. Cloning and characterization of a Drosophila tyramine receptor. *The EMBO Journal*, **11**, pp.3611–3617.

**Scheiner, R. et al.,** 2002. Behavioural pharmacology of octopamine, tyramine and dopamine in honey bees. *Behavioural Brain Research*, **136**, pp.545–553.

**Scheiner, R., Reim, T., et al.,** 2017. Learning, gustatory responsiveness and tyramine differences across nurse and forager honeybees. *The Journal of Experimental Biology*, **220**, pp.1443–1450.

**Scheiner, R., Entler, B. V., et al.,** 2017. The effects of fat body tyramine level on gustatory responsiveness of honeybees (Apis mellifera) differ between behavioral castes. *Frontiers in Systems Neuroscience*, **11**, 55.

**Schinko, J.B.** et al., 2010. Functionality of the GAL4/UAS system in Tribolium requires the use of endogenous core promoters. *BMC Developmental Biology*, **10**, 53.

**Schlegel, P. et al.,** 2016. Synaptic transmission parallels neuromodulation in a central food-intake circuit. *eLife*, **5**, e16799.

**Schneider, A. et al.,** 2012. Neuronal basis of innate olfactory attraction to ethanol in Drosophila. *PLoS ONE*, **12**, e52007.

**Schneider, M. et al.,** 2005. Two-photon activation and excitation properties of PA-GFP in the 720–920-nm region. *Biophysical Journal*, **89**, pp.1346–1352.

**Schoofs, L. & Baggerman, G.,** 2003. Peptidomics in Drosophila melanogaster. *Briefings in Functional Genomics & Proteomics*, **2**, pp.114–20.

**Schoofs, L., De Loof, A. & Van Hiel, M.B.,** 2017. Neuropeptides as regulators of behavior in insects. *Annual Review of Entomology*, **62**, pp.35–52.

**Schroll, C. et al.,** 2006. Light-induced activation of distinct modulatory neurons triggers appetitive or aversive learning in Drosophila larvae. *Current Biology*, **17**, pp.1741–1747.

**Schröter, U., Malun, D. & Menzel, R.,** 2007. Innervation pattern of suboesophageal ventral unpaired median neurones in the honeybee brain. *Cell and Tissue Research*, **327**, pp.647–667.

**Schubert, F.K. et al.,** 2018. Neuroanatomical details of the lateral neurons of Drosophila melanogaster support their functional role in the circadian system. *Journal of Comparative Neurology*, **526**, pp.1209–1231.

**Schwaerzel, M. et al.,** 2003. Dopamine and octopamine differentiate between aversive and appetitive olfactory memories in Drosophila. *The Journal of Neuroscience*, **33**, pp.10495–502.

**Selcho, M. et al.,** 2014. Characterization of the octopaminergic and tyraminergic neurons in the central brain of Drosophila larvae. *Journal of Comparative Neurology*, **522**, pp.3485–3500.

**Selcho, M. et al.,** 2012. The role of octopamine and tyramine in Drosophila larval locomotion. *Journal of Comparative Neurology*, *520*, pp.3764–3785.

**Sellami, L. et al.,** 2012. In-source decay and pseudo tandem mass spectrometry fragmentation processes of entire high mass proteins on a hybrid vacuum matrix-assisted laser desorption ionization-quadrupole ion-trap time-of-flight mass spectrometer. *Analytical Chemistry*, **84**, pp.5180–5185.

**Shafer, O.T. et al.,** 2006. Reevaluation of Drosophila melanogaster's neuronal circadian pacemakers reveals new neuronal classes. *Journal of Comparative Neurology*, **193**, pp.180–193.

**Shang, Y. et al.,** 2013. Short neuropeptide F is a sleep-promoting inhibitory modulator. *Neuron*, **80**, pp.171–183.

**Shang, Y., Griffith, L.C. & Rosbash, M.,** 2008. Light-arousal and circadian photoreception circuits intersect at the large PDF cells of the Drosophila brain. *Proceedings of the National Academy of Sciences*, **105**, pp.19587-19594.

**Shanta, S.R. et al.,** 2012. A new combination MALDI matrix for small molecule analysis: Application to imaging mass spectrometry for drugs and metabolites. *Analyst*, **137**, pp.5757–5762.

**Shariatgorji, M. et al.,** 2012. Deuterated matrix-assisted laser desorption ionization matrix uncovers masked mass spectrometry imaging signals of small molecules. *Analytical Chemistry*, **84**, pp.7152–7157.

**Shariatgorji, M. et al.,** 2014. Direct targeted quantitative molecular imaging of neurotransmitters in brain tissue sections. *Neuron*, **84**, pp.697–707.

**Shariatgorji, M. et al.,** 2015. Pyrylium salts as reactive matrices for MALDI-MS imaging of biologically active primary amines. *Journal of the American Society for Mass Spectrometry*, **26**, pp.934–939.

**Shariatgorji, M. et al.,** 2016. Simultaneous imaging of multiple neurotransmitters and neuroactive substances in the brain by desorption electrospray ionization mass spectrometry. *NeuroImage*, **136**, pp.129–138.

**Shen, P. & Cai, H.N.,** 2001. Drosophila neuropeptide F mediates integration of chemosensory stimulation and conditioning of the nervous system by food. *Journal of Neurobiology*, **47**, pp.16–25.

**Shin, M., Copeland, J.M. & Venton, B.J.,** 2018. Drosophila as a model system for neurotransmitter measurements. *ACS Chemical Neuroscience*, **9**, pp.1872–1883.

**Siegmund, T. & Korge, G.,** 2001. Innervation of the ring gland of Drosophila melanogaster. *Journal of Comparative Neurology*, **431**, pp.481–491.

**da Silva, R. & Lange, A.B.,** 2008. Tyramine as a possible neurotransmitter/neuromodulator at the spermatheca of the African migratory locust, Locusta migratoria. *Journal of insect physiology*, **54**, pp.1306–1313.

**Sinakevitch, I., Niwa, M. & Strausfeld, N.J.,** 2005. Octopamine-like immunoreactivity in the honey bee and cockroach: Comparable organization in the brain and subesophageal ganglion. *Journal of Comparative Neurology*, **488**, pp.233–254.

**Sinakevitch, I. & Strausfeld, N.J.,** 2006. Comparison of octopamine-like immunoreactivity in the brains of the fruit fly and blow fly. *Journal of Comparative Neurology*, **494**, pp.460–475.

**Sloley, B.D.,** 2004. Metabolism of monoamines in invertebrates: The relative importance of monoamine oxidase in different phyla. *NeuroToxicology*, **25**, pp.175–183.

**Sloley, B.D. & Juorio, A. V.,** 1995. Monoamine neurotransmitters in invertebrates and vertebrates: An examination of the diverse enzymatic pathways utilized to synthesize and inactivate blogenic amines. *International Review of Neurobiology*, **38**, pp.253–303.

**Söderberg, J.A.E., Carlsson, M.A. & Nässel, D.R.,** 2012. Insulin-producing cells in the Drosophila brain also express satiety-inducing cholecystokinin-like peptide, drosulfakinin. *Frontiers in Endocrinology*, **3**, pp.1–13.

**Sombati, S. & Hoyle, G.,** 1984. Generation of specific behaviors in a locust by local release into neuropil of the natural neuromodulator octopamine. *Journal of Neurobiology*, **15**, pp.481–506.

**Sotnikova, T.D. & Gainetdinov, R.R.,** 2010. Octopamine and other monoamines in invertebrates. *Encyclopedia of Neuroscience*, pp.9–15.

**Southey, B.R. et al.,** 2006. NeuroPred: A tool to predict cleavage sites in neuropeptide precursors and provide the masses of the resulting peptides. *Nucleic Acids Research*, **34**, pp.267–272.

**Spengler, B.,** 2015. Mass spectrometry imaging of biomolecular information. *Analytical Chemistry*, **87**, pp.64–82.

**Spengler, B., Kirsch, D. & Kaufmann, R.,** 1992. Fundamental aspects of postsource decay in matrix-assisted laser desorption mass spectrometry. *The Journal of Physical Chemistry*, **96**, pp.9678–9684.

**Sporhase-Eichmann, U. et al.,** 1992. Octopamine-immunoreactive neurons in the central nervous system of the cricket , Gryllus bimaculatus. *Cell & Tissue Research*, **268**, pp.287–304.

**Stern, M. et al.,** 1995. Octopaminergic neurons in the locust brain: morphological, biochemical and electrophysiological characterisation of potential modulators of the visual system. *Journal of Comparative Physiology A*, **177**, pp.611–625.

**Stern, M.,** 2009. The PM1 neurons, movement sensitive centrifugal visual brain neurons in the locust: Anatomy, physiology, and modulation by identified octopaminergic neurons. *Journal of Comparative Physiology A: Neuroethology, Sensory, Neural, and Behavioral Physiology*, **195**, pp.123–137.

**Stevenson, P. a et al.,** 2000. The fight and flight responses of crick. *Journal of Neurobiology*, **43**, pp.107–20.

**Stevenson, P.A. et al.,** 1994. Octopamine-like immunoreactive neurones in locust genital abdominal ganglia. *Cell and Tissue Research*, **275**, pp.299–308.

**Stevenson, P.A.,** 2005. Octopamine and experience-dependent modulation of aggression in crickets. *Journal of Neuroscience*, **25**, pp.1431–1441.

**Stevenson, P.A. et al.,** 2000. The fight and flight responses of crickets depleted of biogenic amines. *Journal of Neurobiology*, **43**, pp.107–120.

**Stolz, T.,** 2018. *Descending Octopaminergic Neurons in the Stick Insect: Their Inputs and their Output Effects on the Locomotor System*. Ph.D. Thesis, University Cologne.

**Strausfeld, N.J. & Hirth, F.,** 2013. Deep homology of arthropod central complex and vertebrate basal ganglia. *Science*, **6129**, pp.157–161.

**Suster, M.L. et al.,** 2004. Refining GAL4-driven transgene expression in Drosophila with a GAL80 enhancer-trap. *Genesis*, **39**, pp.240–245.

**Svatoš, A. & Ibáñez, A.J.,** 2014. Single-cell imaging for the study of oncometabolism. *Methods in Enzymology*, **543**, pp.199–215.

**Sweeney, S.T. et al.,** 1995. Targeted expression of tetanus toxin light chain in Drosophila specifically eliminates synaptic transmission and causes behavioral defects. *Neuron*, **14**, pp.341–351.

**Taghert, P.H. & Nitabach, M.N.,** 2012. Peptide Neuromodulation in invertebrate model systems. *Neuron*, **76**, pp.82–97.

**Terhzaz, S. et al.,** 2015. Insect capa neuropeptides impact desiccation and cold tolerance. *Proceedings of the National Academy of Sciences*, **112**, pp.2882–2887.

**Terhzaz, S. et al.,** 2012. Mechanism and function of drosophila capa GPCR: A desiccation stress-responsive receptor with functional homology to human neuromedinu receptor. *PLoS ONE*, **7**, e29897.

**Titlow, J.S., Johnson, B.R. & Pulver, S.R.,** 2015. Light activated escape circuits: A behavior and neurophysiology lab module using Drosophila optogenetics. *Journal of Undergraduate Neuroscience Education*, **13,** pp.166–173.

**Toue, S. et al.,** 2014. Microscopic imaging mass spectrometry assisted by on-tissue chemical derivatization for visualizing multiple amino acids in human colon cancer xenografts. *Proteomics*, **14**, pp.810–819.

**Tseng, H.-M., Li, Y. & Barrett, D.A.,** 2010. Bioanalytical applications of capillary electrophoresis with laser-induced native fluorescence detection. *Bioanalysis*, **9**, pp.1641–1653.

**Tuteja, R.,** 2005. Type I signal peptidase: An overview. *Archives of Biochemistry and Biophysics*, **441**, pp.107–111.

**Tuthill, J.C. & Wilson, R.I.,** 2016. Mechanosensation and adaptive motor control in insects. *Current Biology*, **26**, pp.1022–1038.

**Týčová, A., Ledvina, V. & Klepárník, K.,** 2017. Recent advances in CE-MS coupling: Instrumentation, methodology, and applications. *Electrophoresis*, **38**, pp.115–134.

**Ueno, T. & Kume, K.,** 2014. Functional characterization of dopamine transporter in vivo using Drosophila melanogaster behavioral assays. *Frontiers in Behavioral Neuroscience*, **8**, 303.

**Unoki, S., Matsumoto, Y. & Mizunami, M.,** 2005. Participation of octopaminergic reward system and dopaminergic punishment system in insect olfactory learning revealed by pharmacological study. *European Journal of Neuroscience*, **22**, pp.1409–1416.

**Unoki, S., Matsumoto, Y. & Mizunami, M.,** 2006. Roles of octopaminergic and dopaminergic neurons in mediating reward and punishment signals in insect visual learning. *European Journal of Neuroscience*, **24**, pp.2031–2038.

**Urbach, R. & Technau, G.M.,** 2003. Molecular markers for identified neuroblasts in the developing brain of Drosophila. *Development*, **130**, pp.3621–3637.

**Veenstra, J.A.,** 1989. Isolation and structure of corazonin, a cardioactive peptide from the American cockroach. *FEBS Letters*, **250**, pp.231–234.

**Veenstra, J.A.,** 1994. Isolation and Structure of the Drosophila Corazonin Gene. *Biochemical and Biophysical Research Communications*, **204**, pp.292–296.

**Veenstra, J.A.,** 2000. Mono- and dibasic proteolytic cleavage sites in insect neuroendocrine peptide precursors. *Archives of Insect Bioghemistry and Physiology*, **43**, pp.49–63.

**Veenstra, J.A.,** 2014. The contribution of the genomes of a termite and a locust to our understanding of insect neuropeptides and neurohormones. *Frontiers in Physiology*, **5**, 454.

**Verleyen, P. et al.,** 2003. Expression of a novel neuropeptide, NVGTLARDFQLPIPNamide, in the larval and adult brain of Drosophila melanogaster. *Journal of Neurochemistry*, **88**, pp.311–319.

**Verlinden, H. et al.,** 2015. The pleiotropic allatoregulatory neuropeptides and their receptors: A mini-review. *Journal of Insect Physiology*, **80**, pp.2–14.

**Verlinden, H. et al.,** 2010. The role of octopamine in locusts and other arthropods. *Journal of Insect Physiology*, **56**, pp.854–867.

**Vickrey, T.L., Condron, B. & Venton, B.J.,** 2009. Rapid detection of endogenous dopamine changes in drosophila melanogaster using fast-scan cyclic voltammetry. *Analytical Chemistry*, **81**, pp.9306–9313.

**Vömel, M. & Wegener, C.,** 2008. Neuroarchitecture of aminergic systems in the larval ventral ganglion of Drosophila melanogaster. *PLoS ONE*, **3**, e1848.

**Wang, C. et al.,** 2012. Defining the contribution of select neuropeptides and their receptors in regulating sesquiterpenoid biosynthesis by Drosophila melanogaster ring gland/corpus allatum through RNAi analysis. *General and Comparative Endocrinology*, **176**, pp.347–353.

**Wang, L. et al.,** 2011. Hierarchical chemosensory regulation of male-male social interactions in Drosophila. *Nature Neuroscience*, **14**, pp.757–762.

**Wang, S. et al.,** 2016. Matrix-assisted laser desorption/ionization mass spectrometry imaging of cell cultures for the lipidomic analysis of potential lipid markers in human breast cancer invasion. *Rapid Communications in Mass Spectrometry*, **30**, pp.533–542.

**Warzecha, A.-K., Horstmann, W. & Egelhaaf, M.,** 1999. Temperature-dependence of neuronal performance in the motion pathway of the blowfly Calliphora erythrocephala. *The Journal of Experimental Biology*, **202**, pp.3161–3170.

**Watanabe, K. et al.,** 2017. A circuit node that integrates convergent input from neuromodulatory and social behavior-promoting neurons to control aggression in Drosophila. *Neuron*, **95**, p.1112–1128.e7.

**Wegener, C. et al.,** 2006. Direct mass spectrometric peptide profiling and fragmentation of larval peptide hormone release sites in Drosophila melanogaster reveals tagma-specific peptide expression and differential processing. *Journal of Neruochemistry*, **96**, pp.1362–1374.

**Wegener, C. & Veenstra, J.A.,** 2015. Chemical identity, function and regulation of enteroendocrine peptides in insects. *Current Opinion in Insect Science*, **11**, pp.8–13.

**Weidler, D. & Diecke, F.,** 1969. The role of cations in conduction in the central nervous system of the herbivorous insect Carausius morosus Von mir zitiert. *Zeitschrift für vergleichende Physiologie*, **399**, pp.372–399.

**Weiss, L.A. et al.,** 2011. The molecular and cellular basis of bitter taste in Drosophila. *Neuron*,

**69**, pp.258–272.

**Wen, T. et al.,** 2005. Drosophila neuropeptide F and its receptor, NPFR1, define a signaling pathway that acutely modulates alcohol sensitivity. *Proceedings of the National Academy of Sciences*, **102**, pp.2141–2146.

**Westlund, K.N. et al.,** 1985. Distinct monoamine oxidase A and B populations in primate brain. *Science*, **4722**, pp.181-183.

**Westmark, S., Oliveira, E.E. & Schmidt, J.,** 2009. Pharmacological analysis of tonic activity in motoneurons during stick insect walking. *Journal of Neurophysiology*, **102**, pp.1049–1061.

**De Wied, D.,** 1971. Long term effect of vasopressin on the maintenance of a conditioned avoidance response in rats. *Nature*, **5305**, pp.58–60.

**De Wied, D.,** 2000. Peptide hormones and neuropeptides: birds of a feather. *Trends in Neurosciences*, **23**, 113.

**De Wied, D., van Wimersma Greidanus, T.B. & Bohus, B.**, 1974. Pituitary peptides and behavior: influence on motivational, learning and memory processes. *Proceedings of the IXth Congress of the Collegium International Neuropsychopharmacology*. pp. 653–658.

**Williams, M.J.** et al., 2014. Regulation of aggression by obesity-linked genes TfAP-2 and Twz through octopamine signaling in Drosophila. *Genetics*, **196**, pp.349–362.

**Windhorst, U.,** 2007. Muscle proprioceptive feedback and spinal networks. *Brain Research Bulletin*, **73**, pp.155–202.

**Wright, T.R.F.,** 1987. The genetics of biogenic amine metabolism, sclerotization, and melanization In Drosophila Melanogaster. *In J. G. Scandalios & E. W. Caspari, eds. Molecular Genetics of Development.* Advances in Genetics. Academic Press, pp. 127–222.

**Wu, Q. et al.,** 2003. Developmental control of foraging and social behavior by the Drosophila neuropeptide Y-like system. *Neuron*, **39**, pp.147–161.

**Wu, Q., Zhao, Z. & Shen, P.,** 2005. Regulation of aversion to noxious food by Drosophila neuropeptide Y- and insulin-like systems. *Nature Neuroscience*, **10**, pp.1350–1355.

**Wu, Z.S. et al.,** 2015. Ion channels gated by acetylcholine and serotonin: Structures, biology, and drug discovery. *Acta Pharmacologica Sinica*, **36**, pp.895–907.

**Xu, J., Li, M. & Shen, P.,** 2010. A G-protein coupled neuropeptide Y-like receptor suppresses behavioral and sensory response to multiple stressful stimuli in Drosophila. *The Journal of Neuroscience*, **30**, pp.2504–2512.

**Yamamoto, K. & Vernier, P.,** 2011. The evolution of dopamine systems in chordates. *Frontiers in Neuroanatomy*, **5**, pp.1–21.

**Yang, B. et al.,** 2018. Single-cell mass spectrometry reveals changes in lipid and metabolite expression in raw 264.7 cells upon lipopolysaccharide stimulation. *Journal of the American Society for Mass Spectrometry*, **29**, pp.1012–1020.

**Ye, H. et al.,** 2015. Defining the neuropeptidome of the spiny lobster Panulirus interruptus brain using a multidimensional mass spectrometry-based platform. *Journal of Proteome Research*, **14**, pp.4776–4791.

**Ye, J.H. et al.,** 2006. Patch-clamp studies in the CNS illustrate a simple new method for obtaining viable neurons in rat brain slices: glycerol replacement of NaCl protects CNS neurons. *Journal of Neuroscience Methods*, **158**, pp.251–259.

**Yeoh, J.G.C. et al.,** 2017. DINeR: Database for insect neuropeptide research. *Insect Biochemistry and Molecular Biology*, **86**, pp.9–19.

**Yew, J.Y. et al.,** 2009. Analysis of neuropeptide expression and localization in adult Drosophila melanogaster central nervous system by affinity cell-capture mass spectrometry. *Journal of Proteome Research*, **8**, pp.1271–1284.

**Yin, P. et al.,** 2011. Neuropeptidomics: mass spectrometry-based qualitative and quantitative analysis. *Methods in Molecular Biology*, **789**, pp.223–236.

**Yoon, J.G. & Stay, B.,** 1995. Immunocytochemical localization of Diploptera punctata allatostatin-like peptide in Drosophila melanogaster. *The Journal of Comparative Neurology*, **363**, pp.475–88.

**Yoshihara, M. & Ito, K.,** 2012. Acute genetic manipulation of neuronal activity for the functional dissection of neural circuits - A dream come true for the pioneers of behavioral genetics. *Journal of Neurogenetics*, **26**, pp.43–52.

**Yousuf, M.S. & Kerr, B.J.,** 2016. *The Role of Regulatory Transporters in Neuropathic Pain* 1st ed., Elsevier Inc.

**Yuan, Q. et al.,** 2014. Female contact modulates male aggression via a sexually dimorphic GABAergic circuit in Drosophila. *Nature Neuroscience*, **17**, pp.81–88.

**Zhang, L. & Vertes, A.,** 2018. Single-cell mass spectrometry approaches to explore cellular heterogeneity. *Angewandte Chemie*, **57**, pp.4466–4477.

**Zhou, C., Rao, Y. & Rao, Y.,** 2008. A subset of octopaminergic neurons are important for Drosophila aggression. *Nature Neuroscience*, **11**, pp.1059–1067.

**Zitnan, D.,** 1996. Identification of ecdysis-triggering hormone from an epi tracheal endocrine system. *Science*, **271**, pp.88–91.

**Zitnan, D., Sehnal, F. & Bryant, P.J.,** 1993. Neurons producing specific neuropeptides in the central nervous system of normal and pupariation-delayed Drosophila. *Developmental Biology*, **156**, pp.117–135.

**Zuberovic, A. et al.,** 2009. CE MALDI-TOF/TOF MS for multiplexed quantification of proteins in human ventricular cerebrospinal fluid. *Electrophoresis*, **30**, pp.1836–1843.

**Zwarts, L. et al.,** 2011. Complex genetic architecture of Drosophila aggressive behavior. *Proceedings of the National Academy of Sciences*, **108**, pp.17070–17075.

# 11. Part Publications

Diesner, M.; Neupert, S (2018); **Quantification of biogenic amines from individual GFP-labeled *Drosophila* cells by MALDI-TOF mass spectrometry.** *Analytical chemistry, 2018, 90(13), 8035-8043, DOI: 10.1021/acs.analchem.8b00961.*

Diesner, M; Predel, R; Neupert, S (2018); **Neuropeptide mapping of Dimmed cells of adult *Drosophila* brain.** *Journal of the American Society of Mass Spectrometry, 2018, 25(5), 890-902, DOI: 10.1007/s13361-017-1870-1.*

## Talks

Diesner, M (2018); **Mass spectrometry based single cell analysis for the detection and quantification of neuroactive substances in insect morphology and behavior.** *Invited Talk by Prof. Dr. Wegener, University Würzburg, Germany.*

Diesner, M; Neupert, S (2017); **Probing the soma: Identification and quantification of biogenic amines from single insect somata by direct MALDI-TOF MS.** *15th Rauischholzhausen Seminar: Development and Plasticity of the insect nervous system, 2017, Rauischholzhausen, Germany.*

Diesner, M; Neupert, S (2016); **Identification and quantification of biogenic amines from individual Drosophila somata by MALDI-TOF MS.** *4th ANN Satellite Symposium, 2016, Kiel, Germany.*

Diesner, M; Neupert, S (2016); **Identification and quantification of biogenic amines from individual Drosophila somata by MALDI-TOF MS.** *NeuroDoWo (Neurobiological Doctoral Workshop, 2016, Bielefeld, Germany.*

Diesner, M; Neupert, S (2015); **Detection of octopamine from single *Drosophila* neurons by direct MALDI-TOF MS.** *13th Rauischholzhausen Seminar: Development and Plasticity of the insect nervous system, 2015, Rauischholzhausen, Germany.*

## Poster presentations

Diesner, M; Neupert, S (2016); **Quantification of biogenic amines from single *Drosophila* cells by direct MALDI-TOF MS.** *64th Conference on Mass Spectrometry and allied Topics, 2016, San Antonio, TX, USA.*

Diesner, M; Neupert, S (2015); **Profiling of octopamine from single *Drosophila* cells by direct MALDI-TOF MS.** *63rd Conference on Mass Spectrometry and allied Topics, 2015, St. Louis, MO, USA.*

# 12. Acknowledgments

I want to thank the following people:

I want to express my sincere gratitude to my advisor Dr. Susanne Neupert for providing this interesting topic, the support throughout the project, her patience, the stimulating discussions, motivation and career advice. It has been an honor to be her first Ph.D. student.

Prof. Dr. Marcus Krüger for kindly agreeing to take on the task as second reviewer of this thesis,

Prof. Dr. Reinhard Predel for letting me be a part of his workgroup, numerous fruitful discussions, providing laboratory space and reagents, access to the MALDI-TOF MS instrument as well as Thuringian sausages,

All of the past and current members of the Predel Lab for the always relaxed and funny atmosphere in our office, their support, scientific and non-scientific discussions, long evenings in numerous bars and pubs, as well as company on diverse conferences,

Manuela Ruppert (University of Cologne) and Prof. Dr. Christian Wegner (University Wurzburg) for providing fly lines and many helpful tips regarding fly culture and genetics,

My collaboration partners at the University of Cologne, Dr. Thomas Stolz and PD Dr. Joachim Schmidt,

Leo Lesson, Tobias Schulze, Jörg Schramm and the remaining team from the central workshop of the University of Cologne for their relentless help and support throughout many hardware and software repairs as well as the construction of laboratory equipment,

Dr. Richard Jacoby (University of Cologne) for insightful discussions and the light speed proof-reading of this thesis,

The workgroup Büschges and Wellmann for support inside and outside the Lab, (It's been a great time!)

My family as well as all the friends in Cologne and elsewhere who always supported me throughout my way,

And finally my love Hellena Binz who always believed in me, her understanding for the numerous occupied weekends, for our little man Yoshi and so much more. I have no idea how to pay you back. I love you!

# 13. Erklärung

Ich versichere, dass ich die von mir vorgelegte Dissertation selbstständig angefertigt, die benutzten Quellen und Hilfsmittel vollständig angegeben und die Stellen der Arbeit-einschließlich Tabellen, Karten und Abbildungen -, die anderen Werken im Wortlaut oder dem Sinn nach entnommen sind, in jedem Einzelfall als Entlehnung kenntlich gemacht habe; dass diese Dissertation noch keiner anderen Fakultät oder Universität zur Prüfung vorgelegen hat; dass sie - abgesehen von oben angegebenen Teilpublikationen - noch nicht veröffentlicht worden ist sowie, dass ich eine solche Veröffentlichung vor Abschluss des Promotionsverfahrens nicht vornehmen werde. Die Bestimmungen dieser Promotionsordnung sind mir bekannt. Die von mir vorgelegte Dissertation ist von Dr. Susanne Neupert betreut worden.

Köln, den 12.11.2018

## 14. Curriculum vitae

# Max Diesner

## Personal Data

| | |
|---|---|
| Date of birth | **March 5th 1987** |
| Place of birth | **Frankfurt am Main** |
| Nationality | **German** |
| Email | **maxdiesner@gmx.de** |

## Work experience

| | |
|---|---|
| 04/2018 - | **Research assistant**, Workgroup „Functional cell morpholgy“, Prof. Dr. Aberle, Heinrich Heine University Dusseldorf, Dusseldorf, Germany. |
| 01/2018 – 03/2018 | Unemployed |
| 04/2014 – 12/2017 | **PhD student**, within the framework of the DFG project: „*Weiterentwicklung massenspektrometrischer Detektionsverfahren zur Analyse von Neurotransmittern/ Neuromodulatoren aus identifizierbaren Neuronen der Taufliege D. melanogaster*“ NE911/3-1, Advisor: Dr. Susanne Neupert, University of Cologne, Cologne, Germany. |
| 12/2016 – 02/2017 | Parental leave |
| 10/2013 – 03/2014 | **Lecturer (Studienrat)**, Lecturer for special tasks, University of Cologne, Cologne, Germany. |
| 06/2013 – 09/2013 | **Research assistant**, Workgroup „Functional peptidome analysis“, Prof. Dr. Predel, University of Cologne, Cologne, Germany. |
| 12/2012 – 05/2013 | **Lecturer (Studienrat)**, Lecturer for special tasks, University of Cologne, Cologne, Germany. |

## Education and Academic Studies

| | |
|---|---|
| 04/2014 – 1/2019 | **PhD student**, within the framework of the DFG project: „*Weiterentwicklung massenspektrometrischer Detektionsverfahren zur Analyse von Neurotransmittern/ Neuromodulatoren aus identifizierbaren Neuronen der Taufliege D. melanogaster*“ NE911/3-1, Supervisor: Dr. Susanne Neupert, University of Cologne, Cologne, Germany. Title of the thesis: „Qualitive and quantitive mass spectrometric analysis of neuroactive substances from single insect neurons“. |
| 03/2010 – 11/2012 | **Master studies**, Master of Molecular and Cellular Biology, University Marburg, Marburg, Germany. Master-Thesis: „*Distribution of neuropeptides in two discrete populations of interneurons in the antennal lobe of D. melanogaster*“, Supervisor: Prof. Dr. Joachim Schachtner, Grade 1,0 (Cumulative grade 1,2). |
| 10/2007 – 02/2010 | **Bachelor studies**, University Marburg, Marburg, Germany. Bachelor-Thesis: “*Neuropeptides in the antennal lobe of D. melanogaster*“ Supervisor: Prof. Dr. Joachmin Schachtner, Grade 1,0 (Cumulative grade 1,8). |
| 06/2006 | General qualification for university entrance, Gymnasium Oberursel, Oberursel, Germany. |

## Publications (peer review)

Diesner, M.; Neupert, S (2018); **Quantification of biogenic amines from individual GFP-labeled *Drosophila* cells by MALDI-TOF mass spectrometry.** *Analytical chemistry, 2018, 90(13), 8035-8043, DOI: 10.1021/acs.analchem.8b00961.*

Diesner, M; Predel, R; Neupert, S (2018); **Neuropeptide mapping of Dimmed cells of adult *Drosophila* brain.** *Journal of the American Society of Mass Spectrometry, 2018, 25(5), 890-902, DOI: 10.1007/s13361-017-1870-1.*

Diesner, M; Gallot, A; Binz, H; Vitecek, S; Kahnt, J; Schachtner, J; Jacquin-Joly, E; Gadenne, C (2018); **Mating-induced differential peptidomics of neuropeptides and protein**

**hormones in *Agrotis ipsilon* moths.** *Journal of Proteome research, 2018, 17(4), 1397-1414, DOI: 10.1021/acs.jproteome.7b00779.*

Gálliková, M; Diesner, M, Klepsatel, P, Hehlert, P; Xu, Y; Bickmeyer, I; Predel, R; Kühnlein, RP (2015); **Energy homeostasis control in *Drosophila* adipokinetic hormone mutants.** *Genetics, 2015, 201(2), 665-83, DOI: 10.1534/genetics.115.178897.*

Carlsson, MA; Diesner, M; Schachtner, J; Nässel, DR (2010); **Multiple neuropeptides in the *Drosophila* antennal lobe suggest complex modulatory circuits.** *The Journal of Comparative Neurology, 2010, 518(16), 3359-80, DOI: 10.1002/cne.22405.*

## Talks

Diesner, M (2018); **Mass spectrometry based single cell analysis for the detection and quantification of neuroactive substances in insect morphology and behavior.** *Invited Talk by Prof. Dr. Christian Wegener, University Würzburg, Germany.*

Diesner, M; Neupert, S (2017); **Probing the soma: Identification and quantification of biogenic amines from single insect somata by direct MALDI-TOF MS.** *15th Rauischholzhausen Seminar: Development and Plasticity of the insect nervous system, 2017, Rauischholzhausen, Germany.*

Diesner, M; Neupert, S (2016); **Identification and quantification of biogenic amines from individual Drosophila somata by MALDI-TOF MS.** *4th ANN Satellite Symposium, 2016, Kiel, Germany.*

Diesner, M; Neupert, S (2016); **Identification and quantification of biogenic amines from individual Drosophila somata by MALDI-TOF MS.** *NeuroDoWo (Neurobiological Doctoral Workshop, 2016, Bielefeld, Germany.*

Diesner, M; Neupert, S (2015); **Detection of octopamine from single *Drosophila* neurons by direct MALDI-TOF MS.** *13th Rauischholzhausen Seminar: Development and Plasticity of the insect nervous system, 2015, Rauischholzhausen, Germany.*

## Poster presentations

Diesner, M; Neupert, S (2016); **Quantification of biogenic amines from single *Drosophila* cells by direct MALDI-TOF MS.** *64th Conference on Mass Spectrometry and allied Topics, annual ASMS conference, 2016, San Antonio, TX, USA.*

Diesner, M; Neupert, S (2015); **Profiling of octopamine from single *Drosophila* cells by direct MALDI-TOF MS.** *63rd Conference on Mass Spectrometry and allied Topics, annual ASMS conference, 2015, St. Louis, MO, USA.*

Diesner, M; Schachtner, J (2012); **Allatostatin A expressing interneurons in the adult and larval antennal lobe of *D. melanogaster*.** *105th DZG meeting, Konstanz, Germany.*

Diesner, M; Christ, P; Kollmann, M; Götz, B; Schachtner, J (2011); **Cell proliferation in the brain of the red flour beetle *T. castaneum*.** *104th DZG meeting, Saarbrücken, Germany.*

Carlsson, MA; Diesner, M; Schachtner, J; Nässel, DR (2009); **Neuropeptides in the *Drosophila* antennal lobe.** *21st European Drosophila Research Conference (EDRC), Nice, France.*

## Funding accquisition

DAAD Travel stipend for the visit of the 63rd Conference on Mass Spectrometry and allied Topics, 2015, in St. Louis, MO, USA.

ASMS travel stipend for the visit of the 63rd Conference on Mass Spectrometry and allied Topics, 2015, in St. Louis, MO, USA.